Mechanical behaviour of human enamel and the relationship to its structural and compositional characteristics

by

Lihong He

A thesis submitted in fulfillment of the

requirements for the degree of

Doctor of Philosophy

Biomaterials Science Research Unit, Faculty of Dentistry, the University of Sydney

May 2008

Declaration

Candidate's Certificate

This is to certify that the work presented in this thesis was carried out by the candidate in the Discipline of Biomaterials Science, Faculty of Dentistry, the University of Sydney, and has not been submitted to any other university or institution for a higher degree.

_____

Lihong He, May 2008

Abstract

Objectives

As the outer cover of teeth structure, enamel is the hardest, stiffest and one of the most durable load-bearing tissues of the human body. Also, enamel is an elegantly designed natural biocomposite. From a material science point of view, scientists are interested in the structure and function of the nature material. How does nature design the material to meet its functional needs? From a dental clinic point of view, dental practitioners are keen to know the properties of enamel and compare it with different dental materials. What kind of dental materials can best simulate enamel as a restoration in the oral cavity? The research presented in this thesis on the mechanical behaviour of enamel in respect of its structural and compositional characteristics will attempt to provide answers or indications to the above questions.

Theoretical analysis, as well as experimental investigations of both man-made and natural composites materials, has shown that hierarchical microstructure and organic matrix glues the inorganic particles together and plays an important role in regulating the mechanical properties of the composite. Bearing this finding in mind, in the current investigations, we assume the hierarchical microstructure and trace protein remnants in enamel regulate the mechanical behaviour of the natural biocomposite to meet its functional needs as a load bearing tissue with superb anti-fatigue and wear resistant properties.

One of the important reasons that dental hard tissues haven't been thoroughly investigated is due to the limited sample volume. Fortunately, with the development of nanoindentation technique and equipment, it is now possible to explore the mechanical properties of small volume samples. The application of nanoindentation on dental hard tissues has been documented. However, most investigations have concentrated on only reporting the basic mechanical properties such as elastic modulus and hardness. Very few of them have taken the role of microstructure and composition of these natural biocomposites into their considerations. The main aim of this investigation is to interpret how microstructural and compositional features of enamel regulate its mechanical behaviour. To achieve this goal, the analytical methods considering nanoindentation data

need to be expanded so that more information not only elastic modulus and hardness but also stress-strain relationship, energy absorption ability, and creep behaviour may be evaluated with this technique. These new methods will also be of benefit to dental material evaluation and selection.

Materials and methods

Based on the Oliver-Pharr method[1] for the analysis of nanoindentation data, Hertzian contact theory[2] and Tabor's theory[3], a spherical nanoindentation method for measuring the stress-strain relationship was developed. Furthermore, nanoindentation energy absorption analysis method and nanoindentation creep test were developed to measure the inelastic property of enamel.

With the above methods, sound enamel samples were investigated and compared with various dental materials, including dental ceramics and dental alloys.

- Firstly, using a Berkovich indenter and three spherical indenters with 5, 10 and 20 μm nominal radius, the elastic modulus, hardness and stress-strain relationship of different samples were investigated and compared.
- Secondly, mechanical properties of enamel in respect to its microstructure were investigated intensively using different indenters by sectioning teeth at different angles.
- Thirdly, inelastic behaviour of enamel such as energy absorption and creep deformation were observed and compared with a fully sintered dense hydroxyapatite (HAP) disk to illustrate the roles of protein remnants in regulating the mechanical behaviour of enamel.
- Fourthly, to confirm the functions of protein remnants in controlling mechanical behaviour of enamel, enamel samples were treated under different environments such as burning (300°C exposure for 5 min), alcohol dehydration and rehydration to change the properties of proteins before the nanoindentation tests.
- Lastly, micro-Raman spectroscopy was employed to measure and compare the indentation residual stresses in enamel and HAP disk to evaluate the role of both hierarchical microstructure and protein remnants in redistributing the stresses and reinforcing the mechanical response of enamel to deformation.

Results and significance

Nanoindentation is an attractive method for measuring the mechanical behaviour of small specimen volumes. Using this technique, the mechanical properties of enamel were investigated at different orientations and compared with dental restorative materials. From the present study, the following results were found and conclusions were drawn.

- Although some newly developed dental ceramics have similar elastic modulus to enamel, the hardness of these ceramic products is still much higher than enamel; in contrast, despite the higher elastic modulus, dental metallic alloys have very similar hardness as enamel. Furthermore, enamel has similar stress-strain relationships and creep behaviour to that of dental metallic alloys. SEM also showed enamel has an inelastic deformation pattern around indentation impressions. All of these responses indicated that enamel behaves more like a metallic material rather than a ceramic.
- Elastic modulus of enamel is influenced by highly oriented rod units and HAP crystallites. As a result, it was found to be a function of contact area. This provides a basis to understand the different results reported in the literature from macro-scale and micro-scale tests. Anisotropic properties of enamel, which arise from the rod units, are well reflected in the stress-strain curves. The top surface (perpendicular to the rod axis) is stiffer and has higher stress-strain response than an adjacent cross section surface because of the greater influence of the prism sheaths in the latter behaviour.
- Enamel showed much higher energy absorption capacity and considerably more creep deformation behaviour than HAP, a ceramic material with similar mineral composition. This is argued to be due to the existence of minor protein remnants in enamel. Possible mechanisms include fluid flow within the sheath structure, protein “sacrificial bond” theory, and nano-scale friction within sheaths associated with the degustation of enamel rods.
- A simple model with respect of hierarchical microstructure of enamel was developed to illustrate the structural related contact deformation mechanisms of human enamel. Within the contact indentation area, thin protein layers between HAP crystallites bear most of the deformation in the form of shear strain, which is approximately 16 times bigger than contact strain in the case of a Vickers indenter. By replotting energy absorption against mean strain value of a protein layer, data from different indenters on enamel superimposed, validating the model. This model partially explained the

non-linear indentation stress-strain relationship, inelastic contact response and large energy absorption ability of enamel and indicated the inelastic characteristics of enamel were related to the thin protein layers between crystallites.

- Following different treatments, mechanical properties of enamel changed significantly. By denaturing or destroying the protein remnants, mechanical behaviour, especially inelastic abilities of enamel decreased dramatically, which indicates matrix proteins endow enamel better performance as a load bearing calcified tissue.
- Comparison of Raman derived residual maps about indentations in enamel and a sintered homogeneous HAP showed the hierarchical structure influenced the residual stress distribution within enamel. Moreover, less residual stresses were found in enamel and were a consequence of the protein remnants. These are evidence as to how the microstructure meets the functional needs of the enamel tissue.

In general, evidence from different approaches indicated that the hierarchical microstructure and small protein remnants regulated the mechanical behaviour of enamel significantly at various hierarchical levels utilising different mechanisms. This investigation has provided some basis for understanding natural biocomposites and assisting with dental clinic materials selection and treatment evaluation procedures.

References

1. Oliver WC, Pharr GM. An improved technique for determining hardness and elastic modulus using load and displacement sensing indentation experiments. J Mater Res. 1992;7(6):1564-83.
2. Hertz H. Miscellaneous Papers. London: Jones and Schott, Macmillan; 1863.
3. Tabor D. Hardness of Metals. Oxford: Clarendon Press; 1951.

Acknowledgments

My last remaining task is to acknowledge all those people that have contributed to the work described in this thesis. This is an impossible task, given the many people that have helped to design, implement, apply, criticize, sponsor and evangelize the work. I am going to try anyway, and if your name is not listed, rest assured that my gratitude is not less than for those listed below.

A few lines are too short to make a complete account of my deep appreciation for my supervisor Professor Michael Swain. His curiosity, dedication and passion for research impressed and influenced me deeply. It was his unflattering trust and constant encouragements which have been essential to my success through the last two years. I wish to thank him for his steady support in the most difficult times. His trust and honesty, his efforts in understanding a student's personality and tailoring his approach accordingly translated for me into, although away from home, a very pleasurable 3-year stay at Sydney. My apprentice pursuit into the world of science would not have been the same without Professor Swain's approach to research and science, which made me take the decision, after long internal struggles, to embrace the amazing field of dental materials. I want to extend my appreciation for his patience, for his full devotion to others, for his great understanding, and for the lessons he gave me on the importance of details for the success of the biomaterial project. His contribution has been more than essential for the completion of this thesis and has gone far beyond the commitment of a supervisor. It has been a distinct privilege for me to work with Prof. Swain and the Material Science Research Unit group.

Also, I am grateful for my co-supervisor Dr. Wei Li who provided valuable suggestion to my work and was always available when I needed her help. Dr. Li was the first person I met at Sydney. Her warm heart and kindness touched me deeply from the first second. Without her self-giving assistance, it was impossible for me to settle down and start my research so quickly.

I would like to thank Dr. Ian Kaplin and all the staff of the Australian Key Centre for Microscopy for their assistance and training with the microscopes. Special thanks to Dr. E.A. Carter at Vibrational Spectroscopy Facilities, School of Chemistry, for enthusiastic help and training on Raman micro-spectroscopy. It was an unforgettable experience to work with them.

The episode of acknowledgement would not be complete without the mention of my colleague Mr. Ken Tyler, Dr. Tiffany Huang and Dr. Naoki Fujisawa. Thanks them for valuable technical advice as well as warm friendship, which gave me the feeling of being at home at work. It was a particular pleasure to work with them. The unforgettable group lunches, coffee breaks and free chats with them have become part of my spirit treasures.

Gratefully acknowledge the Australian Department of Education, Science and Training (DEST), Westmead Millennium Institute and The University of Sydney for Providing International Postgraduate research Scholarship (IPRS) support. Research grants from the Australian Dental Research Foundation (ADRF) are also much appreciated.

Finally, I wish to thank my parents for their love and patience during the past thirty years. My parents have always put education as a first priority in my life, and raised me to set high goals for myself. They taught me to value honesty, courage, and humility above all other virtues. I have always needed to work hard to achieve my goals in life and they have always been there for me as an unwavering support. Also, I need to show my special sincere thanks to my wife Joanne, who scarified her good life and promising job in China and came here just for looking after me. I know she suffered a lot depressions and loneliness in the past years by staying in this unacquainted place. Any words are weak here to express my awful regret to her. I wish I can dedicate this thesis to them, and thank them with all my heart for their love, care and patience.

The chain of my gratitude would be definitely incomplete before I express my deepest and sincere gratitude for all the rest who inspired and guided this humble being.

Lihong He

May 2008

Table of Contents

Chapter 1 Introduction 1

1.1 Statement of the problem 1

1.2 Aims of the study 2

1.3 Presentation 3

Chapter 2 Literature review 6

2.1 Brief overview on nature hard tissue and materials 6

2.2 Developmental and structural details of human enamel 10

2.2.1 The ontogeny of human enamel 10

2.2.2 Structure of mature enamel 17

2.3 Composition of mature enamel 23

2.3.1 Inorganic component of enamel 23

2.3.2 Organic component of enamel 24

2.3.3 Vibrational spectroscopy analyses 27

2.4 Research on enamel mechanical behaviour 32

2.4.1 Brief introduction to basic mechanical property definitions 33

2.4.2 Elastic modulus and hardness of enamel 36

2.4.3 Fracture toughness of enamel 40

2.4.4 Inelastic properties of enamel 41

2.5 How enamel structure fits its functional needs? 43

2.5.1 Mechanical advantages of human enamel microstructures 43

2.5.2 Possible functions of protein fragments 46

2.5.3 Numerical and mechanical models 49

2.6 Summary 56

2.7 References 57

Chapter 3 Materials, Methods and Theoretical Basis 63

3.1 Theories 65

3.1.1 Method for stress-strain relationship with spherical indenters 65

3.1.2 Method for energy absorption by nanoindentation 69

3.1.3 Method for nanoindentation creep analysis 71

3.2 Calibration of the indenters 73

3.3 Sample Preparation 76

3.4 References 78

Chapter 4 Nanoindentation Analysis of Enamel and Dental Materials 80

4.1 Material and Methods 81

4.2 Results 82

4.2.1 Sample spherical load-displacement curves 82

4.2.2 Elastic modulus and hardness 82

4.2.3 stress-strain relationship 83

4.2.4 Contact yield point 84

4.2.5 SEM analysis 86

4.2.6 EDX analysis of amalgam 89

4.3 Discussion 90

4.3.1 Load-displacement curve 90

4.3.2 Elastic modulus and hardness 90

4.3.3 Stress-strain response 91

4.3.4 Contact yield point 93

4.3.5 SEM results 93

4.3.6 Differences between enamel and HAP 95

4.3.7 The metallic-like deformation properties of enamel 96

4.4 Conclusions 97

4.5 References 98

Chapter 5 Size Dependent Properties of Enamel 100

5.1 Material and Methods 102

5.2 Results 103

5.2.1 Sample load-displacement curves 103

5.2.2 Elastic modulus of enamel in both directions 103

5.2.3 Stress-strain response 105

5.2.4 SEM observation 106

5.3 Discussion 107

5.3.1. Elastic modulus of enamel 107

5.3.2. Stress-strain response of enamel 109

5.4 Conclusions 110

5.5 References 111

Chapter 6 Non-linear mechanical behaviour of enamel 112

6.1 Energy absorption ability of enamel 114

6.1.1 Materials and methods 114

6.1.2 Results 115

6.1.3 Discussion 118

6.1.4 Conclusions 122

6.2 Nanoindentation creep behaviour of enamel 124

6.2.1 Materials and Methods 131

6.2.2 Results 125

6.2.3 Discussion 129

6.2.4 Conclusions 138

6.3 Numerical analysis of non-linear behaviour of enamel 139

6.3.1 Contact deformation model 140

6.3.2 Discussion 143

6.3.3 Conclusions 146

6.4 References 147

Chapter 7 Influence of environment on the mechanical behaviour of human enamel 150

7.1 Material and Method 152

7.2 Results 154

7.2.1 Indentation elastic modulus and hardness 154

7.2.2 Indentation creep behaviour 156

7.2.3 SEM and EDX analysis 158

7.3 Discussion 160

7.3.1 Possible roles of proteins in regulating mechanical behaviour of enamel 160

7.3.2 Experimental support 161

7.3.3 Consideration of hierarchical structure of enamel 164

7.3.4 Clinical implications 165

7.4 Conclusions 166

7.5 References 167

Chapter 8 Characterization of nanoindentation induced residual stresses in human enamel by Raman micro-spectroscopy 169

8.1 Material and methods 171

8.1.1 Enamel Samples 171

8.1.2 Raman Micro-spectroscopy 171

8.2 Results 173

8.2.1 Force-displacement curves of nanoindentation 173

8.2.2 Representative Raman spectra 174

8.2.3 The influence of fluorescence on $\nu_1(PO_4)$ band position 175

8.2.4 Representative Raman stress maps 176

8.2.5 Comparison of 830-nm and 514.5-nm excitation wavelengths 177

8.3 Discussion 179

8.3.1 Raman spectrum of hydroxyapatite in enamel 179

8.3.2 Factors influence stress detection 179

8.3.3 Residual Stress within different materials 181

8.4 Conclusions 183

8.5 References 184

Chapter 9 Conclusions and Implications 186

List of Tables

Table 2-1 Amino acid composition of human adult enamel protein 26

Table 2-2 Raman and infrared spectroscopic band assignments for mineralized tissue 29

Table 2-3 Conditions under which teeth operate 32

Table 2-4 Elastic modulus and hardness of sound enamel from different measurements 38

Table 2-5 Fracture toughness of sound enamel from different measurements 40

Table 3-1 Summary of the grinding and polishing steps 77

Table 4-1 Indentation elastic modulus and hardness of different materials 83

Table 6-1 Creep rate sensitivity of different enamel samples 129

Table 6-2 Comparison of h_t, h_p values and their ratio 132

Table 7-1 Elastic modulus and hardness of enamel with different treatments 155

Table 8-1 Band shift range of ν_1 vibrational mode from different excitation sources 177

List of figures

Fig. 2-1 Schematic illustration of hierarchical structure of bone 6

Fig. 2-2 Schematic illustration of hierarchical structure of nacre 7

Fig. 2-3 Anatomy of the tooth 9

Fig. 2-4 Secretary stage ameloblast and its relationship with enamel rod structure 13

Fig. 2-5 Proposed scheme for the development of enamel crystallites from mineral/protein subunit precursors 16

Fig. 2-6 Transmission electron microscope images of a rod surrounded by inter-rod enamel 17

Fig. 2-7 Enamel keyhole-shape rod structure 18

Fig. 2-8 Longitudinal section of enamel illustrating Hunter-Schreger bands 20

Fig. 2-9 Rose diagram illustrating amino acid composition of normal permanent human enamel 26

Fig. 2-10 Typical FT-IR spectrum of sound enamel and dentine 28

Fig. 2-11 Raman spectra of natural incisor surface and lased incisor surface 28

Fig. 2-12 C-H stretching mode for enamel 30

Fig. 2-13 Two-dimensional schematic model of indentation fracture on enamel 45

Fig. 2-14 A force extension curve obtained by stretching of a single Ig8 titin fragment 47

Fig. 2-15 Possible kinds of sacrificial bonds involved in the glue between the mineralized collagen fibrils 49

Fig. 2-16 Deformation of enamel parallel and perpendicular to crystal orientation at an ultrastructural level 50

Fig. 2-17 A representation of the crystalline structure in 3-D views 51

Fig. 2-18 Predicted elastic modulus 52

Fig. 2-19 Two adjacent elementary cells of the staggered model 53

Fig. 2-20 Models of biocomposites 54

Fig. 3-1 Schematic illustration of contact between a spherical indenter and a flat specimen 65

Fig. 3-2 Schematic drawing of *P*-*h* curve from nanoindentation 69

Fig. 3-3 Plots of contact radius versus penetration depth for 5 and 20μm tip 73

Fig. 3-4 Plots of contact radius versus penetration depth for 10 μm tip 74

Fig. 3-5 Diagram indicating different specimen directions 76

Fig. 4-1 Comparison of P - h_t curve of three different dental materials and enamel 82

Fig. 4-2 Stress-strain (H-a/R) relationship of different materials 84

Fig. 4-3 h_p/h_t-H curve of dental materials 85

Fig. 4-4 SEM observations of spherical indenter residual impressions 86

Fig. 4-5 SEM pictures of Berkovich indenter impressions on different materials 88

Fig. 4-6 Sample EDX spectra of amalgam sample 89

Fig. 5-1 Sample force-displacement curves for the 20μm spherical indenter 103

Fig. 5-2 Elastic modulus and hardness as a function of penetration depth 104

Fig. 5-3 Nano-indentation stress-strain curves 105

Fig. 5-4 SEM images of indenter impressions on enamel 106

Fig. 5-5 Elastic modulus plotted against contact radius 108

Fig. 6-1 Typical force displacement curves of different indenters on enamel 115

Fig. 6-2 Comparison of *P*-*h* curves at different force loading rates 115

Fig. 6-3 Energy expenditure for the different indenters 116

Fig. 6-4 Comparison of energy absorption ability between enamel and HAP 117

Fig. 6-5 Relationship for enamel between volume of residual indent impression, V_R, and unrecoverable energy loss, U_P. 117

Fig 6-6 SEM image of Berkovich impression on enamel 119

Fig. 6-7 Typical force-displacement results from traditional nanoindentation loading-unloading method showing creep 126

Fig. 6-8 Indentation depth against time, h_t'-t, curves of (a) creep and (b) backcreep of different materials 127

Fig. 6-9 Sample curve of double logarithmic plot of contact pressure (hardness) versus indentation strain rate for enamel 128

Fig. 6-10 Average curve of, a) Logarithmic plot of hardness versus creep time. b) Hardness versus logarithm of time 133

Fig. 6-11 a) Strain rate and b) normalized strain against time plots for enamel compaing both creep and backcreep data 134

Fig. 6-12 Crystal orientation of hydroxyapatite (HAP) crystallites in a rod unit of enamel, showing the crystal and protein layer composite structure 140

Fig. 6-13 Schematic illustration of contact induced deformation of enamel with pointed and spherical indenters 141

Fig. 6-14 Energy expenditure versus mean strain from 10 μm spherical and Berkovich indentations on enamel 143

Fig. 6-15 A schematic illustration of protein peptide chain with sacrificial bonds deforming during indentation contact 145

Fig. 7-1 Elastic modulus and hardness of enamel under different treatments with a Berkovich indenter 154

Fig. 7-2 Indentation depth against time curves of creep and backcreep of enamel under different treatments 156

Fig. 7-3 SEM images comparing sound and burnt enamel 158

Fig. 7-4 Comparison of EDX spectrum on sound and burnt enamel 159

Fig. 7-5 Staggered model illustrates the functional response to shear strain of matrix proteins between HAP crystallites 161

Fig. 7-6 Schematic illustration of peptide chain maintained by water and changes in the presence of ethanol 162

Fig. 8-1 Sample force-displacement curves 173

Fig. 8-2 Sample spectra of enamel and HAP using different excitation sources 174

Fig. 8-3 Comparing of bleaching on the influence of the enamel spectrum 175

Fig. 8-4 $\nu_1(PO_4)$ band position of all three experiments from two different sound areas of enamel 175

Fig. 8-5 Sample stress maps of Berkovich and 10 μm spherical indenters from both HAP and enamel samples 176

Fig. 8-6 Sample stress map of 10 μm spherical indent impression on enamel and its correlated SEM image 182

Publications and scientific meeting presentations arising from this research

Journal publications

1. **HE, L.H.** & SWAIN, M.V. (2008) Nanoindentation creep behavior of human enamel. J Biomed Mater Res, In press.
2. **HE, L.H.**, STANDARD O., HUANG T.T.Y., LATELLA B.A., & SWAIN, M.V. (2008) Mechanical Behaviour of Porous Hydroxyapatite. Acta Biomater,4, 577-586
3. **HE, L.H.** & SWAIN, M.V. (2008) Understanding the mechanical behaviour of human enamel from its structural and compositional characteristics. J Mech Behavior Biomed Mater, 1, 18-29.
4. **HE, L.H.** & SWAIN, M.V. (2007) Influence of environment on the mechanical behaviour of mature human enamel. Biomaterials, 28, 4512-4520.
5. **HE, L.H.** & SWAIN, M.V. (2007) Contact induced deformation of enamel. Appl Phys Lett, 90, 171916.
6. **HE, L.H.** & SWAIN, M.V. (2007) Enamel --- a "metallic-like" deformable biocomposite. J Dent, 35, 431-437
7. **HE, L.H.**, CARTER, E.A. & SWAIN, M.V. (2007) Characterization of nanoindentation induced residual stresses in human enamel by micro-Raman spectroscopy. Anal Bioanal Chem, 389, 1185- 1192.
8. **HE, L.H.**, FUJISAWA, N. & SWAIN, M.V. (2006) Elastic modulus and stress–strain response of human enamel by nanoindentation. Biomaterials, 27, 4388-4398.
9. **HE, L.H.** & SWAIN, M.V. (2006) Energy absorption characterization of human enamel using nanoindentation. J Biomed Mater Res, 81A, 484-492.
10. **HE, L.H.** & SWAIN, M.V. (2006) Nanoindentation derived stress-strain properties of dental materials. Dent Mater, 23, 814-821.
11. SCHNEIDER, G.A., **HE, L.H.**, SWAIN, M.V. (2008) Viscous flow model of creep in enamel. J Appl Phys, 103, 014701
12. AMANAT, N., **HE, L.H.**, SWAIN, M.V. & LITTLE, D.G. (2007) The effect of zoledronic acid on the intrinsic material properties of healing bone: An indentation study. Medical Engineering & Physics, doi:10.1016/j.medengphy.2007.09.008.
13. SHIBATA, Y., **HE, L.H.**, KATAOKA, Y., MIYAZAKI, T. & SWAIN, M.V. (2008) Micromechanical property recovery of human caries dentin achieved with colloidal

nano β-tricalcium phosphate. J Dent Res, 87, 233-237.

14. HUANG T.T.Y, JONES, A.S., **HE, L.H.**, DARENDELILER, M.A. and SWAIN, M.V. (2007) Characterisation of Enamel White Spot Lesions with X-Ray Micro-Tomography. J Dent, 35, 737-743.

Book Chapter:

SWAIN, M. V. & **HE, L. H.** (2007) Mechanical properties of bioceramics. IN KOKUBO, T. (Ed.) *Bioceramics and their clinical applications.* Cambridge, Woodhead Publishing Limited.

Scientific meetings

International Meetings

15. **HE, L. H.** & SWAIN, M. V. Stress-strain properties of dental materials from nanoindentation. 84th General Session & Exhibition of the IADR. Brisbane, Australia. 2006, Oral Representation.
16. SWAIN, M. V. & **HE, L. H.** Size dependence of elastic modulus of enamel. 84th General Session & Exhibition of the IADR. Brisbane, Australia. 2006, Oral Representation.
17. Huang T.T.Y, **HE, L.H.** DARENDELILER, M.A. & SWAIN, M.V. Mechanical Properties of Enamel White Spot Lesions from Nanoindentation. 84th General Session & Exhibition of the IADR. Brisbane, Australia. 2006, Oral Representation.
18. **HE, L.H.**, CARTER, E.A. & SWAIN, M.V. Detection of nanoindentation induced residual stresses on human enamel by Raman microspectroscopy. 4th International Conference on Advanced Vibrational Spectroscopy (ICAVS4). Corfu, Greece. 2007, Oral presentation.

National Meetings

1. **HE, L.H.** & SWAIN, M.V. Investigation of the Influence of Different Environments on the Mechanical Behavior of Mature Human Enamel. 17th Annual Conference of Australian Society for Biomaterials. Melbourne, Australia, 2007. Poster.
2. HUANG T.T.Y, **HE, L.H.** DARENDELILER, M.A. & SWAIN, M.V. Characterisation of Enamel White Spot Lessions with X-ray Microtomography. 17th Annual Conference of Australian Society for Biomaterials. Melbourne, Australia,

2007. Poster.

3. **HE, L.H.** & SWAIN, M. V. Nanoindentation test on enamel. 2nd Australia Nanoindentation Workshop. Kiola, Australia, 2007. Best oral presentation winner.
4. **HE, L.H.**, CARTER, E.A., & SWAIN, M.V. Monitoring stress distribution in human enamel using Raman microspectroscopy. 7th Australian Conference on Vibrational Spectroscopy (ACOVS7). Wollongong, Australia, 2007. Poster.

Chapter 1

Introduction

1.1 Statement of the problem

Over the long period of evolution and adaptation, hard tissues from different species have developed their own unique structures to meet their functional needs. What can we learn from these smart designed natural materials? In the material science field, material development has come to the bio-mimetic and bio-duplication era. In the dental clinic area, we need better tooth replacement materials. Therefore, here we have investigated the excellent mechanical behaviours of human mature enamel in respect of its structural and compositional characteristics to illustrate the smart design developed by nature and how to improve dental material microstructural design and selection.

Enamel, the outer cover of a tooth, is the hardest and stiffest structure of mammals. It is also one of the most critical load bearing tissues in the body. Under critical conditions, the contact stress at the surface of enamel can range from 0.45-2.5 GPa[1,2]. The functional requirements of teeth for the survival of the species are that they are able to bear a wide range of imposed loads and consequent contact induced stresses without failure and retain their shapes while doing so. Besides the normal loads, enamel will be exposed to shear forces because of the direct contact with oppositing teeth and external objects during mastication. Moreover, unlike other calcified skeletal structures, fracture of dental tissue is not repairable. Why does enamel have such perfect mechanical properties? What can we learn from this natural biocomposite? These questions can be traced back to the compositional and structural characteristics of enamel. Generally speaking, enamel is a well designed biocomposite with more than 95wt% inorganic apatite crystals, 1-2wt% protein remnants and 3-4wt% water. These inorganic and organic components are arranged within specific hierarchical structures, which reinforce the mechanical properties of the material dramatically.

From a materials science point of view, the mechanical properties and the mechanisms responsible in relation to the compositional and hierarchal micro-structural characteristics

of enamel are an essential factor to understand this natural material. But, till now, due to the limitation of test methods and sample size, the relationship between mechanical properties and structural characteristics is still not very clear. What is the importance of this hierarchical structure to the function of this natural biocomposite?

From a dental clinical point of view, we need new restorative materials with similar mechanical behaviour as enamel for dental fillings and prostheses. As a successful replacement of alloys and other metallic materials, dental ceramics have been widely used in clinic due to their good aesthetics and high strength. But, dental ceramics have higher hardness in comparison to enamel, which may lead to excessive wear on opposing natural teeth. On the other hand, composite materials which are evermore popular in the dental clinic and are much softer than ceramics, have significant problems such as micro-leakage and failure because of the shrinkage and aging of the material. How can dental material researchers learn from this lesson of nature and develop a new generation of synthetic composites? Based on the mechanical characteristics of enamel, what should be the proper criteria to evaluate and select dental materials in the clinic?

In short, studies on mechanical properties of enamel in respect of its compositional and structural characteristics will benefit the material science, dental material development and clinical communities in the form of material selection significantly.

1.2 Aims of the study

The aims of the study are summarised as follows:

- To determine the basic mechanical properties including elastic modulus, hardness and stress-strain relationship of enamel by nanoindentation and compare them with different dental materials;
- To study and explain the nanoindentation inelastic behaviour including energy absorption and creep behaviour of enamel;
- To explore the influence of the hierarchical structure of enamel on its mechanical properties;
- To investigate the function of the organic components of enamel in regulating the mechanical properties of the biocomposite;

- To develop a nanoindentation based material evaluation and test method for dental material comparison and selection;

1.3 Presentation

The present study consists of eight main chapters.

The histological and structural background of the human enamel and previous investigations on its compositional characteristics and mechanical properties are reviewed in Chapter 2. In this review, the histological origin of the hierarchical microstructure is briefly summarized and explained. Furthermore, several typical scanning electronic microscopy (SEM) images from the author as well as from the literature have been included to illustrate the specific hierarchical microstructure of enamel. The literature review of mechanical tests of enamel also indicates the anisotropic properties of the material due to its hierarchical microstructure. In addition, the possible mechanical functions of protein remnants in enamel are also reviewed. The literature review concludes by predicting the possible mechanics of compositional and structural characteristics of enamel in regulating its mechanical behaviours.

Chapter 3 summarizes most methods and underlying theoretical basis that are used in the following studies. A spherical nanoindentation method for investigation of stress-strain relationship is described. Moreover, the energy absorption and creep behaviour analyses based on nanoindentation method are also illustrated in this part. At the end, the general sample preparation procedure is described to avoid duplication in the following chapters.

In Chapter 4, a thorough investigation and report on the nanoindentation mechanical properties of enamel and the comparison with variety of dental materials is presented. Enamel is compared with sintered hydroxyapatite (HAP) disk, dental ceramics and dental alloys in terms of the elastic modulus, hardness, indentation stress-strain curves as well as deformation patterns. It is concluded that, although enamel contains more than 95wt% HAP crystals, it behaves more like metallic materials rather than ceramics. In other words, enamel is much softer and more plastic deformable than its major composition, HAP disk and most dental ceramics.

Chapter 5, which concentrates on the elastic modulus of enamel, is an extension of Chapter 4. In this chapter, elastic modulus of enamel was investigated by different indenters including Berkovich, 5 and 20 micron spherical tips. Size dependent phenomenon, such as for the elastic modulus, is observed and depicted including its relationship to enamel microstructure is discussed.

Chapter 6 is an expansion of nanoindentation method into an investigation of the inelastic behaviour of enamel, which includes energy absorption and indentation creep. Although the major component of enamel is HAP, a typical elastic and brittle material, experiments show significant inelastic behaviour of enamel. These phenomena are correlated with the small volume fraction of protein remnants in mature enamel. Further more, to better illustrate the issue, a simple numerical model based on the above assumptions is developed and illustrated at the last part of the chapter.

To verify our assumptions on the function of organic components in regulating mechanical behaviours of enamel, we undertook further investigations, which are addressed in Chapter 7. In this study, enamel is subject to different environments such as burning, alcohol dehydration and water rehydration. We do observe differences in the elastic modulus, hardness and indentation creep behaviour in these environments. Because HAP crystals are assumed to be thermally and chemically inactive, the differences between different treatments are related to the organic components of mature enamel. These observations suggest that, although proteins are only a minor part of the enamel composition, they may regulate the mechanical properties of enamel by redistributing stresses inelastically via some unknown mechanism.

In chapter 8, Raman micro-spectroscopy was employed to investigate the indentation induced residual stress in enamel. The results are compared with dense sintered HAP disk. Raman wave number shift derived stress mapping indicates that the hierarchical microstructure of enamel regulates the stress distribution. This became another evidence to support our assumption, namely that the mechanical properties of enamel have been optimized by its microstructure and organic composition.

References

1. Hayasaki H, Okamoto A, Iwase Y, Yamasaki Y, Nakata M. Occlusal contact area of mandibular teeth during lateral excursion Int J Prosthodont. 2004;17(1):72-6
2. Waltimo A, Kononen M. Maximal bite force and its associations with signs and symptoms of craniomandibular disorders in young Finnish non-patients. Acta Odontol Scand. 1995;53:254-8.

Chapter 2

Literature review

Part of this chapter has been published as an invited review paper named “Understanding the mechanical behaviour of human enamel from its structural and compositional characteristics” in the first issue of *Journal of Mechanical Behaviour of Biomedical Materials*.

2.1 Brief overview on nature hard tissue and materials

Nature endows different natural hard materials unique structures. These are all good lessons from nature. Although the aim of this review is focussed only on human mature enamel, a quick scan of some other typical natural hard tissues can help us to appreciate some general concepts of the excellent designs from nature.

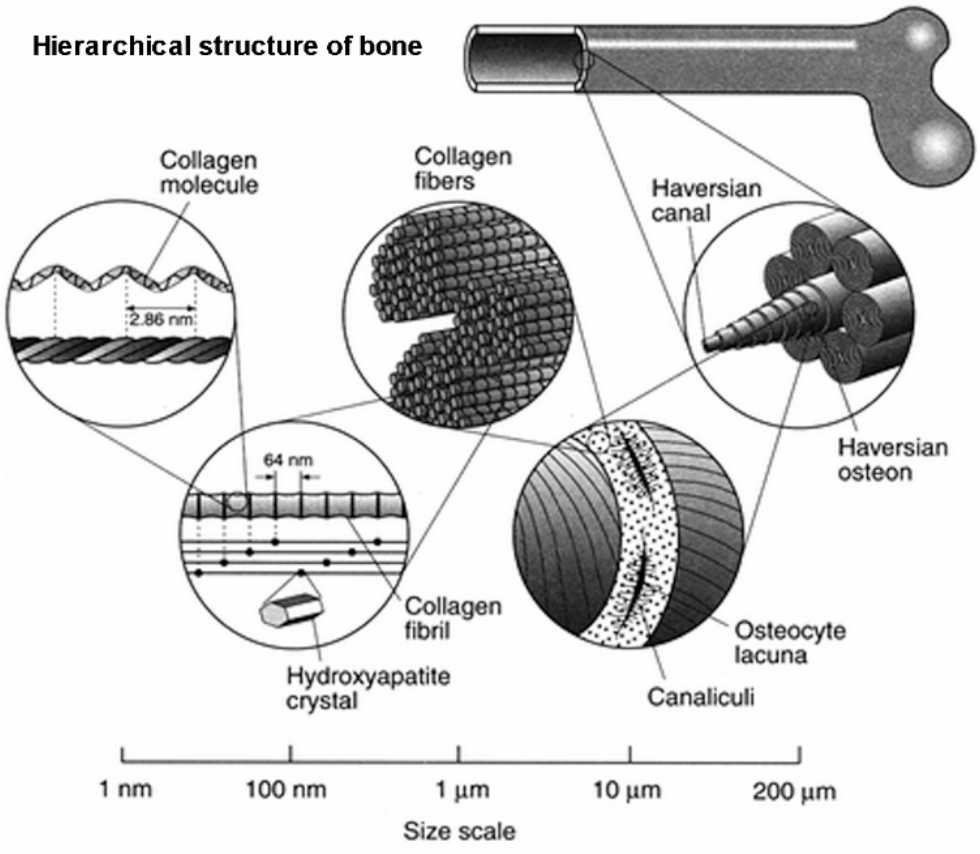

Fig. 2-1 Schematic illustration of hierarchical structure of bone (http://pubs.rsc.org/ej/JM/2000/b000950o/b000950o-f1.gif)

Bone, as a mineralized biomaterial, consists of directional structural features across several unique hierarchical scales, ranging from nano-scale crystals and molecules to the macroscopic shape (Fig. 2-1). However, the foundational structural unit across the hierarchical scales is a relatively simple two phase arrangement of anisometric bone mineral (apatite) preferentially oriented in a collagen matrix. The combination of apatite crystals and collagen fibres in different patterns at different levels forms a light but tough structure that is bone. The growing database of measurements for the mechanical anisotropy of cortical bone depicts the functional advantages of the natural designed structure.

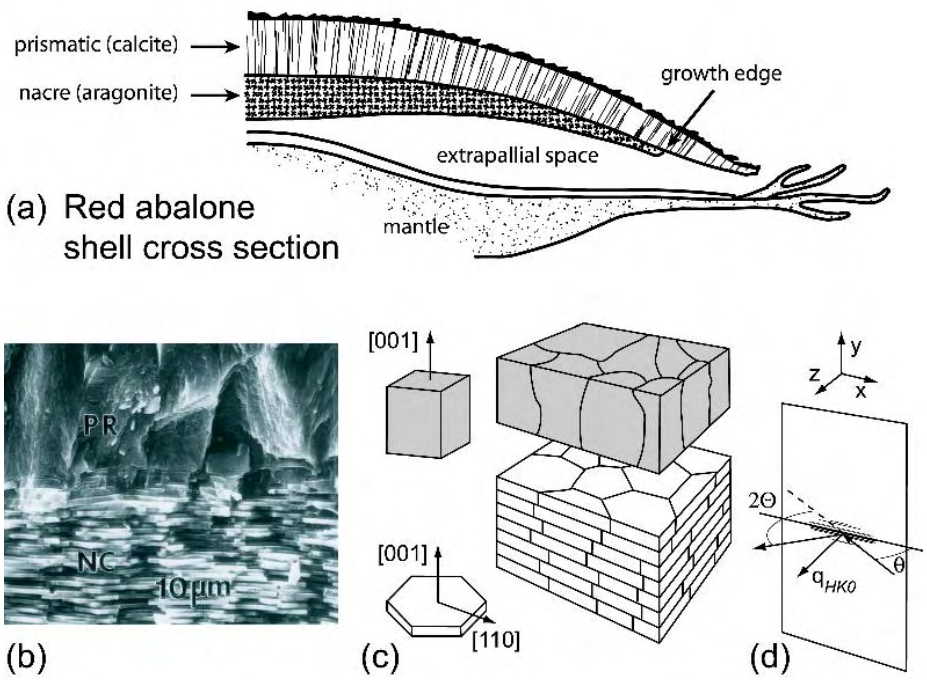

Fig. 2-2 (a) Cross section of the shell of the red abalone. The outer, calcite mineral layer imparts hardness to the shell, while the nacre layer is a laminate that provides toughness. New nacre layers are deposited onto the rod layer at the growth edge. (Vertical scale is exaggerated.) (b) Scanning electron micrograph of the nacre-rod boundary. The larger calcite columns and the thin aragonite tablets can be seen. (c) Idealized view of the crystal orientation at the interface; both mineral types have the c-axis roughly aligned normal to the boundary. (d) Reflection geometry for microbeam diffraction experiments. Under the idealization in (c), the observed peaks will be at [HK0] Bragg reflections. The illuminated spot is of order 5 by 10 µm. (http://www.solids.bnl.gov/home/dimasi/bones/abalone/index.html)

Similar to bone, nacre also has hierarchical structures: crystals combined into platelets and platelets piled into nacre (Fig. 2-2). The key strengthening and toughening mechanisms in nacre can be described as[1]:

- Material properties of aragonite and organic matrix, especially the unique properties of the organic phase in the confined space between platelets.
- Structure at micro scale: size, shape of platelets etc.
- Interlocking of aragonite platelets: progressive failure of interlocks guides the fracture path.
- Molecular interactions at the organic–inorganic interface.

From the above two typical examples, it is easy to see that the hierarchical structure is important to nature hard tissues and plays an important role in regulating the mechanical properties of the materials. As Currey summarized in his paper[2], the main mechanical function of these hierarchical arrangements, is almost certainly, to produce interfaces that will open up in the presence of potentially dangerous cracks, deflecting the cracks and making their travel energetically expensive. This makes biomineralized skeletons surprisingly tough, given that they are made almost entirely of mineral. Bone is a special case, despite having less mineral than most other biomineralized skeletons; it can be remarkably tough. Apart from their hierarchical arrangement, two other features of biominerals contribute to the superior mechanical properties of skeletons made from them. First, at the lowest level, they are often made of tiny crystals that are smaller than the "Griffith length" necessary for cracks to spread. Second, the precision with which they can be laid down (changing their main orientation over a few micrometers, for instance) allows exquisite adaptations to the loads applied to these skeletal tissues.

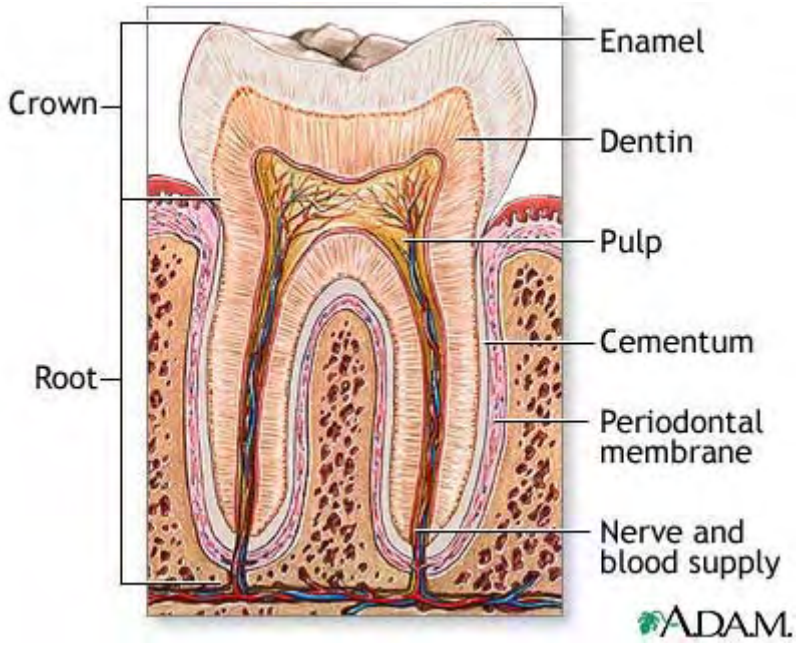

Fig. 2-3 Anatomy of the tooth.

(http://www.nlm.nih.gov/medlineplus/ency/imagepages/1121.htm)

In a manner similar to bone and nacre, human mature enamel, the hardest organ in our body, owes much to its hierarchical structure. As the cover layer of teeth (Fig. 2-3), enamel must retain its shape as well as resist fracture and wear during load-bearing function for the life of the individual. Teeth experience a range of loading situations[3]: firstly, they contact directly other objects and/or opposing teeth; secondly, they encounter normal and sliding contact resulting in wear, and thirdly, unlike bone, damage of teeth is not reparable. To meet all of these functional requirements, teeth have evolved with a unique hierarchical microstructure. In this chapter, enamel will be thoroughly summarized from different aspects including embryo development, microstructure, mechanical properties and possible strengthening mechanisms.

2.2 Developmental and structural details of human enamel

Human enamel is the hardest tissue in the human body. It has the ability to retain its shape and resist fracture during severe load-bearing events. Enamel makes direct contact with opposing teeth. Furthermore, any types of abrasion, fracture and any other damage are unrepairable. Therefore, the structure of enamel should have the characteristics and abilities to satisfy these critical requirements.

2.2.1 The ontogeny of human enamel

The improvement of microscopy and tissue preparation, cell biological and molecular biological techniques have stimulated the study of ontogenetic research during the past three decades. The field now has entered the gene and cell molecular level. The thorough investigation of the ontogeny of this special structure provides us with a fairly good base to explore its functional characteristics. Briefly speaking, the development of enamel experiences several stages, named as cytodifferentiation, matrix secretion and maturation. The detailed procedures will be reviewed in the following sections briefly.

2.2.1.1 Embryo generation of enamel.

Dental enamel is produced by epithelial cells, which may be ectodermal or endodermal in origin[4]. A series of inductive interactions between epithelium and mesenchyme determines the sequence of events in tooth development: the initial establishment of dental primodia, sequential stages of morphogenesis, cytodifferentiation of odontoblasts, deposition of dentin matrix, cytodifferentiation of ameloblasts, deposition of enamel matrix and maturation of enamel. Each successive stage requires conditions and interactions that have been determined in the preceding stage[5].

2.2.1.2 Amelogenesis

Only three main stages will be described in this review: cytodifferentiation, matrix secretion and enamel maturation.

2.2.1.2.1 Ameloblast cytodifferentiation

This process of cytodifferentiation occurs in two steps: the transformation from dental epithelial cell to preameloblasts and the subsequent differentiation from preameloblasts to secretary ameloblasts. The secretary ameloblasts have several typical characteristics. First is that they are polarized, tall and columnar cell shaped. Second is the appearance of Tomes' process (Fig. 2-4a) at the apical, secretary, end of the cell. Third is an increase in the number of organelles (Fig. 2-4a), specifically those organelles that are involved in protein synthesis and secretion. Fourth is the appearance of junctional complexes between neighbouring cells. The apparent absence of a continuous, tight seal between the developing ameloblasts and the extracellular space leaves open the possibility of intercellular movement of ions and low molecular weight substances. The gap junction between secretory ameloblasts are believed to enable these cells to coordinate their secretory activity[6]. The last one is the development of cytoskeleton in the form of microtubules, intermediate filaments and microfilaments. The significance of this cytoskeleton is its proposed role in the movement of horizontal (circumferential) rows of secretory ameloblasts[7].

2.2.1.2.2 Enamel matrix secretion

The newly differentiated ameloblasts start depositing enamel matrix as soon as the adjacent dentin matrix undergoes its initial calcification. Shortly after the secretory activity has started, the ameloblasts develop at their apical (secretory) surface a single, fairly large cell process, the Tomes' process. The Tomes' process is a unique feature of the secretory ameloblast and is present only during the secretory stage.

(A) Enamel matrix proteins.

Initially secreted enamel matrix contains 80-90% matrix protein and fluid with only 10-20% mineral by volume. This is in sharp contrast with mature enamel, which contains 80-90% mineral by volume. The enamel matrix is composed of at least two major types of enamel-specific matrix proteins: amelogenins and enamelins. The cell also produces several enzymes which indicates that the cell is removing and degrading a small quantity of matrix components even during the secretory stage[8].

Amelogenins are proline-rich, hydrophobic proteins. Amelogenins constitute approximately 90% of the enamel matrix proteins prior to maturation[9]. Their role remains elusive. They are capable of binding apatite and have been shown to exhibit an inhibitory action on hydroxy-apatite formation in solution[10]. Amelogenins may regulate the mineralization of enamel. Experimental inhibition of amelogenin translation can result in interference of crystal growth and orientation[11]. During enamel secretion, and particularly during its maturation, amelogenins are degraded and gradually removed from the matrix[12]. Proteolytic enzymes are present throughout the thickness of the newly formed enamel matrix and amelogenin (and enamelin) fragments of different sizes may be encountered[13,14]. During enamel maturation the amelogenins are lost almost entirely from the matrix and the amino acid composition of the enamel is changed significantly[15].

Enamelins, which are highly conserved during evolution, are acidic, hydrophilic glycoproteins, considerably larger than amelogenins. They are mainly attached to the hydroxyapatite crystallites and continue to be present in the mature enamel, although possibly in fragmented form[8]. They are thought to act as nucleators in the mineralization process, resembling in their action the acidic phosphoproteins in bone and dentin[15].

Non-amelogenins. A third class of proteins, named non-amelogenins, was reported as a small molecular size (13-17 kDa) protein remnants in immature bovine enamel[16]. These proteins were observed predominantly in the rod sheaths. The existence of yet another type of enamelin, 'tuftelin', has been postulated by Deutsch et al.[17], while others claim that the proteins found in tufts are all enamelins[9]. Basically, different enamelins and amelogenins are synthesized initially, but additional protein remnants of several sizes observed in different studies may be the results of the action of proteolytic enzymes on enamelins and amelogenins during the mineralization of the enamel matrix[10,14,18].

(B) Function of Tomes' process.

The presence and the shape of Tomes' processes (Fig. 2-4) are significant for the structure of the developing enamel. Their shape controls both the orientation of the matrix proteins and in doing so the alignment of the hydroxyapatite crystallites.

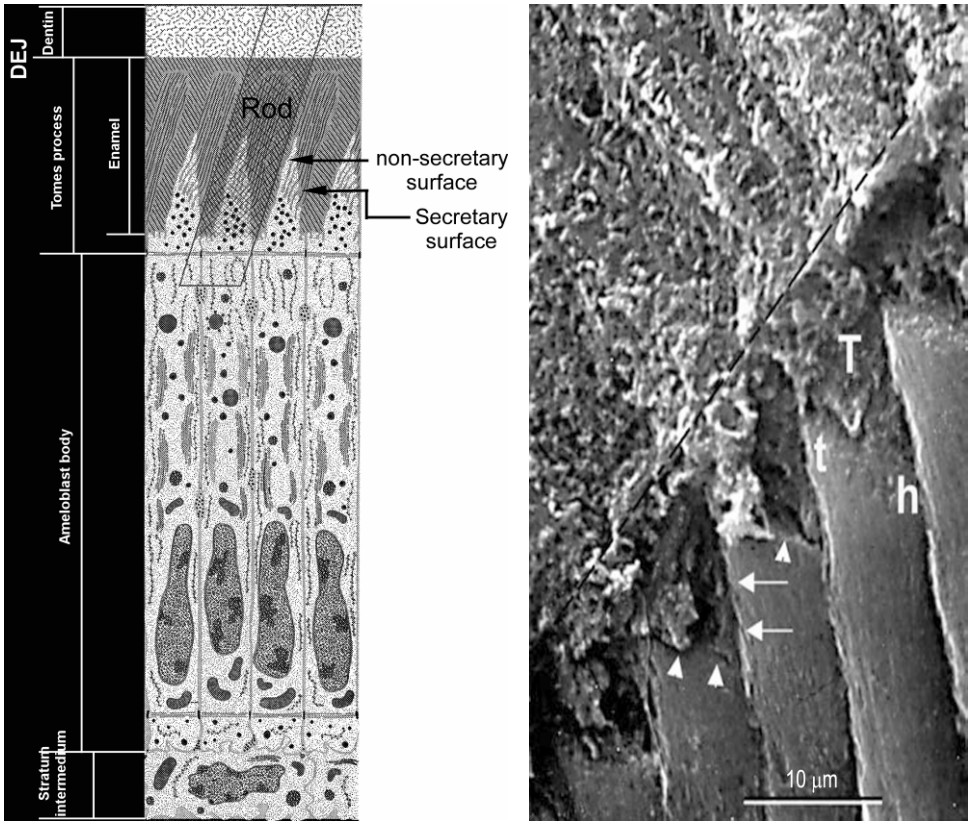

(a) (b)

Fig. 2-4 (a) Schematic illustration of secretary stage ameloblast and its relationship with enamel rod structure[19]; (b) Fractured enamel with intact secretory-stage ameloblasts adhering to the forming enamel surface. The axis of the cells is ~22° to the longitudinal axis of the enamel rods. The apical terminal web (dotted line) separates the cell body from the Tomes process. In the lateral view, Tomes processes (T) appear triangular and connect the divergent angles of the cells and rods. The pattern of stepped Tomes processes, and consequently the stepped forming enamel rods, is clearly seen in the lateral view. The head (h) and tail (t) region of a forming enamel rod surface (arrowheads) are indicated. The arrows point to the adjacent enamel rod confining the head region of the Tomes process[20].

Crystal formation begins early during the secretory phase of amelogenesis within the newly deposited enamel matrix and in close proximity to the secretory apical surface of the ameloblast.

The initial mineralization occurs in small nuclei near the dentino-enamel junction within the supramolecular aggregates of amelogenins and enamelins. Soon thereafter, these

hydroxyapatite crystallites become confluent with the smaller hydroxyapatite crystallites in the neighboring dentin[21]. The early mineralization process of enamel yields thin, ribbon-like crystallites[22], which may be grouped in distinct domains: Rods and interrod regions. Since the crystallites are oriented at right angles to the apical secretory surfaces of the ameloblasts and the Tomes' processes, any abrupt reflection of the cell membrane will produce a similarly abrupt change in crystallite orientation resulting in a boundary, as is found between a rod and an interrod region.

It is generally recognized that non-rod enamel is formed by ameloblasts that do not possess Tomes' processes. In mammals, non-rod enamel may be found near the dentino-enamel junction and may represent enamel formed before Tomes' processes were present. Similarly, non-rod enamel is often found near the surface of the tooth, and may represent enamel formed after Tomes' processes have disappeared.

Tomes' processes have both secretory and non-secretory surfaces. The secretory surfaces are characterized by deep membrane infoldings and the ultrastructural features of exocytosis, while the non-secretory surfaces may show tubular structures, as well as coated pits and vesicles. An ameloblast involved in the formation of rod enamel generally has a Tomes' process with a well-defined secretory surface that may be on the most apical face of the process or on a curved crescent surface, which is slanted cervically. While the secretory surface of a Tomes' process is responsible for the formation of a rod, the apical surface of the ameloblast, which forms a 'shoulder' surrounding the base of Tomes' process, represents the interrod secretion site. The lateral surfaces of Tomes' process are non-secretory. These are the sites where the rod sheaths develop, at the boundaries between two rods or between a rod and an interrod region.

2.2.1.2.3 Enamel maturation

When an ameloblast has completed its principal secretory activities and the developing enamel has reached its full thickness locally, the secretory stage comes to an end. The ameloblast next undergoes a series of cytological changes in preparation for the subsequent stage of amelogenesis: enamel maturation.

During enamel maturation, significant changes occur in the organic matrix and in the

mineral (hydroxyapatite). There is a sharp increase in matrix degradation and replacement by tissue fluid during the maturation stage. After most of the matrix (specifically the amelogenins) and the fluid have been removed, the mineral component increases steeply from 10-20% to 80-90% as a percentage of volume. It should be noted that the maturation stage ameloblasts continue to secrete some proteins well into the maturation period.

One of the most important steps in enamel maturation process is the organization of hydroxyapatite (HAP) crystals into bulk enamel. This organization is achieved by extracellular protein matrices, which are secreted from the Tomes' processes of ameloblasts. Amelogenin is the dominant protein in this enamel matrix.

Amelogenin undergoes self-assembly to form nanospheres in vitro and in vivo[23]. These nanospheres are located adjacent to the a- and b-surfaces of the HAP crystallites in vitro, possibly favouring crystallite elongation along the *c*-axis[23,24]. This would result in long and thin crystals arranged in parallel[23]. As enamel mineralization proceeds, the organic matrix is progressively removed allowing the crystallites to grow in thickness. The resulting mineral phase forms as a consequence of a unique organic matrix that is competent to direct its own replacement by mineral. Recently, there has been a report that the HAP crystallites derived from rat incisor enamel has a uniform banding pattern along their *c*-axis[24]. These data have been derived using chemical force microscopy. The in vitro banding pattern observed consisted of repeating units (high friction and low friction bands) of some 45-65 nm in length. Experimentally, the bands were related to regular nanosphere assembly of hydroxyapatite[24]. These data add significantly to the emerging model of protein-mineral interactions as they relate to enamel formation.

As described by Robinson et al.[25], the rather elaborate matrix processing seen during early enamel development would serve two functions. Firstly, degradative processing of protein within the spheres could affect mineral ion binding or water content, initiating mineral nuclei. Further degradation of the amelogenin would then allow such nuclei to fuse, forming the collinear globular crystal structures seen in secretory enamel by AFM. Secondly, further more complete degradation and removal of the matrix during the maturation stage and its replacement by fluid would permit these crystals to grow in thickness. This proposal has been outlined in Fig. 2-5.

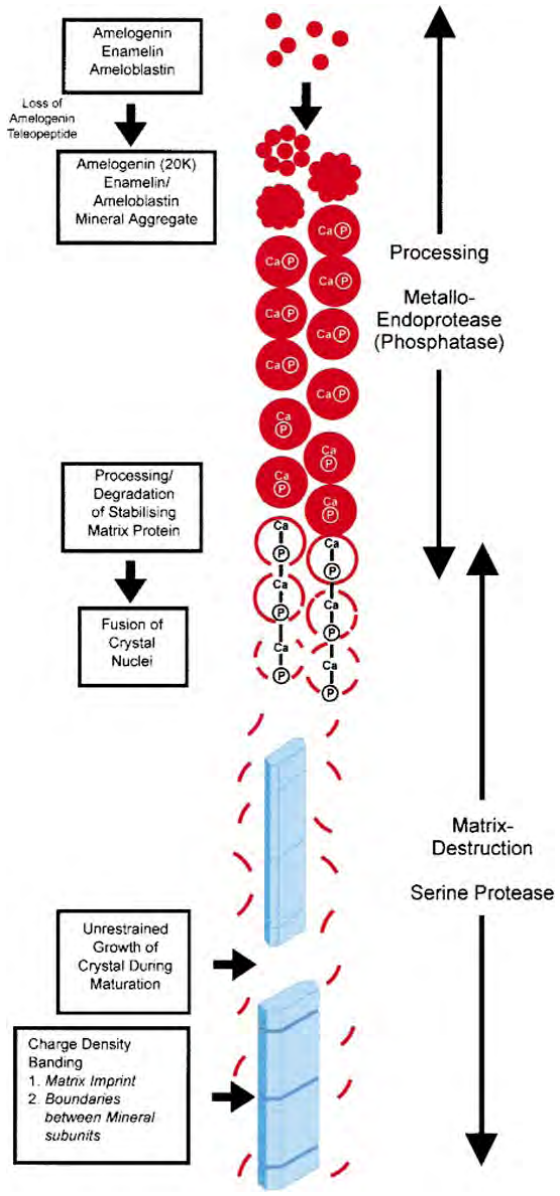

Fig. 2-5 Proposed scheme for the development of enamel crystallites from mineral/protein subunit precursors[25].

Amelogenin protein contains a lectin binding activity[26]. This lectin binding activity may serve to orient the amelogenin nanospheres by tethering them to the retracting glycocalyx on the Tomes' processes, or the amelogenin nanospheres may interact with another glycosylated enamel protein. The resulting interaction may serve to provide a vector of force orientating the nanospheres and the entire proteinaceous matrix relative to the retracting ameloblast, and in turn this would control crystallite orientation.

The crystallites grow first in length and later in width. As the rate of crystallite thickening varies considerably between mammalian species: those in which the teeth last longer grow more mineral at an earlier stage of development. Longer-surviving enamel usually

also has a longer maturation history, enabling it to become harder (i.e. the permanent molar teeth may spend more than 5 years to achieve total maturation).

2.2.2 Structure of mature enamel

The result of such a highly precise regulation of the bio-mineralization procedure during amelogenesis is the prominent hierarchy of enamel structure[27]. The least complex and smallest structural units are needle or plate-like HAP (Fig. 2-6). In healthy human enamel, these hydroxyapatite crystallites are organized and bundled together by protein films into larger-scale structures, called 'keyhole-shaped' enamel rods (Fig. 2-7). On a larger and more complex scale, numerous rod units bound together and twist together or change their direction slightly to reinforce the whole structure[28], which form the Hunter and Schreger bands (Fig. 2-8).

2.2.2.1 Apatite Crystals

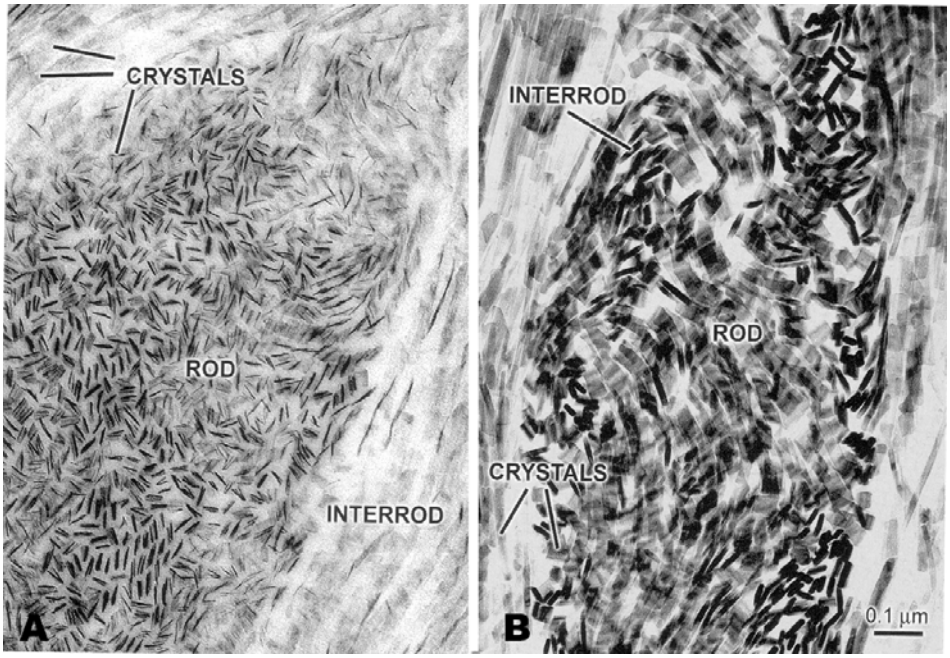

Fig. 2-6 Transmission electron microscope images of a rod surrounded by inter-rod enamel from (A) young and (B) older forming enamel of a rodent. The crystals that make up the rod and interred enamel are long, ribbonlike structures that become thicker as enamel matures. They are similar in structure and composition but appear in different planes of sections because they have different orientations[19]. (Two images have same resolution and share same scale bar at the left bottom.)

At the smallest level, enamel is built from closely packed and long, ribbonlike carbonated apatite crystals which are roughly hexagonal in cross-section[29] (Fig. 2-6) with width of 60-70 nm and thickness of 25-30 nm[30]. Due to difficulties of sample preparation, the length of these crystallites varies from different reports. In other words, the crystals are too long for their true length to be determined[31]. Some investigators believe that the length of the crystals actually spans the entire thickness of the enamel layer[19]. Between two neighbour crystals, there is a ~1 nm thin protein film that "glues" the crystals together.

2.2.2.2 Keyhole-shape rod unit

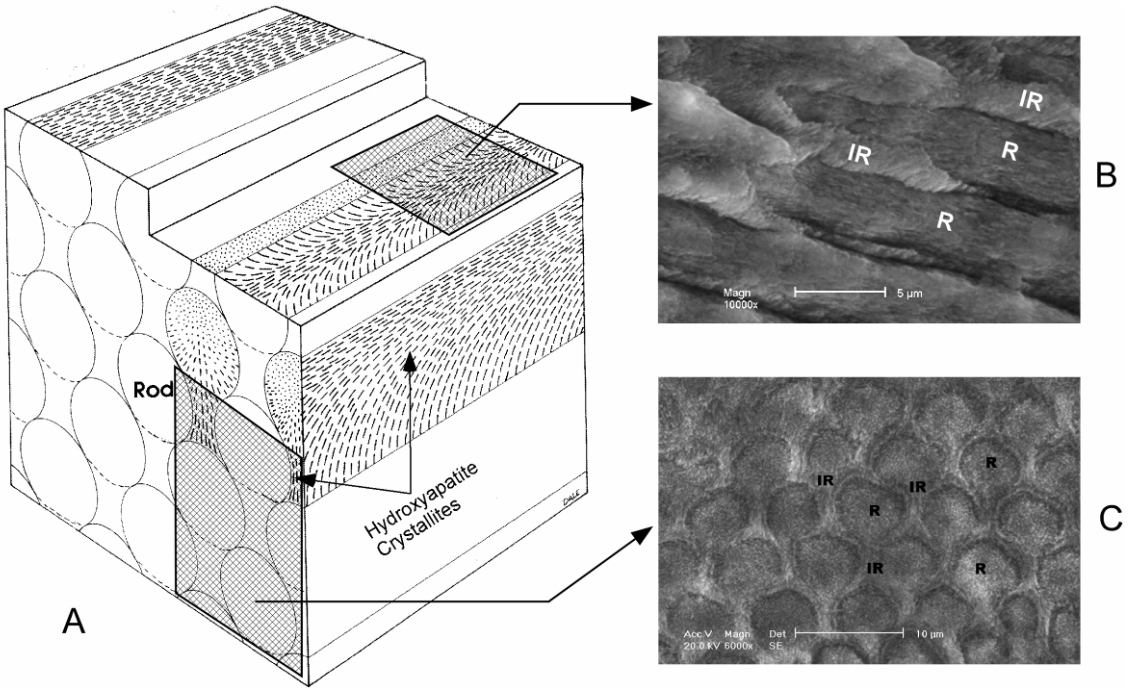

Fig. 2-7 (A) Schematic illustration of enamel keyhole-shape rod structure; (B) and (C) SEM images of different faces.

The arrangement of apatite crystallites determines the next level unit, enamel rod unit. Human enamel consists of ~5 μm diameter rods encapsulated by ~1 μm thick protein rich sheathes that are arranged parallel in a direction perpendicular to the dentino-enamel junction (EDJ) from dentin to the outer enamel surface (Fig. 2-7). Within rod units, the directional arrangement of the apatite crystallites varies. Crystallite plates in the central part of the rod are parallel to the rod axis while those near the edge of the rod usually

have an angle of near 15-45° to the longitudinal axis of the rods[32]. As shown in Fig. 2-7B, the crystal direction of the interrod region is almost vertical to those in its neighbouring rod region. The variation of crystal directions can be explained by the function of Tomes' process mentioned in the above section. It appears that the rod is primarily contributed by the basal tip of the Tomes' processes, whereas, the interrod is primarily determined by the sides of the Tomes' processes, especially by their longer incisal surfaces. Hence, the shape of the secretory part of the process may govern the ratio of the rod to interrod. Likewise, the angle between the crystallite orientations in rod and interrod is a reflection of the angle between the parts of the process that contribute to their respective matrices. In human enamel, the merging of rod and interrod matrices is accomplished by gradual curves connecting the different secretory surfaces of the process.

The rod unit is the most important level in understanding the microstructure and function of enamel. Numerous interpretations of the mechanical properties of enamel are based on this unit structure. Paine et al.[33] proposed a model of human enamel microstructure. This model contains several important elements. First, the paths of the Tomes' processes create a staggering between adjacent layers of rod, governing the possible spatial and temporal relationships among forming rods, and the possible connections between them. Second, the orientation of the crystallites within a rod and interrod is related to shape and orientation of the secretory sites of the Tomes' processes and the vectors of movement of the ameloblasts. Third, it appears the rod is primarily determined by the tip of the Tomes' processes, whereas, the interrod is dominated by the sides of the process, especially by the longer incisal surfaces. Fourth, the dominant rod and interrod crystallite orientations differ by an angle of approximately 15-45° in the sagittal plane. Fifth, boundaries or potential fracture planes are maintained at the incisal surfaces of the rods where rod-interrod continuity is limited, but the apical surfaces of the rod blend into a continuum with interrod.

2.2.2.3 Hunter-Schreger Band

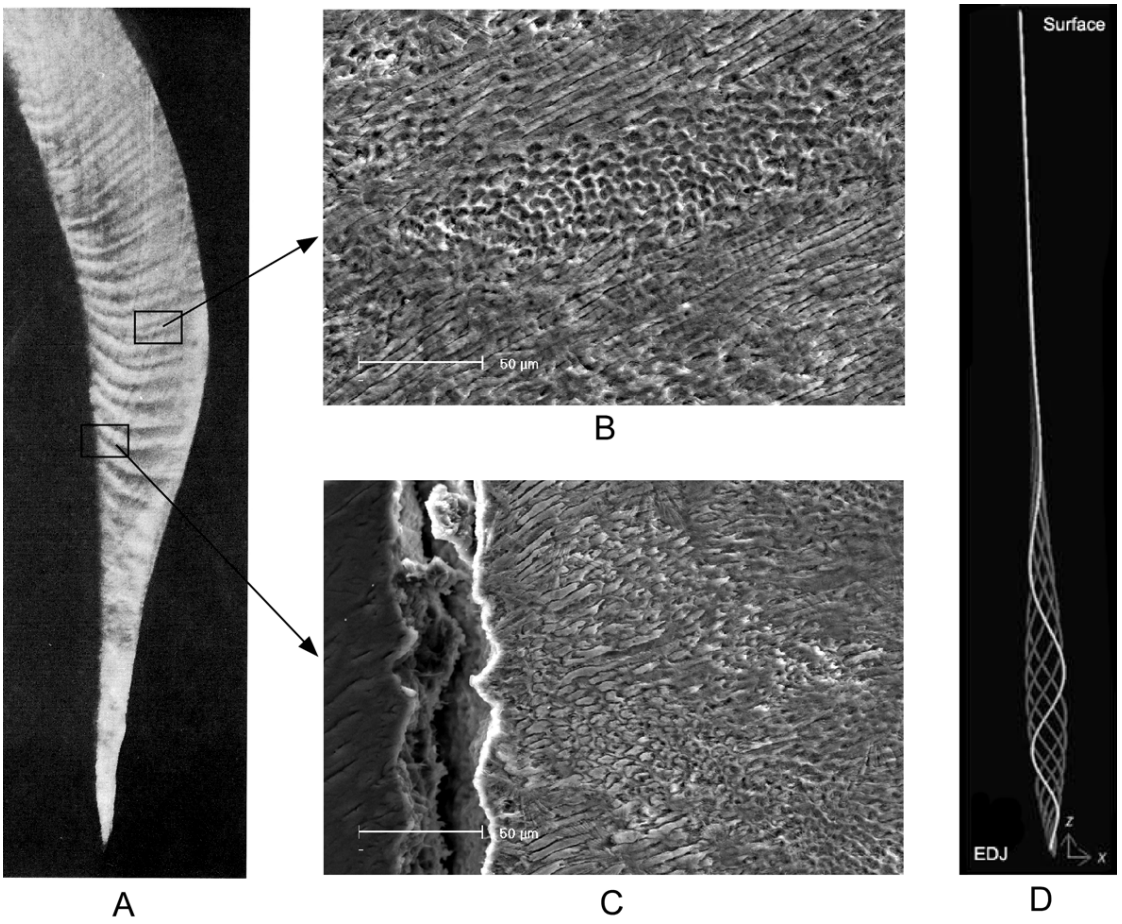

Fig. 2-8 (A) Longitudinal section of enamel viewed by incident light. The series of alternation light and dark Hunter-Schreger bands are apparent[19]; (B) and (C) are SEM images of different areas showing details of the Hunter and Schreger bands; (D) schematic illustration of the wavy direction of one rod unit from enamel surface to enamel dentin junction (EDJ)[28], which may be helpful to understand the Hunter and Schreger band.

The Hunter-Schreger bands are an optical phenomenon produced by changes in direction between adjacent groups of rods. The bands are seen most clearly in longitudinal ground sections viewed by reflected light and are found in the inner two thirds of the enamel. SEM clearly reveals the difference in orientation of groups of rods within these zones (Fig. 2-8). Recently, a 3D study of enamel microstructure also revealed several patterns of rod twisting and suggested this may be an adaptation to functional demands (e.g., a crack stopping mechanism in large-bodied, thick-enameled species, such as the orangutan, which are capable of large bite forces)[28]. From the point of view of developmental

histology, the origin of the Hunter-Schreger bands may be traced to the vector of movement of the ameloblast, as cells move outwards away from the EDJ, may also influence the orientation of its protein matrix and the orientation of the resultant crystallites and rod units[34,35].

2.2.2.4 Porosity and permeability of enamel

Using polarising light microscopy, enamel was shown to be a molecular sieve[32,36]. Pore sizes within enamel vary from 0.15 nm to more than 6 nm from different reports. Firstly, methanol, which has a mean molecular radius of 0.15 nm, seems to enter all pores in enamel, whereas ethanol (r=0.17 nm) is excluded to some extent. Secondly, Krypton only penetrates into large pores due to the large size of this molecule[37]. Calculations suggested that the krypton-accessible pores correspond to the rod/interrod junctions[38] and these pores have a laminar form with the mean width of 6 nm[37]. Thirdly, nitrogen and water gave rise to a greater fraction of enamel pores[39]. Pore–size distribution from water-sorption data indicate peaks at about 2-3 and 4-6 nm radius[40-42]. In conjunction with ultrastructural data, these sorbates enter some intercrystalline pores.

As described in the above sections, enamel is a biocomposite with both crystals and matrix proteins. The matrix may influence the properties of enamel pores in several ways[43], namely: (1) effective pore sizes may be reduced; (2) protein hydration may reduce water mobility within the pores; (3) diffusion of charged solutes may be altered by interactions with the negative charge of the protein; and (4) the lipid component may influence diffusion of solutes according to their hydrophobicity.

Because of its porous nature, enamel is permeable to water[44,45], ions[46], inorganic solutes[47,48], small organic solutes[44] and dyes[49-51]. Ultrastructural observations show that the rod/interrod junctions provide the main pathways[49,51], although in inner enamel some transport was observed within the rod unit[45]. Because of the gradient in density and porosity, permeability of enamel increases from the outer surface towards the EDJ[45]. The matrix may also influence the permeability of enamel. Evidence has shown that proteins restrict ionic diffusion[46]. By considering the positive pressure of the pulp (15-30 cm water)[52], the penetration of other chemical components will be more difficult in vivo.

In general, enamel is permeable to a variety of chemicals and may be classified as an imperfect semi-permeable membrane in which water is transported through the tissue under the influence of an osmotic gradient and solute moves in the opposite direction[44,53].

2.3 Composition of mature enamel

Enamel is a highly mineralised crystalline structure. It contains on average 95% inorganic substance, 4% water and 1% organic substance by weight or 87% inorganic, 11% water and 2% organic component by volume[54]. Crystalline calcium phosphate (hydroxyapatite) substituted with carbonate (CO_3^{2-}) and hydrogen phosphate (HPO_4^{2-}) ions are the largest mineral constituent, 90-92% by volume. Various ions such as strontium, magnesium, lead, and fluoride, if present during enamel formation, may be incorporated into the crystals. Young enamel has a higher magnesium and carbonate content than for mature enamel[55]. The remaining constituent is organic matter and water.

2.3.1 Inorganic component of enamel

As shown by Yanagisawa with high-resolution TEM[56], a cross-cut view of the hydroxyapatite c-axis shows an elongated hexagonal configuration with a central dark line. Three sets of lattice striations with 8.17 Å intervals intersect at 60° angles, indicating that hydroxyapatite is an accumulated rhombic unit cell composed of $Ca_5(PO_4)_3(OH)$. Numerous white spots are frequently observed near the central dark line. Detailed observations reveal many such abnormalities as being edge dislocations, screw dislocations, small angle boundaries, atomic vacancies and atom rotations near the white spots. These abnormalities indicate missing atoms and/or atomic groups or distortion of the atomic arrangement.

The inorganic substances have been reported to vary from the outer enamel surface to EDJ. The mineral content[57,58] and the density[57,59] were reported to decrease towards the EDJ, the volume not occupied by mineral being 50-100% greater in inner than in outer enamel. Both enamel protein[57] and water[40,41] are more abundant in inner enamel close to the DEJ. The mineral content of outer enamel falls off from the cusps towards the cervical region[60,61]. There may also be localised subsurface regions of low density enamel, often near the cusps[60,61].

The overall solubility of enamel in the oral environment decreases with distance from the enamel surface to the EDJ. Fluoride concentration has been found to be higher near the enamel surface (< 100 μm) and decreases dramatically towards the EDJ[62]. Fluoride ions replace the PO_4^{-3}, Cl^{-1}, CO_3^{-2} in the lattice and form fluorapatite which has a hexagonal

space group, $P6_3/m$, with lattice parameters a = 9.367 and c = 6.884 Å [63]. In contrast, pure hydroxyapatite is only pseudohexagonal with a doubled b-axis (a = 9.4214 Å, b = 2a, c = 6.8814 Å, γ = 120°) and monoclinic space group $P2_1/b$ [64]. Of course, two apatite crystals have different chemical and physical properties and this influences the hardness, chemical reactivity, and stability of enamel[65]. Reports[66,67] have declared that fluorapatite has better resistance to acid dissolution, which is the major reason for the widespread use of fluoride in preventive dentistry.

Water in permanent enamel is in the form of free and bound water[68,69]. Free water refers to those components located in small spaces of enamel, while bound water means those combined with peptide chains or crystal lattices. Water released from enamel by heating to 100-200℃ is considered to include the free water, together with "loosely bound" water. Permanent enamel dried in this way after prior equilibration at 100% RH at 37℃ loses about 2% w/w (*c.* 6% v/v) water[70,71] and the same fraction is exchangeable with ^3H_2O[69]. Studies with hydroxyapatite suggest that some of the water in enamel will be more firmly bound to the mineral[72,73]. However, due to technical difficulties, the amount of firmly bound water has not been quantified exactly. Clearly, because of structural heterogeneities, the relative proportions of free, loosely and firmly bound water will vary considerably.

Although it is only a minor part of enamel, water plays an important role in enamel's function, because dehydration changes the mechanical properties of enamel significantly[74]. This may be explained as: (1) water forms hydrogen-bond bridges across adjacent peptide chains and maintains functional conformation of protein remnants and collagen fibres in mature enamel[75]; (2) water fluid is essential in explaining load-bearing behaviour of enamel as for instance the "stiff sponge" model proposed by Fox[76], in which enamel was considered as a stiff sponge from which liquid was expelled in compression and drawn in again when the load is released.

2.3.2 Organic component of enamel

As mentioned in the above sections, although enamel begins as a protein matrix, it becomes a mineralized tissue that is approximately 85% mineral by volume and 96% by weight. The protein content of enamel changes dramatically during normal development

ranging from about 20% protein by weight during the secretory stage to 7% at the beginning of the maturation stages. Ultimately, the ameloblasts remove almost the entire original matrix as mineralization progresses. As a result, fully developed normal human enamel contains only ~1% protein by weight, which is the remnant component of the development matrix proteins.

What is the detailed composition of proteins in mature human enamel? Unfortunately, due to the difficulties in sample preparation and application of protein analysis techniques on such a highly mineralized tissue, there are only limited reports on this topic till now. Usually, the conformation and tertiary structure of these proteins were destroyed during protein extraction and purification. Therefore, only limited compositional reports are found and summarised here.

Several studies have reported amino acid compositions for the human enamel matrix[77-81]. The main amino acids described were alanine, glutamic acid, glycine, proline, and serine. However, these results were not directly comparable since different preparative techniques were used with varying sample purity and protein heterogeneity being additional complicating factors. A typical amino acid composition of human enamel protein is listed in Table 2-1 and Fig. 2-9. Recently, type I collagen was also detected in mature enamel samples[82]. In short, the organic matrix in mature enamel is a multi-component protein/peptide mix, which is lying between crystallites clearly and has the function of gluing hydroxyapatite crystallites together thereby maintaining the hierarchical structure of enamel. However, the exact composition and conformation of these proteins and their biological functions are still unresolved.

Table 2-1. Amino acid composition of human adult enamel protein[80]

Amino Acid	%
Asp	6.9
Thr	4.1
Ser	11.3
Glu	13.5
Pro	11.2
Gly	25.2
Ala	5.8
Cys*	1.8
Val	2.9
Met	0.9
Ile	1.1
Leu	3.0
Tyr	1.0
Phe	2.2
Lys	1.9
His	2.3
Arg	3.0
Hyp	1.9

*Measured as cysteic acid after performic oxidation

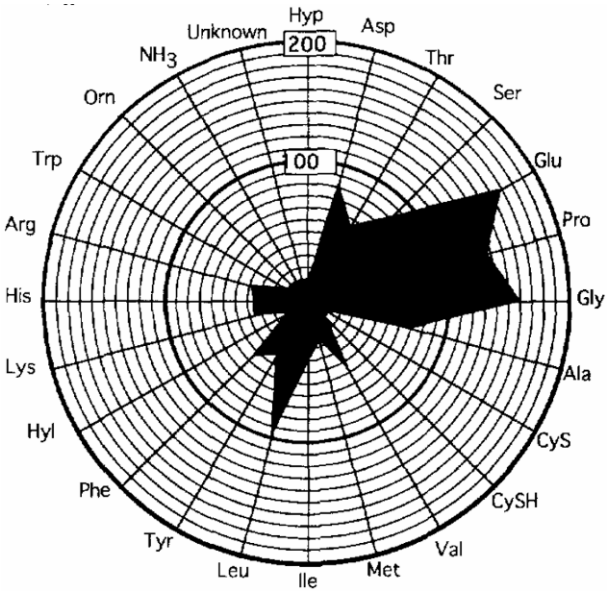

Fig. 2-9 Rose diagram illustrating amino acid composition of normal permanent human enamel[83]

2.3.3 Vibrational spectroscopy analyses

In the last decade or so, vibrational spectroscopy, both infrared (IR) and Raman, has been employed by an increasing number of researchers in the study of dental hard tissues and relative materials. Vibrational spectroscopy has the considerable advantage of being sensitive to both the mineral and organic components of mineralized tissues, thus allowing the study of mineral-matrix interactions as well as each individual component's properties. Sample preparation is relatively simple for both types of spectroscopy and once the specimen is excised and sectioned, no further preparation is necessary (though the sections must be thin for IR absorbance measurements). This nondestructive approach allows for spatial distribution mapping of mineralized tissues' components as well as compositional analysis. Furthermore, traditionally prepared light microscopy specimens may also be examined using either Raman or IR spectroscopy, allowing for correlative studies. These spectroscopic techniques thus help to provide a complete picture of the composition unattainable by other commonly used methods such as X-ray diffraction or nuclear magnetic resonance (NMR). Most importantly, IR and Raman spectroscopies enable studies at micron-scale spatial resolution. The diffraction-limited spatial resolution achievable when using IR spectroscopy is 10–20 μm, while the shorter wavelengths examined using the visible excitation of Raman spectroscopy yield a diffraction-limited spatial resolution of 1 μm or less. These fine spatial resolutions allow the observation of phenomena occurring at the microscopic level; these phenomena can then be used to help explain the macroscopic observations made using more traditional techniques. Finally, both IR and Raman spectroscopy are useful in the study of abnormal or diseased mineralized tissues, providing clues to the causes and effects of the diseases.

Raman and infra-red spectroscopy has been used frequently to study teeth. Dental enamel has a similar composition as other mineralized tissues but with more crystalline and more highly oriented mineral. Typical IR and Raman spectrum of sound enamel are shown in Figs. 2-10 and 2-11 and the relative band assignments and position are summarized in Table 2-2.

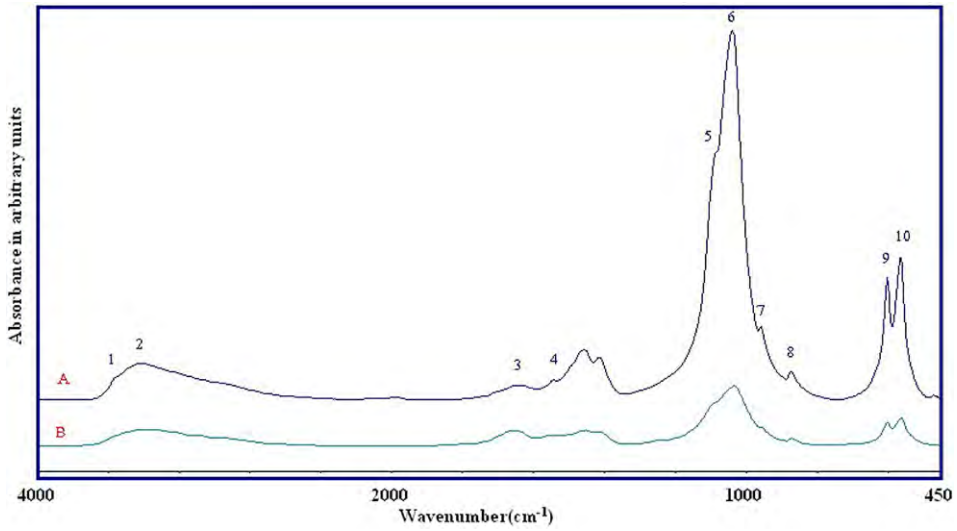

Fig. 2-10 Typical FT-IR spectrum of sound enamel (A) and dentin (B)[84].

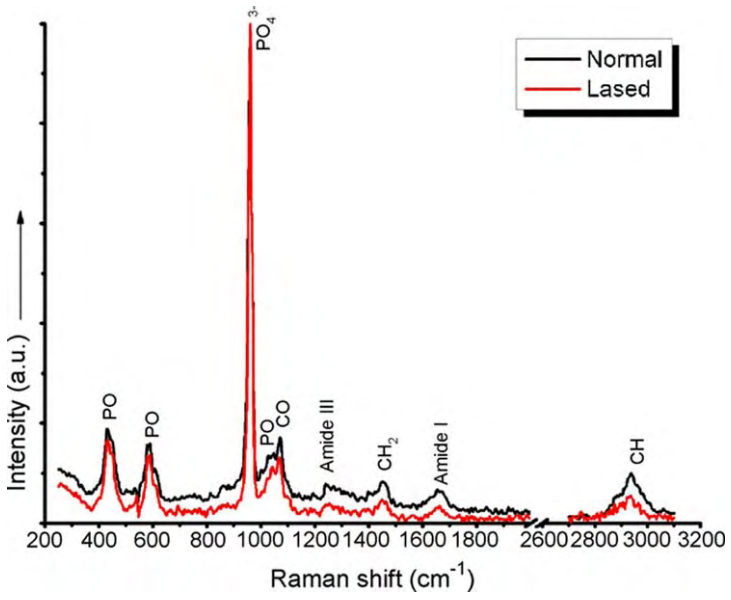

Fig. 2-11 Raman spectra of natural incisor surface (upper curve) and lased incisor surface (lower curve)[85].

Table 2-2 Raman and infrared spectroscopic band assignments for mineralized tissue[84-88]

Assignment	Wave number range (cm^{-1})	Observed in
PO_4^{3-} $v2$	422-454	Raman
PO_4^{3-} $v4$	578-617	Raman/IR
C-C stretching	815-921	Raman
CO_3^{2-} $v2$	850-890	IR
PO_4^{3-} $v1$	957-962	Raman/IR
HPO_4^{2-} $v3$	1003-1005	Raman/IR
PO_4^{3-} $v3$	1026-1071	Raman/IR
CO_3^{2-} $v1$	1065-1103	Raman/IR
Amide III	1243-1269	Raman/IR
CH_2 wag	1447-1452	Raman/IR
Amide II	1540-1580	IR
CO_3^{2-} $v3$	1544	IR
H_2O	1642	IR
Amide I	1595-1720	Raman/IR
C-H (CH_2) stretching	2840-2986	Raman
H_2O	2900-3550	IR
O-H and N-H stretching	3369	IR
OH stretch	3567-3575	Raman

Polarized Raman studies[89,90] on enamel crystallites illustrated the distinct polarization dependence of apatite crystallites in Raman spectra, which indicate that crystallites in enamel are well arranged in certain directions. Moreover, based on their polarized Raman results, Leroy et al.[90] proposed a new structure of apatite crystal of enamel, which is a box of Ca^{2+} ions which surrounds and isolates the PO_4^{3-} ions from one another, decreasing the influence of substitutions. Micro-Raman spectroscopy was also used for an investigation of the EDJ area based on the PO_4^{3-} band and C-H (CH_2) stretching mode, in which evidence of the existence of organic components in enamel was clearly illustrated with a long acquisition time (see Fig. 2-12). The evidence of organic components in enamel came from another investigation on laser treated enamel samples[85], in which the organic matrix in enamel was believed to be thermally decomposed by laser treatment. Also, another investigation on deproteinated enamel showed distinctive decreasing of Raman bands intensity at 1100-1700 cm^{-1} and around 2900 cm^{-1} spectra region which are all due to organic materials[91].

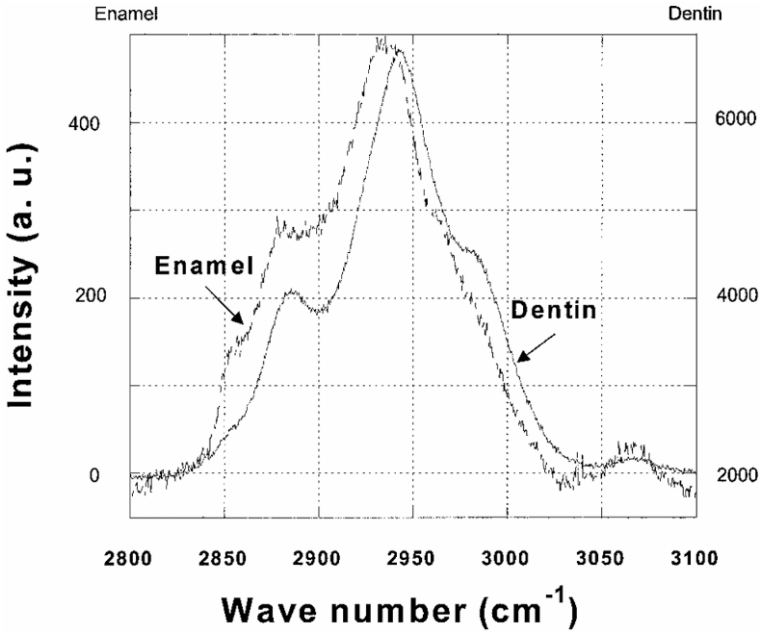

Fig. 2-12 C-H stretching mode for enamel shows a pronounced shift to 2934 cm^{-1} compared to the C-H stretching mode at 2937 cm^{-1} for dentin. Acquisition time for enamel was 72 h and for dentin 600 s[92].

Moreover, Raman spectroscopy has enabled the measurement of stress in mineralized tissues by observing the PO_4^{3-} $\nu 1$ band shift[93,94]. The relationship between the peak position of Raman vibrational modes of interest and applied stress can be investigated and calibrated by using standard samples with a loading apparatus. By assuming the axes of principal stress correspond to the main crystallographic directions of the crystal, the relationship can be expressed as: $\Delta\nu = \Pi_{ij}\sigma_{ij}$, where $\Delta\nu$ is the spectral shift of the selected Raman band, σ_{ij} and Π_{ij} are the stress and the piezo-spectroscopic coefficient, respectively[93]. Pezzotti reported the Π value of ν_1 phosphate band of a standard hydroxyapatite (HAP) sample under uniaxial stress, as 2.45 - 2.95 cm^{-1}/GPa[93,94]. This technique has been used in the research of deformation[95] and fatigue[96] mechanisms of bone.

In addition apatite minerals, water and proteins are also good infrared absorbers. IR spectroscopy has some advantages in observing water in enamel. As mentioned in the above sections, water is an important component of enamel. Between 4000 and 400 cm^{-1} of enamel IR spectrum, four absorption bands associated to the water molecule are observed[97], while another report indicated a broad band at 3500-2900 cm^{-1} and another less intense band near 1642 cm^{-1} [88]. This will be very helpful in exploring the location and

function of water in enamel. Moreover, infrared is a high sensitive technique for the detection of organic matrix in enamel. FT-IR photoacoustic phase analysis indicated a dramatic increase in the protein content relative to the phosphate content with increased depth from the enamel surface to a depth of about 200 μm[98]. Another IR investigation on the bleaching treatment on enamel illustrated the frequency of the Amide A and Amide I bands were significantly changed for enamel tissue after the treatment of high concentrations of bleaching agent[84]. P. Fattibene et al.[91] also reported the decrement of IR band intensity above 1500 cm^{-1} after enamel deproteination.

In short, vibrational spectroscopy is a powerful tool for dental researchers. It has significant advantages for compositional analysis of dental tissue[92], in situ nano-mechanical observation[93], evaluation of dental treatments such as laser[85] and bleaching[84], and detection of early caries lesions[99].

2.4 Research on enamel mechanical behaviour

As the outer cover of teeth, enamel must retain its shape as well as resist fracture and wear during load-bearing function for the life of the individual. Teeth experience a range of loading situations; firstly, they contact directly other objects and/or opposing teeth; secondly, they encounter normal and sliding contact resulting in wear, and thirdly, unlike bone, damage of teeth is not reparable. Some typical physiological conditions of oral/teeth have been listed in Table 2-3 by Waters[100]. Recently, investigations indicated that masticatory forces range from 28 N to more than 1200 N[101,102]. At the same time, the contact area can be as small as a few square millimetres. It is amazing that enamel can sustain and survive such high forces for millions of cycles.

Table 2-3 Conditions under which teeth operate[100]

Rate of chewing	60-80 cycles/min
Forces: maximum biting force overall teeth	640 N
maximum biting force on a single tooth	265 N
normal forces on a single tooth	3-18 N
Contact time: time maximum pressure sustained	0.07 S
Total contact time: normal	10 min
Bruxist (over 24 h)	30 min - 3 h
Mean sliding distance	1.0 mm
Contact area (1^{st} molar region)	15 mm^2
Maximum stress	20 MPa

To illustrate the excellent performance of enamel, people commenced mechanical tests on this optimised natural material. Moreover, knowledge of the mechanical properties and microstructural features of dental enamel is important to understanding stress dissipation in the tooth, for developing biomimetic restorative materials and for the execution of clinical dental preparations. Hierarchical microstructures endow enamel unique anisotropic mechanical properties, which ensure its life-time survival in the mouth as a load bearing organ. Although numerous tests have been conducted to explore the

mechanical properties of enamel from different aspects since the 19th century, this is still an area of intense research in the biomaterial field because from the basis of this fantastic natural biocomposite are still poorly understood.

2.4.1 Brief introduction to basic mechanical property definitions

2.4.1.1 Stress/strain

The stress-strain relationship is the basic parameter to describe and evaluate a material. The quantitative treatments of deformation usually employ the concept of *stress*, which is the pressure at any point in a body submitted to a load and expressed as:

$$\sigma = \frac{F}{A}, \quad (2\text{-}1)$$

where F is the force on the supporting area A. Because force, F, has direction, the stress, σ, should be defined by not only in terms of its magnitude but also direction. From this point of view, stress can be divided into three types: tensile stress, compressive stress and shear stress. Material will experience deformation under the application of stress. *Strain* quantifies the deformation response of a body to stress and is defined as the ratio between the total deformation in one direction of a specimen and the length of the specimen in the same direction. Setting original length and increment of length as L and ΔL, separately, the strain, ε, can be expressed as:

$$\varepsilon = \frac{\Delta L}{L}. \quad (2\text{-}2)$$

This equation doesn't consider the change of reference axes and is known as the nominal or engineering strain. More correctly, the true strain should be used,

$$\varepsilon = \int_{L_0}^{L_1} \frac{dL}{L} = \ln \frac{\Delta L}{L}. \quad (2\text{-}3)$$

This equation takes into account the change in the reference length L from its initial value L_0 to its value L_1 at each step of deformation.

When a given force (described by stress, σ) is applied to a material, the associated deformation can be specified by the resulting strain, ε. Therefore, the stress-strain curve has long been considered as one of the most important parameters to evaluate a material.

With the resultant curve, the deformation, which is strain, for any stress value can be predicted.

2.4.1.2 Elastic modulus

From Hooke's law, we know that, within the elastic range, the strain has a linear relationship with stress. And the term *Hookean behavior* is used to describe the usual case in which a given strain component varies linearly with stress in components[103]. From this point of view, *elastic modulus* is known as the ratio of stress to strain below the proportional limit. It represents the magnitude of the interatomic stiffness of a material within the elastic range when tensile or compressive forces are applied. It is also an indication of the amount of reversible deformation that will occur in a structure when a load is applied. From the definition of stress and strain, elastic modulus can be derived as follows:

$$E = \frac{\sigma}{\varepsilon} = \frac{F/A}{\Delta L/L} = \frac{FL}{\Delta LA}. \quad (2\text{-}4)$$

Elastic modulus is a basic parameter to describe the material. Not only researchers, but also clinicians are interested in this value, because it may assist with the selection of restorative biomaterials with similar deformable properties to those of the material it is replacing.

For force bearing structures, a high elastic modulus is often required to limit the deflection on loading and still return to its original shape after being stressed. It has been reported that increasing the elastic modulus of a supporting core structure of a dental restorative material might be a way of improving the fracture resistance of all-ceramic dental crown/bridge structures[104].

2.4.1.3 Hardness

Hardness may be the most widely used parameter for evaluating and comparing materials. The *hardness* of a material usually is considered as a measure of the resistance to permanent indentation[105]. The principle purpose of the hardness test is to determine the suitability of a material, or the particular treatment to which the material has been

subjected. The ease with which the hardness test can be made has made it the most common method of inspection for most materials.

The general procedure for hardness assessment can be summarised as: a standardised force or weight is applied to an indenter pressing into the surface of a material to create a symmetrical shaped indentation (residual impression). The dimensions of the indentation (area, depth or width) are measured at a microscopic level, and entered in a specific hardness formula according to the type of tests. Therefore, the hardness value is different for different test methods. The most commonly used hardness test methods include: Brinell hardness test, Knoop hardness test, Vickers hardness test and nano-indentation hardness test.

2.4.1.4 Fracture strength

Strength can be defined as the maximum tensile stresses that a material can endure before fracture occurs. It might also be defined as force per unit area required to initiate and propagate a crack to the fracture point. Strength is an important mechanical property to evaluate the performance of brittle materials like bioceramics. The inability of ceramics to reduce the tensile stresses at the tip of the cracks by deformation in an inelastic manner explains why they are much weaker in tension rather than in compression and also why bioceramics normally fail in areas of tensile stresses. Therefore, tensile strength is considered more significant that compressive strength in the brittle material field.

2.4.1.5 Fracture toughness

Since crack propagation and subsequent fracture is known to be the major problem that leads to ultimate structural failure, it is important to know the threshold condition of crack propagation. Therefore, fracture mechanics concepts have been applied to characterise the criteria of crack propagation of brittle materials such as bioceramics. The strength of a brittle material, σ_a, is related to the critical stress intensity factor, K_c, at a crack tip which can be calculated with the following equation:

$$K = Y\sigma_a\sqrt{c}\,, \quad (2\text{-}5)$$

in which c is the radius of a crack, and Y is a geometrical factor. Irwin[106] analysed the crack propagation procedure from a critical stress point of view and concluded the criteria

of crack propagation, which is stress field intensity, K, of crack tip should exceed a certain value K_c. K_c is the critical stress intensity level at which a given flaw starts growing.

In a mode I (uniaxial tension) crack model, this threshold value is also named as the fracture toughness, K_{Ic}, which indicates the ability of a material to resist crack propagation and its consequent catastrophic failure. The definition of fracture toughness in ASTM E-24 is: the resistance to crack propagation under plain strain conditions, which means strain value about the crack tip should be kept constant while the crack begins propagating.

Fracture toughness is one of the most important mechanical properties that delineates the fracture behaviour of a specific material. It has gained wide acceptance as a technique suitable for the assessment of ceramic materials ability to resist crack propagation. In the biomaterials field, fracture toughness values may help us to evaluate the serviceability, long-term clinical success and performance of brittle materials. It has been proven that materials with high fracture toughness demonstrate improved clinical performance and reliability than low fracture toughness ones[107].

2.4.2 Elastic modulus and hardness of enamel

The mechanical tests to determine elastic modulus and hardness of enamel have experienced several stages from macro scale to micro and nano scale over the last several decades. The major contributions are summarized in Table 2-4. Due to the size limit of human enamel samples, it has been difficult to perform macro scale tests. Therefore, only limited reports with big variation of the results can be found. In contrast, a number of reports on bovine enamel could be found because of the bigger sample size. With the development of indentation technique and relative facilities, micro-indentation and nano-indentation were widely employed in the investigation of mechanical properties of human enamel, as shown in Table 2-4. Also, the variation of the results reduced considerably due to the precise control of the test area.

By comparing data from table 2-4, several trends can be summarized as follows:

1. Macro scale tests gave lower elastic modulus than micro and nano scale test;

2. Cross section has lower elastic modulus and hardness than top surface;
3. The higher the load applied, the lower the elastic modulus measured.

The elastic modulus of enamel varies in a wide range, from more than 100 GPa to less than 50 GPa,. What is the key factor to regulate the elastic modulus of enamel under different conditions? What is the contribution of enamel hierarchical structure to its elastic modulus and hardness? These are interesting topics for further research.

Table 2-4 Elastic modulus and hardness of sound enamel from different measurements

	Author(s)	Surface and site	Test method	Test load ()	Hardness (GPa)	Elastic modulus (GPa)
Macro-scale tests	Stanford et al.[108]	Variable (cusp) Cross section (side) Top surface (occlusal)	compressive	\	\	47.5 30.3 8.96
	Stanford et al.[109]	Canine: Variable (cusp) Cross section (side) Variable (cusp) Molar: Variable (cusp) Cross section (side) Top surface (side)	compressive	\	\	 47.5±5.5 33±2.1 20±6.2 46.2±4.8 32.4±4.1 9.65±3.45
	Craig et al. [110]	Top surface Cross section	compressive	\	\	84.1±6.2 77.9±54.8
	Tyldesley[111]	\	4 point bending	\	\	131±16
	Reich et al.[112]	Top surface	Acoustic impedance	\	\	76.5
	Staines et al.[113]	Top surface	Spherical indentation	Up to 800 N	\	83±8
Micro- and Nano- scale tests	Xu et al.[114]	Top surface Cross section	Standard Vickers indentation	2-50 N	3.23±0.38 3.03±0.09	\
		Top surface Cross section	Modified Vickers indentation	1.9 N	3.62±0.2 3.37±0.15	94±5 80±4
	Willems et al[115]	Top surface	nanoindentation	10 mN	3.39±0.18	90.59±16.13
	Cuy et al[116]	Cross section: Outer enamel EDJ	nanoindentation	Depth control (400 & 800 nm)	2.7-6.4 >6 <3	47-120 >115 <70

Micro- and Nano- scale tests	Zhou et al[117]	Top surface	nanoindentation	Depth control (100-2000 nm)	5.7-3.6	104-70
	Ge et al[118]	Top surface: rod Interrod	nanoindentation	1 mN 0.3 mN	4.3±0.8 1.1±0.3	83.4±7.1 39.5±4.1
	Mahoney et al[119]	Cross section (primary molar)	nanoindentation	50 & 150 mN	4.9±0.4	80.4±7.7
	Marshall et al[120]	Cross section (EDJ area)	AFM indentation	Up to 14 mN	3.51±0.13	63.55±1.46
	Poolthong[121]	Cross section: Buccal side Cusp tip	nanoindentation	50 & 150 mN	4.74±0.2 4.45±0.3	90.79±2.2 83.83±6.3
	Fong et al[122]	Top surface Cross section	nanoindentation	0.3-2.5 mN	4.78±0.36 4.53±0.26	98.3±5.9 95.6±4.9
	Habelitz et al.[123]	Top surface Cross section Head of rod Tail of rod interrod	nanoindentation	1.5 mN	3.8±0.31 3.3±0.35 4.3±0.4 3.7±0.4 3.9±0.4	87.5±2.1 72.7±4.4 88.0±8.6 80.3±7.2 86.4±11.7
	Habelitz et al.[124]	Cross section	nanoindentation	0.75 & 1.5 mN	3.2±0.4 – 3.7±0.5	74±4 - 80±9.1
	Barbour et al.[125]	Top surface	nanoindentation	3 mN 5 mN 7 mN	4.81±0.15 4.77±0.13 4.75±0.12	99.6±1.8 101.9±1.6 105.2±1.3

2.4.3 Fracture toughness of enamel

Understanding fracture properties and crack propagation procedure of enamel is important for both clinicians and material scientists. It has been long hypothesized that anti-fracture ability of enamel is controlled by the anisotropic microstructure, such as rod orientation, and organic components. Many reports on this topic may be found in the literature and textbooks. Due to the size limit of human enamel sample, most investigations have been based on the indentation technique. This is an indirect method for the measurement of fracture toughness. Several equations and methods have been developed for indentation fracture toughness calculation of brittle materials such as glass. Investigation of dental materials and enamel have generated results from the indentation method were different and depended on the equation chosen[126].

Fracture toughness values of enamel from different reports have been summarised in Table 2-5.

Table 2-5 Fracture toughness of sound enamel from different measurements

Author(s)	Method	Test direction	Test load (N)	Fracture toughness ($MPa \cdot m^{-1/2}$)
Hassan at al.[127]	Vickers microindentation	Top surface	2.94 & 4.9	0.7-1.27
Xu et al. [114]		Top surface Cross section 45° tilted rod	2 - 10	0.77±0.05 0.52±0.06 1.30±0.18
White et al.[128]		Top surface Cross section	4.9	1.3±0.3 0.9±0.22

Hassan at al.[127] also reported that a pattern of increasing fracture toughness values existed from incisal to cervical incisor enamel; the molar enamel was more brittle than either the canine or incisor enamel; it was also observed that the cracks emanating from the corners of an indentation propagated along preferential directions, with the weakest path of fracture usually extending along the cervical-incisal axis.

Another approach using a bending test for the measurement of fracture properties of enamel[129] illustrated that fracture in enamel is anisotropic with respect to the orientation

of the enamel rods, with the work of fracture (W_f) for fracture parallel to the rods being 13 J/m^2 but of the order of 200 J/m^2 for fracture perpendicular to the rods; fractographs of enamel showed that the enamel rods behaved as integral units during controlled fracture.

In their microindentation testing, Xu et al.[114] illustrated that the cracks in the enamel axial section were significantly longer in the direction perpendicular to the occlusal surface than parallel. The cracks propagating toward the EDJ were always arrested and unable to penetrate dentin. The fracture toughness of enamel was not single-valued but varied by a factor of three as a function of enamel rod orientation.

By comparison with dense hydroxyapatite material, White et al.[128] found that enamel was approximately three times tougher than geologic HAP, which only has a K_{Ic} value of ~0.45 MPa·m$^{1/2}$ [130], demonstrating the critical importance of biological manufacturing. Moreover, their measurements suggested that enamel is a composite ceramic with the crystallites oriented in a complex three-dimensional continuum.

In short, all these studies show some common treads:

- Hierarchical microstructure resulted in enamel having anisotropic fracture behaviour. Top surface (occlusal surface), which is the functional surface of enamel in oral condition, has higher fracture toughness than manually cut cross section surface;
- The rod-interrod junction may be the weakest pathway for crack propagation;
- Organic matrix in enamel improves the anti-crack ability of natural biocomposites significantly.

2.4.4 Inelastic properties of enamel

Although enamel has long been regarded as a hard and brittle material, recently, evidence of the inelastic behaviour of the natural biocomposite has begun to mount. As described above, enamel is a two phase biocomposite with well arranged hierarchical structure. The remnant protein remnants within the structure may endow enamel with some in-elastic properties.

Recently, with the understanding of “sacrificial bonds” between the individual subdomains in a protein molecule[131], more people are believing that this can be a possible

mechanism for explaining the mechanical behaviour of organic matrix of biomineralized tissues. As the protein molecule is stretched, these sacrificial bonds break first to protect its backbone and dissipate extra energy; after unloading, these bonds recover automatically and pull deformed material back to its original shape[132].

Creep, which is defined as the time dependent deformation under constant loading, is one of major inelastic response of viscous materials. For metallic and polymeric materials, traditional tensile and/or compressive tests are used to investigate the creep response of a specimen. For natural materials such as enamel, two main problems limit the usage of these methods. Firstly, these tests need multiple identical specimens, which are hard to prepare upon considering the direction of hierarchical structures of each sample. Secondly, the sample size is too small and with limited creep restricts the accuracy of these methods. Due to the difficulties of macro creep tests on small samples, indentation creep tests were introduced into the nanoindentation field by Lucas and Oliver as a powerful technique for studying the rheological properties and relaxation dynamics of different materials[133].

Recently, Zhou and Hsiung[134] undertook rate-dependent deformation tests on enamel and found that enamel demonstrated better resistance to penetration deformation and greater elastic modulus values were measured at higher strain rates. The origin of this rate-dependent deformation was rationalized to be the shear deformation of nanoscale protein matrix surrounding each hydroxyapatite crystal rod and the shear modulus of protein matrix depended on strain rate given by the relationship $G_p=0.213+0.021 \ln\dot{\varepsilon}$. This report indicates that the minor organic matrix does regulate the mechanical behaviour of enamel significantly. But, this is just the start of research on mechanical roles of the organic matrix. There is a long way to go before we understand the functions of organic matrix in biocomposites thoroughly.

2.5 How does enamel structure fit its functional needs?

Almost all mammals have enamel-covered teeth. The microstructural architecture of enamel varies from species to species and appears to have evolved to cope with the specific requirements associated with the source of food[135]. Of particular importance is the ability of enamel to survive sustained localized contact over millions of chewing and non-specific loading cycles. It is also known from comparative observations of primates that the structure of enamel was influenced by different food type and evolved to meet these functional needs[136,137]. In a word, enamel structure is the result of long-term evolution and functional adaptation.

2.5.1 Mechanical advantages of human enamel microstructures

2.5.1.1 Apatite crystallites

Based on Griffith theory of brittle fracture[138], the smaller the individual sample, the higher the strength is, because smaller samples contain less and smaller defects. From this fracture mechanical point of view, nano-scale hydroxyapatite crystallites will have higher strength than bulk materials. This will definitely increase the strength of the enamel as a composite structure. Based on this assumption, Gao et al.[139] developed a theoretical relationship as to the critical thickness of mineral crystallites of biocomposites. The result showed the crystallites with the thickness of around 30 nm can reach its theoretical strength. This is very coincident with TEM observations on enamel HAP crystallites. The study also indicated that the structure of biocomposites may be the result of stress optimization.

The organization of hydroxyapatite crystallites to form enamel reflects a balance between its two main, but very different, mechanical functions, wear resistance and fracture resistance. The dominant rods are primarily oriented so as to approach the outer tooth surface in an approximately perpendicular orientation. This is in order to increase hardness and reduce wear. Interconnections between rod and interrod, and complex cleavage planes limit critical crack size and uncontrolled crack propagation that would otherwise lead to premature fracture[55]. The amount of anisotropy may not only reflect the balance between wear and fracture resistance, but may also reflect a balance between

differing vectors of functional stress as well as the transfer of occlusal loads to the resilient supporting dentin[140]. Hence, differences in structural organization might be found within different parts of a tooth[141].

Connections between adjacent rods via the interrod region and the presence of interrod crystallites oriented in a plane different from the main rod direction have been discerned in cross-sectional and long-sectional scanning electron micrographs[34,142,143]. The variation of crystal directions is the result of bio-fabrication process during the maturation of enamel, which is essential in shielding the cracks. From a fracture mechanical point of view, the crystal directions and thin protein films between crystals are the two major contributors to the high fracture toughness of natural biocomposites.

2.5.1.2 Rod unit

Although most of the enamel organic matrix is removed during mineralization and maturation, some protein, notably ameloblastin, is retained, primarily at the incisal edges and proximal sides of rod boundaries defining a rod sheath[143]. Ameloblastin remnants help to define the rounded discontinuity seen around the top of the 'fish scale' on rods viewed in occlusal section, as well as the linear demarcations between rods viewed in the cross section. These discontinuities have two very important mechanical functions. First, they define three-dimensional cleavage planes that will deflect cracks[55,142]. This prevents cracks from advancing straight through enamel to cause catastrophic macro-mechanical failure, but instead spreads the damage laterally and hence energy absorbed over a larger volume. Second, the presence of minute quantities of protein remnants could allow limited differential movement between adjacent rods. Limited slippage could reduce stresses without crack growth. The minor components of enamel, protein remnants and water, have a profound plasticizing effect. Enamel is known to be much more flexible and softer than its major component, crystalline hydroxyapatite[110,141,142]. In addition to ameloblastin, the amino-terminal remnants of amelogenin, the so-called tyrosine rich amelogenin peptide (TRAP) and portions of the enamelins are also retained in mature enamel and are candidate peptides that may contribute to altering the physical properties of the crystallites.

Well arranged rod units are believed to contribute to the high fracture toughness of the

biocomposites. Several schematic illustrations propose explanations for the proposed advantage of rod units in controlling the propagating of a crack (Fig. 2-13). Also, recent numerical studies on layered biocomposites indicated crack tip-stress concentration was prominently weakened by the composite structure[144,145]. This structural advantage helps enamel resist catastrophic crack failure.

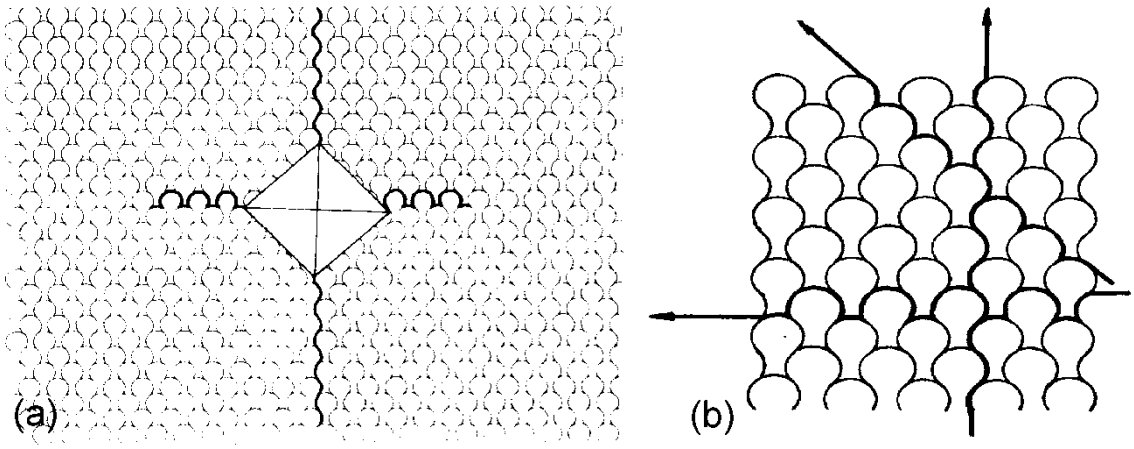

Fig. 2-13 (a) Two-dimensional schematic model of indentation fracture with indenter diagonal oriented 0° to the incisal-cervical axis[127]. (b) Two-dimensional figure of fracture parallel to enamel rods. Arrows represent three different fracture paths that pass around rods[129].

2.5.1.3 Hunter-Schreger band

The complex oblique migratory paths of the cells from the EDJ out to the external surface produce the potential for interweaving among the enamel protein matrices. Human enamel has two levels of decussation, a small angle between adjacent layers of ameloblasts, and a large angle (Hunter-Schreger bands) between neighbouring cohorts of approximately 10 layers of ameloblasts. This complex interweaving provides the possibility for ordered connections between the matrices of many ameloblasts. The greater complexity of human enamel, the additional level of decussation, may be a reflection of differing masticatory function or the need for increased durability due to the much longer human life span. Despite their critical importance to the structural organization of enamel, the mechanisms governing the complex migratory patterns of ameloblasts remain unknown.

2.5.2 Possible functions of protein remnants

Protein is a type of biopolymer with viscoelastic properties stemming from the configurational rearrangements, disposition and interaction among the macromolecules in both their short- and long-range interrelations[146]. Under indentation load, these macromolecular chains may deform by changing their angulation, unfolding and even moving their positions, just like ordinary polymers. The response to local redistribution is rapid and the response to long-range interactions is slow before a new assortment of configurations is obtained. From a thermodynamics perspective, these changes of macromolecules are unstable. Upon unloading, the molecules have a tendency to return to their initial form and positions.

Nano-mechanical properties of biological macromolecules have attracted considerable interest recently, because it has been possible to measure the stiffness of micro- to nano-scale biological specimens with atomic force microscope (AFM) and unfold single protein molecules. The associated force-displacement curve is the basic data recorded by AFM. This technique has been extended to the measurement of mechanical properties of different samples, such as structural proteins[131], bone[147], antigen/antibody pair[148] and DNA strands[149]. Since proteins are heterogeneous and anisotropic in their basic architecture down to the atomic level, the mechanical properties of these single molecular structures are totally different from bulk volumetric materials. Several unique nano-mechanical behaviours of protein macro-molecular have been reported and reviewed by Ikai[150].

Generally speaking, the peptide chains of protein molecules are folded together and form secondary and tertiary structures, which are maintained mainly by hydrogen bonding between amino acids. Force-displacement curves from AFM stretching tests are a reflection of mechanical properties of different secondary and tertiary structures. Evidence supporting this conclusion are: (1) experiments on α-helical protein[151] and a knotted protein[152] indicated that different secondary structures have different stretching responses. For example, although the stretching force may break down the three-dimension structure of α-helix into random coil, it would tighten the knotted structure of protein molecules. (2) Chemically, hydrogen bonds maintaining the three-dimensional structure of protein molecules which are sensitive to denaturant reagents. Denaturing

conditions change the nano-mechanical properties of proteins dramatically[153], although some proteins have a core structure which is highly resistant to denaturing conditions[154].

As a consequence of this technique, the unique mechanical responses of such a recoverable domain bond within protein, named “sacrificial bond”, was reported[131,155]. Molecules that contain these bonds reveal saw-tooth pattern force-displacement curves under tensile force (Fig. 2-14), with every peak of the saw-tooth curve being interpreted as representing the force required to break down each individual “sacrificial bond” unit of the protein. The experiment also found the peak force has a dependence on the speed of pulling of protein samples; the greater the pulling speed, the larger the force is needed[156,157]. In addition, such a domain structure showed recovery upon unloading. The longer the delay before the next application of force, the more reformation of the bond occurred during relaxation; refolding of protein domains was also observed in this process[131]. Moreover, the saw-tooth curve is claimed to result from the presence of a critical set of hydrogen bonds that will be disrupted at the beginning of the mechanical breakdown of the three-dimensional structure due to stretching force[158]. Recently, a stochastic kinetic model has been proposed to study the unfolding process of titin domains[159]. Also, the domains have been simulated at the atomic level by a novel computer simulation method named steered molecular dynamics (SMD)[160]. Furthermore, in recent work, Fantner et al.[161] proposed various types of sacrificial bonds, their combination, and how they appear in single molecule force spectroscopy measurements to aid the analysis of the force spectroscopy curves, by which additional information can be obtained about the molecules and their bonds to the native constructs. These theoretical studies explained and reinforced the experimental findings.

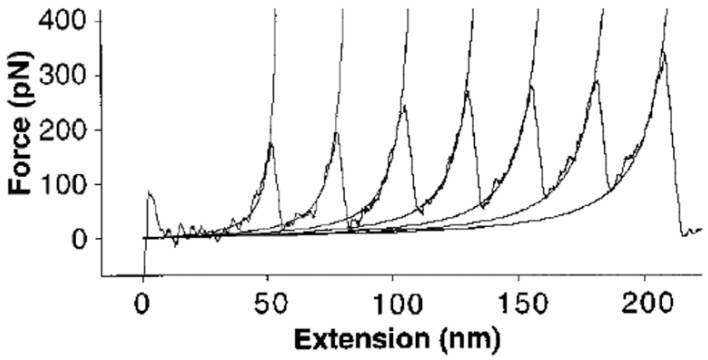

Fig. 2-14 A force extension curve obtained by stretching of a single Ig8 titin fragment. The force extension curve shows a characteristic saw-tooth pattern with seven peaks.[131]

Although the individual components of this type of bond may be weak (hydrogen bridges, hydrophobic interactions, etc.), because of the number in any one molecule, this multiple rupturing bond adds significantly to the strength and toughness of the material. Moreover, the energy dissipated during mechanical unfolding and extension of proteins is typically an order of magnitude greater than their folding free energy while the sample was under the atomic force microscopy-based external force[162]. Jager and Fratzl have developed a numerical model to simulate the mechanical responses of such special bonds for understanding the tensile response of bone[163].

The most relevant research to the topic of this study may be investigations on bone. Recently, the above mentioned "sacrificial bond" phenomena have also been found in bone deformation processes (Fig. 2-15)[132,147]. This new evidence shows that molecular bonds can temporarily sacrifice themselves to absorb impacts[164]. Moreover, micro-tensile deformation at different strain rates resulted in an activation energy of 1.1 eV associated with the basic step involved in the plastic deformation of bone at the molecular level[165]. Interestingly, this activation energy is much higher than the energy of hydrogen bonds but lower than the energy required for breaking covalent bonds inside the collagen fibrils, which indicated an origin of charge interactions between molecules. Similarly, sacrificial bonds in bone were also reported as ion sensitive[132]. In addition, this energy is consistent with the energy associated with the "sacrificial bonds" in bone[161]. These findings reinforced the molecular basis of bone's toughness, strength and fatigue properties. Moreover, similar sacrificial bonds have been found in other natural biocomposites such as nacre[155]. This indicates that most natural biocomposites may have similar molecular mechanics in reinforcing the bulk materials.

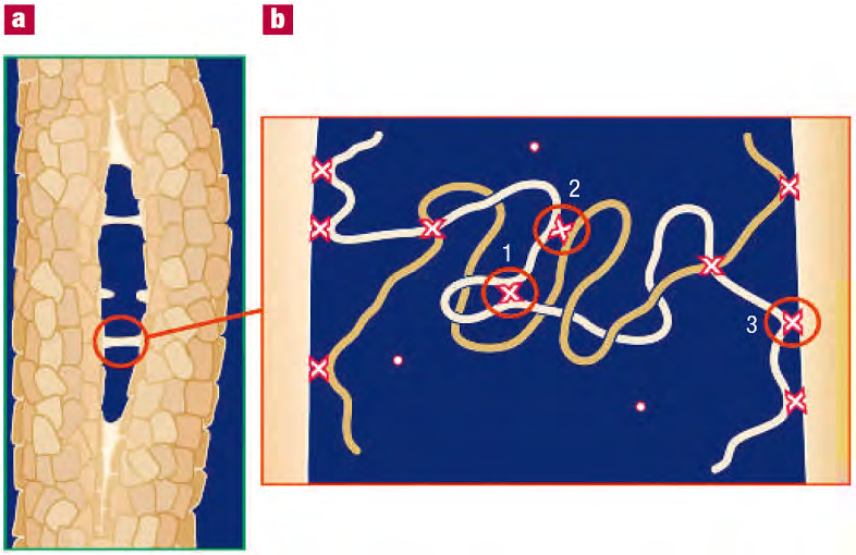

Fig. 2-15 Possible kinds of sacrificial bonds involved in the glue between the mineralized collagen fibrils. (a) Glue filaments could resist the separation of mineralized fibrils. (b) The suspected, calcium-mediated sacrificial bonds in the bone could form between (1) two binding regions on one polymer, (2) two polymers or (3) a polymer and a mineral plate or a combination of these. For all cases the sacrificial bond might involve multiple weak bonds in parallel.[147]

As a result, irrespective of whether the proteins behave as a biopolymer or show the special nano-mechanical properties, the mass response of the bulk material will be non-linear or inelastic. These findings on the nano-mechanics of proteins may help us to understand the basis for the excellent mechanical properties of enamel, namely because this hard tissue contains protein films between HAP crystallites.

Based on the above knowledge of the nano-mechanics of proteins and other findings on natural hard bio-composites such as bone and nacre[147,155], it is reasonable to assume that similar mechanisms may be associated with the proteins in mature enamel and regulate the mechanical behaviour of enamel significantly.

2.5.3 Numerical and mechanical models

The complex hierarchical structure of enamel has elicited a number of attempts to model it[140,166-168]. Here, several widely accepted models will be summarized as a reference to the future work investigated in this thesis.

2.5.3.1 Finite element model by Spears[166]

Finite element analysis (FEA) is a mathematical modeling technique which examines the deformations of a model composed of a meshwork of elements with given material properties. The earliest FEA on teeth can be traced back to Yettram[169] who compared normal and restored teeth in 1976. But, the most successful and widely accepted FE model of enamel was developed by Spears at 1997.

Basically, Katz's composite model[170] can help us to understand the anisotropic behaviour of enamel. Following Katz, Spears derived a simple two-phase composite model on the mechanical structure of enamel at the crystallite level (Fig. 2-16).

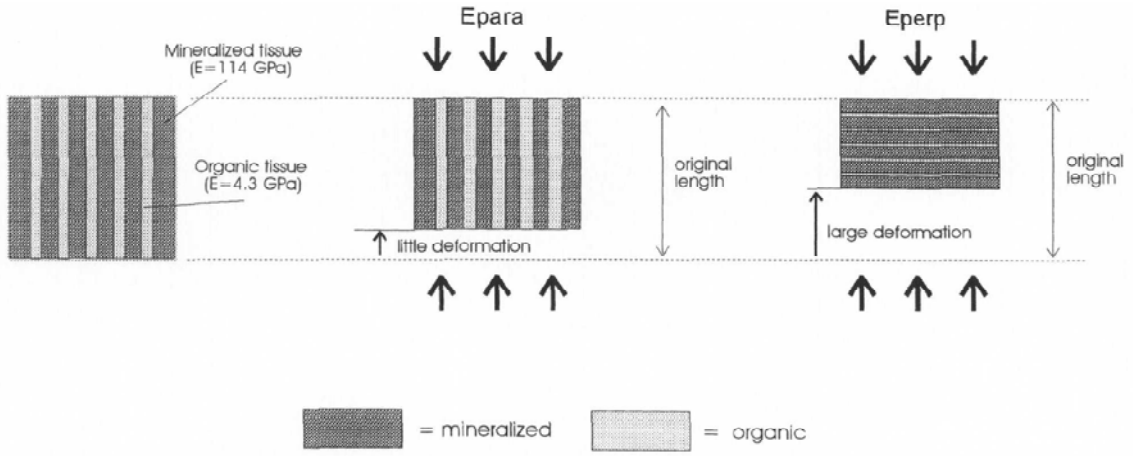

Fig. 2-16 Deformation of enamel parallel and perpendicular to crystal orientation at an ultrastructural level, where E_{para} is the stiffness of enamel along the orientation of crystals and E_{perp} is the stiffness across the orientation of crystals.

The stiffness of the composite in the direction parallel to the direction of crystals can be calculated by means of the equivalent strain equation model: $E_{para} = V_{crys}E_{crys} + (1-V_{crys})E_{org}$, while stiffness perpendicular to the direction of crystals can be calculated by means of the equivalent stress model: $1/E_{perp} = (1-V_{crys})/E_{crys} + (1-V_{crys})/E_{org}$. Unfortunately, this model could not reproduce any of the experimental values from previous works. This is because the variation of crystal orientations within the rod unit was not included into the model. Therefore, with the help of better computer and FE software (ANSYS), Spears built a more appropriate FE model as shown in Fig. 2-17.

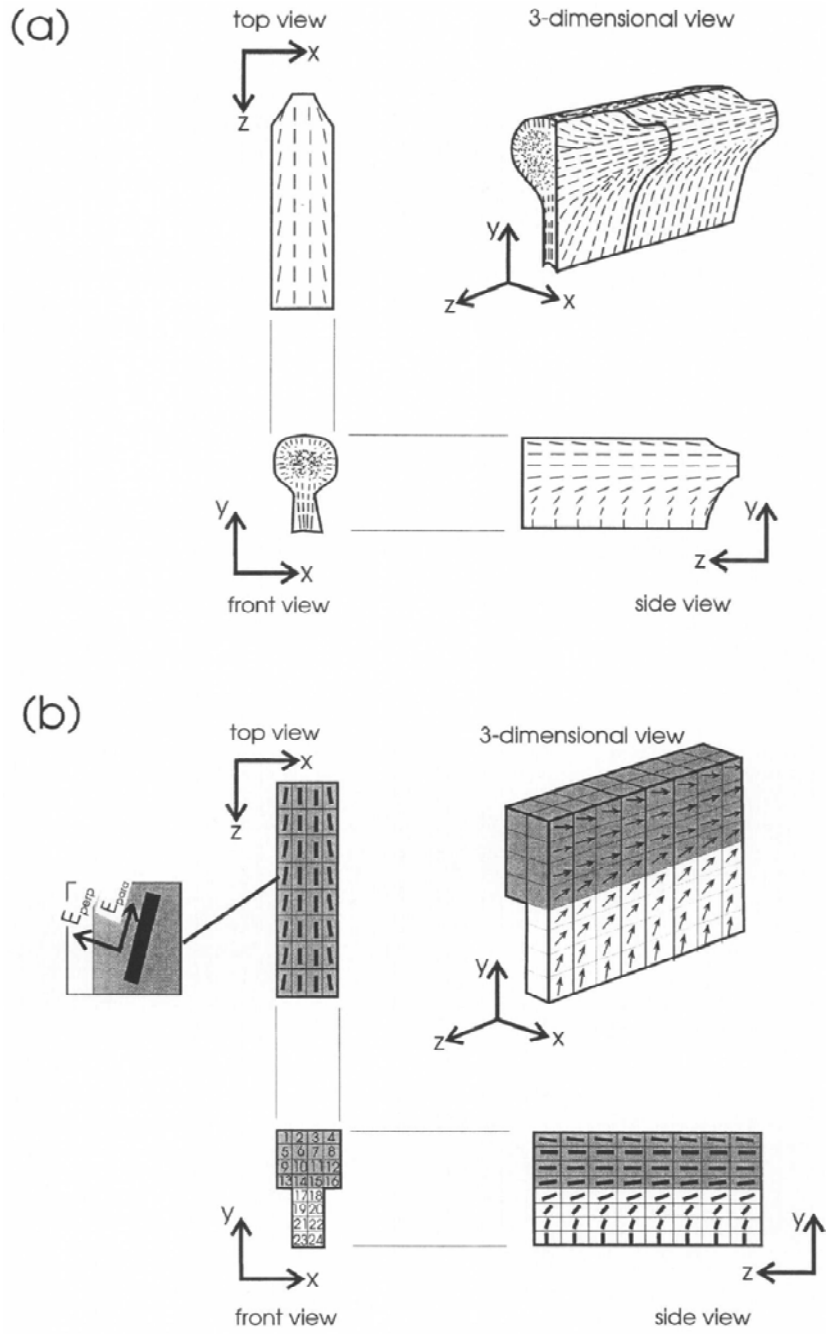

Fig. 2-17 (a) A representation of the crystalline structure in a pattern 3 rod, as seen from top, front, side, and three-dimension views. (b) The elements at the surface of an individual rod model as seen from top, front, and three-dimensional views. The vector directions illustrate the assumed crystal orientations, and thus, the assigned directions of high stiffness (E_{para}).

By considering the elastic modulus of apatite crystallites as 114 GPa and the organic tissue as 4.3 GPa (definitely, this is higher than reality), the elastic modulus of enamel as a composite was estimated in a range of volumetric fractions (V_{crys}) between 0.81 and

0.99. The result was shown in Fig. 2-18. This result is consistent with other experimental findings. Also, this has become the base of many later studies.

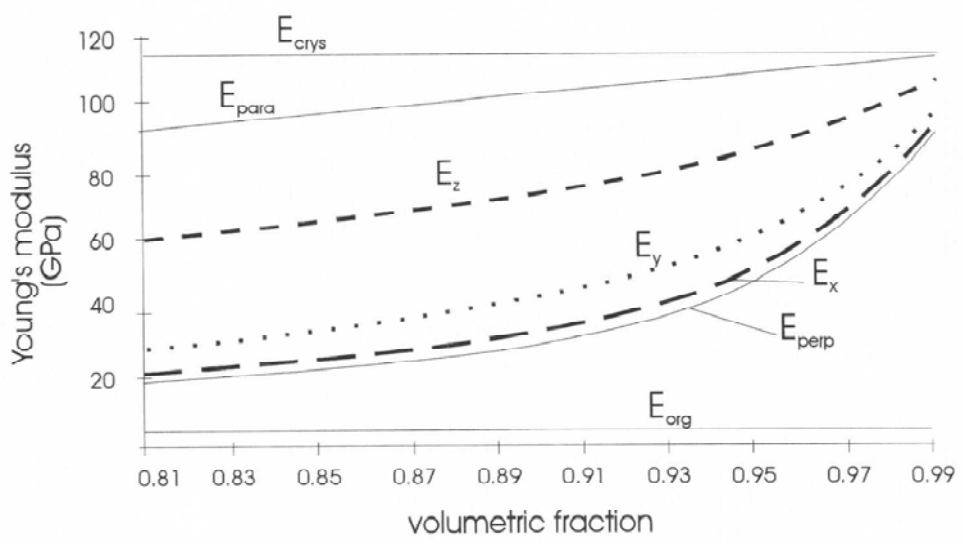

Fig. 2-18 Predicted elastic modulus along (E_z), horizontally across (E_x), and vertically across (E_y) the direction of rod. Also shown are the calculated values of stiffness (E_{para}) along and across (E_{perp}) crystals.

2.5.3.2 "Stiff sponge" model by Fox[171]

With a servo-hydraulic machine and a 3 mm diameter steel ball, Fox made cyclic compressive loading on fifty sound premolars. He found hysteresis between loading and unloading curve. He proposed the area under the hysteresis loop is a measure of the energy required to squeeze out the liquid within enamel. Upon cyclic loading, the area under the hysteresis loop was found to diminish with the number of cycles but was recoverable after an interruption. In addition, the loading hysteresis could be influenced by liquid environments such as stannous fluoride solution.

Based on the above findings, the major argument from the author was: tooth enamel behaves like a stiff sponge from which liquid is expelled through the narrow channels between the hydroxyapatite fibers in compression and drawn in again when the load is released. The effect of repeated loading on the energy absorbing capacity of the enamel was argued as the result of disruption of the diffuse double layer on squeezing the liquid from the pores. For the influence of liquid environment, because hydroxyl groups in hydroxyapatite can be easily replaced by fluoride ions and lead to the change of surface charges of the narrow channels, based on the theory of flow through narrow channels, the

viscosity of fluid within the surface charged channels was changed significantly, which formed the base of different hysteresis cycles.

2.5.3.3 Staggered model by Jäger[172]

By reviewing the microstructure of bone and comparing other parallel-serial models, Jäger developed this staggered deformation model (Fig. 2-19) [172], which is more realistic and accurate by introducing shear stresses in the collagen phase between the overlapping mineral platelets.

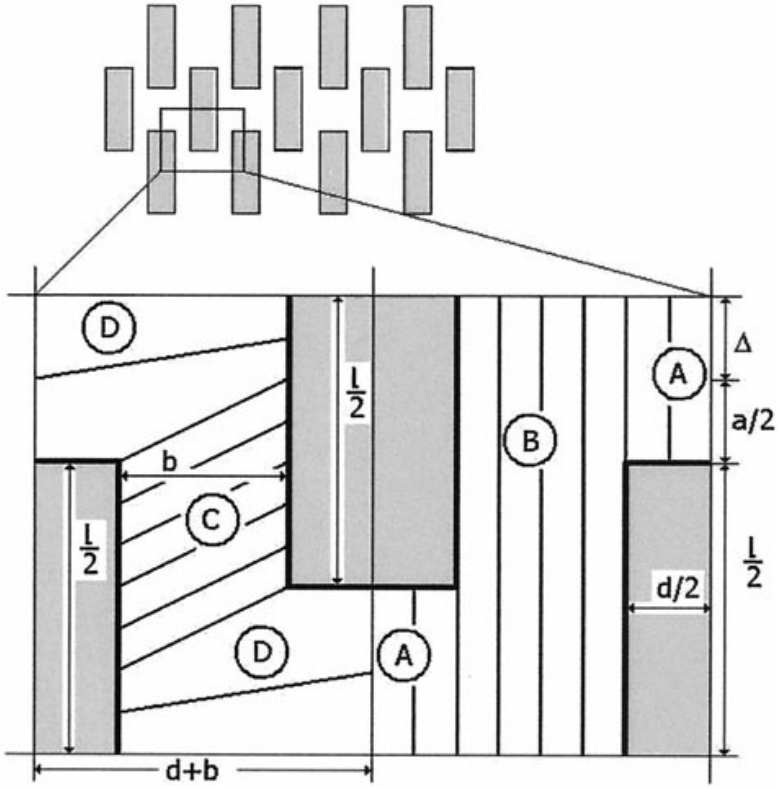

Fig. 2-19 Two adjacent elementary cells of the staggered model showing the regions of tensile (regions *A* and *B*), and shear (regions *C* and *D*) stresses separately. The dimensions of the mineral, *l* and *d*, are indicated as well as the distances between them, *a* and *b*. The elementary cells are shown strained by an amount Δ.[172]

By replacing the nonlinear and anisotropic collagen by an "effective" elastic medium with a Poisson's ratio of $v = 0.25$, and ideal coherence between mineral platelets and collagen at their respective interfaces, the elastic modulus, E', and the maximum strain, ε'_{max}, of the mineralized biocomposite can be estimated.

Based on this staggered model of bone fibrils, Gao et al.[139] proposed a one-dimensional composite model to study the nanoscale effective stiffness of bone, dentin and shells, as illustrated in Fig. 2-20. The mineral crystals have large aspect ratios and are much harder than the soft protein matrix, and the tensile zone in protein matrix near the ends of mineral crystals is assumed to carry no mechanical load. The load transfer is largely accomplished by the high shear zones of proteins between the long sides of mineral platelets. Under an applied tensile stress, the mineral platelets carry most of the tensile load while the protein matrix transfers the load between mineral crystals via shear. The path of load transfer in the composite is thus simplified to a one-dimensional serial spring system consisting of mineral elements (tension) interspersed among protein elements (shear). Hence the model can be called a tension–shear chain model of the biological nanostructure. The large aspect ratio of the mineral platelets ensures that the force transferred between the platelets is distributed over a large shear region with a relatively small stress within the protein. Assuming that the stress distribution along the length of the mineral crystals is linear, shown in Fig. 2-20(c), the maximum and average tensile stress in the mineral can be written as:

$$\sigma_{\mathrm{m}} = \rho\tau_{\mathrm{p}}, \quad \bar{\sigma}_{\mathrm{m}} = \rho\tau_{\mathrm{p}}/2, \quad (2\text{-}6)$$

where $\rho = L/h$ is the aspect ratio of mineral platelets, L being the length and h the thickness of the platelets, and τ_{p} is the shear stress of the protein. These equations show that the tensile stress in mineral is amplified by the aspect ratio ρ from the shear stress in the protein.

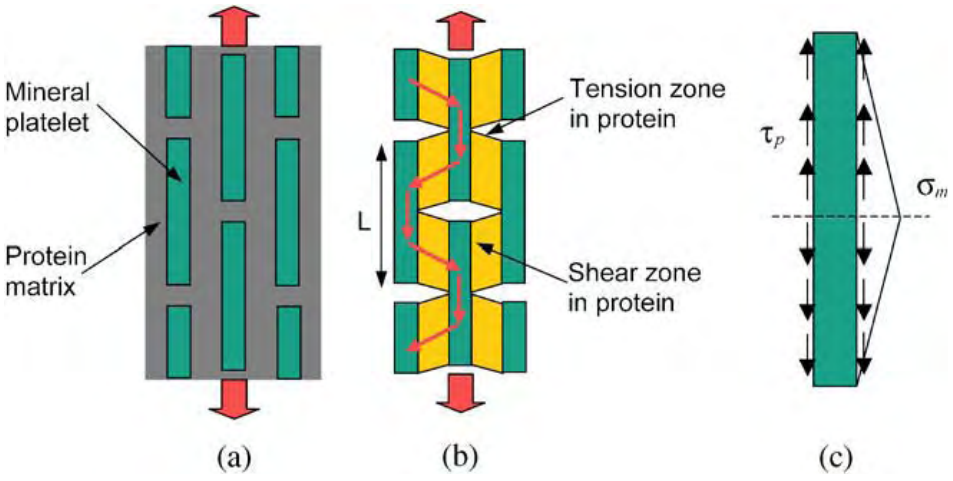

Fig. 2-20 Models of biocomposites. (a) Perfectly staggered mineral inclusions embedded in protein matrix. (b) A tension–shear chain model of biocomposites in which the tensile regions of protein are eliminated to emphasize the load transfer within the composite structure. (c) The free body diagram of a mineral crystal.[146]

In this simplified one-dimensional model, the large aspect ratio of mineral platelets compensates for the low modulus of the protein phase. According to this simple model, the stiffness (elastic modulus) E of the composite can be expressed as:

$$\frac{1}{E} = \frac{4(1-\Phi)}{G_{\mathrm{p}}\Phi^2\rho^2} + \frac{1}{\Phi E_{\mathrm{m}}}, \quad (2\text{-}7)$$

where E_{m} is the elastic modulus of mineral, G_{p} is the shear modulus of protein, Φ is the volume concentration of mineral, and ρ is the aspect ratio of the mineral platelets. This equation indicated that, the elastic modulus of the biocomposite is controlled by the mineral volume concentration and aspect ratio of the mineral platelets. There should be an optimized value for the aspect ratio:

$$\rho^* = \frac{1}{\tau_p^f}\sqrt{\frac{\pi E_{\mathrm{m}}\gamma}{h}}, \quad (2\text{-}8)$$

where γ is surface energy, h is the thickness of the crystal, and τ_p^f is the shear strength of protein matrix.

This explains why the mineral platelets in human bone have much smaller size and larger aspect ratios in comparison with those found in seashells. Because, to achieve the same level of stiffening, a lower volume fraction Φ must be compensated for by a large aspect ratio ρ, and larger aspect ratio means smaller thickness.

2.6 Summary

In this literature review, compositional and hierarchical microstructural characteristics of enamel have been well illustrated and the embryological origin of them was also briefly introduced. Review on mechanical investigations of enamel confirmed the assumption that hierarchical microstructure regulated the mechanical behaviour of the biocomposite significantly. Moreover, numerical studies also supported the argument. On the other hand, there is a rapid progress on the investigation of mechanical behaviour of protein molecules, some researchers relative to biomaterials have been summarized in this chapter as well. Based on their findings, we assume that similar mechanisms may play an important role in enamel. Unfortunately, we could not find any literature evidence to support this hypothesis. This may be an interesting direction for future research on mechanical behaviour of dental hard tissues and relative materials.

Based on the review, the purposes of the thesis were to investigate the nano-mechanical properties of sound human enamel in respect of its hierarchical structure and the protein components inside, which would provide experimental and theoretical bases on the excellent mechanical behaviour of enamel and illustrate some implications on the development of new composites.

2.7 References

1. Katti KS, Katti DR. Why is nacre so tough and strong? Mater Sci Eng C. 2005;26:1317-24.
2. Currey JD. Hierarchies in Biomineral Structures. Science. 2005;309:253-4.
3. Rensberger JM. Mechanical adaptation in enamel. Rotterdam: Balkema; 1997. 237-57 p.
4. Smith MM, Hall BK. A development model for evolution of the vertebrate exoskeleton and teeth. The role of cranial and trunk neural crest. In: Hecht MK (ed). Evolutionary Biology. Volume 27. New York: Plenum Press, 1993:387-448.
5. Slavkin HC. Molecular determinants of tooth development: a review. Crit Rev Oral Biol Med. 1990;1:1-16.
6. Warshawsky H. A freeze-fracture study of the topographic relationship between inner enamel secretory ameloblasts in the rat incisor. Am J Anat. 1978;152:153-208.
7. Nishikawa S. Correlation of the arrangement pattern of enamel rods and secretory ameloblasts in pig and monky teeth: a possible role of the terminal webs in ameloblast movement during secretion. Anat Rec. 1992;232:466-78.
8. Inage T, Shimokawa H, Teranishi Y, Iwase T, Toda Y, Moro I. Immunocytochemical demonstration of amelogenins and enamelins secreted by ameloblasts during the secrectory and maturation stages. Arch Hist Cytol. 1989;52:213-29.
9. Chen E, Piddington R, Decker S, et al. Regulation of amelogenin gene expression during tooth deleopment. Develop Dynamics. 1994;19:189-98.
10. Fincham AG, Lau EC, Simmer J, Zeichner-David M. Amelogenin biochemistry form and function. In: Slavkin H, Price P (eds). Chemistry and biology of mineralized tissues. Amsterdam: Elsevier Science Publishers, 1992:187-201.
11. Diekwisch T, David S, Bringas P, Santos V, Slavkin HC. Antisense inhibition of AMFL translation demonstrates supramolecular controls for enamel HAP crystal growth during embryonic mouse molar development. Development. 1993;117:471-82.
12. Kallenbach E. Fate of horseradish peroxidase in the secretion zone of the rat enamel organ. Tissue Cell. 1980;12:491-501.
13. Nagasaka S. Electron microscopy of biochenically characterized, newly secreted enamel proteins. Arch Oral Biol. 1994;39:105-10.
14. Tanabe T, Fukae M, Shimizu M. Degradation of enamelins by proteinases found in porcine secretory enamel in vitro. Arch Oral Bioly. 1994;39:277-81.
15. Deutsch D, Alayoff A. Changes in the amino acid composition and protein distribution during development of human deciduous enamel. Growth. 1987;51:342-54.
16. Fukae M, Tanabe T, Uchida T, Yamakoshi Y, Shimizu M. enamelins in the newly formed bovine enamel. Calcif Tiss Int. 1993;53:257-61.
17. Deutsch D, Palmon A, Fisher LW, Kolodny N, Termine JD, Young MF. Sequencing of Bovine enamelin ('Tuftelin'): A novel acidic enamel protein. J Biol Chemy. 1991;266:16021-8.
18. Brookes SJ, Robinson C, Kirkham J, Bonass WA. Biochemistry and molecular biology of amelogenin proteins of developing dental enamel. Arch Oral Biol. 1995;40:1-14.
19. Nanci A. Enamel: Composition, Formation, and Structure. In: Nanci A (ed). Ten Cate's Oral Histology: Development, Structure, and Function. St. Louis: Mosby, 2003.
20. Skobe Z. SEM evidence that one ameloblast secretes one keyhole-shaped enamel rod in monkey teeth. Eur J Oral Sci. 2006;114(Suppl. 1):338-42.
21. Diekwisch T, Berman BJ, Gentner S, Slavkin HC. Initial enamel crystals are not spatially associated with mineralized dentin. Calcif Tissue Res. 1995;279:149-67.
22. Cuisinier FJG, Voegel JC, Yacaman J, Frank RM. Structure of initial crystals formed during human amelogenesis. J Cryst Growth. 1992;116:314-8.
23. Fincham AG, Luo W, Moradian-Oldak J, Paine ML, Snead ML, Zeichner-David M. Enamel biomineralization: the assembly and dissassembly of the protein extracellular organic matrix. In: Teaford MF, Meredith-Smith M, Ferguson, M.W.J. (eds). Development, Function and Evolution of Teeth. Cambridge: Cambridge University Press, 2000:37-61.
24. Kirkham J, Zhang J, Brookes SJ. Evidence for charge domains on developing enamel crystal surfaces. J Dent Res. 2000;79:1943-7.
25. Robinson C, Shore RC, Wood SR, et al. Subunit Structures in Hydroxyapatite Crystal Development in Enamel: Implications for Amelogenesis Imperfecta. Connet Tissue Res. 2003;44(Suppl. 1):65-71.
26. Ravindranath RMH, Moradian-Oldak J, Fincham AG. Tyrosyl motif in amelogenins binds N-acetyl-D-glucosamine. J Biol Chem. 1999;274:2464-71.

27. Koenigswald Wv, Sander PM. Tooth enamel microstructure. In: Cate RT (ed). Oral histology : development, structure, and function (5th Edition). Rotterdam: Balkema, 1997:267-80.
28. Macho GA, Jiang Y, Spears IR. Enamel microstructure—a truly three-dimensional structure. J Hum Evol. 2003;45:81-90.
29. Frazier PD. Adult human enamel: an electron microscopic study of crystallite size an morphology. J Ultrastruct Res. 1968;22:1-11.
30. Kerebel B, Daculsi G, Kerebel LM. Ultrastructural studies of enamel crystallites. J Dent Res. 1979;57:306-12.
31. Orams HJ, Phakey PP, Rachinger WA, Zybert JJ. Visulization of micropore structure in human dental enamel. Nature. 1974;252:584-5.
32. Poole DFG, Brooks AW. The arrangement of crystallities in enamel prisms. Arch Oral Biol. 1961;5:14-26.
33. Paine ML, White SN, Luoa W, Hanson Fongc, Mehmet Sarikayac, Sneada ML. Regulated gene expression dictates enamel structure and tooth function. Matrix Biology. 2001;20:273-92.
34. Risnes S. Growth tracks in dental enamel. J Hum Evol. 1998;35:331-50.
35. Smith CE. Cellular and chemical events during enamel maturation. Crit Rev Oral Biol Med. 1998;9:128-61.
36. Darling AI, Mortimer KV, Poole DFG, Ollis WD. Molecular sieve behavious of normal and carious human enamel. Arch Oral Biol. 1961;5:251-73.
37. Dibdin GH. The internal surface and pore structure of enamel. J Dent Res. 1969;48:771-6.
38. Dibdin GH. Surface area of dental enamel" comparison of experimental calues with calues calculated for its structural components. J Dent Res. 1972;51:1256-7.
39. Misra DN, Bowen RL, Mattamal GJ. Surface area of dental enamel, bone and hydroxyapatite: chemisorption from solution. Calcif Tissue Res. 1978;26:139-42.
40. Dibdin GH, Poole DFG. Surface area and pore size analysis for human enamel and dentin by water vapour sorption. Arch Oral Biol. 1982;27:235-41.
41. Zahradnik RT, Moreno EC. Structural features of human dental enamel as revearled by isothermal water vapour sorption. Arch Oral Biol. 1975;20:317-25.
42. Moreno EC, Zahradnik RT. The pore structure of human dental enamel. Arch Oral Biol. 1973;18(8):1063-8
43. Shellis RP, Dibdin GH. Enamel microporosity and its functional implications. In: Teaford MF, Smith MM, Ferguson MWJ (eds). Development, Function and Evolution of Teeth. Cambridge: Cambridge University Press, 2000:242-51.
44. Poole DFG, Tailby PW, Berry DC. The movement of water and other molecules through human enamel. Arch Oral Biol. 1963;8:771-2.
45. Linden LA. Microscopic observation of fluid flow through enamel in vitro. Odontologisk Revy. 1968;19:349-65.
46. Arwill T, Myrberg N, Soremark R. Penetration of radioactive isotopes through enamel and dentin II. Transfer of ^{22}Na in fresh and chemicallytreated dental tissues. Odontologisk Revy. 1969;20:47-54.
47. Linden LA, Bjorkman W, Hattab F. The diffusion in vitro of fluoride and chlorhexidine in the enamel of human deciduous and permanent teeth. Arch Oral Biol. 1986;31:3-37.
48. Thitinanthapan W, Satamanont P, Vongsavan N. In vitro penetration of the pulp chamber by three brands of carbamide peroxide. J Esthet Dent. 1999;11:259-64.
49. Tarbet WJ, Fosdick LS. Permeability of human dental enamel to acriflavine and potassium fluoride. Arch Oral Biol. 1971;16:951-61.
50. Berggren H. Experimental studies on the permeability of enamel and dentin. Swed Dent J. 1947;40:6-109.
51. Jansen MT, Visser JB. Permeable structures in normal enamel. J Dent Res. 1950;29:622-32.
52. Vongsavan N, Matthews B. The permeability of cat dentin in vivo and in vitro. Arch Oral Biol. 1991;36:641-6.
53. Atkinson HF. An investigation into the permeability of human enamel using osmotic methods. Br Dent J. 1947;83:205-14.
54. Simmelink JW. Histology of enamel. In: Avery JK (ed). Oral development and histology. Baltimore: Williams & Wilkins, 1987:140-51.
55. Boyde A. Microstructure of enamel. In: Chadwick DJ, Cardew G (eds). Ciba Foundation Symposium 205 Dental Enamel. New York: Wiley, 1997:18-31.
56. Yanagisawa T, Miake Y. High-resolution electron microscopy of enamel-crystal demineralization and remineralization in carious lesions. J Electron Microscopy. 2003;52(6):605-13.
57. Robinson C, Weatherell JA, Hallsworth AS. Variation in composition of dental enamel within thin ground tooth sections. Caries Res. 1971;5:44-57.

58. Robinson C, Weatherell JA, Hallsworth AS. Distribution of magnesium in mature human enamel. Caries Res. 1981;15:70-7.
59. Weatherell JA, Robinson C, Hallsworth AS. Variations in the chemical composition of human enamel. J Dent Res. 1974;53:180-92.
60. Weatherell JA, Weidmann SM, Hamm S. Density patterns in enamel. Caries Res. 1967;1:42-51.
61. Crabb HSM. Structural patterns in human dental enamel revealed by the use of microradiography in conjunction with two dimensional microdensitometry. Caries Res. 1968;2:235-52.
62. Weatherell JA, Robinson C, Hallsworth AS. Assimilation of fluoride by enamel throughout the life of the tooth. Caries Res. 1977;11:85-115.
63. Sudarsanan K, Machkie PE, Young RA. Comparison of synthetic and mineral fluorapatite, $Ca_5(PO_4)_3F$, in crystallographic detail. Mater Res Bull. 1972;7:1331-8.
64. Elliott JC, Mackie PE, Young RA. Monoclinic hydroxyapatite. Science. 1973;180:1055-7.
65. Troy B, Sluder JB. Clinical dental anatomy, histology, physiology, and occlusion. In: Sturdevant CM (ed). The art and science of operative dentistry. St. Louis: Mosby, 1995.
66. Volker JF. The effect of fluorine on solubility of enamel and dentin. Proc Soc Exp Biol Med. 1939;42:725-7.
67. Jenkins GN. Theories on the mode of action of fluoride in reducing dental decay. J Dent Res. 1963;42:444-54.
68. Burnett GW, Zenewitz J. Studies on the composition of teeth VII. The moisture content of calcified tooth tissues. J Dent Res. 1958;37:581-9.
69. Dibdin GH. The water in human dental enamel and its diffusional exchange measured by clearance of tritiated water from enamel slabs of varying thickeness. Caries Res. 1993;27:81-6.
70. Bernett GW, Zenewitz J. Studies on the composition of teeth VII. The moisture content of calcified tooth tissues. J Dent Res. 1958;37:581-9.
71. LeFevre ML, Manly RS. Miosture, inorganic and organic contents of enamel and dentin from carious teeth. J Am Dent Assoc. 1938;25:233-42.
72. Rootare HM, Craig RG. Vapor phase adsorption of water on hydroxyapatite. J Dent Res. 1977;56:1437-48.
73. Elliott JC. Structure, crystal chemistry and density of enamel apatites. In: Chadwick DJ, Cardew G (eds). Dental Enamel. Chivhester: Wiley, 1997:54-72.
74. Nalla RK, Kinney JH, Tomsia AP, Ritchie RO. Role of alcohol in the fracture resistance of teeth. J Dent Res. 2006;85(11):1022-6.
75. Pashley DH, Agee KA, Carvalho RM, Lee KW, Tay FR, Callison TE. Effects of water and water-free polar solvents on the tensile properties of demineralized dentin. Dent Mater. 2003;19(5):347-52.
76. Fox P. The toughness of tooth enamel, a natural fibrous composite. J Mater Sci. 1980;15:3113-21.
77. Hess WC, C.Y L, Neidig BA. The amino acid composition of enamel protein. J Dent Res. 1953;32:585-7.
78. Battistone GC, Burnett GW. Studies of the composition of teeth. IV. The amino acid composition of human enamel protein. J Dent Res. 1956;35:260-2.
79. Weidmann SM, Eyre DR. Amino acid composition of enamel protein in the fully' developed human tooth. Caries Res. 1967;1:349-55.
80. Belcourt A, Gillmeth S. EDTA soluble protein of human mature normal enamel. Calcif Tissue Int. 1979;28:227-31.
81. Klein J-P, Scholler M, Frank RM. Soluble and insoluble proteins of normal human mature enamel. Arch Oral Biol. 1982;27:133-9.
82. Acil Y, Mobasseri AE, Warnke PH, Terheyden H, Wiltfang J, Springer I. Detection of Mature Collagen in Human Dental Enamel. Calcif Tissue Int. 2005;76:121–6.
83. Wright JT, Chen SC, Hall KI, Yamauchi M, Bawden JW. Protein characterization of fluorosed human enamel. J Dent Res. 1996;75(12):1936-41.
84. Gökduman K. Effects of hydrogen peroxide bleaching on human denin and enamel mictostructure and function: Middle East Technical University, 2005. 75 p.
85. Liu Y, Hsu C-YS. Laser-induced compositional changes on enamel: A FT-Raman study. J Dent. 2007;35:226-30.
86. Carden A, Morris MD. Application of vibrational spectroscopy to the study of mineralized tissues (review). J Biomed Opt. 2000;5(3):259-68.
87. Penel G, Leroy G, Rey C, Bres E. MicroRaman Spectral Study of the PO_4 and CO_3 Vibrational Modes n Synthetic and Biological Apatites. Calcif Tissue Int. 1998;63:475-81.
88. Bachmann L, Diebolder R, Hibst R, Zezell DM. Infrares absorption bands of enamel and dentin tissues from human and bovine teeth. Appl Spectr Rev. 2003;38(1):1-14.

89. Tsuda A, Arends J. Orientational micro-Raman spectroscopy on hydroxyapatite single crysals and human enamel crystallites. J Dent Res. 1994;73(11):1703-10.
90. Leroy G, Penel G, Leroy N, Bres E. Human tooth enamel: a Raman polarized approach. Appl Spectr. 2002;56(8):1030-4.
91. Fattibene P, Caros A, De Coste V, et al. A comparative EPR, infrared and Raman study of natural and deproteinated tooth enamel and dentin. Phys Med Biol. 2005;50:1095-108.
92. Schulze KA, Balooch M, Balooch G, Marshall GW, Marshall SJ. Micro-Raman spectroscopic investigation of dental calcified tissues. J Biomed Mater Res. 2004;69A:286-93.
93. Pezzotti G. Raman piezo-spectroscopic analysis of natural and synthetic biomaterials. Anal Bioanal Chem. 2005;381:577-90.
94. Pezzotti G. Introducting a unique measurement for biomaterial nanomechanics. Key Eng Mater. 2003;240-242:893-900.
95. Carden A, Rajachar RM, Morris MD, Kohn DH. Ultrastructural Changes Accompanying the Mechanical Deformation of Bone Tissue: A Raman Imaging Study. Calcif Tissue Int. 2003;72:166-75.
96. Timlin JA, Carden A, Morris MD, Rajachar RM, Kohn DH. Raman spectroscopic imaging markers for fatigue-related microdamage in bovine bone. Anal Chem. 2000;72:2229-36.
97. LeGeros RZ, Bonel G, Legeros R. Types of H_2O in human enamel and in percipitated apathies. Calcif Tissue Res. 1978;26:111-8.
98. Sowa MG, Mantsch HH. FT-IR photoacoustic depth profiling spectroscopy of enamel. Calcif Tissue Int. 1994;54:481-5.
99. Sowa MG, Popescu DP, Werner J, et al. Precision of Raman depolarization and optical attenuation measurements of sound tooth enamel. Anal Bioanal Chem. 2007;387:1613-9.
100. Waters NE. Some mechanical and physical properties of teeth. In: Vincent J, Curry J (eds). The mechanical properties of biological materials. Cambridge: Cambridge University Press, 1980:99-134.
101. Ferrario VF, Sforza C, Zanotti G. Maximal bite forces in healthy young adults as predicted by surface electromyography. J Dent. 2004;32:451-7.
102. Fernandes CP, Glantz P-OJ, Svensson SA. A novel sensor for bite force determinations. Dent Mater. 2003;19:118-26.
103. Guy AG. Introduction to Materials Science. New York: McGraw-Hill Book Company; 1972.
104. Lee SK, Wilson PR. Fracture strength of all-ceramic crowns with varying core elastic moduli. Au Dent J. 2000;45:103-7.
105. Boyer HE. Hardness Testing. Metals Park, OH: ASM International; 1987.
106. Irwin GR. Fracture. In: Fluegge S (ed). Handbuck der Physik. Berlin: Springer-Verleg, 1958.
107. Fischer H, Marx R. Fracture toughness of dental ceramics: comparison of bending and indentation method. Dent Mater. 2002;18:12-9.
108. Stanford JW, Paffenberger GC, Kampula JW, Sweeney AB. Determination of some compressive properties of human enamel and dentin. J Am Dent Assoc. 1958;57:487-95.
109. Stanford JW, Weigel KV, Paffenberger GC, Sweeney WT. Compressive properties of hard tooth tissues and some restorative materials. J Am Dent Assoc. 1960;60:746-51.
110. Craig RG, Peyton FA, Johnson W. Compressive properties of enamel, dental cements, and gold. J Dent Res. 1961;40:936-43.
111. Tyldeslsy WR. Mechanical properties of hunman dental enamel and dentin. Br Dent J. 1959;106:269-78.
112. Reich FR, Brenden BB, Porter NS. ultrasonic imaging of teeth. Washington: Batelle Memorial Institue, 1967.
113. Staines M, Robinson WH, Hood JAA. Spherical indentation of tooth enamel. J Mater Sci. 1981;16:2551-6.
114. Xu HHK, Smith DT, Jahanmir S, et al. Indentation damage and mechanical properties of human enamel and dentin. J Dent Res. 1998;77:472-80.
115. Willems G, Celis JP, Lambrechts P, Braem M, Vanherle G. Hardness and Young's modulus dertermind by nanoindentation technique of filler particles of dental restorative materials compared with human enamel. J Biomed Mater Res. 1993;27:747-55.
116. Cuy JL, Manna AB, Livi KJ, Teaford MF, Weihs TP. Nanoindentation Mapping of the Mechanical Properties of Human Molar Tooth Enamel. Arch Oral Biol. 2002;47:281-91.
117. Zhou J, Hsiung LL. Depth-dependent mechanical properties of enamel by nanoindentation. J Biomed Mater Res. 2007;81A:66-74.
118. Ge J, Cui FZ, Wang XM, Feng HL. Property variations in the prism and the organic sheath within enamel by nanoindentation. Biomaterials. 2005;26:3333-9.

119. Mahoney E, Holt A, Swain M, Kilpatrick N. The hardness and modulus of elasticity of primary molar teeth: an ultra-micro-indentation study. J Dent. 2000;28(8):589-94.
120. Marshall GW, Balooch M, Gallagher RR, Gansky SA, Marshal SJ. Mechanical properties of the dentinoenamel junction: AFM studies of nanohardness, elastic modulus, and fracture. J Biomed Mater Res. 2000;54(1):87-95.
121. Poolthong S. Determination of the mechanical properties of enamel, dentin and cementum by an ultra micro-indentation system [PhD Thesis]. Sydney: University of Sydney, 1998.
122. Fong H, Sarikaya M, White SN, Snead ML. Nano-mechanical properties profiles across dentin-enamel junction of human incisor teeth. Mater Sci Eng C. 2000;7:119-28.
123. Habelitz S, Marshall SJ, Jr GWM, Balooch M. Mechanical properties of human dental enamel on the nanometre scale. Arch Oral Biol. 2001;46:173-83.
124. Habelitz S, Marshall GW, Baloochb M, Marshalla SJ. Nanoindentation and storage of teeth. J Biomech. 2002;35:995-8.
125. Barbour ME, Parker DM, Jandt KD. Enamel dissolution as a function of solution degree of saturation with respect to hydroxyapatite: a nanoindentation study. J Coll Interface Sci. 2003;265:9-14.
126. Sakar-Deliormanli A, Guden M. Microhardness and Fracture Toughness of Dental Materials by Indentation Method. J Biomed Mater Res. 2005;76B:257-64.
127. Hassan R, Caputo AA, Bunshan RF. Fracture Toughness of Human Enamel. J Dent Res. 1981;60(4):820-7.
128. White SN, Luo W, Paine ML, Fong H, Sarikaya M, Snead ML. Biological organization of hydroxyapatite crystallites into a fibrous continuum toughens and controls anistropy in human enamel. J Dent Res. 2001;80(1):321-7.
129. Rasmussen ST, Patchin RE, Scott DB, Heuer AH. Fracture properties of human enamel and dentin. J Dent Res. 1976;55:154-64.
130. Kobayashi S, Kawai W, Wakayama S. The effect of pressure during sintering on the strength and the fracture toughness of hydroxyapatite ceramics J Mater Sci: Mater Med. 2006;17:1089–93.
131. Rief M, Gautel M, Oesterhelt F, Fernandez J, Gaub H. Reversible unfolding of individual titin immunoglobulin domains by AFM. Science. 1997;276:1109-12.
132. Thompson JB, Kindt JH, Drake B, Hansma HG, Morse DE, Hansma PK. Bone indentation recovery time correlates with bond reforming time Nature. 2001;414(6865):773-6
133. Lucas BN, Oliver WC. Indentation power-law creep of high-purity indium. Metall Mater Trans. 1999;30A(3):601-10.
134. Zhou J, Hsiung LL. Biomolecular origin of the rate-dependent deformation of prismatic enamel. Appl Phys Lett. 2006;89:051904.
135. Maas MC, Dumont ER. Built to last: The structure, function, and evolution of primate dental enamel. Evol Anthr. 1999;8(4):133-52.
136. Spears IR, Crompton RH. The mechanical significance of the occlusal geometry of great ape molars in food breakdown J Hum Evol. 1996;31(6):517-35
137. Maas MC, OLeary M. Evolution of molar enamel microstructure in North American Notharctidae (primates). J Hum Evol. 1996;31(4):293-309
138. Griffith AA. The phenomenon of rupture and flow in solids. Phil Trans Roy Soc Lond. 1920;A221:163-98.
139. Gao H, Ji B, Jäger IL, Arzt E, Fratzl P. Materials become insensitive to flaws at nanoscale: Lessons from nature. PNAS. 2003;100(10):5597-600.
140. Spears IR, van Noort R, Crompton RH, Cardew GE, Howard IC. The effects of enamel anisotropy on the distribution of stress in a tooth. J Dent Res. 1993;72:1526-31.
141. Xu HHK, Smith DT, Jahanamir S. Indentation damage and mechanical properties of human enamel and dentin. J Dent Res. 1998;77:472-80.
142. White SN, Luo W, Paine ML, Fong H, Sarikaya M, Snead ML. Biological organization of hydroxyapitite crystallites into a fibrous continuum toughens and controls anisotropy in human enamel. J Dent Res. 2001;80:321-6.
143. Hu C-C, Fukae M, Uchida T. Sheathalin: cloning, cDNA polypeptide sequences, and immunolocalization of porcine enamel sheath proteins. J Dent Res. 1997;76:648-57.
144. Okumura K, Gennes P-Gd. Why is nacre strong? Elastic theory and fracture mechanics for biocomposites with stratified structures. Eur Phys J E. 2001;4:121-7.
145. de Gennes PG, Okumura K. On the toughness of biocomposites. C R Acad Sci Paris. 2000;257(1):257-61.
146. Ji B, Gao H. Mechanical properties of nanostructure of biological materials. J Mech Phys Solids. 2004;52:1963-90.

147. Fantner GE, Hassenkam T, Kindt JH, et al. Sacrificial bonds and hidden length dissipate energy as mineralized fibrils separate during bone fracture. Nature Mater. 2005;4(8):612-6
148. Kirkham J, Andreev I, Robinson C, Brookes SJ, Shore RC, Smith DA. Evidence for direct amelogenin–target cell interactions using dynamic force spectroscopy. Eur J Oral Sci. 2006;114(Suppl. 1):219-24.
149. Lee GU, Chrisey LA, Colton RJ. Direct measurement of the forces between complementary strands of DNA. Science. 1994;266(5186):771-3.
150. Ikai A. Nano-mechanics of proteins with possible applications. Superlattices and Microstructures. 2002;31(1):43-62.
151. Idiris I, Alam MT, Ikai A. Spring mechanics of alpha-helical polypeptide. Protein Eng. 2000;13(11):763-70.
152. Ikai A, Wang T. Protein stretching IV: Analysis of force-extension curves Japan J Appl Phys. 2000;39(6B):3784-8.
153. Wang T, Ikai A. Protein stretching III: Force-extension curves of tethered bovine carbonic anhydrase B to the silicon substrate under native, intermediate and denaturing conditions Japan J Appl Phys. 1999;38(6B):3912-7.
154. Semisotnov GV, Uversky VN, Sokolovsky IV, Gutin AM, Razgulyaev OI, Rodionova NA. Two slow stages in refolding of bovine carbonic anhydrase B are due to proline isomerization. J Mol Biol. 1990;213(3):561-8.
155. Smith B, Schaffer T, Viani M, et al. Molecular mechanistic origin of the toughness of natural adhesives, fibres and composites. Nature. 1999;399:761-3.
156. Rief M, Gautel M, Schemmel A, Gaub HE. The mechanical stability of immunoglobulin and fibronectin III domains in the muscle protein titin measured by atomic force microscopy. Biophys J. 1998;75(6):3008-14
157. Carrion-Vazquez M, Oberhauser AF, Fowler SB, et al. Mechanical and chemical unfolding of a single protein: a comparison. PNAS. 1999;96:3694-9.
158. Isralewitz B, Gao M, Schulten K. Steered molecular dynamics and mechanical functions of proteins. Curr Opin Struct Biol. 2001;11(2):224-30.
159. Makarov DE, Hansma PK, Metiu H. Kinetic Monte Carlo simulation of titin unfolding. J Chem Phys. 2001;114(21):9663-873.
160. Gao M, Lu H, Schulten K. Unfolding of titin domains studied by molecular dynamics simulations J Muscle Res Cell M 2002;23(5-6):513-21
161. Fantner GE, Oroudjev E, Schitter G, et al. Sacrificial Bonds and Hidden Length: Unraveling Molecular Mesostructures in Tough Materials. Biophys J. 2006;90:1411-8.
162. Thompson JB, Hansma HG, Hansma PK, Plaxco KW. The Backbone Conformational Entropy of Protein Folding: Experimental Measures from Atomic Force Microscopy. J Mol Biol. 2002;322:645-52.
163. Jäger IL. The "Sticky Chain": A Kinetic Model for the Deformation of Biological Macromolecules. Biophys J. 2001;81(4):1897-906.
164. Currey J. Biomaterials-Sacrificial bonds heal bone. Nature. 2001;414:699.
165. Gupta HS, Fratzl P, Kerschnitzki M, Benecke G, Wagermaier W, Kirchner HOK. Evidence for an elementary process in bone plasticity with an activation enthalpy of 1 eV. J R Soc Interface. 2007;4:277-82.
166. Spears IR. A three-dimensional finite element model of prismatic enamel: a re-appraisal of the data on the Young's modulus of enamel. J Dent Res. 1997;76:1690-7.
167. Shimizu D, Macho GA, Spears IR. Effect of prism orientation and loading direction on contact stresses in prismatic enamel of primates: Implications for interpreting wear patterns American Journal of Physical Anthropology. 2005;126(4):427-34
168. Jiang Y, Spears IR, Macho GA. An investigation into fractured surfaces of enamel of modern human teeth: a combined SEM and computer visualisation study. Arch Oral Biol. 2003;48(6):449-57
169. Yettram AL, Wright KW, Pickard HM. Finite element stress analysis of the crowns of normal and restored teeth. J Dent Res. 1976;55:1004-11.
170. Katz JL. Hard tissue as a composite material. I. Bounds on the elastic behaviour. J Biomech. 1971;4:455-73.
171. Fox PG. The toughness of tooth enamel, a natural fibrous composite. J Mater Sci. 1980;15:3113-21.
172. Jäger IL, Fratzl P. Mineralized collagen fibrils: a mechanical model with a staggered arrangement of mineral paticles. Biophys J. 2000;79:1737-46.

Chapter 3

Materials, Methods and Theoretical Basis

The instrumented indentation technique has become a popular method to measure the mechanical properties of different materials. However, most investigations use a sharp tip such as a Berkovich indenter from which the hardness and elastic modulus may be determined. Few investigators have chosen a spherical tipped indenter. In the dental materials area, a number of studies have been published on the measurement of specific dental materials and tooth properties using nano-indentation[1-6], but no other investigations with spherical indenter tips was found apart from a study by Poolthong et al[7] to investigate the properties of enamel and dentin. A sharp tipped indenter does not allow the transition from elastic to plastic behavior of a material to be deduced because these indenters produce a nominally-constant plastic strain impression. A spherical tip, in contrast, with increasing depth of penetration develops increasing contact stress with load, the mechanics of which will now be considered, so that the elastic to plastic transition response and the determination of the contact stress-strain property of a material may be investigated[8,9].

The use of spherical tipped indenters has a long history for characterizing metallic materials[10]. Tabor[11] found a simple empirical relationship between contact pressure or hardness and contact strain (contact radius/indenter radius, a/R). This approach and the relationships between hardness and true stress as well contact strain and true strain has been an area of further study such as that by Matthews[12] and only recently has been analytically confirmed by Hill et al[13]. Recently, Lawn and colleagues have investigated the behavior of dental ceramics with a spherical indenter[14-17]. The latter research has mainly concentrated on the macro-scale damage mode of brittle material and multilayer structures.

With the development of high resolution instrumented indentation devices, new methods are available to measure the mechanical properties of materials. Oliver and Pharr[18] proposed a method based on the contact mechanics analysis developed by Sneddon[19] to analyse any axi-symmetric indentation generated *P-h* curves to determine the Hardness and Elastic Modulus mechanical properties of materials. Field and Swain[20] developed an alternate method to analyze force-displacement data using a spherical tipped indenter. Later, Oliver and Pharr[21] and Suganuma and Swain[22] verified the equivalence of the two approaches.

In this chapter, new methods were developed to measure the indentation stress-strain relationship, energy absorption ability and creep behaviour of the sample by nanoindentation.

3.1 Theories

3.1.1 Method for stress-strain relationship with spherical indenters

The models chosen to interpret the indentation data were that of Hertz[10], Oliver and Pharr[18] and Tabor[11]. Unfortunately, on a micro-scale level, it is impossible to produce a perfect polished diamond spherical indenter with a constant radius. In the case of a spherical tipped indenter Hertz's analysis provides an elastic contact relationship between indenter and samples (see Fig. 3-1).

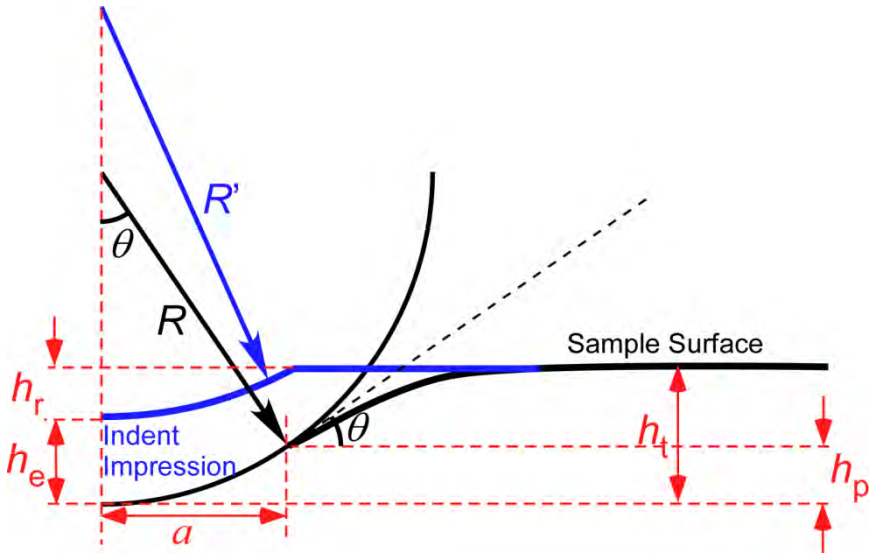

Fig. 3-1 Schematic illustration of contact between a spherical indenter and a flat specimen

The radius of contact circle, a, can be calculated as[10],

$$a^3 = \frac{3}{4}\frac{PR}{E_{\text{eff}}}, \qquad (3\text{-}1)$$

in which $\frac{1}{E_{\text{eff}}} = \frac{1-\nu^2}{E} + \frac{1-\nu'^2}{E'}$, E, E' and ν, ν' are Young's modulus and Poisson's ratio of specimen and indenter (usually diamond), P is the contact load and a is the contact radius.

The total depth of penetration, h_t, is given by:

$$h_t^3 = \left(\frac{3}{4E_{eff}}\right)^2 \frac{P^2}{R}. \quad (3\text{-}2)$$

Contact pressure, P_m, can be calculated by the definition of the pressure,

$$P_m = \frac{P}{\pi a^2} \quad . \quad (3\text{-}3)$$

Hertz also established the simple relationship between the elastic total displacement into the sample, h_t, and the contact depth, h_p,

$$h_t = 2h_p. \quad (3\text{-}4)$$

Combining Eqs. (3-1) and (3-3), the relationship between the contact pressure, P_m, and the contact radius, a, is,

$$P_m = \left(\frac{4E_{eff}}{3\pi}\right)\frac{a}{R}, \quad (3\text{-}5)$$

where E_{eff} is the reduced or indentation modulus and R is the nominal radius of the indenter tip. This expression establishes the linear relationship between contact pressure and contact strain, a/R, during the elastic loading of a material.

In the case of a conical tipped indenter Tabor[11] showed that

$$\varepsilon_r \approx 0.2 \tan\theta \quad , \quad (3\text{-}6)$$

$$\sigma \approx P_m / 3, \quad (3\text{-}7)$$

are appropriate expressions for representative strain, ε_r, and stress, σ, where β is the angle between the indenter flank and the original surface. Matthews[12] on the other hand suggested that the divisor in equation 3-13 should be 2.8 rather than 3.

For spherical indentation, strain increases continuously with indentation impression depth, and an appropriate equivalent expression is

$$\varepsilon_r \approx 0.2a / R \quad (3\text{-}8)$$

where $\tan\theta \approx \sin\theta \approx a/R$.

In these studies, the approach of Tabor, namely the *H-a/R* curve generated for a material shall be regarded as the contact stress-strain curve.

In the case of elastic plastic response of materials to pointed indenters Oliver and Pharr[18] recommended a simple method to fit the nanoindentation *P*-*h* unloading curve, namely;

$$P = \alpha (h - h_r)^m, \qquad (3\text{-}9)$$

where P is the indenter load, h is the elastic displacement, h_r is the residual impression depth of the indenter, while α and m are constants. This method applies to all axi-symmetric indenters, including spheres. With this equation, the elastic contact stiffness, dP/dh, can be calculated from the upper portion of the unloading data.

There is a constant relationship between the elastic contact stiffness, dP/dh, the projected area of contact, A, and the reduced or indentation modulus E_{eff},

$$\frac{dP}{dh} = \beta \frac{2}{\sqrt{\pi}} E_{\text{eff}} \sqrt{A} \qquad (3\text{-}10)$$

In which $A = \pi a^2$, β is a constant dependent upon indenter shape. For a spherical indenter, β=1.

In this context, by assuming that the E modulus of a material is known, the radius of contact area, a, at certain loading force, can be calculated from equation (3-7), namely

$$a = \frac{dP/dh}{2E_{\text{eff}}}. \qquad (3\text{-}11)$$

At the same time, a relationship between the indenter radius, R, contact radius, a, and contact depth h_p, can be derived from Fig. 3-1,

$$a = \sqrt{2h_p R - h_p^2} \qquad (3\text{-}12)$$

By combining equations (3-8) and (3-9), it is not difficult to show,

$$\frac{a}{R} = \frac{\dfrac{dP/dh}{E_{\text{eff}}} h_p}{\left(\dfrac{dP/dh}{2E_{\text{eff}}}\right)^2 + h_p^2}. \qquad (3\text{-}13)$$

Based on the definition of hardness, H,

$$H = \frac{P_{\max}}{A}, \qquad (3\text{-}14)$$

the nanoindentation system can record the *P*-*h* response of a material from which P_{max}, h_p and *dP*/*dh* maybe automatically calculate. Thus, a relationship between *H*-*a*/*R* curve of the sample may be determined.

Because of the inevitable deviation of the tip shape from that of a sphere, which is to say, the real radius of the tip at different contact depths may not be as constant as the nominal value reported by the manufacturer. Therefore, we need a better method to avoid using the parameter of tip radius, *R*, in the calculation.

From Fig. 3-1, it is not difficult to show that the contact area of a spherical indenter with a specimen can be described by the h_p-*a* curve. The tangent angle of this curve, θ, may also be easily calculated from the derivative of the function $h_p(a)$. Moreover, to facilitate calculation, the equation of the curve can be expressed as $a = f(h_p)$ and its derivative as $a' = \tan\beta = f'(h_p)$, in which β is the tangent angle of the curve. In this way, the stress-strain curve of any material can be acquired by collecting *P* and h_p data alone. For $\theta + \beta = 90^\circ$, $\tan\theta$ can be calculated as,

$$\tan\theta = 1/\tan\beta = 1/f'(h_p). \qquad (3\text{-}15)$$

Contact pressure, *H*, can be calculated as,

$$H = \frac{P_t}{A}, \qquad (3\text{-}16)$$

in which $A = \pi a^2$ and $a = f(h_p)$. With equations (3-15) and (3-16), the stress-strain curve (*H*-tanθ curve) may be calculated. Another geometrical relationship in Fig. 1 is

$$a/R = \sin\theta = 1/\sqrt{\left(\tan^{-2}\theta + 1\right)}. \qquad (3\text{-}17)$$

By combination of equations (3-8) and (3-17), an effective indenter radius, *R*, may be determined. The elastic modulus of the sample may be calculated from equation (3-3) as

$$E_{eff} = \frac{dP/dh}{2a}. \qquad (3\text{-}18)$$

With the help of tip shape function $a = f(h_p)$, the elastic modulus of any sample can be measured with spherical tips by using only h_p and *dP*/*dh* data.

3.1.2 Method for energy absorption by nanoindentation

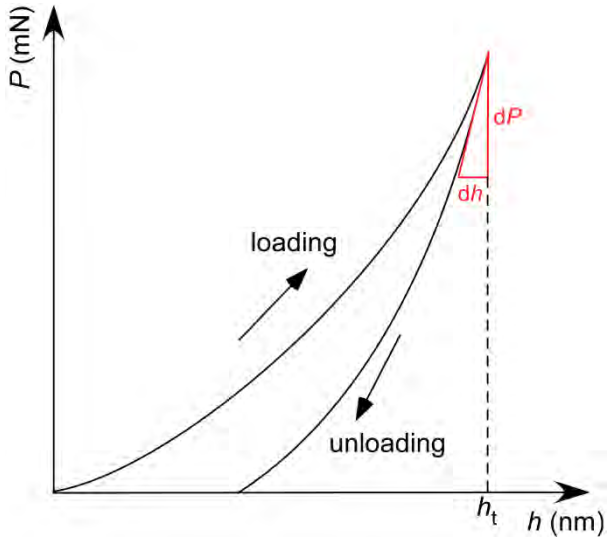

Fig. 3-2 Schematic drawing of *P*-*h* curve from nanoindentation.

Mechanical work is defined as the product of force and displacement. Therefore, the area below the loading curve in the load-displacement (*P*-*h*) diagram (Fig. 3-2) corresponds to the total energy spent pressing an indenter into the material, U_T. The area below the unloading curve corresponds to the elastic energy recovered from the system during unloading, U_E. Their difference, $U_P = U_T$-U_E, (the area between loading and unloading curve), expresses the unrecoverable energy, consisting of the work spent in plastic deformation or other irreversible processes (e.g. cracking), and stored elastic energy associated with the residual stresses caused by the resultant impression. All the energies can be easily calculated from *P*-*h* curves. However, since all these values correspond to a particular test with special values of load and depth, it is more informative to normalize them. In this study, the ratio of the unrecoverable energy to the total energy, $U\% = U_P/U_T \times 100\%$, is used to normalize the energy expenditure of each test. This value may also be denoted the "plasticity index" to characterize the plasticity of the material. This U_P/U_T ratio ranges from 0 for an ideally elastic material (all energy is returned on unloading) to 1 for an ideally plastic material (no energy is returned). In addition the concept of "work of indentation"[23,24] is considered as the basis for analysis. The energy to create a unit volume of indentation is called the "work of indentation" and is given by:

$$W = \frac{U}{V}, \qquad (3\text{-}19)$$

in which, U is the energy used to create the indentation volume, V, at the surface of the sample. During loading procedure, the energy used to create the volume, V_T, at maximum load should be U_T. After unloading, the residual impression with the volume V_R is a reflection of unrecoverable energy, U_P. The volume of indent produced by spherical indenter is a segment of a sphere which can be calculated with the following equation:

$$V = \frac{\pi}{3} h^2 (3R - h). \qquad (3\text{-}20)$$

As there is a geometrical relationship between contact radius, a, contact depth, h, and tip radius, R, namely

$$R = \frac{h^2 + a^2}{2h}, \qquad (3\text{-}21)$$

equation (3-20) can be rewritten as:

$$V = \frac{\pi}{6} h(h^2 + 3a^2), \qquad (3\text{-}22)$$

in which, h is generated from the analysis software and contact radius, a, is calculated using a tip calibration function, $a=f(h_P)$, established with fused silica.

For a Berkovich indenter, the volume of an equivalent conical shape was determined by using the nominal angle indenter face angle of 70.3°. Therefore, the volume can be calculated by,

$$V = \frac{1}{3} \pi a^2 h, \qquad (3\text{-}23)$$

in which, contact radius, a, is calculated by,

$$a = \eta \tan \alpha \cdot h_p, \qquad (3\text{-}24)$$

With η the area function ratio between a perfect indenter (η = 1) and the actual indenter[22].

For the residual impression V_R after unloading, h in the above equations is the residual depth, h_r, of the indentation (see Fig. 3-1). To calculate the residual volume V_R, based on Stilwell and Tabor's observation[25], we assume the elastic recovery in horizontal direction is small enough so that the radius of residual impression is the same as the maximum

contact radius of the indentation, a, in equation (3-21) and (3-22). With U_P and V_R values, the plastic work of indentation ("true hardness" defined by Sakai), W_P, values can calculated with equation (3-19).

Energy expenditure analysis provides a novel way to explore the mechanical properties of enamel and compare enamel with other materials, especially dental restorative materials. This may provide guidance for future material development and evaluation.

3.1.3 Method for nanoindentation creep analysis

The rapid progress of depth-sensing indentation test method provides a new method to explore mechanical properties of materials and has been extended to measuring creep behavior. Lucas and Oliver[26] reviewed the depth-sensing creep tests and recognized four types: (1) indentation load relaxation tests, (2) constant rate of loading tests, (3) constant-load indentation creep tests, and (4) impression creep tests. The most common method is constant-load indentation creep test, which records the change of the depth with time.

In some non-linear solids, especially power-law creep materials, the mechanical response depends upon the strain rate, namely[23]:

$$\sigma = K\dot{\varepsilon}^m, \qquad (3\text{-}25)$$

where K and m are material constants and m is the creep rate sensitivity. This equation is derived from Norton's finding that $d\varepsilon/dt = (\sigma/\sigma_c)^n$, where ε, σ, t are strain, stress and time respectively and σ_c, n are material parameters[27].

The complex stress state beneath an indenter tip requires a somewhat different approach to evaluate the creep response generated. Because of geometrical similarity for conical and pyramidal indenter tips the Berkovich tip has a constant effective strain value, from Tabor's empirical relationship the effective contact strains is $\varepsilon_r \approx 0.2\tan\theta$[11]. Therefore,

the strain rate of an indentation test can be extracted from the *h-t* curve as the indenter displacement velocity divided by the plastic depth of penetration[28]:

$$\dot{\varepsilon} = \dot{h} / h, \qquad (3\text{-}26)$$

where the indentation rate $\dot{h} = \mathrm{d}h / \mathrm{d}t$. Strictly speaking, h should be the contact depth of indenter, h_p. However, to facilitate the measurement and calculation, total displacement, h_t, is generally used in this equation. By assuming a constant ratio of h_p/h_t, which is what we saw in our preliminary tests on most materials including enamel, the using of h_t instead of h_p will not influence the final result.

Another independent analysis derived from the definition of hardness also supports the concept of strain rate dependence in equation 3-26[26]. As has been mentioned in equation 3-16, the definition of contact hardness, H, can be written as,

$$H = \frac{P}{A} = \frac{P}{ch^2}, \qquad (3\text{-}27)$$

where H is hardness, P is the load, h is the contact depth (and total depth, h_t, was chosen here), and c is a geometrical constant of the indenter (24.5 for perfect Berkovich tip). Equation 3-27 can be differentiated and reorganized into,

$$\frac{\dot{h}}{h} = \frac{1}{2}\left(\frac{\dot{P}}{P} - \frac{\dot{H}}{H}\right) = \dot{\varepsilon}, \qquad (3\text{-}28)$$

in which $\dot{\varepsilon}$ is the strain rate defined in equation 3-26 This equation suggests that, during the holding period of a creep test, because the force is kept constant ($\dot{P}$ =0), strain rate $\dot{\varepsilon}$ is expressed by $\dot{h} / h$. This conclusion is the same as equation 3-26.

Based on the above analysis, the creep behavior, creep rate sensitivity, m, of material can be calculated from the depth-time (h - t) curve of the creep test at maximum load. By fitting and differential h_e depth-time (h - t) curve, the indentation rate $\dot{h} = \mathrm{d}h / \mathrm{d}t$ needed by equation 3-26 can be calculated. From equation 3-27, the contact pressure (hardness, H) can be acquired. Therefore, creep rate sensitivity value of the sample can be read from the logarithmic plot of H-$\dot{\varepsilon}$ curve.

3.2 Calibration of the indenters

The calibration tests were performed using a nano-based indentation system [Ultra Micro-Indentation System, UMIS-2000, CSIRO, Australia]. A standard fused silica specimen with known elastic modulus of 72.5 GPa was chosen to calibrate a Berkovich and three spherical indenters with nominal radius of 5, 10 and 20 microns [Synton, Switzerland]. Fused silica was mounted on a metal base which contained a strong magnet to ensure adequate contact was obtained with the test base in the UMIS. More than 100 tests were done for each indenter within the load range of the system from 1-500 mN to calibrate the indenters. For the Berkovich indenter, the software generated the calibrated area function automatically. For the spherical indenter, the contact area, a, was calculated and the contact radius a determined versus contact depth of penetration, h_p, which represents the shape of the indenter tip.

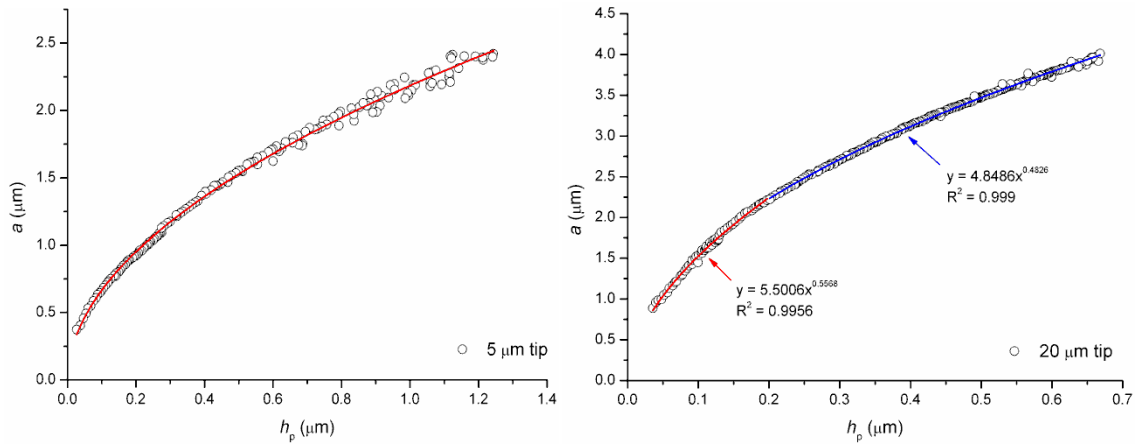

a) b)

Fig. 3-3 Plots of contact radius versus contact depth of penetration for the a) 5 μm, and b) 20 μm spherical indenter tips along with fitting equations.

The Berkovich indenter tip was calibrated with fused silica using the approach outlined by Oliver and Pharr[18]. The two spherical indenters were calibrated with fused silica using the methods described above to acquire the a-h_p curve and its functional form. The results from more than 200 individual indentation tests on fused silica for each indenter were fitted to power law functions as shown in Figures 3-3a and 3-3b. The curve generated for

the nominally 5 μm radius spherical tip (Fig. 3-3a) was fitted with the following expression:

$$a = 2.1818 h_p^{0.5151} \quad (h_p \in [0,1.3]\mu m,\ R^2=0.9975) \qquad (3\text{-}29)$$

For the nominally 20 μm radius spherical indenter, two separate fitting functions were used because a single fitting equation was not sufficiently accurate over the entire range. The curve fitting functions are:

$$\begin{cases} a = 5.5006 h_p^{0.5568} & (h_p \in [0,0.2]\mu m,\ R^2=0.9956) \\ a = 4.8486 h_p^{0.4826} & (h_p \in [0.2,0.7]\mu m,\ R^2=0.999) \end{cases} \qquad (3\text{-}30)$$

True tip radii, *R*, of both indenters at specific depths were calculated using equation (3-17). The initial contact radii of the tips were almost 5 μm and 20 μm, but thereafter the radii decreased with depth. The R^2 values associated with each equation indicate the quality of fit.

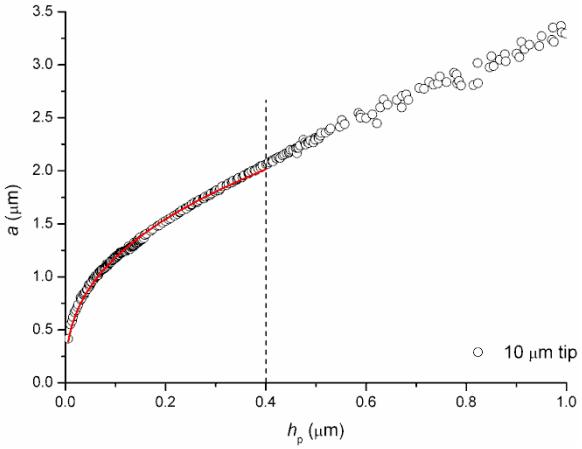

Fig. 3-4 Plots of contact radius versus contact depth of penetration for the 10 μm tip

Because of the imperfection of 10 μm indenter, we could not generate a proper equation to describe the tip shape in the full range (Fig. 3-4). It seems at the contact depth, h_p, of more than 0.4 μm, the tip becomes a conical shape. Even for the spherical part, the tip shape is not perfect. Therefore, in the following chapters, all data from this indenter were calculated with the method from equation 3-10.

The stresses and deflections arising from the contact between two elastic solids are of particular interest to those undertaking indentation testing. From Fig. 3-1, it is not difficult to see that if we plot the data of contact depth, h_p, against contact radius, a, the figure should be in the same nominal shape as contact surface of the indenter. Fig. 3-3 shows the effective shape of the indenters. It is found that the indenters have a parabolic shape rather than standard spherical. That is, the radius of spherical indenter is changing with contact depth, hp. However, Oliver and Pharr[21] have shown that the method used to calculate the contact pressure is applicable to any asymmetrical indenter, including this parabolic one.

Based on Tabor's work, the stress-strain function (H-a/R) is a unique function for a given deformable material, regardless of the nature of deformation and independent of sphere size[11]. However, reports[29-31] have shown that in micro and nano scale indentation field, indentation size effect (ISE) is a major influence on test results. That is to say, different size of indenter may lead to different results. In the case of crystalline materials this phenomenon can be explained by the concept of "geometrically necessary dislocations". Based on this concept, with the changing of the tip radius, the onset of the plastic response of the stress-strain curve may change. Moreover, enamel and dentin, which are typical anisotropic materials, may have prominent ISE. These will be important and interesting areas of future work.

3.3 Sample Preparation

Samples were collected from Sydney Dental Hospital under the ethical approval from Ethics Review Committee of Sydney South West Area Health Service with the protocol No X08-0012 & HREC Ref. 08/RPAH/25.

Healthy premolar teeth extracted for orthodontic reasons without any caries and hard tissue defects were collected from donators ranged 18-30 years old with written permit consent. After disinfection with Milton's solution for 3 min and washed with copious distill water, samples were embedded with a cold-curing epoxy resin (Epofix, Struers, Copenhagen, Denmark). The cutting directions were well selected so that the enamel prism direction was perpendicular to the top surface and parallel to the cross section as illustrated in Fig. 3.4. A low speed saw (Isomet, Buehler Ltd., Lake Bluff, USA) was used to cut the tooth under water irrigation. All the specimens were polished with two machines (Grinder-Polisher, Buechler UK Ltd., Coventry, England; RotoPol-22, Struers, Copenhagen, Denmark) to 0.6 μm alumina polishing paste (see Table 3-1). Once prepared, the tooth was briefly stored in distilled water at room temperature and the tests were conducted shortly after sample preparation. While previous work by Habelitz et al[32] has established the importance of storing enamel and dentin in Hank's solution after polishing on the subsequent nano-indentation results. The latter work used very low loads (<1.5 mN) with a sharp corner cube indenter that penetrated less than 400 nm into the surface, whereas based on previous nano-indentation investigations at loads comparable to those used in this study by Poolthong[33], there was no discernable change in the long-term stability (over three months) of the hardness and elastic modulus of enamel stored at 4°C in de-ionized water.

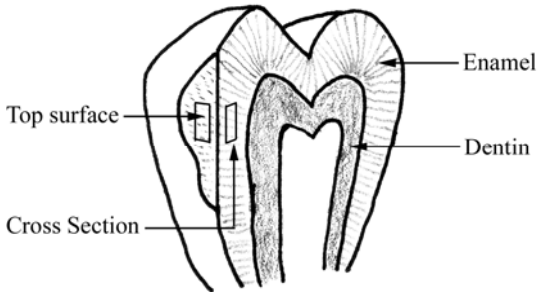

Fig. 3-5 Diagram indicating different specimen directions where indentations were made on the tooth. (Black boxes indicate the test areas.)

Table 3-1. Summary of the grinding and polishing steps

Step	1	2	3	4	5
Abrasive	Silicon-carbide	Silicon-carbide	Diamond paste	Diamond paste	Alumina paste
Grit/grain size	#500	#1000	9 μm	1μm	0.6μm
Lubricant	Water	Water	DP-Green	DP-Red	water
Rotational speed [rpm]	300	300	300	300	300
Polish time [min]	5	10	20	30	40
Ultrasonic clean time [sec]	30	30	30	30	30

The indentation experiments were performed using a nano-based indentation system (Ultra Micro-Indentation System, UMIS-2000, CSIRO, Australia). The finished specimens were mounted on metal bases with wax using a paralleling machine (Leitz, Wetzlar, Germany). The mounting base contained a strong magnet to ensure adequate contact was obtained with the test base in the UMIS. All the tests on enamel samples were done in distilled water at room temperature.

Similar as hydrogen peroxide, sodium hypochlorite can change the properties of protein by generating free radicals. Thus, some investigators believe it has potential influence on the mechanical behavior of enamel[34,35]. However, our samples were only soaked in Milton's solution briefly and have been thoroughly washed by distill water. Furthermore, the experimental regions were at least 100 μm underneath the natural surface. Therefore, it is safe to assume that brief disinfection by Milton's solution did not influence the mechanical properties of the samples significantly.

3.4 References

1. Angker L, Nockolds C, Swain MV. Correlating the Mechanical Properties to the Mineral Content of Carious Dentin--a Comparative Study Using an Ultra-Micro Indentation System (Umis) and SEM-BSE Signals. Archives of Oral Biology. 2004;49(5):369-78.
2. Angker L, Swain MV, Kilpatrick N. Characterising the Micro-Mechanical Behaviour of the Carious Dentin of Primary Teeth Using Nano-Indentation. Journal of Biomechanics. 2005;38(7):1535-42.
3. Drummond JL. Nanoindentation of Dental Composites. Journal of Biomedical Materials Research Part B: Applied Biomaterial. 2005: Early View (Online only from Wiley Interscience Journals).
4. Ge J, Cui FZ, Wang XM, Feng HL. Property Variations in the Prism and the Organic Sheath within Enamel by Nanoindentation. Biomaterials. 2005;26(16):3333-9.
5. Low D, Swain MV. Mechanical Properties of Dental Investment Materials. Journal of Material Science: Material in Medicine. 2000;11(7):399-405.
6. Mahoney EK, Rohanizadeh R, Ismail FS, Kilpatrick NM, Swain MV. Mechanical Properties and Microstructure of Hypomineralised Enamel of Permanent Teeth. Biomaterials. 2004;25(20):5091-100.
7. Poolthong S, Mori T, Swain MV. Determination of elastic modulus of dentin by small spherical diamond indenters. Dent Mater J. 2001;20(3):227-36.
8. Swain MV. Mechanical Property Characterisation of Small Volumes of Brittle Materials with Spherical Tipped Indenters. Materials Science and Engineering A. 1998;253(1-2):160-6.
9. Fujisawa N, Li W, Swain MV. Observation and numerical simulation of an elastic-plastic solid loaded by a spherical indenter. Journal of Material Research. 2004;19(12):3474-83.
10. Hertz H. Miscellaneous Papers. London: Jones and Schott, Macmillan; 1863.
11. Tabor D. Hardness of Metals. Oxford: Clarendon Press; 1951.
12. Matthews JR. Indentation hardness and hot pressing. Acta Metallurgica. 1980;28:311-8.
13. Hill R, Storakers B, Zdunek AB. A Theoretical Study of the Brinell Hardness Test. Proc R Soc (Lond). 1989;A423:301-30.
14. Lawn BR, Deng Y, Lioyd IK, Janal MN, Rekow ED, Thompson VP. Materials Design of Ceramic-Based Layer Structures for Crowns. Journal of Dental Research. 2002;81(6):433-8.
15. Lawn BR, Deng Y, Thompson VP. Use of contact testing in the characterization and design of all-ceramic crownlike layer structures: A review. Journal of Prosthetic Dentistry. 2001;86:495-501.
16. Lawn BR, Pajares A, Zhang Y, et al. Materials Design in the Performance of All-Ceramic Crowns. Biomaterials. 2004;25(14):2885-92.
17. Peterson IM, Pajares A, Lawn BR, Thompson VP, Rekow ED. Mechanical Characterization of Dental Ceramics by Hertzian Contacts. Journal of Dental Research. 1998;77(4):589-602.
18. Oliver WC, Pharr GM. An improved technique for determining hardness and elastic modulus using load and displacement sensing indentation experiments. Journal of Material Research. 1992;7(6):1564-83.
19. Snedden IN. The reguation between load and penetration in the axisymmetric Bossinesq problem for a punch of arbitrary profile Int J Engng Sci. 1965;3:47-57.
20. Field JS, Swain MV. A simple predictive model for spherical indentation. Journal of Material Research. 1993;8(2):297-305.
21. Oliver WC, Pharr GM. Measurement of hardness and elastic modulus by instrumented indentation:

Advances in understanding and refinements to methodology. Journal of Material Research. 2004;19(1):3-20.

22. Suganuma M, Swain MV. Simple Method and Critical Comparison of Frame Compliance and Indenter Area Function for Nanoindentation. Journal of Material Research. 2004;19(12):3490-502.
23. Fischer-Cripps AC. Nanoindentation. New York: Springer; 2002. 110-1 p.
24. Sakai M. Energy principle of the indentation-induced inelastic surface deformation and hardness of brittle materials Acta Metallurgica et Materialia 1993;41(6):1751-8.
25. Stilwell NA, Tabor D. Elastic recovery of conical indentations. Proc Phys Soc. 1961;78:169-79.
26. Lucas BN, Oliver WC. Indentation power-law creep of high-purity indium. Metallurigical and Materials Transactions. 1999;30A(3):601-10.
27. Norton FH. Creep of Steel at High Temperatures. New York: McGraw-Hill; 1929.
28. Mayo MJ, Nix WD. A micro-indentation study of superplasticy in Pb, Sn, and Sn-38 wt% Pb. Acta Metall. 1988;36(8):2183-92.
29. Bull SJ, Page TF, Yoffe EH. An explanation of the indentation size effects in ceramics. Phil Mag Lett. 1989;59(6):281-8.
30. Nix WD, Gao H. Indentation size effects in crystalline materials: a law for strain gradient plasticity. J Mech Phys Solids. 1998;46(3):411-25.
31. Qian LM, Li M, Zhou ZR, Yang H, Shi XY. Comparison of Nano-Indentation Hardness to Microhardness. Surface & Coatings Technology. 2005;195:264-71.
32. Habelitz S, Marshall SJ, Marshall GW, Balooch M. Mechanical properties of human dental enamel on the nanometre scale. Archives of Oral Biology. 2001;46:173-83.
33. Poolthong S. Determination of the mechanical properties of enamel, dentin and cementum by an ultra micro-indentation system [PhD Thesis]. Sydney: University of Sydney, 1998.
34. Attin T, Muller T, Patyk A, Lennon AM. Influence of different bleaching systems on fracture toughness and hardness of enamel. Operative Dentistry. 2004;29(2):188-95.
35. Hairul Nizam BR, Lim CT, Chng HK, Yap AUJ. Nanoindentation study of human premolars subjected to bleaching agent. J Biomech. 2004;38:2204–11.

Chapter 4

Nanoindentation Analysis of Enamel and Dental Materials

General mechanical property characterization of materials has become an essential requirement for their successful application as structural elements. For metallic materials, these properties are well described and numerous handbooks are available enabling comparison for structural design purposes. In the field of dental materials, such properties, especially stress-strain behaviour, are not available for most materials. This deficiency is considered to be a major short coming especially with the wide spread use of ceramics in dentistry, the elastic-plastic mechanical properties of these materials is of considerable interest.

Among all the mechanical properties, stress-strain behaviour is one of the most important because this property determines the deformation response of the material. At the same time, the ductility and yield ability are also important for the application of the material as a structural element undergoing contact loading. Moreover, this property has a close relationship with the wear or abrasive nature of the material, which is very important for dental material. For the new generation of dental ceramics which exhibit quasi-plastic behaviour, quantifying this property becomes more important.

With the methods described in chapter 3, elastic modulus, hardness and the stress-strain curve of enamel were investigated and compared with some typical dental materials.

This chapter is based on the following published manuscripts:

- HE, L.H. & SWAIN, M.V. (2007) Nanoindentation derived stress-strain properties of dental materials. *Dental Materials*, 23, 814-821.
- HE, L.H. & SWAIN, M.V. (2007) Enamel --- a “metallic-like” deformable biocomposite. *Journal of Dentistry*, 35, 431-437.

4.1 Material and Methods

Several commonly used dental materials were chosen for comparison with sound tooth enamel extracted for orthodontic reasons. Sintered hydroxyapatite (HAP) was selected as a ceramic equivalent of enamel. The dental ceramics were Cerec®2 VitaBLOCS® Mark II CAD/CAM ceramic (A3,5C, V5-12) and its veneer porcelain Vita VM9 (Base Dentin, 1M1) [VITA Zahnfabrik, Germany]. The metal materials were cast alloy [Wiron® 99, BEGO, Germany], type IV gold alloy [ITI® Straumann, Switzerland], commercial pure Titanium [T-alloy, GC, Japan] and amalgam. The amalgam sample came from a tooth with a class I amalgam filling extracted because of periodontal disease. Optical microscopy observation on the mesial-distal section of the sample illustrated that the filling was clinically successful.

Elastic modulus and hardness of specimens were measured with the calibrated Berkovich indenter. The force applied during testing ranged form 10 to 300 mN, and was dependent upon the evaluated material. The software calculated elastic modulus and hardness as a function of penetration depth, h_p, for each indentation. At least 15 indents at different forces were done on each material to acquire the average values.

All the samples were indented with the spherical indenter at loading forces from 1 to 400 mN. The distance between two indents on the surface of the sample was more than 40μm to avoid the influence of residual stresses from other impressions. The *H-a*/*R* curves were generated using the methods outlined above

After indentation testing an SEM (XL-30, Philips, Netherlands) was used to check the deformation and damage associated with the indents. All the specimens were ultrasonically cleaned with ethanol and then gold coated. Both secondary electron detector and back-scattered electron detectors were selected for the SEM observation. Amalgam was also investigated with energy dispersive X-ray analysis (EDX) to determine its composition using an area collection method at 1250 magnification. EDX composition analysis was repeated 5 times at different areas and the average and standard deviation were calculated and reported in the next section.

4.2 Results

4.2.1 Sample spherical load-displacement curves

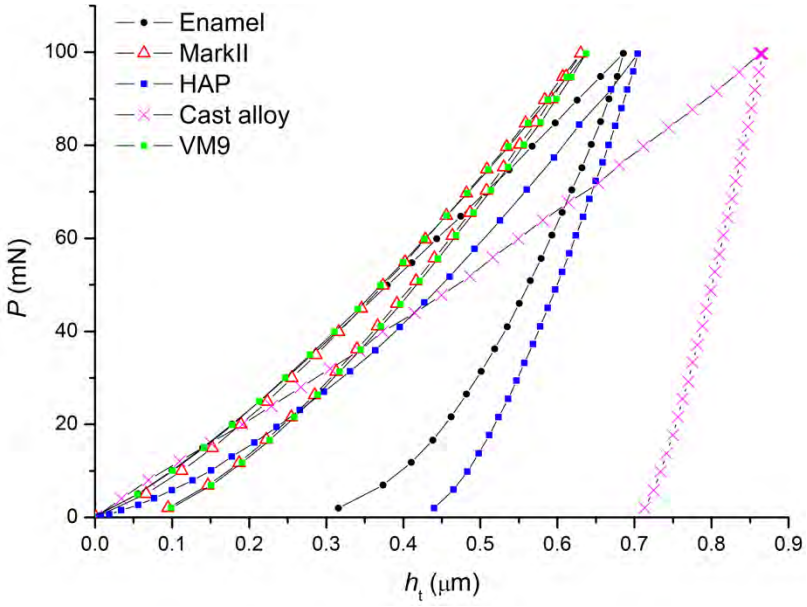

Fig. 4-1 Comparison of P - h_t curve of three different dental materials and enamel under 100mN loading force

Load-displacement data is the basic response acquired from the depth-sensing indentation system and is the loading-unloading history of the sample. Fig. 4-1 illustrates typical load-unloading curves of four materials indented to a maximum force of 100mN. Dental ceramics showed mostly elastic recovery upon unloading. In comparison with dental ceramics, the metallic alloy showed almost a totally plastic response. Enamel, as a structure with both inorganic and organic composition, has the response between elastic and plastic.

4.2.2 Elastic modulus and hardness

The indentation elastic moduli and hardness' measured are listed in table 4-1. Here, the indentation hardness value is the contact pressure of the indenter on the surface of the sample. Indentation elastic modulus, E_{eff}, has the following relationship with the true elastic modulus of the material, namely: $\frac{1}{E_{\text{eff}}} = \frac{1-\nu^2}{E} + \frac{1-\nu'^2}{E'}$, E, E' and ν, ν' are Young's modulus and Poisson's ratio of specimen and diamond indenter. We assume E' and ν' as 1050 GPa and 0.07, respectively. The values of our results are within the normal range of other reports[1,2].

The alloy has the highest elastic modulus among all the samples. Enamel has a higher elastic modulus than ceramics. As the veneer part of the ceramic structure, VM9 has a slightly lower elastic modulus than its core, Mark II. When it comes to hardness, ceramics have the highest value of nearly 10GPa, which is double that of the enamel. The amalgam has the lowest hardness of around 2 GPa.

At the same time, based upon Tabor's theory and the relationship $\tan\beta \approx \sin\beta \approx a/R$, we calculated the effective hardness from spherical indenter data, regarding the effective angle of the Berkovich indenter as 70.3 °. The values are similar for the hardness value acquired from Berkovich indenter and spherical indenter.

Table 4-1 Indentation elastic modulus and hardness of different materials

Material	Elastic modulus, E_{eff} (GPa)	Hardness, H (GPa)	Effective Hardness (GPa)
Enamel	94.1 ± 5.4	4.2 ± 0.2	5.3
Hydroxyapatite	130.0 ± 4.7	8.1 ± 0.1	8
Mark II	78.9 ± 2.94	10.64 ± 0.46	11.5
VM9	65.52 ± 2.89	9.5 ± 0.35	8.5
Amalgam	57.6 ± 9.2	2.1 ± 0.5	1.9
Cast alloy	209.8 ± 9.8	3.2 ± 0.1	4.9
Gold alloy	122.3 ± 4.5	3.5 ± 0.1	3.7
Titanium	145.1 ± 2.9	2.8 ± 0.2	2.5

4.2.3 stress-strain relationship

Based on Tabor's empirical relationship[3] and the more recent work by Lawn and colleagues[4,5], *H-a/R* curves can be used to represent the stress-strain relationship of materials. In Fig. 4-2, the elastic part of the materials (short doted lines) were calculated with Hertz equation: $H = \left(4E_{eff}/3\pi\right)a/R$, in which E_{eff} of each material was read from Table 1. The numerical predictions of elastic responses of materials coincided very well with the real spherical indentation data, especially for HAP. Fig. 4-2 shows that, although it's major component is hydroxyapatite, enamel displayed similar stress-strain responses

to that of the metallic materials, especially cast alloy and gold alloy rather than HAP, which had a well defined yield point at ~7 GPa. Enamel showed a smooth stress-strain curve without any prominent elastic-plastic transition point. It was not possible to predict the initial elastic response of enamel with the Hertz equation because, in our preliminary tests, even with very small forces with a larger radius spherical indenter, no pure elastic responses were found. Also, HAP had much higher stress-strain curve than enamel. The flat horizontal stress-strain response beyond yielding for titanium and amalgam indicate that these two materials did not appear to exhibit work-hardening.

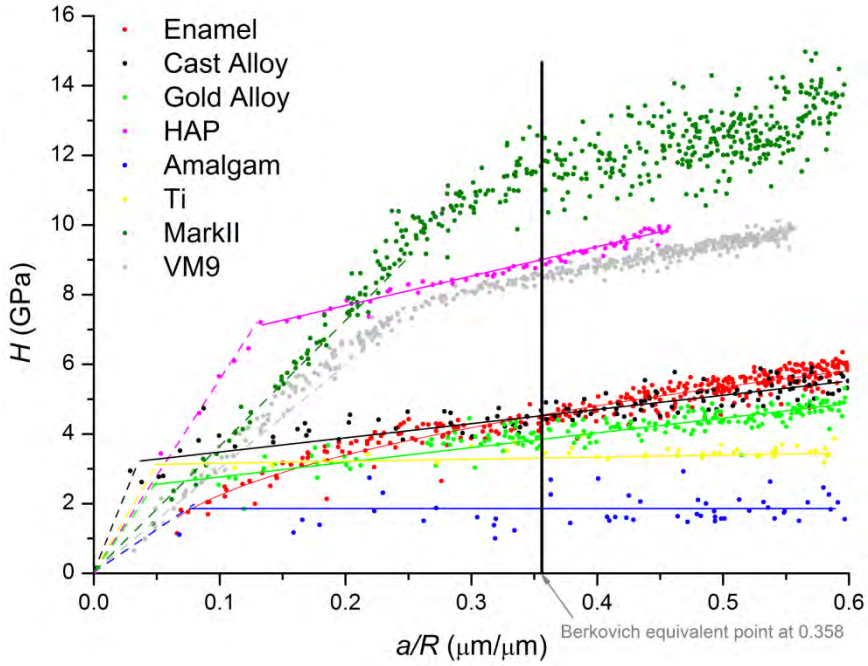

Fig. 4-2 Stress-strain (*H-a/R*) relationship of different materials. (Solid lines represent plastic part and short dots lines represent elastic part of materials, which was calculated from Hertz equation.)

4.2.4 Contact yield point

From equation (1), within the elastic limit, the contact depth h_p and total depth h_t have a relationship of $h_p/h_t = 0.5$. With the increasing of loading force, the total depth increases gradually. When the stress-strain response of the material enters the plastic zone, the aforementioned relationship no longer holds and the ratio of h_p over h_t will increase. Therefore, theoretically, from the figure of h_p/h_t-H, we can read the yielding strength of the material (see Fig. 4-3). Within the low contact pressure or elastic region, both

ceramics show a trend of slightly decreasing h_p/h_t values from nearly 0.5 to 0.45. Nevertheless, in an effort to make use of the acquired data, it was decided to select the point at which the shape of curve changed dramatically to represent the yielding point from elastic to plastic. The arrow in the figure indicates the points. The yielding contact pressure is approximately 7GPa for VM9 porcelain and near 10GPa for Mark II ceramic.

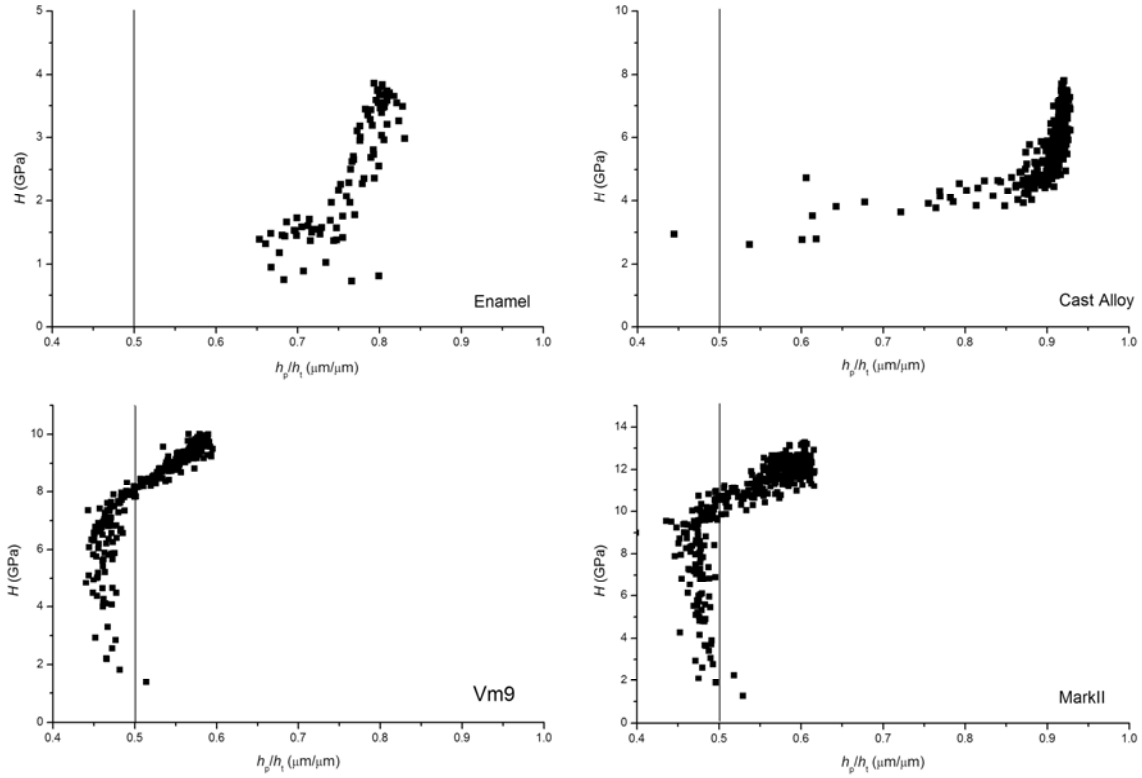

Fig. 4-3 h_p/h_t-H curve of dental materials

4.2.5 SEM analysis

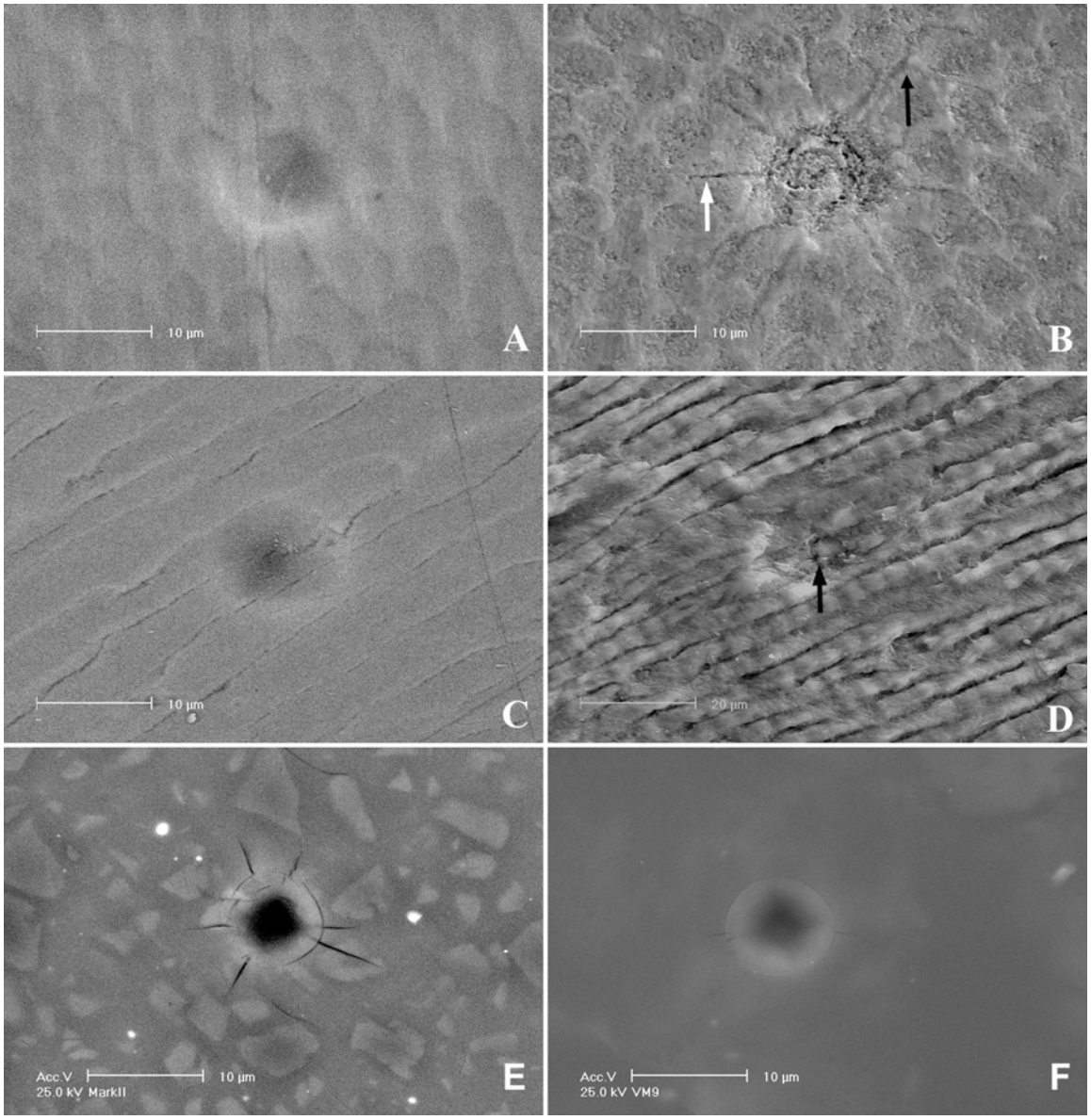

Fig. 4-4 SEM observations of the nominally 10 µm spherical indenter residual impressions on enamel (A-D) after loading to 350mN and dental ceramics (E is MarkII and F is VM9) after loading to 450mN. A is polished and B is etched (37% H_3PO_4 gel for 5 seconds) top surface, while C is polished and D is etched (37% H_3PO_4 gel for 5 seconds) cross-sectional surface of enamel. Arrows indicate cracks and damage which are considered in the discussion.

Fig. 4-4 summarizes the SEM images of spherical indents on the surface of both directions of enamel specimen with images A and B from the top surface while C and D are from the cross section surface. The maximum force for all indents in the figure was

350mN. These observations show that human enamel has a typical prism diameter of approximately 4 to 5μm and the thickness of organic rich sheath of nearly 1μm. Without etching, all indents looked smooth (A and C) and the diameter of the residual impression is nearly 10μm. This value is very similar to that determined from analysis of the force-displacement data using the expressions given in section 2.1. After being etched using 37% H_3PO_4 gel for 5 seconds, radial cracks were seen on the top surface (see B). Most of these radial cracks occurred within the sheath area between the prisms. Ring like cracks and across prism cracks within, and at the periphery of the contact area, are observed on the etched surface of the indented cross section (D).

Fig. 4-4 E and F are SEM photos of spherical indents on the surface of Mark II and VM9 specimen. Both pictures show cracks generated by the spherical indenter. For Mark II ceramic, the indenter produced not only cone cracks but also radial cracks. VM9, in contrast, had a damage mode of mainly cone cracks. From the figure E we can also see that Mark II ceramic contains many particulates in its structure. It is interesting to notice that indentation induced radial cracks pass through these particles. VM9, on the other hand, has a homogeneous structure.

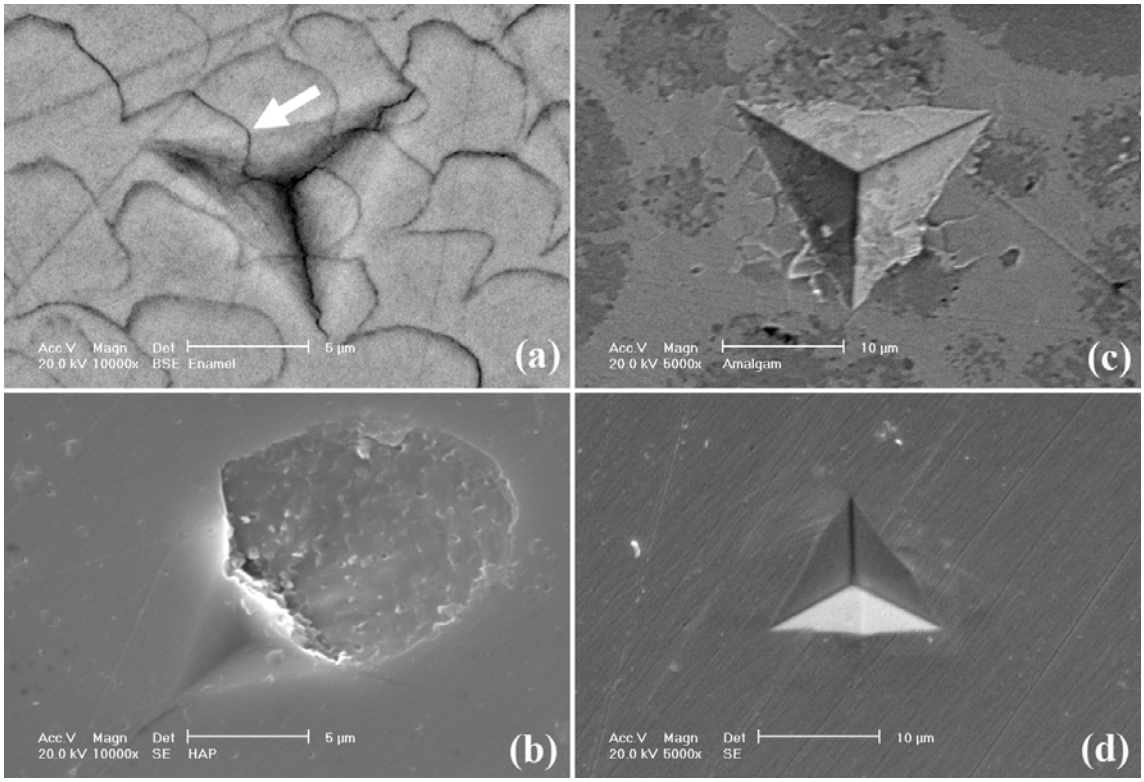

Fig. 4-5 SEM pictures of Berkovich indenter impressions on different materials: (a) enamel after 250 mN loading. Surface was etched with a mild polyacrylic acid (10%) solution (Dentin Conditioner Liquid, GC, Japan) for 30 seconds. (b) HAP after 200mN loading. (c) Amalgam after 150 mN loading, and (d) gold alloy after 250 mN.

Fig.4-5 compares the residual indentation impressions and surrounding deformation for different materials. HAP exhibited typical brittle behaviour under sharp indentation. At loads of 200 mN, radial and lateral cracks formed with the latter extending to the surface resulting in chipping of the sample (Fig. 4-5b). In contrast, enamel showed residual deformation without any prominent cracks (Fig. 4-5a). The white arrow in Fig. 4-5a illustrates that even at a prism gap at the boundary of the indent impression, no crack formation occurred. Because of its low hardness, amalgam had larger indents at lower forces (Fig. 4-5c). Also, as is typical with plastic metallic materials such as gold alloy (Fig. 4-5d), no cracks were detected around the indents in amalgam. Because of the morphological similarities, indentation impressions on other materials were not shown.

4.2.6 EDX analysis of amalgam

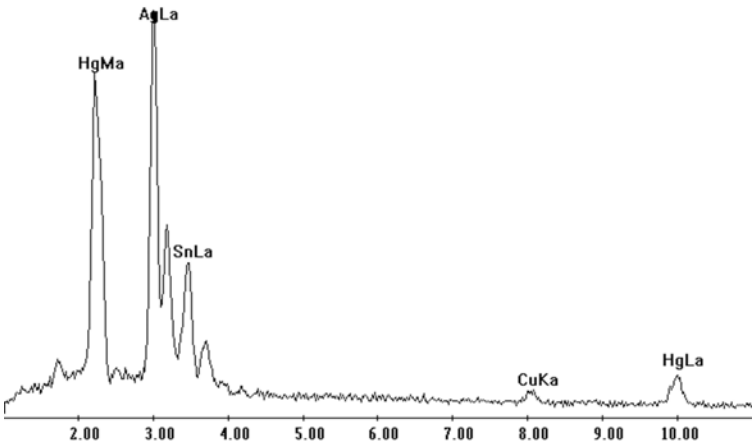

Fig. 4-6 Sample EDX spectra of amalgam sample showing the major Hg, Ag and Sn peaks with minor amounts of Cu.

As shown in Fig. 4-6, EDX spectra of amalgam indicated that, the main elements are Hg, Ag and Sn, with just a little Cu. Elemental analysis indicated the composition of the sample is Ag 42.48±0.69%, Hg 33.89±0.7%, Sn 21.74±0.62% and Cu 1.9±0.09%. This product may be considered a low copper amalgam. The dark area of amalgam contained mainly Ag and Sn while the bright area only contained Hg and Ag.

4.3 Discussion

In the field of materials evaluation, one needs different parameters to rank materials for different aspects. Elastic modulus, or the ratio of stress to strain below the proportional limit, can reflect the elastic deformation ability of a material; the hardness of a material is usually considered as the resistance to permanent indentation deformation; while the stress-strain response reflects the elastic-plastic mechanical behaviour of a material usually on a large scale and creep behaviour is a reflection of viscous property of a material. These basic parameters reflect the mechanical properties of materials and, therefore, may be used to compare and select materials for specific applications.

4.3.1 Load-displacement curve

The use of spherical tipped indenters enables the initial elastic response prior to commencement of elastic-plastic displacement during loading. On the other hand, the unloading procedure is generally regarded as a purely elastic process. From the energy point of view, the area between the loading and unloading curve represents the irrecoverable energy loss (W_i) because of plastic deformation. The total energy (W_t) is the area under the loading curve, represents the total energy expended in forming the indentation, and includes both the elastic and plastic components. The energy absorption ratio is calculated from $W_i/W_t \times 100\%$. Wiron alloy has the highest energy absorption ratio while the ceramic materials have the lowest ratio. This means that the alloy has the capacity to absorb severe localized loading by deformation thereby reducing the contact stresses with an opposing tooth during contact. In contrast, ceramic has limited ability to deform and so develops high-localized stresses, which may be harmful to the opposing dentition. Details of energy absorption in enamel, will be considered in section 1 of chapter 6.

4.3.2 Elastic modulus and hardness

The results of the elastic modulus and hardness of enamel are a little higher than the value from Habelitz at al.[6] where an elastic modulus of 87.5±2.2 GPa and the hardness of 3.9±0.3 GPa were reported. This difference may come from the different depth of enamel below the surface investigated. Cuy et al.[2] have shown that the mechanical response of

enamel depends upon location, chemical composition, and prism orientation. The hardness value of enamel decreases from more than 6GPa at the top surface of the tooth to less than 3GPa near the Enamel-Dentin Junction area. The current investigation was done very near the top lingual surface of the premolar tooth. Based on the conclusion of Cuy et al., the hardness value of this area should be somewhat higher than the inner part of the enamel. On the other hand, since the functional area of a tooth or denture should be the occlusal surface area, the investigation of mechanical properties of this area will have more practical significance than inner parts.

For the cast dental alloy Wiron® 99, the elastic modulus is very similar to that listed in the manufacturer's data sheet, namely 205GPa. In Lawn's paper[7], the elastic modulus of Mark II is 68GPa. David[8] also reported that the elastic modulus of this material is much closer to that of tooth structure. All these results coincide with those of the current study very well. This suggests that the UMIS system and the area function created are reliable.

4.3.3 Stress-strain response

In the theoretical section (Chapter 3), Tabor's equation to convert H-a/R value into σ-ε value was considered. Should we follow Tabor's idea and regard the later value as the true stress-strain curve? To answer this question, two things should be made clear. Firstly, Tabor's work is an empirical relationship based on experimental observation for metallic materials. It is still not clear if this relationship applies to brittle materials. Secondly, the contact stress distribution is complex and it is difficult to compare this type of stress-strain relationship with uniaxial tensile/compression test. Herbert et al.[9] for an aluminium alloy have shown that the indentation derived stress-strain relationship has a big difference to the uniaxial one. This maybe anticipated as a consequence of the indentation size effect and the respective volumes of material involved in the two types of tests. Recently, some researchers have made progress in relating spherical indentation stress-strain curve with the uniaxial tests for metallic materials[10-12]. It is uncertain whether this method is universal or not and if it can be extended into the ceramic field. Therefore, in this work, we retain the data as H-a/R curves and these plots adequately represent the indentation stress-strain response of different materials.

In Table 4-1, we compared the hardness values from Berkovich (Hardness) and spherical indenters (Effective Hardness) by using Tabor's equation. The results are similar between the two kinds of indenters. This implies that the a/R values are reliable. The small difference may come from the approximation of the relationship that is $\tan\beta \approx \sin\beta = a/R$. Moreover, Tabor's expression is an empirical one which is not absolutely accurate.

From the standpoint of structure reliability and integrity, two issues are important. The first one is the need for materials with higher strength as well as a better elastic response. Materials with high elastic to plastic transition point (yield point) can bear bigger force within its elastic limits. In the oral functional environment, because ceramic has a higher yield point than enamel, we can predict that the ceramic structure (crown/bridge) can sustain higher bite forces than enamel provided it does not fracture. Therefore, this kind of material and its structure is strong enough to serve as dental restorations. Moreover, Mark II, as the core material, has a higher yield strength and elastic limit than its veneer part, VM9. This coincides with the structural design criteria, which requires a stronger core to support the whole structure. The higher yield strength of Mark II may come from the ceramic particles dispersed in the glass matrix. Of course, other factors that influence the integrity of a structure include fatigue and fracture toughness. Second, when it comes to the contact damage and surface fatigue wear, the condition may be totally different. At the micro scale level, the actual contact surface consists of numerous asperities because of surface roughness. For each contact pair over the contact area, the two opposite parts bear the same force. If the difference of mechanical properties, especially the stress-strain property, between the contact pair is too big, the soft one will be destroyed while the hard one remains intact. Therefore, the component with lower stress-strain response will wear. Clinically, if Mark II serves as an inlay in posterior teeth, it will be in contact directly with the opposing teeth. During the surface contact period, the contact pressure on the contact point may exceed the elastic limit of enamel while still remaining within the elastic range of ceramic. Under this condition, permanent plastic deformation or even damage may occur on the surface of enamel. Thus, the surface of the opposing teeth will be at risk of excessive wear. However, other researchers[13,14] have suggested that mechanical properties are only one factor that influence the wear between enamel and dental restorations. Moreover, it is becoming increasingly clear that hardness may not be

a good predictor of potential abrasivity of dental materials[15]. Wear properties of materials, especially of ceramics, also depend upon microstructure, fracture toughness, and the mechanism of contact damage[15-17]. In general, contact damage characteristics are known to be a function of the fracture toughness of ceramics, microstructural scale (grains, filler phases, pores), and local property variations in its microstructure[15,17]. The stress-strain response provides a novel means to re-evaluate the study of wear and contact damage. Future work shall attempt to correlate the stress-strain property with the abrasive ability of dental materials.

4.3.4 Contact yield point

The results in Fig. 4-3 indicate that the ratio of the contact depth to total indenter displacement is a function of the contact pressure rather than a constant within the elastic range of the ceramic materials. Unfortunately, the ratio is slightly less than anticipated from Hertz's contact theory. This is similar to what Herbert et al. saw with the aluminium alloy 6061-T6[9]. Understanding the cause of these different results will be an integral part of future work. However, the trend of the curves also gives us some indications about the yield of the materials investigated. The arrows illustrate the inflexion points of the ratio, which may be regarded as the yield point of the materials. The yield contact pressure should be approximately 7GPa for VM9 porcelain and near 10GPa for Mark II ceramic, which coincides with the trend of the H-a/R curves.

For Wiron alloy and enamel, plastic deformation dominates their indentation response, as even with an initial loading force of 5mN, the contact pressure exceeds the elastic limit of these materials. The initial ratio of h_p/h_t is larger than 0.6 and we cannot obtain the elastic part of the H-a/R curve with this spherical indenter. With a larger spherical tip, it should be possible to investigate the elastic response range of these materials. However, with the help of Hertz equation, we can predict the transition point of these plastic materials like that drawn in Fig. 4-2. The transition point from elastic to plastic may be nearly 2GPa.

4.3.5 SEM results

Fig. 4-4B shows the presence of radial cracks surrounding the contact impression of enamel. Two types of radial cracks may be distinguished in the picture. The first and most

predominant types are inter-rod cracks growing along the sheath and propagating between prisms (black arrow in Fig. 4-4B). The second types are the inner-rod cracks that propagate within the prisms (white arrow in Fig. 4-4B). The first type of cracks indicate that fracture occurred around the enamel prisms rather than through them. This is in agreement with other tests on composite materials which showed that cracks tend to follow weak interfaces[18,19] as well as with previous observations on enamel by Rasmussen et al.[20] and White et al.[21]. The second form of cracks may have resulted from the acid etching procedure. After loading and unloading, residual stress accumulated in the enamel structure, especially in highly mineralized prism. During acid etching, the surface of the impression was damaged and the balance of residual stress changed and as a result a crack may propagate within the prism. The issue of indentation residual stress within enamel will be taken up in Chapter 8.

On the cross section surface, the prisms and apatite crystallite directions are perpendicular to the loading force and act as strong integral units or fibres. Every prism is wrapped by a very thin organic sheath. The deformation in this direction is similar to the bending of beams. By comparing pictures C and D in Fig. 4-4, it is clear that, after surface etching, substantial damage almost twice that of the surface impression is evident. In picture D, cracked prisms within the contact area had been exposed by acid and ring-like cracks restricted in one prism are present (Black arrow in Fig. 4-4D).

These preliminary observations of cracks in the indented surfaces indicate that the fracture mechanisms of enamel are influenced by the prism-sheath unit structure as also proposed by other researchers[21]. Further study is required to explore the exact fracture mechanisms of enamel especially inter prism fracture.

Cerec2 Mark II ceramic is a feldspathic ceramic with a composition of SiO_2、Al_2O_3、K_2O、Na_2O SiO_2 and Al_2O_3 sintered together and develops a microstructure with particulates of 1-7 μm diameter, as observed by SEM. Fig. 4-4E shows that these particles are well distributed in the glass matrix. No microcracks were found along the interface of the particle and the matrix. It is these particles which are considered to cause the scatter of the indentation data in Fig. 4-2. VM9, in contrast, has more glass phase than Mark II. Therefore, Fig. 4-4F shows a homogenous structure and less scatter of data than in Fig. 4-

4E. The damage mode observed in Fig. 4-4E and F are similar to Lawn's results[7,22,23], which showed that cone cracks are a common damage mode and in less brittle, tougher ceramics, the ‘quasi-plasticity’ of the materials may lead to a ‘yield’ zone of distributed shear microcracks.

4.3.6 Differences between enamel and HAP

HAP, a typical crystalline ceramic material, is composed of sintered small apatite crystals with minimal dislocations present within crystal lattices and at the boundary of adjacent crystals. This predominant ceramic character determines the mechanical properties of HAP as a hard and brittle material. The indentation stress-strain behaviour of HAP was similar to that previously reported for a range of porcelain and restorative ceramic materials[24].

Although the primary component of enamel is also hydroxyapatite, the mechanical responses of enamel were totally different to those of pure HAP, such as lower elastic modulus and hardness (Table 4-1), lower stress-strain response (Fig. 4-2), and no brittle cracks about indentation impressions (Fig. 4-4 and 4-5). These results confirm the declaration that the hierarchy of enamel structure and the small protein fragments within the enamel may regulate the mechanical properties of enamel, as mentioned in literature review (Chapter 2).

Protein films act as a cushion between the crystallites and prisms. The inelastic properties of proteins like bio-polymers can help to dissipate and redistribute the stresses and protect crystallites from fracture[25]. Structural hierarchy also regulates the mechanical properties of enamel at the prism level. Nano-scale investigations[6,26] have shown that, compared to those in the head area of the rods, elastic moduli and hardness were lower in the tail area and in the inter-prism enamel, which can be attributed to changes in crystal orientation and the higher content of soft organic tissue in these areas. Moreover, the staggered mineral crystallites may deflect and bridge the cracks and strengthen the bulk material on a large scale. As a result, enamel has higher fracture toughness than pure hydroxyapatite[27]. This has also been confirmed in the SEM pictures which showed that even the sheath area at the contact boundary, the presumed weak area, did not form any cracks (white arrow in Fig. 4-5a).

4.3.7 The metallic-like deformation properties of enamel

From a functional point of view, enamel needs metallic-like deformation properties to withstand millions of cyclic occlusal loadings. A comparable example to understand this requirement is, for some mechanical structures needing to sustain cyclic loadings such as bridge frames, where tough ductile materials are prefered rather than stiff but brittle ceramics. The reason is metals are more plastic deformable and flaw insensitive and are better able to withstand random overloads as cyclic-force bearing structures. During its evolutionary development, enamel has been optimized structurally and endowed with metallic-like deformation properties to sustain multiple impact and sliding contact events.

Enamel has similar elastic modulus, hardness and stress-strain responses to those of widely accepted dental metallic (gold alloy and amalgam) materials. By comparing with hard brittle materials such as ceramics, lower hardness values of metals mean these materials have better plastic deformation abilities. Plastic metallic materials can dissipate more energy before catastrophic failure. SEM comparative observations also illustrated that elastic-plastic materials such as enamel, gold alloy and amalgam could survive under bigger loading forces without cracking. Moreover, enamel showed very similar stress-strain response to those of metals rather than ceramics. From these perspectives, metallic materials may be more suitable than ceramics for dental fillings and crown/bridge because of similar basic mechanical responses.

Previous studies have shown that gold alloy causes less wear on the opposing dentition than dental ceramics[28-30]. This statement is supported by our observations (Fig 4-2) of the stress-strain relationship of a number of dental ceramic materials[24], where it is shown that the onset of non-linear behaviour occurred at much higher stress levels than enamel. It is thus apparent that the stress-strain properties, which reflect the hardness, have a close relationship with the wear behaviour of materials and materials with similar stress-strain response as enamel may have less abrasive or better protective effects on opposing teeth. The detailed relationship between stress-strain response and wear property of materials will be an interesting direction of future studies.

4.4 Conclusions

From the nanoindentation investigation on enamel and the comparison with other dental materials, the following conclusions are possible:

- Although some newly developed dental ceramics have similar elastic moduli to that of enamel, the hardness of these ceramic products is still much higher than enamel;
- In contrast, despite the higher elastic modulus, dental alloys have very similar hardness as enamel;
- Enamel has similar stress-strain relationship as dental alloys which are much lower than dental ceramics;
- In general, enamel behaves more like a metallic rather than a ceramic material . The evidence for this is its metallic like stress-strain curve and indentation deformation pattern from SEM observations.

These conclusions may need some attention from clinical practitioners. To avoid excessive wear damage of opposing teeth, it is better to choose materials with similar stress-strain behaviour as enamel. Elastic modulus can not be the only criteria in choosing materials.

4.5 References

1. Boyer R, Welsh G, Collings EW (eds). Materials properties handbook: titanium alloys. Materials Park, OH: ASM International; 1994.
2. Cuy JL, Manna AB, Livi KJ, Teaford MF, Weihs TP. Nanoindentation Mapping of the Mechanical Properties of Human Molar Tooth Enamel. Arch Oral Biol. 2002;47:281-91.
3. Tabor D. Hardness of Metals. Oxford: Clarendon Press; 1951.
4. FischerCripps AC, Lawn BR. Indentation stress-strain curves for "quasi-ductile" ceramics Acta Mater. 1996;44(2):519-27
5. Hu XZ, Lawn BR. A simple indentation stress–strain relation for contacts with spheres on bilayer structures Thin Solid Films. 1998;322(1-2):225-32
6. Habelitz S, Marshall SJ, Jr GWM, Balooch M. Mechanical properties of human dental enamel on the nanometre scale. Arch Oral Biol. 2001;46:173-83.
7. Lawn BR, Deng Y, Thompson VP. Use of contact testing in the characterization and design of all-ceramic crownlike layer structures: A review. J Prosth Dent. 2001;86:495-501.
8. David SB, LoPresti JT. Tooth-Colored Posterior Restorations Using a Cerec Method (CAD/CAM)-Generated Ceramic Inlays. Compend Contin Educ Dent. 1994;15:802.
9. Herbert EG, Pharr GM, Oliver WC, Lucas BN, Hay JL. On the measurement of stress-strain curve by spherical indentation. Thin Solid Films. 2001;398-399:331-5.
10. Beghini M, Bertini L, Fontanari V. Evaluation of the Stress-Strain Curve of Matallic Materials by Spherical Indentation. International Journal of Solids and Structures. 2006;43:2441-59.
11. Taljat B, Zacharia T, F K. New analitical procedure to determine stress-strain curve from spherical indentation data. International Journal of Solids and Structures. 1998;35:4411-26.
12. Zhao M, Ogasawara N, Chiba N, Chen X. A New Approach to Measure the Elastic-Plastic Properties of Bulk Materials Using Spherical Indentation. Acta Materialia. 2006;54:23-32.
13. Mair LH, Stolarski TA, Vowles RW, Lloyd CH. Wear: mechanisms, manifestations and measurement. Report of a workshop Journal of Dentistry. 1996;24:141-8.
14. Oh W-s, DeLong R, Anusavice KJ. Factors affecting enamel and ceramic wear: A literature review. J Prosth Dent. 2002;87:451-9.
15. Larsen-Basse J. Abrasive Wear of Ceramics. Friction and Wear of Ceramics. New York: Dekker; 1994. 99-115 p.
16. Gentile MJ, Kelly JR. Intra-Oral Wear Mechanisms on Dental Ceramics. J Dent Res. 1996;75:50, Abstr. A264.
17. Kelly JR, Nishimura I, Campbell SD. Ceramics in Dentistry: Historical Roots and Current Perspectives. J Prosth Dent. 1995;75:18-32.
18. Rice JR. Elastic fracture mechanics concepts for interfacial cracks. J Appl Mech. 1988;55:98-103.
19. He MY, Hutchinson JW. Crack deflection at an interface between dissimilar elastic materials. Int J Solids Struct. 1989;25:1053-67.
20. Rasmussen ST, Patchin RE, Scott DB, Heuer AH. Fracture properties of human enamel and dentin. J Dent Res. 1976;55:154-64.
21. White SN, Luo W, Paine ML, Fong H, Sarikaya M, Snead ML. Biological organization of hydroxyapatite crystallites into a fibrous continuum toughens and controls anistropy in human enamel. J Dent Res. 2001;80(1):321-7.
22. Lawn BR, Deng Y, Lioyd IK, Janal MN, Rekow ED, Thompson VP. Materials Design of Ceramic-Based Layer Structures for Crowns. J Dent Res. 2002;81(6):433-8.
23. Lawn BR, Pajares A, Zhang Y, et al. Materials Design in the Performance of All-Ceramic Crowns. Biomaterials. 2004;25(14):2885-92.
24. He LH, Swain MV. Nanoindentation derived stress-strain properties of dental materials. Dental Materials. 2006;27:4388-4398.
25. Gao H, Ji B, Jäger IL, Arzt E, Fratzl P. Material become insensitive to flaws at nanoscale: Lessons from nature. PNAS. 2003;100(10):5597-600.
26. Ge J, Cui FZ, Wang XM, Feng HL. Property variations in the prism and the organic sheath within enamel by nanoindentation. Biomaterials. 2005;26:3333-9.
27. White SN, Luo W, Paine ML, Fong H, Sarikaya M, Snead ML. Biological organization of hydroxyapatite crystallites into a fibrous continuum toughens and controls anistropy in human enamel. J Dent Res. 2001;80(1):321-7.
28. Ramp MH, Suzuki S, Cox CF, Lacefield WR, Koth DL. Evaluation of wear: Enamel opposing three ceramic materials and a gold alloy. J Prosth Dent 1997;77(5):523-30.
29. Hacker CH, Wagner WC, Razzoog ME. An in vitro investigation of the wear of enamel on porcelain and gold in saliva. J Prosth Dent 1996;75(1):14-7.

30. Hudson JD, Goldstein GR, Georgescu M. Enamel wear caused by three different restorative materials. J Prosth Dent 1995;74(6):647-54

Chapter 5

Size Dependent Properties of Enamel

As outlined in Chapter 2, enamel is composed of inorganic mineral crystals and a small volume of water and protein that holds the inorganic crystals together. The inorganic part of enamel is a form of carbonate hydroxyapatite and the organic part is mainly protein. Though free water and protein comprise only a minor part of mature enamel, they are crucial to its development and are important in understanding its structural organization and physical properties[1]. After maturation, some acidic proteins called enamelins and tuftelins remain inside enamel[2] and act as a "glue" between crystallites[3] and as the cover sheath of the prisms or rods that extend from the dentin enamel junction to the enamel surface. Most free water within enamel is bound within the sheath structure and has an influence on enamel's compressibility, permeability and ionic conductivity[4]. The resulting composite material is much tougher than apatite mineral alone[5]. The mineral and non-mineral components are organized into a complex textured nano-crystallite material that very effectively dissipates forces applied to teeth and protects them from fracture.

Although the high mineral content accounts for enamel's hardness, it is the arrangement and organization of its inorganic and organic constituents (enamel microstructure) that modulates the way enamel responds to stress[1]. Enamel structure may be visualized as having a number of hierarchical levels of increasing complexity and scale from the crystalite level to a pattern level[1,6]. Among them, the most useful and practical model from a mechanical perspective is the rod unit. Human enamel at this level is composed of a rod and inter-rod structure[7]. The diameter of keyhole-like rods is about 5μm. They align parallel from the enamel-dentin junction to the surface of the tooth and are covered by a thin organic sheath. Recently, an FEA model at this level has been developed to predict the orientation and mineral dependence of the elastic properties of enamel[8].

The well arranged prism microstructure results in anisotropy of enamel’s mechanical properties. During the past half century, several methods, including both macroscopic and microscopic approaches, were used to determine the mechanical properties such as elastic modulus, strength and toughness of dental tissues[9-16]. The results of some typical

investigations were listed above in Table 2-4, from which we found that with a decrease in indenter tip size, elastic modulus of enamel had an increasing trend. Furthermore, the cross section surface has a significantly lower elastic modulus than the top surface. Does this indicate that enamel has a size dependent effect? What is the mechanism of this size effect?

This chapter is based on the following published manuscript:

- HE, L.H., FUJISAWA, N. & SWAIN, M.V. (2006) Elastic modulus and stress–strain response of human enamel by nanoindentation. *Biomaterials,* 27**,** 4388-4398.

5.1 Material and Methods

A Berkovich indenter and two spherical tipped indenters (Synton, Switzerland) with a nominal indenter radius of 5 and 20 μm were chosen for this study. Fused silica acted as the standard calibration material.

The tooth samples, both top surface and cross section, as well as fused silica were indented with a Berkovich tip and two spherical indenters under a variety of loading forces from 1 to 450mN. The distance between two separate indents was more than 40μm to avoid the influence of residual stresses from adjacent impressions. The H-tanθ curves were generated using the methods outlined in chapter 3.

After indentation, the samples were ultrasonic cleaned with pure ethanol, gold coated and observed by scanning electron microscopy or SEM (XL-30, Philips, Netherlands).

5.2 Results

5.2.1 Sample load-displacement curves

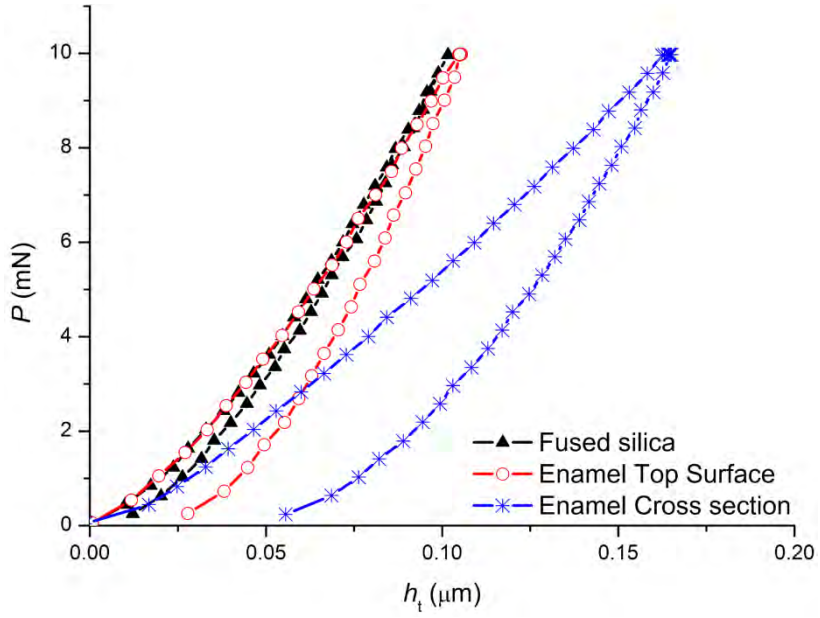

Fig. 5-1 Comparison of force-displacement curves for the 20μm spherical indenter at 10mN on fused silica as well as the top and cross-section surfaces of enamel.

Fig. 5-1 illustrates typical load-unloading curves of the fused silica and enamel indented in this instance using the 20 μm indenter at a maximum force of 10 mN. Fused silica showed almost total elastic recovery upon unloading. In comparison with the top surface, the cross section of enamel showed a greater inelastic response with the penetration depth almost 50% greater than the top surface.

5.2.2 Elastic modulus of enamel in both directions

Elastic modulus and hardness for the spherical tipped indenters at different contact depths in the following figures were calculated using Eq. 3-18 as well as curve fitting Eq. 3-25 and 3-26. The Berkovich results were determined using the Oliver and Pharr[17] analysis. Eq. 3-8 with known values of E and Poisson's ratio for diamond tip (1070 GPa and 0.07) along with a value of Poisson's ratio of enamel of 0.3[18] was used to convert indentation modulus, E_{eff}, into E. Fig. 5-2 shows the variation of the elastic modulus and contact pressure versus indenter contact depth for indentations made on the top and cross section surfaces.

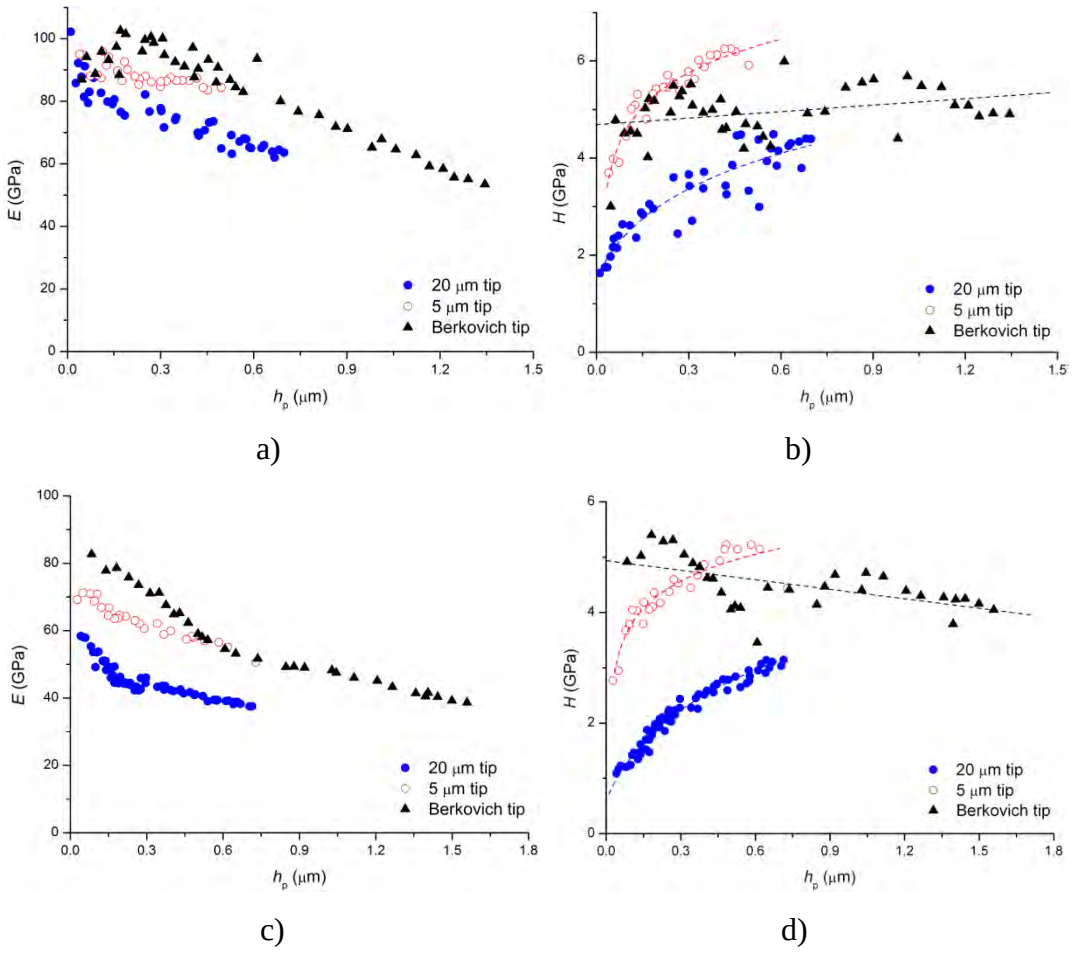

Fig. 5-2 Elastic modulus and hardness as a function of penetration depth of the a), b) top surface and c), d) cross section of enamel obtained with Berkovich as well as the 5 and 20 μm radius indenters.

The above figures show that analysis of the force-displacement data for different tips resulted in different elastic moduli and hardness values. Elastic modulus showed a trend to decrease with an increasing contact depth. The variation of elastic modulus on the top surface was between 100 GPa and 60 GPa, while this value varies between 80 GPa and 40 GPa on the cross section surface.

In the case of hardness or contact pressure the constant strain associated with the Berkovich tip produced a relatively stable hardness value, which was 5±0.45 GPa and 4.5±0.45 GPa on top surface and cross section, respectively. In contrast the hardness or contact pressure for the spherical tips increased with the increment of contact depth because of the increasing strain value. For both indenters the contact pressure at the same depth of penetration was higher for the top surface.

5.2.3 Stress-strain response

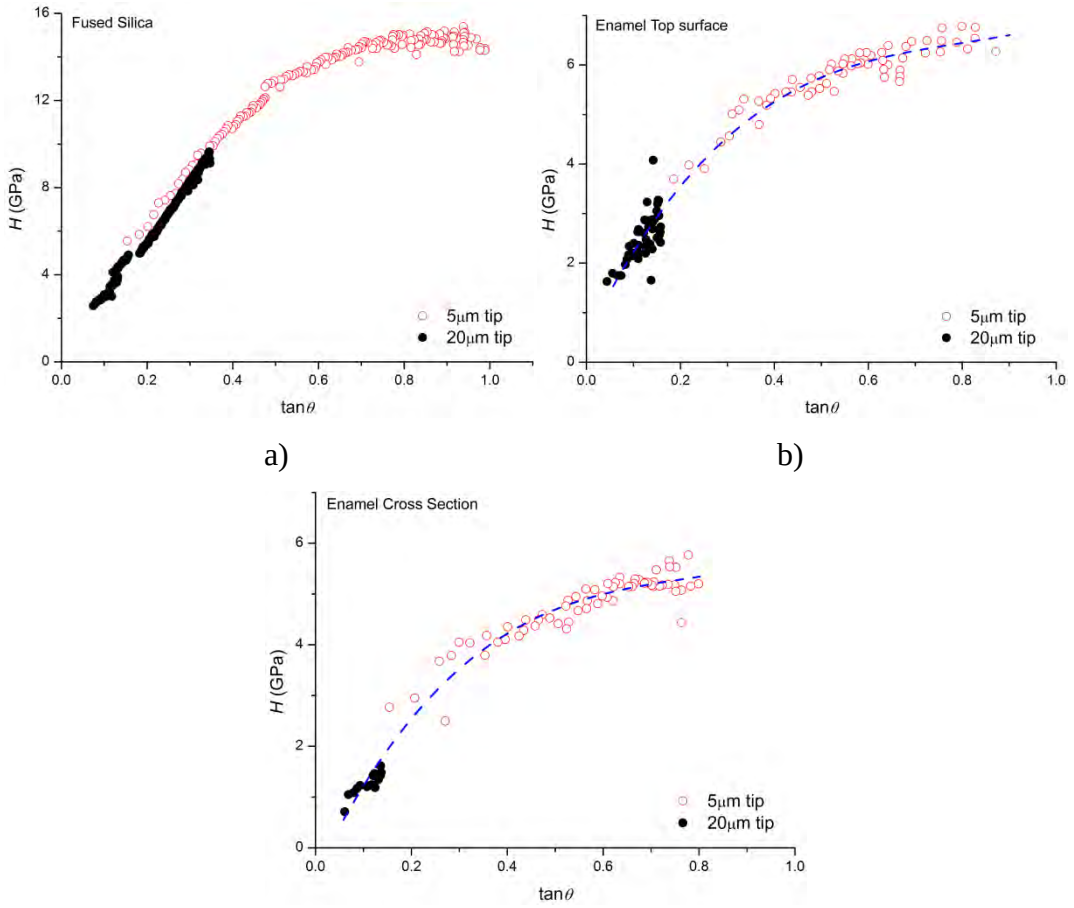

Fig. 5-3 Nano-indentation stress-strain curves on a) fused silica, b) top surface and c) cross section of enamel from two spherical tipped indenters.

Following Eq. 3-15 and 3-16, the stress-strain response curves obtained by including results for the 5 and 20 μm spherical tipped indenters for fused silica and the two directions of enamel were plotted in Fig. 5-3. In these curves, each point is the result of one complete load-unload indentation test. In the case of the fused silica curve, the nominally 20 μm spherical indenter data only covered the purely elastic part of the stress-stain response while the 5μm indenter extended into the elastic-plastic part. Although enamel has similar elastic modulus as fused silica, the stress-strain response is totally different. Even contact at the lowest loads investigated produced slight inelastic deformation on both enamel surface directions. Unlike fused silica, which had an elastic-to-plastic transition value of 10-12 GPa, no prominent transition point was found for enamel. In Fig. 5-3b and 5-3c, only data points whose tan θ value was lower than 0.2

were selected from the 20 μm indenter. This point is taken up in more detail in the discussion.

5.2.4 SEM observation

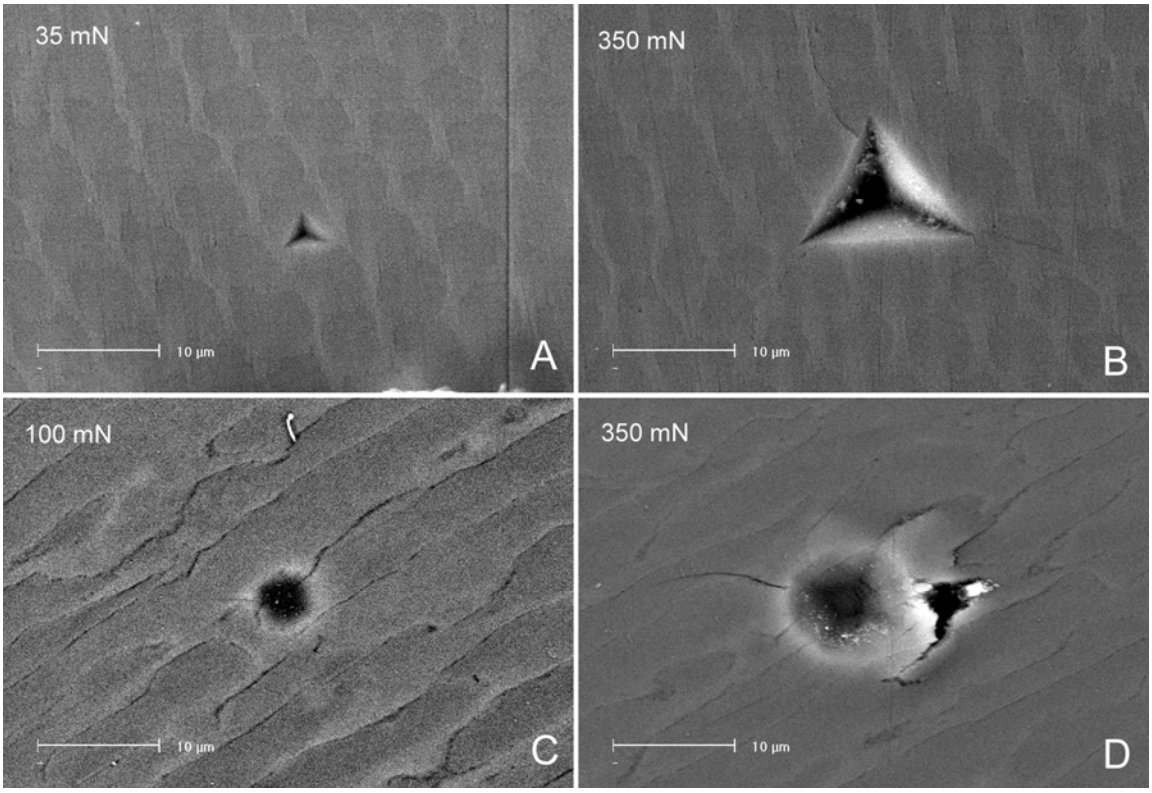

Fig. 5-4 SEM images of Berkovich indenter on top surface (A and B) and 10 μm spherical indenter on cross section surface (C and D) with different peak forces.

Fig. 5-4 compared the indenter impressions from different peak loads. Fig. 5-4A showed, that under a load of 35 mN, the Berkovich impression was located within one prism unit. In contrast, a 350 mN load generated a much bigger impression with the same indenter which covered more than 3 prism units. Similarly, spherical impressions from 100 mN load were approximately equal to one prism unit in Fig. 5-4C, while impressions from the 350 mN load occupied more than 2 prism units on the cross section surface.

5.3 Discussion

Load-displacement curves (Fig. 5-1) illustrate that different surfaces have different mechanical response. Different tips also produced different elastic modulus at the same contact depth and both surfaces tested showed similar trends (see Fig. 5-2). This indicates that prism orientation and structure may play a role in determining the elastic modulus, hardness and stress-strain response.

5.3.1. Elastic modulus of enamel

Many tests have been done to measure the elastic modulus of enamel. Some of them along with the direction of testing and technique used are listed in Table 2-4, which indicates that the value of the elastic modulus of enamel varies dramatically depending upon technique used and orientation investigated. One common point of agreement is that the elastic modulus of the top surface is always greater than the cross section surface. The data generated in this study are within the range of results from other nanoindentation tests. We shall now consider a basis for the differences observed even within a single tooth over a small localized area as investigated in this study.

Enamel consists of two major structures, the prism or rod and surrounding organic rich sheath structure. It has long been recognized that the mechanical properties of these two structures are different[4,8,18]. As a consequence the mechanical properties of enamel may be expected to scale with the diameter of the prisms or rods, that is where the contact diameter is small compared with the rod diameter the elastic response would be dominated by the rod elastic properties whereas if the contact is large compared with the rod diameter then both the rods and sheath structure properties would play a role as modelled by Spears[8] for uniaxial loading. To illustrate this issue more clearly, the calculated elastic modulus values shown in Fig. 5-2a and c are replotted versus contact radius, *a*, for the three indenters as shown in Fig. 5-5a and 5-5b. In the case of the Berkovich indenter this was the effective contact radius determined from the contact area of the triangular impression. The resulting plots show a much more consistent decrease in *E* for all indenters in both rod orientations. This illustrates that elastic modulus, in the case of enamel, is a function of contact area and the effective volume of the contact stress

field from which the elastic modulus is determined, irrespective of what type of indenter tip is used.

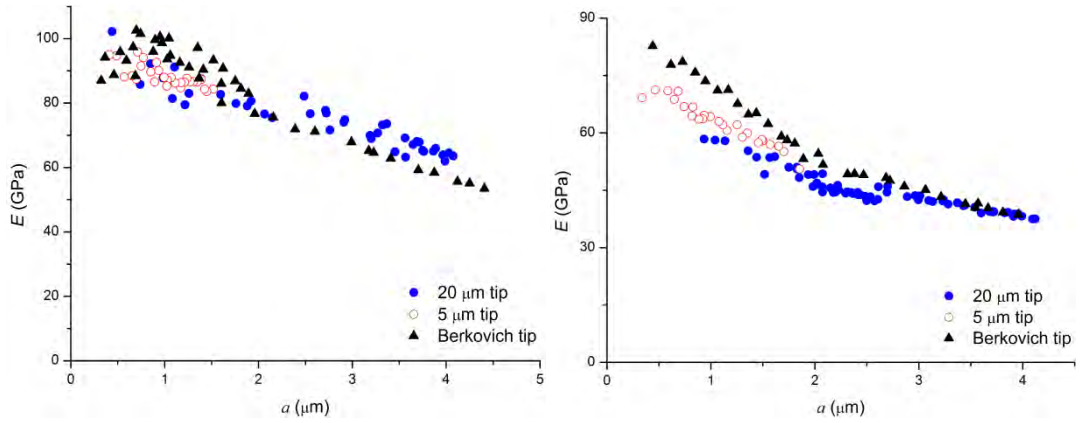

a) b)

Fig. 5-5 Elastic modulus plotted against contact radius for the three different indenters on a) the top surface and b) cross section surface of enamel.

The present observations support the very recent AFM based nano-indentation results of enamel by Ge et al.[15], who reported that the nanohardness and elastic modulus of sheaths were about 73.6% and 52.7% lower than those of the prisms. Such a lower elastic modulus of the organic rich sheath will lower the modulus of the whole system when the contact area incorporates many rods. In an extreme condition, taking the diameter of a prism as 5μm, if the contact area is far smaller than this value and the contact point is on the central area of the prism, the organic sheath will play a reduced role and the elastic modulus will be dominated by the elastic modulus of the prism, which is composed of a high volume fraction of hydroxyapatite and has a high elastic modulus. With the increase of contact area, the stress field expands and the organic rich sheath will play a greater role in the resultant deformation and estimation of the contact area. That is the stiffness of the whole system decreases because of the lower elastic modulus of the sheath.

This prism-sheath unit related response results in the elastic modulus becoming a function of contact area and stress field. This may partially assist in explaining the wide range of elastic modulus reported in former results. For macro-scale tests such as compression tests, the contact area was much larger than the prism-sheath dimension and thus the elastic modulus of the whole prism-sheath unit system was measured. On the other hand, for nanoindentation tests, especially AFM based tests, the contact area is much smaller

than prism diameters. The results of this test reflect only the elastic modulus of prism which has higher volumetric fraction of hydroxyapatite. From Table 2-4, it is evident that macro scale tests generally have lower values of elastic modulus than micro scale, especially nano scale tests. In addition, the top surface values were always higher than cross section values in accordance with Spears' FEA model[8].

SEM images in Fig. 5-4 also supported the above arguments. With the increment of peak load during nanoindentation, more and more prism-sheath units were involved into indentation stress field and contributed to the measurement of nanoindentation elastic modulus. Due to the softness of the sheath region, the more the sheath area was involved, the lower the stiffness of the measured area was. Recently, a similar phenomenon was observed from another similar nanoindentation investigation on enamel[19], which verified our results.

5.3.2. Stress-strain response of enamel

The stress-strain curves in Fig. 5-3 for enamel includes all the 5 µm indenter data but only includes data for the 20 µm radius indenter where the contact diameter is less than the rod diameter. In this manner, a more consistent stress-strain response was found and as discussed above for the elastic modulus, the influence of the sheath structure is less dominant.

Although the difference of the elastic modulus between enamel and fused silica is small, the stress-strain response (Fig. 5-3) is totally different. This is mainly caused by the unique composite prism structure of enamel and its organic rich sheath which makes the whole material more deformable than pure inorganic hydroxyapatite. The stress-strain curves, especially the inelastic part for the top surface, lie well above those for the cross section surface. For indentations on the top surface, the force direction is parallel to the prism with the yield behaviour primarily determined by shear deformation of the very thin protein "glue" between the individual apatite crystallites. In the case of the cross-section surface, the loaded prism deflects under the force because the contact load is supported not only by the prism structure but also by the more deformable and thicker sheath structure surrounding the prism parallel to the surface 3 to 5 µm below the surface.

5.4 Conclusions

Nanoindentation is an attractive method for measuring the mechanical behaviour of small specimen volumes. Using this technique, the mechanical properties of enamel were investigated in directions parallel and perpendicular to the prisms. From the present study using both pointed and spherical tipped indenters the following conclusions are proposed.

- Elastic modulus of enamel is influenced by the prism-sheath structure and in the case of nano-indentation it is a function of contact area. This provides a basis along with the FEA model of Spears[8] to understand the different results previously reported in the literature for macro-scale and micro-scale tests.
- Anisotropic properties of enamel, which arise from the rod like prism-sheath structure, are well reflected in the stress-strain curves. The top surface is stiffer and has higher stress-strain response than an adjacent cross section surface because of the greater influence of the prism sheaths in the latter behaviour.

5.5 References

1. Maas MC, Dumont ER. Built to last: The structure, function, and evolution of primate dental enamel. Evol Anthr. 1999;8(4):133-52.
2. Moss-Salentijn L, Moss ML, Yuan MS-t. The ontogeny of mammalian enamel. Rotterdam: Balkema; 1997. 5-30 p.
3. Boyde A, Martin LB. The microstructure of primate dental enamel. New York: Plenum Press; 1984. 341-67 p.
4. Waters NE. Some mechanical and physical properties of teeth. In: Vincent J, Curry J (eds). The mechanical properties of biological materials. Cambridge: Cambridge University Press, 1980:99-134.
5. White SN, Luo W, Paine ML, Fong H, Sarikaya M, Snead ML. Biological organization of hydroxyapatite crystallites into a fibrous continuum toughens and controls anistropy in human enamel. J Dent Res. 2001;80(1):321-7.
6. Wv K, Clemens WA. Levels of complexity in the microstructure of mammalian enamel and their application in studies of systematics. Scan Microscopy. 1992;6:195-218.
7. Mechel AH, Griebstein WJ, Neal RJ. Structure of mature human dental enamel as observed by electron microscopy. Arch Oral Biol. 1965;10:775-83.
8. Spears IR. A three-dimensional finite element model of prismatic enamel: a re-appraisal of the data on the Young's modulus of enamel. J Dent Res. 1997;76:1690-7.
9. Bowen RL, Rodriguez MS. Tensile strength and modulus of elasticity of tooth structure and several restorative materials. J Am Dent Assoc. 1962;64:378-87.
10. Rasmussen ST. Fracture properties of human teeth in proximity to the dentinoenamel junction. J Dent Res. 1984;63:1279-83.
11. Rasmussen ST, Patchin RE, Scott DB, Heuer AH. Fracture properties of human enamel and dentin. J Dent Res. 1976;55:154-64.
12. Mowafy OME, Watts DC. Fracture toughness of human dentin. J Dent Res. 1986;65:677-81.
13. Lin CP, Douglas WH. Structure-property relations and crack resistance at the bovine dentin-enamel junction. J Dent Res. 1994;73:1072-8.
14. Xu HHK, Smith DT, Jahanmir S, et al. Indentation damage and mechanical properties of human enamel and dentin. J Dent Res. 1998;77:472-80.
15. Ge J, Cui FZ, Wang XM, Feng HL. Property variations in the prism and the organic sheath within enamel by nanoindentation. Biomaterials. 2005;26:3333-9.
16. Kinney JH, Balooch M, Marshall SJ, Marshall GW, Weihs TP. Atomic force microscope measurements of the hardness and elasticity of peritubular and intertubular dentin. J Biomech Eng. 1996;118:133-5.
17. Oliver WC, Pharr GM. An improved technique for determining hardness and elastic modulus using load and displacement sensing indentation experiments. J Mater Res. 1992;7(6):1564-83.
18. Haines D. Physical properties of human teeth enamel and enamel sheath material under load. J Biomech. 1968;1:117-25.
19. Zhou J, Hsiung LL. Depth-dependent mechanical properties of enamel by nanoindentation. J Biomed Mater Res. 2007;81A:66-74.

Chapter 6

Non-linear mechanical behaviour of enamel

Teeth, like other mineralized hard tissue, must retain their shape as well as resist fracture and wear during load-bearing function for the life of the individual. Teeth experience a range of loading situations[1]; firstly, they contact directly other objects and/or opposing teeth; secondly, they encounter normal and sliding contact resulting in wear, and thirdly, unlike bone, damage of teeth is not reparable. To meet all of these functional requirements, teeth have evolved with a unique microstructure, namely a bioceramic composite material with both inorganic and organic components. This exquisite microstructure has attracted considerable interest not only from dentists but also materials scientists, evolutionary and cellular development researchers[1-3].

Under oral functional conditions, masticatory forces range from 28 N to more than 1200 N[4,5]. At the same time, the contact area is restricted to a few square millimeters. It is amazing that enamel can sustain and survive such high stresses for millions of cycles in the abrasive and corrosive environment of the oral cavity. The basic mechanical behaviour of enamel has been widely investigated and models relating its structure and mechanical properties have been reported[6-8]. However, limited investigations of the non-linear characteristics of enamel such as energy dissipation and creep have been reported. Based on a materials science perspective, these properties play an important role in explaining the performance of enamel as a load bearing tissue. Factors contributing to our limited knowledge of such behaviour are the complex shape and small size of specimens of enamel available for testing.

Indentation has been long appreciated as a method for quantifying the mechanical properties and the spatial dependence of such behaviour. Over the past decade with the availability of nano-indenting instruments there has been an upsurge of interest in the mechanical properties of teeth[9-12]. Most of these studies have focused on the determination of the hardness and elastic modulus of tooth structure using both sharp and small spherical tipped indenters. However, some early macro-indentation tests using large

spherical indenters did identify that enamel showed non-linear or hysteretic response even at loads resulting in low contact stresses[13,14].

In this chapter, nanoindentation was employed to investigate the non-linear behaviour of enamel, which was mainly reflected by energy absorption and indentation creep. The results contribute further to our understanding of the relationship of structure, composition and function of enamel.

This chapter is based on the following manuscripts:

- HE, L.H. & SWAIN, M.V. (2006) Energy absorption characterization of human enamel using nanoindentation. *Journal of Biomedical Material Research,* 81A, 484-492.
- HE, L.H. & SWAIN, M.V. (2008) Nanoindentation creep behaviour of human enamel. *Journal of Biomedical Material Research,* In review.
- HE, L.H. & SWAIN, M.V. (2007) Enamel --- a "metallic-like" deformable biocomposite. *Journal of Dentistry,* 35, 431-437.
- HE, L.H. & SWAIN, M.V. (2007) Contact induced deformation of enamel. *Applied Physics Letters,* 90, 171916.

6.1 Energy absorption ability of enamel

As illustrated in chapter 3, nanoindentation can be used for energy absorption investigation. This provides a novel way to explore the mechanical properties of enamel and compare enamel with other materials, especially dental restorative materials. This may provide guidance for future dental clinical materials development and evaluation.

6.1.1 Materials and methods

A Berkovich and three spherical tipped indenters (Synton, Switzerland) with nominal indenter radii of 5, 10 and 20 μm were chosen for this study. Fused silica acted as the standard calibration and sintered hydroxyapatite (HAP) disk were chosen as comparison materials.

Healthy premolar teeth extracted for orthodontic reasons was prepared and tested with the method described in chapter 3. The enamel surface of tooth samples was indented with all four indenters under a variety of loading forces from 1 to 300 mN. A HAP disk was similarly tested with the 10 μm spherical indenter. The distance between two separate indents was more than 40 μm to avoid the influence of residual stresses from adjacent impressions. The U%-ε curve was generated using the methods mentioned above (Chapter 3).

To verify the influence of force loading rate on the mechanical response of enamel, two loading and unloading rates, 10 mN/S and 0.1 mN/S, were selected for tests with both the 20 μm spherical and Berkovich tips, the bluntest and sharpest indenters. The indentation loading force was 100 mN. P-t curve and P-h_t curves were recorded by the indenting system automatically.

6.1.2 Results

6.1.2.1 Sample curves of different indenters on enamel

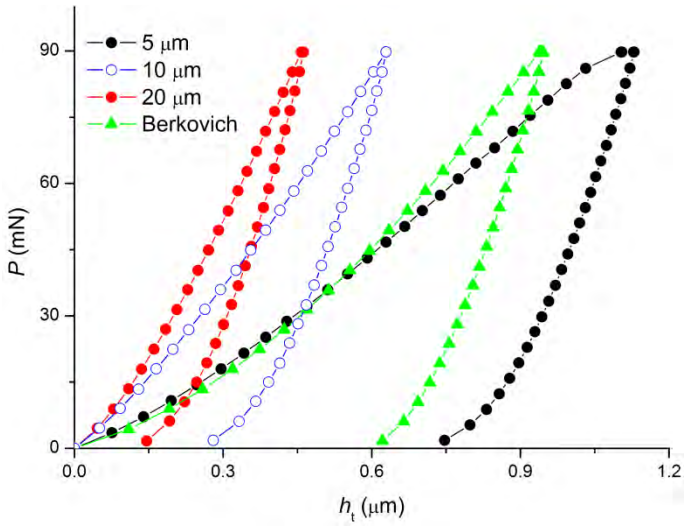

Fig. 6-1 Typical force displacement curves generated with the different indenters on enamel.

Fig. 6-1 shows typical force-displacement curves of the different indenters on enamel at a load of 90mN. The penetration depth for the 5 μm indenter was largest while the 20 μm indenter gave the shallowest value as the smaller radius indenter produces the higher pressure at the same load.

6.1.2.2 Force loading rate tests

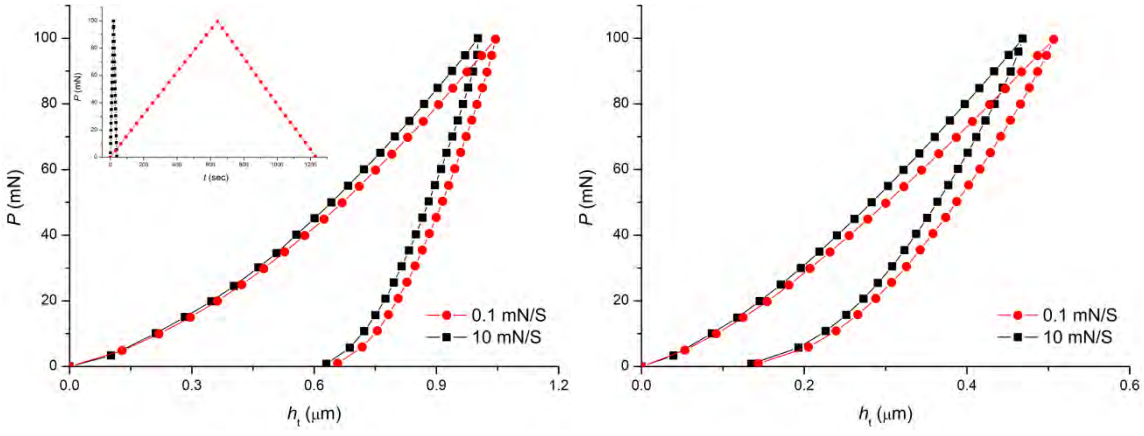

a) b)

Fig. 6-2 Comparison of *P-h* curves at different force loading rates with a) Berkovich tip and b) 20μm spherical tip. The inset figure compares the load-time history of the test.

Force-displacement curves for both indenters as shown in Fig. 6-2 indicate that there was only a slight difference between two force tests despite a 100 fold difference in the loading rates. The slower loading rates for all indenters resulted in a slightly greater penetration depth. This indicates that the energy loss ratio for enamel is almost strain rate independent.

6.1.2.3 Energy expenditure

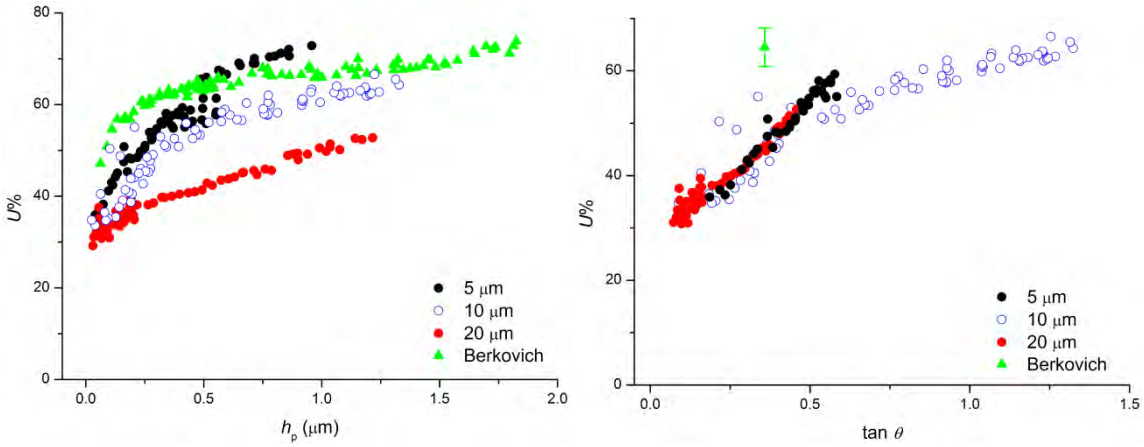

a) b)

Fig. 6-3 Energy expenditure for the different indenters as a function of (a) indenter contact depth and (b) indentation contact strain.

Fig. 6-3a illustrates the relationship between the contact depth and energy expenditure of the three indenters for enamel. The figure showed the significant difference between the different indenters. Different indenters result in different energy loss, *U%*, versus the contact depth, h_p. The 5μm indenter produced higher local strain at the same contact depth resulting in greater energy loss.

In Fig. 6-3b, the results for the enamel shown in Fig. 6-3a were replotted to show energy loss versus effective contact strain as calculated from equation (3-15) in chapter 3. In this way, data from different tips, especially spherical tips, are consistent and form a continuous curve. For enamel, energy expenditure ratio, *U%*, begins at 30% and has a monotonic increase with the contact strain, ε, with no obvious elastic part.

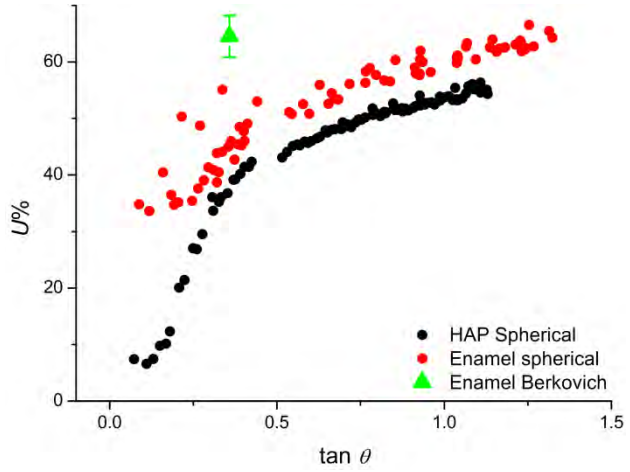

Fig. 6-4 Comparison of energy absorption ability between enamel and HAP disk based on the nominally 10 μm spherical and Berkovich indenters.

Fig. 6-3b also illustrated that data from the 10 μm spherical indenter covered the whole strain range data from other indenters. Therefore, we compared the energy absorption of enamel and HAP disk with only the 10 μm spherical indenter here and data has been depicted in Fig. 6-4. For enamel, energy expenditure ratio, *U%*, begins at 30% and has a monotonic increase with the strain, ε, with no obvious elastic part. For HAP, there was a linear *U*%-ε part for strain values less than 0.5. As is well known, HAP has a prominent elastic response in the stress-strain curve (see Fig. 4-2). The initial slighter higher *U*% values (which started at 5%) in the case of the HAP were caused by inherent noise of the UMIS system especially at low loads.

6.1.2.4 Work of indentation

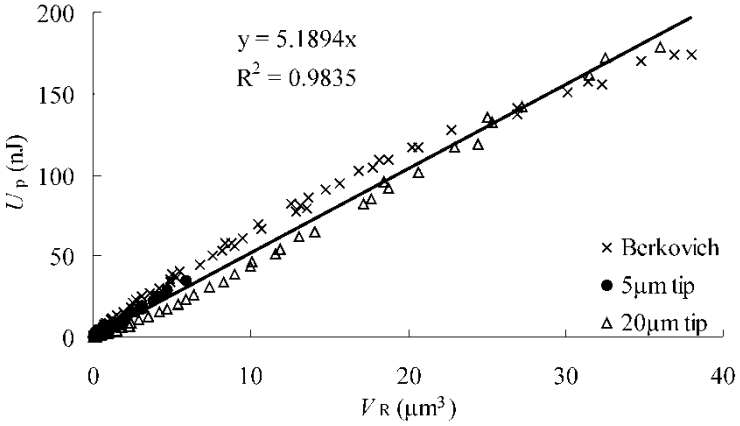

Fig. 6-5 Relationship for enamel between volume of residual indent impression, V_R, and unrecoverable energy loss, U_P. (The fitting line covered all data from different indenters.)

Fig. 6-5 illustrates that the work of indentation for inelastic deformation is independent of the tip shape. The slope of the fitting line representing work of inelastic indentation is approximately 5.2 nJ/μm^3.

6.1.3 Discussion

Like other biocomposites such as nacre and bone, enamel is composed of an inorganic part (hydroxyapatite), organic part (protein fragments) and water. The protein fragments in the mature enamel are residues following the development and maturation of enamel[15,16] and serve as a "glue" between crystallites[17] and as part or cover of the sheath of the prisms. Although these protein fragments occupy only a small volume of the whole enamel, they change the mechanical properties of enamel dramatically by softening the enamel tissue, deflecting cracks and imparting enamel with inelastic properties. The resulting composite material, enamel, is much tougher than mineral, hydroxyapatite alone[8]. The following discussion will consider whether the high energy dissipation ability may arise from the organic sheath component of the enamel.

Fig. 6-2 illustrates that the force loading rate has only a minor influence on the indentation force-displacement response. The difference in energy loss between the two loading rates for the different indenters is less than 2%. This independence of energy loss as a consequence of loading rate suggests that viscous behaviour of enamel is not the major basis of the energy loss mechanism. This may be because the primary component of enamel is hydroxyapatite.

Fig. 6-3 shows different indenters have different energy absorption curves; the smaller the indenter radius or effective indenter radius as for the Berkovich tip, the higher the energy loss at the same contact depth. The Berkovich indenter shows a nearly horizontal line on the $U\%$-h_p diagram, Fig. 6-3a. This is because a Berkovich indenter has a constant strain value of nearly 0.0716 (calculated from Eq. 3-15). The initial increasing part of the Berkovich curve may arise because the indenter tip is not sharp, with a radius of approximate 0.1 μm.

Fig. 6-3b illustrates that the plasticity index (energy loss ratio), $U\%$, for spherical indenters in contact with enamel was fitted together by counting the contact strain values.

At the same nominal strain value, the Berkovich tip has higher *U%* value than spherical indenters. The origin of such behaviour may be because the Berkovich indenter has a sharp tip and ridges with higher local stresses in their vicinity and in addition may cause cracks, which is another source of unrecoverable energy dissipation. Another possible reason may be that the contact strain across the area of contact beneath a spherical tip is not constant but is a maximum at the edge of contact. Whereas for a Berkovich indenter the contact strain is constant across the contact area, that is the mean contact strain beneath a Berkovich indenter is greater than that or a spherical indenter of nominally equivalent contact strain ($\tan\theta = a/R$). In Fig. 6-6, SEM showed that, even at loads of 35 mN, the Berkovich indenter produced radial cracks on the enamel surface. Fig. 6-3b also shows there was no lower load limit in our experiments where purely elastic recovery occurs during loading and unloading even with the bluntest (20 μm) indenter. The initial energy loss is nearly 30% at an initial contact stress which is only 0.6 GPa. This value is higher than the inelastic stress limit of enamel 0.33 GPa measured by Staines et al[14] using a 6.35 mm radius WC indenter. Compared with fused silica, a typical ceramic material with similar elastic modulus, enamel has much greater energy absorption ability.

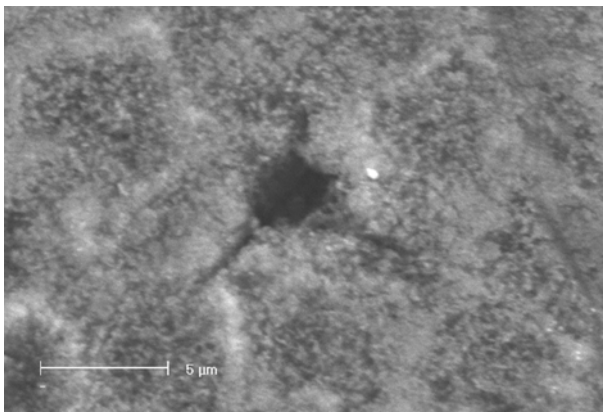

Fig. 6-6 SEM image of Berkovich impression on enamel after 35mN peak load (Surface was etched by 37% H_3PO_4 for 5 seconds).

The plastic work of indentation, W_P, reflects the unrecoverable energy expenditure per unit volume of plastic deformation. Sakai[18] has discussed the physical significance of W_p, in terms of "true hardness" of pure plastic deformation. The true hardness is considered as the irreversible energy consumption, i.e. plastic energy dissipation and the elastic stored energy associated with plastic deformation induced residual stresses, to create a unit volume of indentation impression. For brittle materials, plastic energy loss also includes

other irreversible behaviour such as cracking. As shown in chapter 4, the Berkovich tip produced radial cracks while spherical tips at much heavier loads generated radial and cone cracks. But, as no “pop-in” or any other discontinuities in the load-displacement curve were observed, it is considered that fracture surface energy expenditure is minor compared with plastic deformation. Sakai[18] suggests that even for brittle ceramic materials, the energy loss due to cracking is less than 1% of the plastic dissipation energy.

Where is the extra energy in enamel dissipated? Enamel has a prism microstructure composed primarily of aligned hydroxyapatite crystallites with a very thin protein layer between them surrounded by a thicker organic rich sheath. Various energy loss mechanisms may occur in enamel. If we initially consider the apatite crystals, their very small size would, as Gao et al.[19] suggest, have near theoretical strength, approximately 10% of the shear modulus or ~10GPa. The mean contact stresses for enamel do not approach this value and only in the vicinity of the tip in the case of the Berkovich indenter may such stresses be achieved. Hence, it is not considered that energy loss by conventional dislocation based plastic deformation of the inorganic phase is important for enamel. Therefore, the remainder of this discussion will focus on the role of the organic protein components between and surrounding hydroxyapatite crystallite rods.

Spears[6] cited the elastic modulus of hydroxyapatite crystals and organic tissues as 114 GPa and 4.3 GPa, respectively, in his FEA model. Moreover, AFM nanoindentation[11] also reinforced the argument that the protein rich sheath has a lower elastic modulus and hardness than crystal containing rods: the nanohardness and elastic modulus of the sheaths were reported as being 73.6% and 52.7% lower than those of the prisms, respectively. The nano-indentation curves shown by Ge et al.[11], although not commented upon, showed that sheaths had more energy absorption than prisms. White et al.[8] also established that mineral apatite crystals had a micro-hardness approximately 1.8 times greater than human enamel. These studies indicate that the minor components of enamel, namely protein and water, have a profound softening or plasticizing effect. Other possible mechanisms responsible for the greater energy loss include: fracture of the apatite crystallites, deformation of the very thin protein layers between the crystallites within the prisms or by deformation of the protein and movement of fluid in the slightly porous structure.

Fox[20], who investigated energy loss under cyclic loading conditions with a 3 mm diameter steel ball to a load of 10 kg, considered enamel as a "stiff sponge" like material in which fluid flow occurs in the narrow sheath channels between the enamel prisms. The enamel behaves like a stiff sponge from which liquid is expelled in compression and drawn in again when the load is released. Within the prism region of tooth enamel, the crystallites are very closely spaced with nanometer thick protein layers and provide limited opportunity for fluid transport. Human enamel does have a very fine pore structure with inter- and intra-prismatic spacings[21]. This may provide the mechanism whereby energy is dissipated during indentation even at relatively low contact stresses by forcing liquid through the narrow channels. On the basis of our results in Fig. 6-3a, this model does not appear to be the major contributor to energy loss because nearly hundred fold change in force rate has little influence (2% change) on the indentation force-displacement and energy loss response of enamel.

An alternative explanation is that the energy loss occurs within the proteins in the rods and sheath component of enamel, and is based on the recovery domain bond mechanism within proteins, so-called "sacrificial bond"[22]. In the case of striated muscle[22], the force needed to unfold individual Titin immunoglobulin protein domains and break a sacrificial bond within it was 150-300 pN and depended on the pulling speed. Proteins within the organic sheath and between the apatite crystallites of enamel may deform by gradual unfolding of their domain structures in this form similar to what Smith et al.[23] observed in nacre. This mechanism can absorb a large amount of deformation before the primary structure of the protein, the peptide backbone, is directly stretched. Therefore, during indentation loading, the unfolding of protein fragments within enamel may lead to extra energy dissipation. Rief et al.[22] and Thompson et al.[24] also showed that the energy required to break protein fragments with domain structure and sacrificial bonds can be hundreds or even thousands of times greater than the energy needed to break a covalent bond, because the protein fragment must be re-stretched every time a sacrificial bond breaks and releases more hidden length. That is, some of the indentation energy was absorbed by the sacrificial bonds of the protein between the crystallites and within the surrounding sheath. This is similar to what other research of bone behaviour has proposed[24,25], namely that energy dissipation during the fracture of bone, a composite mix of mineralized fibrils and organic matrix, were partially contributed by extension of sacrificial bonds. Therefore, even the very thin protein layers within enamel prisms,

which are very similar to the situation of proteins in nacre, have such characteristics, and may be a partial contributor to the total energy loss.

Lastly, the arrangement of crystallites within the prism may be another reason for the energy absorption of enamel. It is known that hydroxyapatite crystallites are not all parallel to the long axis of prism. The inter-prism crystallites are at an angle of approximately 60 degrees to the long axes of prisms[6,8]. This will change the surface roughness of two adjacent prisms and will lead to nanoscale friction. Although the organic rich sheath has a thickness of 0.5 to 1μm between two prisms, the interaction of crystals from adjacent rods in such an arrangement may increase the shear resistance of the sheath between enamel prisms. Moreover, studies[26,27] on the morphology of a single enamel prism show that they slightly change direction and shape from enamel-dentine junction to the outer surface resulting in adjacent enamel rods being twisted together (degustation). This will cause the hydroxyapatite crystals in the adjacent prisms to contact directly under an indentation force and will inevitably magnify the nanoscale friction and may cause interlocking at crystal level between two contact surfaces within the sheath. This will initially inhibit the recovery of the enamel after unloading and result in the residual deformation.

Unfortunately, the present observations do not enable us to quantify the energy loss mechanisms between the various proposed mechanisms at this time. Further investigations are required to assist with such identification.

6.1.4 Conclusions

Using nanoindentation, the energy absorption capacity of enamel was investigated. Several conclusions are possible, namely

- Enamel showed much higher energy absorption capacity than HAP, a ceramic material with equivalent composition. This may be because of the minor organic component of enamel.
- Indentation force rate had only a minor influence on the energy loss of enamel.
- For the spherical indenters the energy loss was found to be a function of the contact strain.

- Energy loss with a Berkovich indenter was greater than a spherical indenter at equivalent contact strain.
- The top surface of enamel has a plastic work of indentation of nearly 5.2 nJ/μm^3.

Three different mechanisms were considered to contribute to the measured energy absorption, namely fluid flow within the sheath structure as proposed by Fox[13], protein "sacrificial bond" extension as proposed by Smith et al.[23] for nacre and Fantner et al.[25] for bone, or nano-scale friction within sheaths associated with the degustation of enamel rods as considered by Macho et al[26]. Further work is required to more quantitatively assign the energy loss observations to these or other mechanisms.

6.2 Nanoindentation creep behaviour of enamel

Viscous response of natural biomaterials plays an important role in their function to bear and distribute force, and especially for bone, has attracted considerable attention[28-33]. Jäger[29] summarized the characteristics of typical viscous deformation of biological tissues as: (1) the force necessary for deformation depends on the deformation rate; (2) force-displacement hysteresis occurs during loading and unloading; (3) application of a (constant) force leads to transient and/or permanent creep; (4) after removing the deformation force there is stress-relaxation or recovery. A universal numerical model may be used to describe the visco-elastic relaxation behavior of a material, which is the Kohlrausch-Williams-Watts (KWW) model[34]: $\gamma(t) = \gamma_o \exp[-(t/\tau)^{\beta}]$, where β is a power law exponent with values in the range $0<\beta\leq1$, and γ_o is an instantaneous stress. In the above expressions, τ is an effective relaxation time and γ is the relaxation stress. A specific condition of the model is $\beta=1$, where the above equation may be simplified as: $\gamma(t) = \gamma_o \exp[-t/\tau]$, which is the well-known "Debye" or Maxwell relaxation model[35].

Restricted by measurement methods, the limited viscosity and temperature range over which natural biomaterials operate, the viscous responses of these biological materials, especially creep behaviour, are difficult to quantify. For metallic and polymeric materials, traditional uniaxial tensile and/or compressive tests are used to investigate the creep response of a specimen. Two main problems limit the usage of these methods for biological materials such as enamel. Firstly, these tests need multiple identical specimens and are time consuming to conduct. Secondly, the accuracy of these methods depends on the creep response of the material. For small samples with limited creep, such as enamel, it is not very reliable. In the biomaterials field, only limited indentation creep tests have been done on biological hard tissues. Torsion[30,31] and three-point bending tests[28] were used to measure the relaxation Young's modulus and shear modulus of bovine bone. Furthermore, because of the anisotropic property of natural biomaterials, the loading direction must be controlled. This limitation, along with the size of teeth, severely restricts the usage of bulk methods for the evaluation of dental tissue.

Recently, depth-sensing indentation techniques have become widely used for mechanical property evaluation, and may be used for the determination of creep behaviour. Indentation creep tests are a powerful technique for studying the rheological properties

and relaxation dynamics of different materials such as metals[36], polymers[37,38] and other materials[39,40]. The aim of this study was to investigate the creep of human enamel using the nanoindentation technique.

6.2.1 Materials and Methods

A diamond Berkovich indenter (Synton, Switzerland) was chosen for this study. Due to the imperfection of Berkovich indenters, the contact area of the indenter has been calibrated by fused silica before the study, as described in Chapter 3.

Three healthy premolar teeth, extracted for orthodontic reasons, were prepared and tested by the UMIS system as described in chapter 3. Several commonly used dental metallic materials were chosen for comparison with sound tooth enamel extracted for orthodontic reasons. Pure hydroxyapatite (HAP) was selected as a ceramic equivalent of enamel. The metal materials are cast alloy [Wiron® 99, BEGO, Germany], type IV gold alloy [ITI® Straumann, Switzerland], commercial pure Titanium [T-alloy, GC, Japan] and amalgam. Details of these materials have been well described in Chapter 4.

The top surface of each enamel sample was indented at least 5 times at the maximum force of 250 mN with the one-step loading method. The results reported are the average of these tests. Holding time at maximum load was 900 seconds for all the tests. During one-step unloading, another holding at 5 mN was activated. This unload-holding time was 900 seconds as well. Each group of tests commenced at least 2 hours after a thermal soak period in the instrument, and thermal drift was assessed before each experiment. Thermal drift during all the tests was deemed to be negligible (<0.02nm/sec). The distance between indents was more than 50 μm to avoid the influence of residual stresses from adjacent impressions. The force, P, displacement, h, and time, t, values were recorded. Creep rate sensitivity, m, was calculated with equation 3-25 separately for each test of enamel. After that, the average value was statistically calculated.

After indentation testing, scanning electron microscopy (SEM) (XL-30, Philips, Netherlands) was used to examine the residual indent impressions. Enamel specimens were etched with a mild polyacrylic acid (10%) solution (Dentin Conditioner Liquid, GC, Japan) to better highlight the structures and indentation damage. All samples were

ultrasonically cleaned with absolute ethanol for 10 seconds before gold coating prior to SEM.

6.2.2 Results

6.2.2.1 Description of indentation creep test

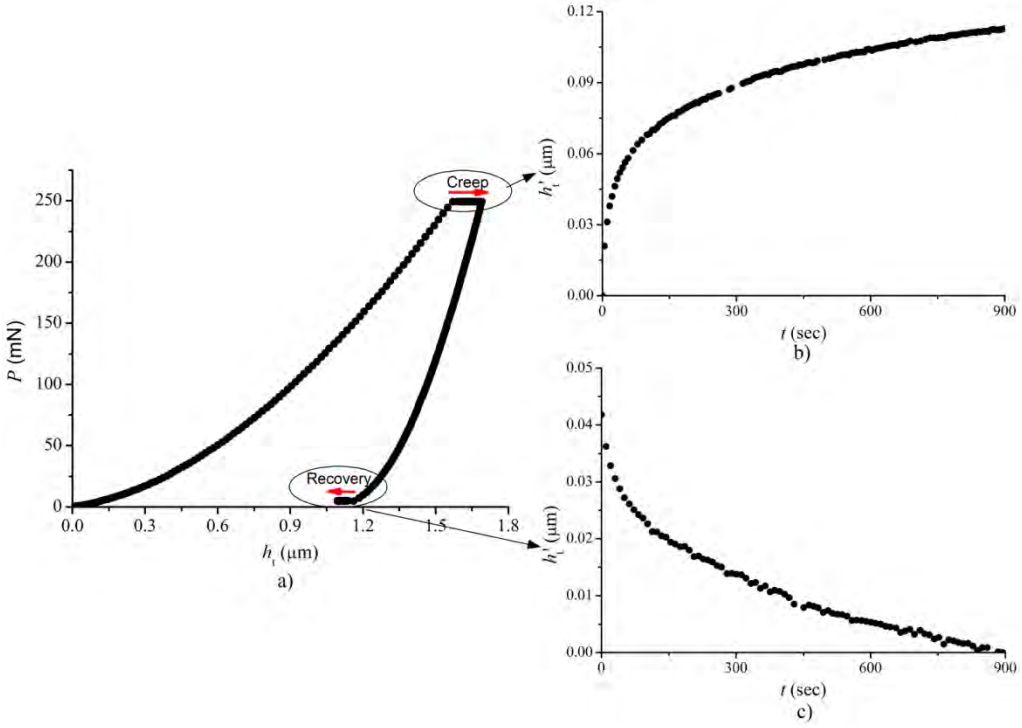

Fig. 6-7 a) Typical force-displacement results from traditional nanoindentation loading-unloading method showing creep during hold period at the maximum and minimum loads; b) Creep at the maximum load as a function of time; c) Creep recovery at the minimum load as function of time. (In the latter curves the initial penetration at the commencement of creep has been subtracted from the observations.)

Due to the difficulty in illustrating the one-step loading-unloading data in force-displacement (*P*-*h*) curve, the results in Fig. 6-7 are used to illustrate the creep phenomenon of enamel at the maximum and minimum loads from a traditional nanoindentation test. The relative penetration depth, h_t', is calculated by subtracting the initial depth at the maximum load from the increasing depths during the holding period at this load. Creep data at maximum load exhibited increasing penetration depth with time (Fig. 6-7b). On the contrary, upon unloading to 5 mN and keeping the force constant, the penetration depth decreased (called *backcreep* after Jäger[29]) (Fig. 6-7c).

6.2.2.2 Indentation creep behaviour of enamel and dental materials

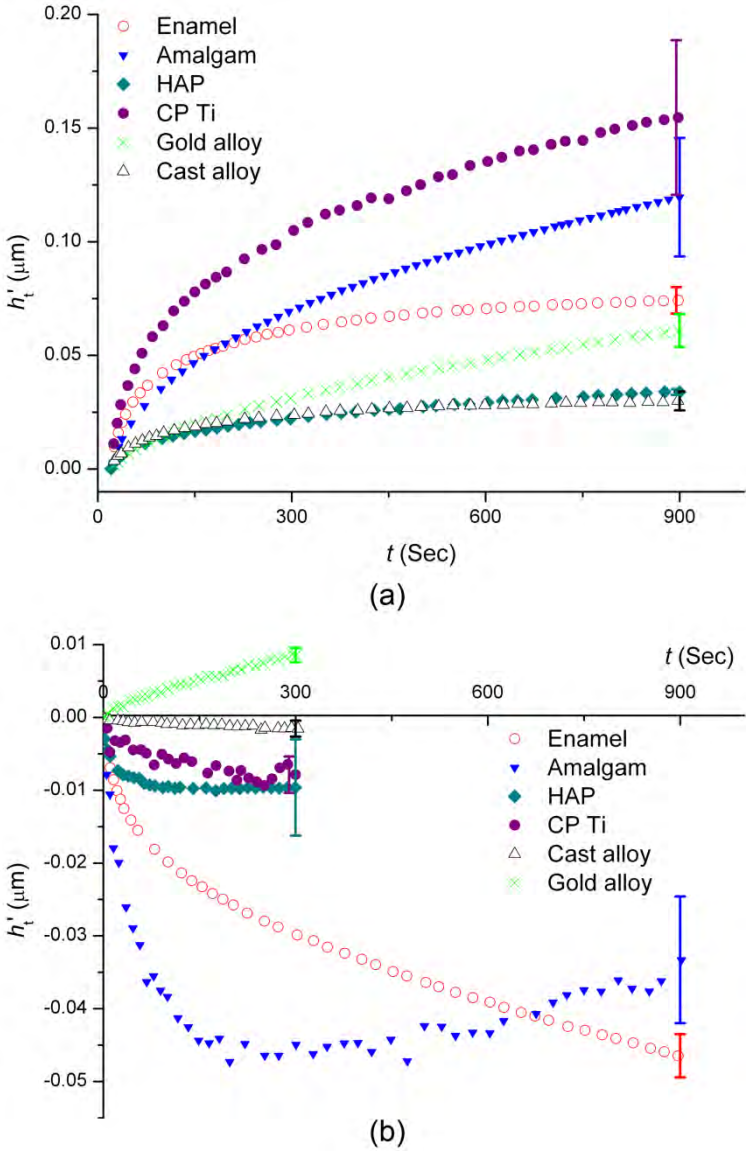

Fig. 6-8 Indentation depth against time, h_t'-t, curves of (a) creep and (b) backcreep of different materials. (h_t' values of amalgam in (a) were divided by 10 to fit onto the diagram.)

All the curves in Fig. 6-8 were the average value of at least 3 tests and the error bars at the end of the curves indicating the deviation of the data. The relative penetration depth, h_t', was calculated by subtracting the initial depth at the beginning of the holding time from the increasing depths during the holding period at maximum and minimum loads.

Creep data at maximum-load holding exhibited increasing penetration depth with time for most investigated materials (Fig. 6-8a). Amalgam showed the maximum creep, followed

by titanium. But they all exhibited considerable scatter in data. Enamel, on the other hand, had a relatively stable creep response. In contrast, the indentation creep depths of hydroxyapatite and cast alloy were very limited (less than 0.025μm during the 900 seconds holding period). Such limited creep response, ~0.03 nm/sec, is within the limit of UMIS system thermal drift stability and implied that the viscous properties of these materials are negligible compared with their elastic/plastic properties.

At the minimum-load holding period (named "*backcreep*" period), the recovery was prominent only for enamel and amalgam samples but remained within the instruments stability range (<0.05 nm/sec) for other samples (Fig. 6-8b). The displacement rate and limited backcreep of hydroxyapatite (~0.03 nm/sec) and cast alloy (~0.01 nm/sec) were all within the limit of system thermal drift. Therefore, only enamel and amalgam exhibited significant backcreep response. When considered in more detail, the backcreep curves of enamel and amalgam were totally different. Enamel showed a progressive recovery while amalgam recovered very quickly in the first 150 seconds and reached the limit of nearly -0.05 μm in h_t' values. The latter portion of the amalgam curve only reflects system thermal drift response.

This part of the results implies that enamel and some dental metallic materials all exhibit creep behaviour but with different characteristics. This indicates different mechanisms are responsible for this behaviour and will be considered in detail in the discussion.

6.2.2.3 Measurement of indentation creep rate sensitivity.

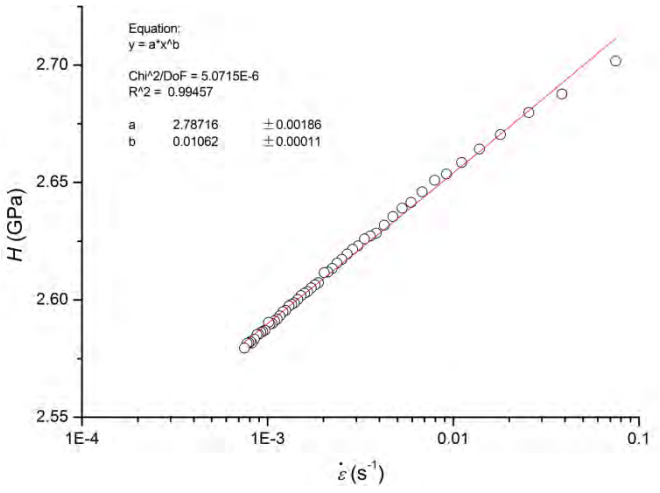

Fig. 6-9 Sample curve of double logarithmic plot of contact pressure (hardness), *H*, versus indentation strain rate, $\dot{\varepsilon}$, for enamel.

Table 6-1 Creep rate sensitivity of different enamel samples

Sample	Creep rate sensitivity
No. 1	0.0113 ± 0.0004
No. 2	0.0103 ± 0.0003
No. 3	0.0133 ± 0.003

Data in Fig. 6-9 according to equation (3-25) illustrates that the test data follows this relation very well. The creep rate sensitivity, *m*, of enamel varied a little between different samples and is ~0.012 in general from all samples (Table 6-1). This is the first time that creep rate sensitivity of enamel was measured.

6.2.3 Discussion

6.2.3.1 Comparison of indentation creep behaviour of dental materials and enamel

The indentation creep ability of enamel was much greater than HAP but similar to some dental alloys. A recent literature review by Li et al.[41] showed that most materials, including hard ceramics, have limited ability to creep at room temperature. The theoretical analysis of the indentation hardness test by Johnson[42] suggested when an indenter is pressed into a flat surface of a homogeneous material, the indenter is encased in a non-deforming hemispherical "core" of material, within which there is assumed to be a hydrostatic pressure. Surrounding this hydrostatic zone, there is a plastic-elastic hemispherical zone. The process of indentation is thus likened to the plastic movement of a series of shells concentric with the hemispherical core. Li et al.[41] also summarized the major possible mechanisms of indentation creep for different engineering materials as: plasticity (dislocation glide), power law creep (climb plus glide), power law breakdown (glide plus climb), recovery (dislocation climb), and diffusion (volume, grain boundary or dislocation pipe). Reports on a titanium alloy described the mechanisms of creep as the rearrangement of the atoms within the crystal lattice, along with formation, movement and pile-up of the dislocations, slip of crystals along grain boundaries and so on[43,44]. All of these mechanisms play a role in the expansion of the elastic/plastic boundary into the material under the contact area at maximum load, and the speed of this expanding procedure determines the creep ability of the material.

Here, because of the structural complexity and similarity in creep mechanisms of other alloys, we consider only amalgam as an example to illustrate the mechanisms of indentation creep on metallic materials. Generally speaking, after setting, an inter-metallic compound of silver and mercury, Ag_2Hg_3 (γ1-phase), and a solid solution of mercury in tin, Sn_7Hg (γ2-phase), form the matrix of the amalgam (bright area in Fig. 4-5c), and some un-reacted Ag_3Sn immersed in the matrix (dark area in Fig. 4-5c). Moreover, some pores and fissures may be generated at the boundary interface of different phases during the setting procedure (pores in figure 4-5d are good examples). These defects and the multiplicity of phases influence the mechanical properties of the material dramatically. This can also partially explain the large data scatter of the material in all the amalgam tests of this study. Theoretically, creep in amalgam occurs by plastic flow and grain-boundary sliding[45]. According to Xu et al.[46], subsurface creep of indentation area is dominated by deformation of individual alloy particles as well as matrix grains, which are associated with the creep-induced shape changes of an individual alloy particles from spherical to irregularly elongated shapes, and the matrix grains separating them from each other possible due to plastic flow and/or grain rotation.

Because of its totally different chemical composition, enamel will have other creep mechanisms than occur in metals, mainly related to the organic protein components existing between the apatite crystallites. This proposition is supported by research on creep of bone[31], in which the stress relaxation curves of bone were found to be similar to those of demineralized bone. Moreover, in comparison with HAP sample, enamel exhibited a much more extensive creep response. All of these observations indicate that proteins were the dominant contribution to creep behaviour. Therefore, it is safe to conclude that creep behaviour of enamel comes mainly from the protein films between the apatite crystallites and the prisms. Moreover, the limited creep response may be because the protein films occupy only a very small volume fraction of the entire enamel.

Most proteins may be regarded as bio-polymers. Like normal polymeric materials, they have viscous properties. Moreover, proteins inside enamel may also contain special bio-molecular structures such as “sacrificial bonds”[22,23]. This type of bond has saw-tooth shaped force-displacement curves because of the gradual break down of the domains and time dependent unfolding of the peptide chains. This may help us to explain the observed creep of enamel. Another characteristic of this bond is, after unloading, the bond can

recover and the peptide chain can be refolded. The reversibility of this bonding coupled with the residual stress surrounding the deformed zone about the indentation impression may explain the prominent backcreep observed for enamel.

Only enamel showed stable backcreep upon partial unloading. Backcreep may be regarded as the behaviour of polymers, which have the ability to reform visco-elastically after unloading. For HAP and most metallic materials, plastic deformation, no matter if it is viscous or not, is permanent and unrecoverable. This also suggests that the more deformable organic protein-rich material in the sheath region and between the apatite crystallites assisted the recovery of the deformed material back towards its initial position. This property may be important in enamel's ability to function as a long-time force bearing tissue and contribute to the superb anti-fatigue behaviour of enamel.

The mechanism of initial rapid back-creep of amalgam is not clear but may be a consequence of similar creep mechanisms as for enamel producing a visco-elastic recovery of the deformed material under the indentation residual stresses. In comparison with the extensive creep of amalgam at peak load, the extent of the backcreep was not significant (only ~5%) whereas in the case of enamel backcreep was much more significant (~60%).

6.2.3.2 Creep behaviour of enamel

In the current study, total depth, h_t, was used in this study instead of contact depth, h_p, to calculate H. This is because, firstly, only current depth, h_t, at a particular time may be read directly from the machine rather than h_p, during the creep process. Secondly, a preliminary SEM observation confirmed the nearly constant ratio of h_p/h_t: a direct measurement of the indentation impressions to calculate h_p with calibrated SEM at x10,000 magnification was compared with h_t values recoded by the nanoindentation system at different holding times with the same load (250 mN). As listed in Table 6-2, the h_p/h_t ratio is relatively stable. Therefore, in the rest of the calculations, we assumed that the H value derived from h_t did not influence the final results.

Table 6-2. Comparison of h_t, h_p values and their ratio

Hold Time (Sec)	h_t (μm) (from UMIS system)	h_p (μm) (From SEM measurement)	h_p/h_t ratio
100	2.307	2.009	87.08%
50	2.147	1.870	87.11%
20	2.094	1.863	88.92%

Although this is mainly a phenomenological investigation, efforts were made to provide a numerical description of the indentation creep behaviour of enamel. In an attempt to determine a nanoindentation creep model, the creep data at maximum load were evaluated to determine the mean contact stress *H* versus time and then plotted in a logarithmic manner (Fig. 6-9). Log*H*-*t* curve from the results may be well fitted by a double exponential function in a form of :

$$y = a_1 \exp(-x/t_1) + a_2 \exp(-x/t_2) + y_0 . \quad (6\text{-}1)$$

Data in Fig. 6-10a can be fitted by equation (6-1) as:

$$H = 0.0251\exp(-t/338.57) + 0.0238\exp(-t/14.87) + 0.471 \ (R^2=0.996), \quad (6\text{-}2)$$

which is green solid line in the diagram. This indicates that the creep response of enamel does not match the predicted Debye/Maxwell relationship. This is in accordance with other findings for bone[28,30-32], namely that the viscous response is too complex to be described by a simple Debye/Maxwell relaxation model. There may be two main reasons for this discrepancy. On the one hand, materially, enamel is a complex biocomposite with at least two phases, linear elastic inorganic phase of hydroxyapatite (more than 90% of the biocomposite) and inelastic organic phases of protein fragments (less than 10% of the biocomposite) and water. The compositional and microstructural complexity of enamel and other calcified tissue biocomposites are more complex than single component polymers in their creep responses. Our finding is similar to that of other biological materials such as bone[28,30-32], for which the viscous response is too complex to be described by a simple Debye/Maxwell relaxation model. Following a similar procedure to what Sasaki did for bovine bone under torsion and three point bending tests[31], creep curves in Fig. 6-10a may be divided into two parts: an initial rapid decreasing response followed by a near linear region. This is similar to what Sasaki observed for bovine bone under torsion and three point bend tests[31]. Initially, the stress relaxation response indicates mixed KWW type and Debye type behaviour. Later, the KWW type relaxation diminishes

and only the Debye type relaxation remains (blue dash line in Fig. 6-10a). On the other hand, methodologically, the indentation test creates a complex three dimensional stress field including compression, tensile and shear stresses. As described by Lucas and Oliver[36], in the indentation test, the inelastically deformed volume of material is continually expanding to encompass previously elastically deformed material. The material underneath the indenter is very often likened to an expanding cavity with a hydrostatic core, where no deformation is occurring, and an expanding elastic/plastic boundary. The creep process is believed to depend upon the rate at which the elastic/plastic boundary can proceed into the material. In contrast to a uniaxial test, the indentation creep process is, therefore, seen to entail an ever-increasing volume of material as deformation proceeds. The requirement of additional displacement rather than a characteristic time to reach a new indentation steady-state value of hardness can perhaps be understood in this light. On this basis and by considering the anisotropic nature of enamel, it is obvious that its behaviour is more complex under nanoindentation than polymers. Therefore, although a linear relationship was found (green solid line in Fig. 6-10b) upon replotting the contact stress, *H*, against time, *t*, in a logarithmic manner, there is no current model of creep behavior that is appropriate for this relationship. All of these results indicate that indentation creep tests, especially those on natural biomaterials, produce complex responses that do not match current mechanical models which are based upon metallic or viscous materials. Therefore, new experimental and theoretical studies are necessary to describe creep behaviour of natural biomaterials such as enamel and bone.

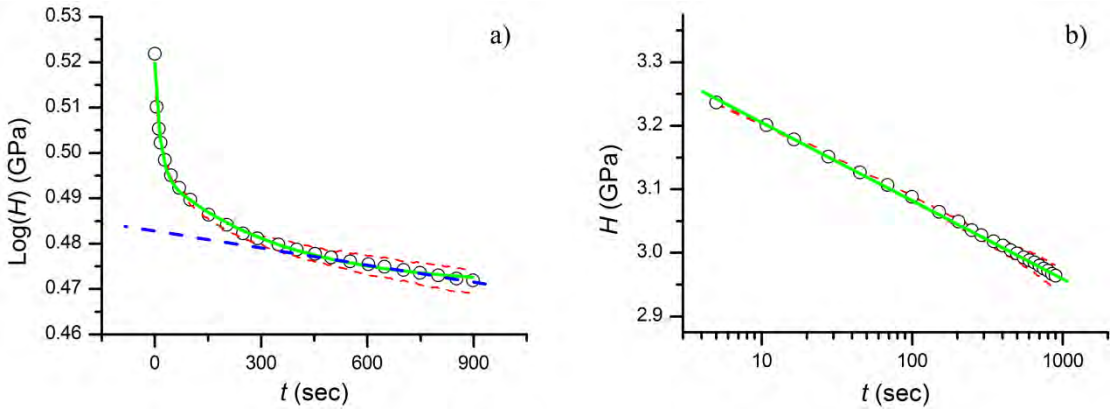

Fig. 6-10 Average curve of, a) Logarithmic plot of hardness, *H*, versus creep time, *t*. b) Hardness versus logarithm of time, at the load of 250 mN. (The thin red dash lines show the upper and lower limits of all data from one sample)

6.2.3.3 Backcreep of enamel

Upon unloading to 5 mN, the enamel appeared to show visco-elastic creep recovery (backcreep). To investigate this response in more detail, the h_t-t curves similar as Fig. 1c were inverted and fitted so that the strain rate, $\dot{\varepsilon}$, was calculated from the derivative function of the curve, that is $\dot{\varepsilon} = (dh/dt)/h$ [47]. The resultant response is compared with creep behaviour at the maximum load as shown in Fig. 4 which illustrates that the strain rate dependence of creep and backcreep both initially show similar trends against time, t, although the backcreep appears to be nearly an order of magnitude lower.

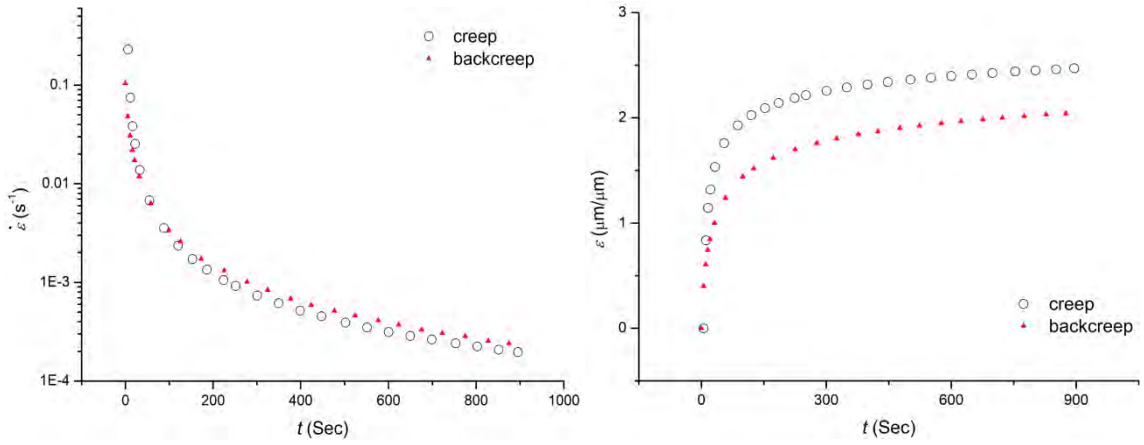

a) b)

Fig. 6-11 a) Strain rate and b) normalized strain, ε, against time, t, plots for enamel compaing both creep and backcreep data.

Fig. 6-11a establishes the relationship of $d\varepsilon/dt = f(t)$, from which the strain value in Fig. 6-11b was integrated and normalized by setting the initial strain as zero. This curve indicates that the strain changed rapidly at the initial stage of the creep process. The strain associated with backcreep was lower than that of creep at maximum load. Both creep and backcreep have the tendency to reach a saturated value after a finite time. This is in accordance with theoretical predictions of a model by Jäger[29].

6.2.3.4 Creep mechanisms of enamel

The microstructure of enamel, a natural biocomposite material, has a typical rod like structure of nearly 5 to 7 μm in diameter which is composed primarily of hydroxyapatite crystallites. These rods are surrounded by a 0.5 to 1 μm thick organic rich sheath and there is a very thin protein layer between the apatite crystallites within the rod structure. This special structure endows enamel with highly advantageous mechanical properties

such as high fracture toughness[8] and the ability to sustain millions of chewing cycles. As shown in an earlier part of this thesis (Chapter 5), the micro-structure of enamel has an influence on its elastic modulus. The protein rich sheath structure plays a significant role in determining the elastic deformation response together with the hydroxyapatite crystals as initially proposed by Spears[6] on the basis of a finite element model.

Research on bone[31], in which the stress relaxation curves were found to be similar to those of demineralized bone, indicated that the protein component was the dominant contributor to the creep behaviour. Other theoretical studies on the viscous property of natural biocomposite materials also assume that the mineral platelet component is linear elastic and only the minor protein component contributes to the viscoelastic properties of these composites[48]. Moreover, our recent study of enamel after different treatments illustrated that treatments such as burning and ethanol dehydration, which can influence the function of proteins, limited the creep ability of the sample significantly (see Chapter 7). Therefore, it is reasonable to deduce that creep behaviour of enamel arises mainly from the protein rich organic sheath and the thin layer between the apatite crystallites within the rods. Moreover, the limited creep response occurs because the organic sheath occupies a very small volume fraction of the entire enamel.

The visco-elastic property of enamel may be considered as follows: First, the proteins and other organic (and water) components within enamel may be regarded as a biopolymer. Viscoplastic properties of these biopolymers stem from the configurational rearrangements, disposition and interaction among the macromolecules in both their short- and long-range network interactions[48]. Under indentation load, the local re-distribution response of the structure is rapid, while the long-range interaction response is slow due to the time-dependent molecular rearrangement. Upon unloading, due to the memory effects associated with the cross-linked network, the molecules have a tendency to return to their initial form and positions[48]. In the case of indentation, the surrounding elastically deformed hinterland about the residual impression provides an additional driving force for such backcreep deformation. These factors result in the recovery of the indentation impression being also time-dependent.

Second, proteins within enamel may behave similar to the recovery domain bond within many proteins, called a “sacrificial bond”[22]. Such a domain structure within titin

immunoglobulin domains exhibited similar recovery upon unloading. These authors noted that the longer the delay before the next application of force, the more reformation of the bond occurred during relaxation; refolding of protein domains was also observed during this process[22]. Similarly, proteins within the organic rich sheath and between the apatite crystallites of enamel may have a similar function and response as those in bone.

In short, this reversible visco-elastic property of enamel may help teeth distribute the localized high contact/impact stresses resulting from chewing forces especially the high localized contacts from asperities or small hard particles trapped between teeth. Also, sliding wear between teeth and food particles may introduce high local tensile, compressive and shear forces around sliding contact area. This reversible inelastic property may be vital to limit damage accumulation and prevent excessive wear in enamel.

6.2.3.5 Creep-rate sensitivity of enamel

Creep rate sensitivity, *m*, is a value that reflects the flow ability of a material. If $m = 1$, the material is considered viscous and to exhibit Newtonian flow; $m < 1$ indicates inhomogeneous non-Newtonian flow. The very small *m* values measured for enamel, suggests that strong localized shear flow inside the material under load condition occurs[39]. Usually, such low values quantify the creep ability of crystalline materials at high temperature, and where the creep response has a relationship with the temperature and activation energy for self-diffusion of the material[36,49]. However enamel and other dental materials function at body temperature of nearly 37℃, which is far lower than the melting point of the mineral apatite material although we have no knowledge of the glass transition temperature of the protein materials that are present in enamel. Future studies may wish to include the temperature dependence of the creep in their consideration.

As outlined in the first part of the discussion, hardness values from different depths of indenter penetration have a proportional relationship because of the definition of hardness (see eq. 3-27). It is possible to deduce that this change of hardness value, *H*, will not interfere with the calculation of creep rate sensitivity, *m*.

When it comes to the problem of equivalence of nanoindentation creep test and universal creep test, it is necessary to initially explain the stress-strain procedures of these two tests. A uniaxial test provides a simple one-dimensional tensile/compressive load. The strain rate of the material under this condition is fairly easy to determine. On the contrary, for indentation test, because the sample experiences a severe three-dimensional strain gradient, a unique strain rate of the material is impossible to define.

During an indentation test, the deforming volume of material under the indenter is continually expanding to encompass previously undeformed material[49]. As the material deforms under the indenter, the material beneath the contact area may be regarded as an expanding cavity with a hydrostatic core, where no further deformation is occurring, while at the same time the elastic/plastic boundary continues to expand. The creep process is believed to depend upon the rate at which the elastic/plastic boundary can grow into the surrounding elastically strained material. As the radius of the elastic/plastic boundary is often related to the radius of the indentation, the instantaneous change in contact area divided by the instantaneous contact area ($\dot{A}/A$) may be the most appropriate definition for the indentation strain rate, as it is a direct measure of the progression of the elastic/plastic boundary into the material. However, for a geometrically similar indenter, the instantaneous displacement rate of the indenter divided by the instantaneous displacement ($\dot{h}/h$) is simply related to $\dot{A}/A$, and the indentation strain rate has typically been defined as $\dot{h}/h$.

Consideration of this issue enables indentation creep tests to be compared with uniaxial creep tests. Other researchers have verified this approach both experimentally and theoretically[36,47,49,50]. Based on all these findings, indentation creep tests may be extended to other biomaterials. This provides us with an alternative approach to evaluate the viscous properties of natural biomaterials and biomedical materials.

6.2.3.6 The phenomenological description of indentation creep and its mechanical correlations

As mentioned above, creep behaviour is a reflection of the visco-elastic properties of a material, which may be described as the variation of the strain under constant stress. Various approaches have been published to describe and/or calculate creep behaviour of

materials using the indentation method[38,40,50-53]. However, because of the complexity of indentation phenomenon which includes both compressive, tensile and shear stresses within the deformation volume, most of these methods are relevant for material specific formal constitutive equations and result in complex solutions. At this stage, it is difficult to describe nanoindentation creep behaviour, especially of biological materials, with accurate and appropriate constitutive models. Thus only phenomenological results are reported in this thesis. Further investigations are required to explore and describe the detailed creep properties and mechanisms of dental natural materials, including not only enamel and dentin, but also cementum and dental alveolar bone.

6.2.4 Conclusions

In this study, the room temperature creep behaviour of enamel was investigated and reported for the first time. This property is considered to be important in understanding the stress redistribution during contact loading and the long service life of teeth. The present results show that enamel has the ability to creep and exhibit a hysteresis response during contact loading and unloading very similar to that reported for bone. This is critical for natural hard tissues so as to cushion and distribute the rapid increasing stresses under functional loading conditions. Furthermore this visco-elastic behaviour associated with the protein component, may help enamel to relax high localized contact stresses, crack tip stresses and dissipate fracture energy under dynamic loads [48]. In addition, the comparison of creep behaviour between enamel and other dental materials indicated that enamel is more like a metallic material rather than ceramic. This may be helpful in guiding clinic material selection.

6.3 Numerical analysis of non-linear behaviour of enamel

Traditionally, enamel has been considered as a ceramic-like material because of its high hardness and elastic modulus. The limited size of enamel specimens and the cellular mitigated microstructural orientation have limited methods for quantifying the mechanical properties of the natural material. Only recently, with the development of nanoindentation instruments, has it been possible to investigate the orientation and spatial dependence of the elastic and non-linear behaviour of enamel. But, only limited numerical analyses have been undertaken.

Spears developed a microstructure based finite element (FE) model[6] that predicted orientation and protein content elastic modulus dependence in good agreement with recent observations[11,54]. Spears' model indicated large differences in elastic modulus between axial versus orthogonal loading relative to the rod direction.

Many authors have investigated the contact induced deformation of enamel. Staines et al. using a 6.35 mm diameter tungsten carbide indenter, were unable to observe specific elastic contact behaviour, even at very low loads, but rather hysteretic behaviour[14]. Xu et al. examined the contact induced damage with Vickers indenter at loads of 2-50 N and showed that damage at high contact stress was related to the hierarchical structure of enamel[55]. More recently, White et al. investigated the fracture toughness of enamel using a pointed indenter and showed it was 3 times higher than pure hydroxyapatite[8]. They argued the protein content played an important role in imparting higher toughness to enamel structure. Also, we have investigated the size and indenter shape dependence of the elastic modulus (chapter 5) and stress-strain response (chapter 4) of enamel, and found that not only did the orientation dependence of elastic modulus agree with Spears model but also an indenter size dependence existed. This work also supported Staines at al. observation as it was not possible to generate elastic contact of enamel with small spherical indenters. Moreover, we found that the extent of energy loss during indentation (section 1 of the chapter) was contact strain as well as indenter shape dependent.

In this section, we proposed a simple model of in-elastic deformation that incorporates the role of the protein, and specifically addresses the role of both microstructure and localised

strain associated with contact deformation to explain the above mentioned non-linear behaviour of enamel.

6.3.1 Contact deformation model

The microstructure of human enamel consists of very fine hydroxyapatite (HAP) crystallites aligned at different hierarchical levels[2,8,17,56-58]. At the crystallite level, HAP crystallites of enamel are roughly rectangular in cross-section with mean width of 68.3 nm and mean thickness of 26.3 nm[59] while the protein film between them is no more than 2 nm. In this paper, and because of the biological development of enamel, we consider Spears FE model[6] as appropriate. That is, enamel consists of a rod unit, which has cylindrical like structure that originates at the dentino-enamel junction, and between such rods there is a protein-rich sheath. Within the rod unit, HAP crystallites are arranged in certain directions and are "glued" together by a thin protein layer (Fig. 6-12).

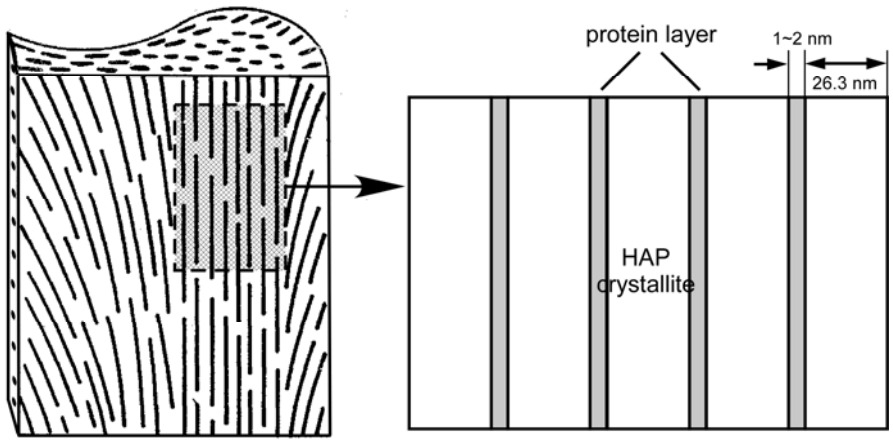

Fig. 6-12 Crystal orientation of hydroxyapatite (HAP) crystallites in a rod unit of enamel, showing the crystal and protein layer composite structure. (Revised from Eisenmann)[56]

During contact loading of enamel, the situation is influenced by the microstructure shown in Fig. 6-12. In Fig. 6-13, we illustrate the deformation response of enamel loaded parallel to the axis of the rods and HAP crystallites with pointed and spherical indenters.

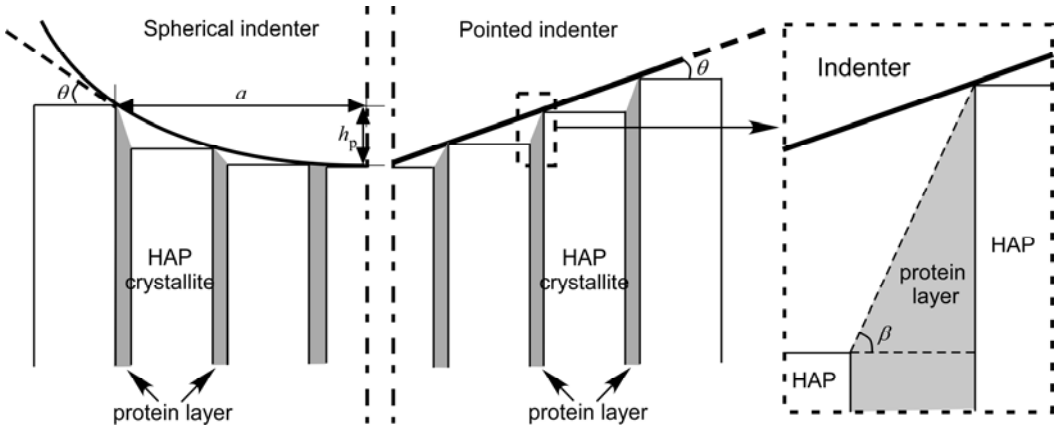

Fig. 6-13 Schematic illustration of contact induced deformation of enamel with pointed and spherical indenters.

As the organic part, protein has much lower mechanical properties than HAP crystals. Spears assumed a value of 4.3 GPa for the elastic modulus of protein in his FE model[6], while Jäger et al. cited 50 MPa as elastic modulus of collagen in their model for bone[33]. By considering the relationship of $G = \frac{E}{2(1+\nu)}$ where E, is elastic modulus, G is shear modulus and ν is Poisson's ratio, shear modulus of protein can be no more than 1.7 GPa from Spears and 20 MPa from Jäger et al. assuming the protein to be an effective elastic medium with Poisson's ratio of ν = 0.25, see Akiva et al[60]. Zhou and Hsiung[61] reported a G value of 0.213 GPa from a rate-dependent nanoindentation test. As the shear modulus of the protein is much lower than HAP (~ 56 GPa), therefore, we assume that HAP are rigid platelets and all contact deformation is accommodated in the protein component, especially under small contact load.

An amplified view of the shear that develops in the thin protein within the rod is shown in Fig. 6-13. In this figure, the HAP platelets behave as rigid blocks and all shear deformation occurs in the protein layer. The shear strain in the protein is given by:

$$\gamma_{\mathrm{p}} = \tan\beta = \tan\theta\left(\frac{l_{\mathrm{p}} + l_{\mathrm{a}}}{l_{\mathrm{a}}}\right), \quad (6\text{-}2)$$

where l_{p} and l_{a} are the thickness of the protein and HAP crystallites. In Fig. 6-12, HAP crystallites are assumed as plates parallel to the axis of contact and the thickness ratio of HAP to protein layer is 15:1. Therefore, for a Berkovich indenter with equivalent contact angle, θ, of 19.7° and with Eq. 6-2, the shear strain, γ_{p}, in protein layer will be 16 times higher than the contact strain.

Another feature of this model is that, as all the contact strain is transferred into the protein layer as shear strain, contact energy is dissipated by the protein phase and energy absorption of enamel should be proportional to the mean shear strain in the protein layer, which will be the integral of shear strains of all protein layers. From Eq. 6-2 in which shear strain, tan β, has a geometrical relationship with the contact angle, θ, the mean shear strain can be calculated as:

$$\bar{\gamma}_{\mathrm{p}} = \int \left(\frac{l_{\mathrm{p}} + l_{\mathrm{a}}}{l_{\mathrm{a}}} \right) \tan\theta d\theta . \quad (6\text{-}3)$$

For a pointed (Berkovich) indenter, mean shear strain in protein layer is constant because of the uniform θ angle. In contrast, for a spherical indenter, the mean shear strain is the integral of tan θ from 0 to θ because of the changing contact angle (Fig. 6-13).

In Chapter 3, we established a method to estimate indentation strain with contact angle, θ, with a calibrated spherical tip, in which the tip-shape was described by a function $a = f(h_{\mathrm{p}})$, where a is contact radius and h_{p} is contact depth (Fig. 6-13). Incorporating this approach in Eq. 6-3, we get

$$\bar{\gamma}_{\mathrm{p}} = \frac{l_{\mathrm{p}} + l_{\mathrm{a}}}{l_{\mathrm{a}}} \int_0^{h_{\mathrm{p}}} \frac{1}{f'(h_{\mathrm{p}})} dh_{\mathrm{p}} . \quad (6\text{-}4)$$

With this equation, mean shear strain for a spherical indenter can be calculated from contact depth.

In section 1 of the chapter, we investigated the contact induced energy loss of enamel using both spherical and pointed indenters and compared energy loss of enamel and sintered dense HAP using a spherical indenter with nominal radius of 10 μm, the results are shown in Fig. 6-4. At a small contact strain region, enamel has much higher energy absorption than HAP (Fig. 6-4). In all instances, the energy loss with a sharp Berkovich indenter was substantially higher than comparable contact strain values with spherical indenters, Fig 6-4. However upon replotting our energy absorption data against mean shear strain, γ_{p}, from Eq. 6-4, the Berkovich data superimposes with the spherical indenter results, Fig. 6-14.

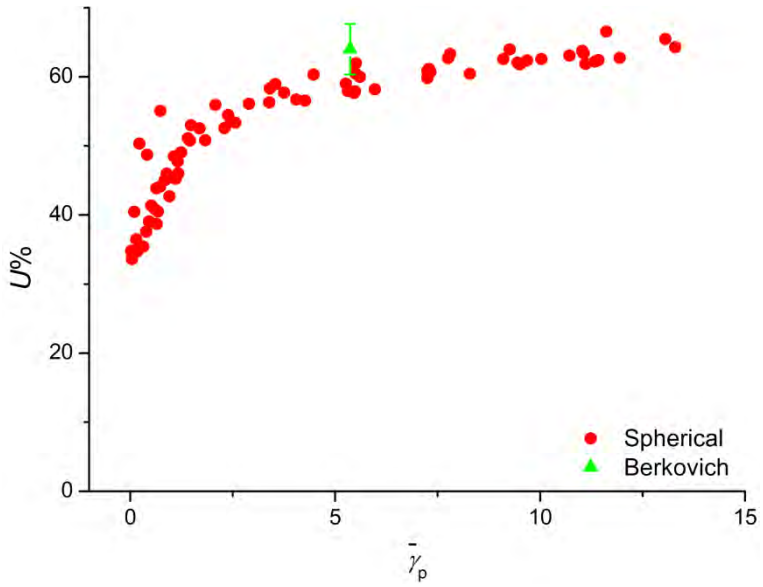

Fig. 6-14 Energy expenditure versus mean strain from 10 μm spherical and Berkovich indentations on enamel

6.3.2 Discussion

Most investigations of enamel to determine hardness and elastic modulus use high modulus indenters such as diamond and tungsten carbide, which may be considered rigid with respect to enamel. The mean contact stress, or hardness, defined simply as Eq. 3-15, $H=P/A$, where P is the peak load and A is the area of contact. The elastic contact stress over the area of contact, however, depends upon the indenter geometry[62]. In the case of pointed indenters, there is a stress singularity at the apex, whereas for the special indenter, the max stress is 1.5 times that of the mean value. In both instances, the contact stress drops to zero at the edge of contact. The strain associated with contact is dependent upon the contact angle of the indenter[63]. For a cone, the contact strain is given by tan θ, where θ is the angle between the original specimen and indenter flank, which remains invariant with depth of penetration. For a sphere, the angle of contact changes with depth of penetration.

As mentioned by other researchers, it is the minor protein component which plays a very important role in regulating the mechanical responses of biomaterials with hierarchical structures such as bone and nacre[19,33,48]. For dental hard tissues, the protein component also endows enamel with specific characteristics such as a distinctive hierarchical microstructure[58], elastic modulus anisotropy[6], effective viscoelastic properties and much higher facture toughness[8].

The present approach establishes a simple model of contact deformation for enamel which incorporates its hierarchical microstructure and explains the experimental phenomena illustrated in the above two sections of this chapter.

Firstly, the non-linear stress-strain response of enamel to indentation can be interpreted by the model. In the case of the elastic loading of a sphere on a flat, the Hertzian relationship may be written as $P = 3E/4\pi\ (a/R)$[64]. Hence, a plot of contact pressure, P, versus contact strain, a/R, should initially generate a linear relationship from which the elastic modulus of the sample may be determined. In Chapter 4, we could not find any linear part on stress-strain curve of enamel. These observations were supported by previous results of Staines et al.[14] and Fox[13]. On the basis of the model proposed in Fig. 6-13, the significant non-linear stress-strain curve of enamel can be explained as follows: indentation stresses result in high shear deformation of the protein and the non-linear stress-strain response was a reflection of inelastic behaviour of proteins.

Secondly, the inelastic response of enamel under small indentation force and contact pressures may also be explained with this model. As the model illustrated, the contact induced strain in the protein layer is approximately 16 times greater than the mean contact strain. Moreover, protein has much lower mechanical properties than HAP crystals. Therefore, even small contact stresses result in large shear strains in the protein layer and inelastic response of the deformed area. That is why we and other investigators could not achieve purely elastic response when indenting enamel[14]. Moreover, Staines et al. estimated the yield stress of enamel as 0.33 GPa by spherical indentation tests with a 6.35 mm diameter tungsten carbide ball[14]. Based on their data, the indentation depth was 1.6 μm at yield point. Therefore, contact radius a = 100.8 μm, $\tan\theta = a/R$ = 0.0317 and, based on Hertzian relationship, contact stress P = 0.6 GPa. The resultant effective shear strain in the protein layers is 0.48, well in excess of the generally considered theoretical elastic limit of materials, namely 0.1. This confirms our assumption that initial inelastic deformation comes from the protein layer.

Thirdly, this model explains the high energy absorption ability of enamel. Experimental data in Fig. 6-4 supports the model's ability to rationalise the energy loss difference between spherical and pointed indenters. Therefore, it is reasonable to assume that shear strain of the protein layer is the primary micro-deformation response during contact

deformation of enamel. By regarding peptide chains as “ropes” linking two adjacent HPA crystallites, as suggested by other authors[48,65], then for a Berkovich indenter, the elongation of peptide chains may be as much as 600% (1/cosβ*100%). The so-called sacrificial bond model in Fig. 6-15 provides a basis understand the mechanisms by which such large deformations of protein peptide chains are possible. A sacrificial bond is associated with folded peptide chain domain within a protein molecule which have the ability to unfold under stretching forces and refold after unloading[22,23,65]. Unfolding of these bonds results in extra energy expenditure[25] and this may explain the high energy absorption during contact deformation of enamel. Also, the auto refolding ability of these bonds endows enamel “self-healing” properties, which was reflected as creep recovery in the indentation creep tests of enamel described in section 2 of the chapter.

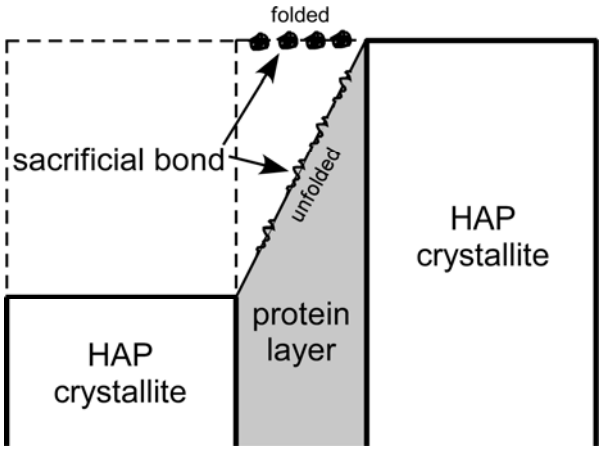

Fig. 6-15 A schematic illustration of protein peptide chain with sacrificial bonds deforming during indentation contact.

The above discussion is centred at the enamel crystallite level. By extending it to the next hierarchical level, the cylindrical rod level, this model may also be used to explain macro-scale contact, by replacing HAP crystallites and protein layers with rods and sheath. During oral function, opposing teeth may have a critical contact area of 0.4-2.2 mm^2 [66] with the maximal bite force of around 1000 N[67]. Even under this critical condition, the contact stress is still only 0.45-2.5 GPa, which is not sufficient to cause fracture or plastic deformation of HAP crystals. Therefore, the organic-rich sheath will play a major role at this level in accommodating the contact strains, which is similar to the crystallite model described above.

Finally, based on the model above, enamel is not a hard elastic ceramic-like material as generally considered. Because of the protein layers, enamel is very sensitive to contact force and may be readily deformed. Therefore, softer materials such as composites or metals may be better choices for antagonist restorations than ceramics and porcelains. Our recent investigation of indentation stress-strain curves of dental materials (Chapter 4) also supports this point of view, as enamel exhibited similar behaviour to that of dental alloys rather than ceramics.

6.3.3 Conclusions

In this section, we developed a simple model with respect to the hierarchical microstructure of enamel to illustrate structure related contact deformation mechanisms of human enamel. Within the contact indentation area, the thin protein layer between two HAP crystallites bears most of deformation in the form of shear strain, which is 16 times bigger than contact strain. By replotting energy absorption against mean strain value of protein layer, data from different indenters becomes superimposed, validating the model. This model may be used to explain the non-linear indentation stress-strain relationship, inelastic contact response and large energy absorption behaviour of enamel. Based on the above deformation model, all of these characteristics are related to the thin protein layers between crystallites. In short, like other biocomposites, the protein component within enamel plays an important role in regulating its mechanical responses and to meet its functional needs.

6.4 References

1. Rensberger JM. Mechanical adaptation in enamel. Rotterdam: Balkema; 1997. 237-57 p.
2. Maas MC, Dumont ER. Built to last: The structure, function, and evolution of primate dental enamel. Evolutionary Anthropology. 1999;8(4):133-52.
3. Paine ML, White SN, Luoa W, Hanson Fongc, Mehmet Sarikayac, Sneada ML. Regulated gene expression dictates enamel structure and tooth function. Matrix Biology. 2001;20:273-92.
4. Ferrario VF, Sforza C, Zanotti G. Maximal bite forces in healthy young adults as predicted by surface electromyography. J Dent. 2004;32:451-7.
5. Fernandes CP, Glantz P-OJ, Svensson SA. A novel sensor for bite force determinations. Dent Mater. 2003;19:118-26.
6. Spears IR. A three-dimensional finite element model of prismatic enamel: a re-appraisal of the data on the Young's modulus of enamel. J Dent Res. 1997;76:1690-7.
7. Spears IR, van Noort R, Crompton RH, Cardew GE, Howard IC. The effects of enamel anisotropy on the distribution of stress in a tooth. Journal of Dental Research. 1993;72:1526-31.
8. White SN, Luo W, Paine ML, Fong H, Sarikaya M, Snead ML. Biological organization of hydroxyapatite crystallites into a fibrous continuum toughens and controls anistropy in human enamel. J Dent Res. 2001;80(1):321-7.
9. Xu HHK, Smith DT, Jahanmir S, et al. Indentation damage and mechanical properties of human enamel and dentin. J Dent Res. 1998;77:472-80.
10. Habelitz S, Marshall SJ, Jr GWM, Balooch M. Mechanical properties of human dental enamel on the nanometre scale. Archives of Oral Biology. 2001;46:173-83.
11. Ge J, Cui FZ, Wang XM, Feng HL. Property variations in the prism and the organic sheath within enamel by nanoindentation. Biomaterials. 2005;26:3333-9.
12. Cuy JL, Manna AB, Livi KJ, Teaford MF, Weihs TP. Nanoindentation Mapping of the Mechanical Properties of Human Molar Tooth Enamel. Archives of Oral Biology. 2002;47:281-91.
13. Fox PG. The toughness of tooth enamel, a natural fibrous composite. J Mater Sci. 1980;15:3113-21.
14. Staines M, Robinson WH, Hood JAA. Spherical indentation of tooth enamel. J Mater Sci. 1981;16:2551-6.
15. Inage T, Shimokawa H, Teranishi Y, Iwase T, Toda Y, Moro I. Immunocytochemical demonstration of amelogenins and enamelins secreted by ameloblasts during the secrectory and maturation stages. Archives of Histology and Cytology. 1989;52:213-29.
16. Hu C-C, Fukae M, Uchida T. Sheathalin: cloning, cDNA polypeptide sequences, and immunolocalization of porcine enamel sheath proteins. Journal of Dental Research. 1997;76:648-57.
17. Boyde A, Martin LB. The microstructure of primate dental enamel. New York: Plenum Press; 1984. 341-67 p.
18. Sakai M. Energy principle of the indentation-induced inelastic surface deformation and hardness of brittle materials Acta Metallurgica et Materialia 1993;41(6):1751-8.
19. Gao H, Ji B, Jäger IL, Arzt E, Fratzl P. Materials become insensitive to flaws at nanoscale: Lessons from nature. PNAS. 2003;100(10):5597-600.
20. Fox P. The toughness of tooth enamel, a natural fibrous composite. J Mater Sci. 1980;15:3113-21.
21. Moreno EC, Zahradnik RT. The pore structure of human dental enamel. Arch Oral Biol. 1973;18(8):1063-8
22. Rief M, Gautel M, Oesterhelt F, Fernandez J, Gaub H. Reversible unfolding of individual titin immunoglobulin domains by AFM. Science. 1997;276:1109-12.
23. Smith B, Schaffer T, Viani M, et al. Molecular mechanistic origin of the toughness of natural adhesives, fibres and composites. Nature. 1999;399:761-3.
24. Thompson J, Klndt J, Drake B, Hansma H, Morse D, Hansma P. Bone indentation recovery time correlates with bond reforming time. Nature. 2001;414:773-5.
25. Fantner GE, Hassenkam T, Kindt JH, et al. Sacrificial bonds and hidden length dissipate energy as mineralized fibrils separate during bone fracture Nature Materials. 2005;4(8):612-6
26. Macho GA, Jiang Y, Spears IR. Enamel microstructure—a truly three-dimensional structure. Journal of Human Evolution. 2003;45:81-90.
27. Radlanski RJ, Renz H, Willersinn U, Cordis CA, Duschner H. Outline and arrangement of enamel rods in human deciduous and permanent enamel. 3D-reconstructions obtained from CLSM and SEM images based on serial ground sections. Eur J Oral Sci. 2001;109:409-14.
28. Goto T, Sasaki N, Hikichi K. Early stage stress-relaxation in compact bone. Journal of Biomechanics. 1999;32:93-7.

29. Jäger IL. Viscoelastic behavior of organic materials: consequences of a logarithmic dependence of force on strain rate. Journal of Biomechanics. 2005;38:1451-8.
30. Sasaki N, Enyo A. Viscoelastic properties of bone as a function of water content. Journal of Biomechanics. 1995;28:809-15.
31. Sasaki N, Yoshikawa M, Enyo A. Stress relaxation function of bone and bone collagen. Journal of Biomechanics. 1993;26:1369-76.
32. McElhaney JH. Dynamic response of bone and muscle tissue. Journal of Applied Physiology. 1966;21:1231-6.
33. Jäger IL, Fratzl P. Mineralized collagen fibrils: a mechanical model with a staggered arrangement of mineral paticles. Biophysics Journal. 2000;79:1737-46.
34. Williams G, Watts DC. Non-symmetrical dielectric relaxation behavior arising from a simple empirical decay function. Transactions of the faraday society 1970;66(565P):80-5.
35. Dorrington KL. The theory of viscoelasticity in biomaterials. Symp Soc Exp Biol. 1980;34:289-314.
36. Lucas BN, Oliver WC. Indentation power-law creep of high-purity indium. Metallurigical and Materials Transactions. 1999;30A(3):601-10.
37. Yang S, Zhang YW, Zeng KA. Analysis of nanoindentation creep for polymeric materials. Journal of Applied Physics. 2004;95(7):3655-66.
38. Oyen M, Cook R. Load-dieplacement behavior during sharp indentation of viscous-elastic-plastic materials. Journal of Materials Research. 2003;18(1):139-49.
39. Wei BC, Zhang TH, Li WH, Xing DM, Zhang LC, Wang YR. Indentation creep behavior in Ce-based bulk metallic glasses at room temperature. Materials Transactions. 2005;46(12):2959-62.
40. Bembey AK, Oyen ML, Bushby AJ, Boyde A. Viscoelastic properties of bone as a function of hydration state determined by nanoindentation Philosiphical Magazine. 2006;86(33-35):5691-703
41. Li WB, Henshall JL, Hooper RM, Easterling KE. The Mechanisms of Indentation Creep. Acta Metallurgica et Materialia. 1991;39(12):3099-110.
42. Johnson KL. The Correlation of Indentation Experiments. Journal of the Mechanics and Physics of Solids 1970;18(2):115-26.
43. Savage MF, Neeraj T, Mills MJ. Observations of room-temperature creep recovery in titanium alloys. Metallurigical and Materials Transactions. 2002;33A(3):891-8.
44. Neeraj T, Hou DH, Daehn GS, Mills MJ. Phenomenological and microstructural analysis of room temperature creep in titanium alloys. Acta Mater. 2000;48:1225-38.
45. Hero H. On creep mechanisms in amalgam. Journal of Dental Research. 1983;62:44-50.
46. Xu HHK, Liao H, Eichmiller FC. Indentation creep behavior of a direct-filling silver alternative to amalgam. Journal of Dental Research. 1998;77(12):1991-8.
47. Mayo MJ, Nix WD. A micro-indentation study of superplasticy in Pb, Sn, and Sn-38 wt% Pb. Acta Metall. 1988;36(8):2183-92.
48. Ji B, Gao H. Mechanical properties of nanostructure of biological materials. Journal of the Mechanics and Physics of Solids. 2004;52:1963-90.
49. Atkins AG, Silverio A, Tabor D. Indentation hardness and the creep of solids. Journal of The Institue of Metals. 1966;94:369-78.
50. Bower AF, Fleck NA, Needleman A. Indentation of a power law creeping solid. Proceedings of the royal society of London series A. 1993;441:97-124.
51. Feng G, Ngan AHW. Effects of creep and thermal drift on modulus measurement using depth-sensing indentation Journal of Materials Research. 2002;17(3):660-8.
52. Ngan AHW, Tang B. Viscoelastic effects during unloading in depth-sensing indentation Journal of Materials Research. 2002;17(10):2604-10.
53. Cheng L, Xia X, Seriven LE, Gerberich WW. Spherical-tip indentation of viscoelastic material. Mechanics of Materials. 2005;37:213-26.
54. Angker L, Swain MV. Nanoindentation: Application to dental hard tissue investigations J Mater Res. 2006;21(8):1893-905
55. Xu HHK, Smith DT, Jahanmir S, et al. Indentation damage and mechanical properties of human enamel and dentin J Dent Res. 1998;77(3):472-80
56. Eisenmann DR. Enamel Structure. In: Cate RT (ed). Oral Histology. St. Louis, Missouri: Mosby, 1998:218-35.
57. Gwinnett AJ. Structure and composition of enamel. Operative Dentistry. 1992;Suppl. 5:10-7.
58. Koenigswald Wv, Sander PM. Tooth enamel microstructure. In: Cate RT (ed). Oral histology : development, structure, and function (5^{th} Edition). Rotterdam: Balkema, 1997:267-80.
59. Kerebel B, Daculsi G, Kerebel LM. Ultrastructural studies of enamel crystallites. J Dent Res. 1979;57:306-12.

60. Akiva U, Wagner HD, Weiner S. Modelling the three-dimentional elastic constants of parallel-fibred and lamellar bone. J Mater Sci. 1998;33:1497-509.
61. Zhou J, Hsiung LL. Biomolecular origin of the rate-dependent deformation of prismatic enamel. Appl Phys Lett. 2006;89:051904.
62. Fischer-Cripps AC. Introduction to Contact Mechanics. New York: Springer; 2000.
63. Tabor D. Hardness of Metals. Oxford: Clarendon Press; 1951.
64. Lawn BR. Indentation of Ceramics with Spheres: A Century after Hertz. J Am Ceram Soc. 1998;81:1977-94.
65. Thompson JB, Kindt JH, Drake B, Hansma HG, Morse DE, Hansma PK. Bone indentation recovery time correlates with bond reforming time Nature. 2001;414(6865):773-6
66. Hayasaki H, Okamoto A, Iwase Y, Yamasaki Y, Nakata M. Occlusal contact area of mandibular teeth during lateral excursion Int J Prosthodont. 2004;17(1):72-6
67. Waltimo A, Kononen M. Maximal bite force and its associations with signs and symptoms of craniomandibular disorders in young Finnish non-patients. Acta Odontol Scand. 1995;53:254-8.

Chapter 7

Influence of environment on the mechanical behaviour of human enamel

An understanding of the mechanical behaviour of enamel is important to both clinicians and material scientists. Numerous researchers have described the mechanical properties of mature enamel[1-6], and tried to explain the unique mechanical characteristics of enamel from different perspectives such as anisotropy[1-3], hierarchy[5,6] and composition[4,6]. Anisotropic and hierarchical characteristics of enamel have been described by numerical models and been used to explain fracture and other mechanical properties of enamel[6-9].

Though organic components such as protein and free water comprise only a minor part of mature enamel, they are crucial to its development and are important in understanding its structural organization and physical properties[10]. After maturation, fragments of some acidic proteins called enamelins and tuftelins remain inside enamel[11] and act as a "glue" between crystallites[12] throughout the rod structure and extend from the dentine enamel junction to the enamel surface. Most free water within enamel is located within the protein matrix and has an influence on enamel's compressibility, permeability and ionic conductivity[13]. The resulting composite material is much tougher than apatite mineral alone[4].

The important role of organic components in calcified tissues has widely been recognized. Theoretically, Ji and Gao predicted the consequences of the juxtaposition of high modulus and high aspect ratio apatite crystals with low modulus binding proteins on the strength and stress-strain response of calcified tissues[14]. These mechanical and microstructural differences endow the protein component as a major regulator of the properties of natural biomaterials, which have been described by Spears' finite element (FE) model[6], Jäger's "staggered" model[15] and Gao's tension-shear-chain (TSC) model[16]. For dental hard tissues, the protein component also endows enamel with specific characteristics such as a distinctive hierarchical microstructure[17], elastic modulus anisotropy[6], effective viscoelastic properties[18] and much higher facture toughness[4]. Recently, with the help of the TSL model, Zhou and Hsiung calculated the shear modulus

of the protein film within rod enamel from nanoindentation tests[18]. All these recent studies emphasize that the minor organic component may be the key to understanding the excellent mechanical properties of calcified tissues.

As is well known, the properties of proteins may be regulated by thermal and chemical mediums. Also, Bembey et al. proved that environmental conditions had significant influence on the mechanical properties of bone tissue[19,20]. Thus an investigation of the mechanical properties of enamel in various environments provides us a method to explore the role of the organic matrix within mature enamel. The aim of this study is to investigate the influence of various environments on the enamel mechanical properties using nanoindentation.

The chapter is based on the following manuscript:

- HE, L.H. & SWAIN, M.V. (2007) Influence of environment on the mechanical behaviour of mature human enamel. *Biomaterials*, 28, 4512-4520.

7.1 Material and Method

Five healthy premolar teeth extracted for orthodontic reasons were selected and disinfected with Milton's solution. Two of the samples (burnt samples) were placed in a dental ceramic furnace [VACUMAT 50, Vita, Germany] and heated to a temperature of 300℃ for 5 min. After the treatment, all samples were cut, embedded and polished as described in chapter 3. The remaining three sound enamel samples were cut into 2 mm thick slices from the epoxy tooth block to ensure full penetration of absolute ethanol through enamel in the following experiments. Once the slice had been prepared and prior to immersion in ethanol, they were briefly stored in distilled water at room temperature prior to testing. The burnt enamel samples were stored in ambient environment. Nanoindentation elastic modulus, hardness and creep behaviour of sound then burnt enamel samples were tested by a UMIS system as mentioned in chapter 3 under water and dry environment, respectively. The sound enamel slices were then soaked in absolute ethanol [100% denatured ethanol alcohol, Chem-Supply, Australia] for 24 hours (dehydration) and the same tests were repeated under ethanol. After that, the slices were returned to distilled water again for another 24 hours (re-hydration) before the same tests were repeated under water. Finally, the samples were dried in ambient environment for another 24 hours (dry) and indentation tests were repeated again.

Elastic modulus and hardness of specimens were measured with a calibrated Berkovich indenter [Synton, Switzerland]. The force applied during testing ranged form 10 to 250 mN. The software calculated elastic modulus and hardness as a function of penetration depth, h_p, for each indentation. At least 16 indents at different forces were done for each test. Results were statistically analyzed (*t*-test, $p<0.05$).

The shear modulus, *G*, maybe determined from the expression developed in Zhou and Hsiung's paper[18], namely;

$$G_p = \frac{4(1-V_h)E_hE_e}{(V_hE_h - E_e)V_h\rho^2}. \qquad (7\text{-}1)$$

With G_p, shear modulus of protein film, V_h, volume fraction of HAP, E_h, elastic modulus of HAP, E_e, elastic modulus of enamel, ρ, aspect ratio of HAP crystals. Again following Zhou and Hsiung [18] who assumed $\rho = 30$, $V_h = 0.95$, $E_h = 144$ GPa, with the E_e value from our investigation, we calculated G_p values for different environmental conditions.

The Berkovich indenter was used to investigate the indentation creep behaviour of different materials at a force of 250 mN. One-step loading and unloading method was set with a maximum-force (250 mN) hold time of 900 seconds and upon unloading a minimum-force (5 mN) hold time of 900 seconds. All tests commenced after at least 2 hours' thermal soak period in the instrument, and thermal drift was deemed to be almost negligible (<0.05 nm/sec) before each experiment commenced.

For all the tests, the distance between indents was more than 40μm to avoid the influence of residual stresses from adjacent impressions because this distance is far larger than the stress field of the indent impression which scales with the contact diameter.

After indentation testing, scanning electron microscopy (SEM) [XL-30, Philips, Netherlands] was used to examine the residual indent impressions. One enamel specimen was slightly etched with a mild polyacrylic acid (10%) solution [Dentin Conditioner Liquid, GC, Japan] to better highlight the structures and indentation damage. All samples were ultrasonic cleaned with pure ethanol for 10 seconds before gold coating prior to SEM. Samples were also investigated with energy dispersive X-ray analysis (EDX) using a frame collection procedure at 5000 magnification with a data collecting time of 50 seconds to compare the composition between untreated and burnt enamel. With the help of standard gold sample, we extracted the Au peak from the spectrum of coated enamel samples for better comparison of compositions.

7.2 Results

7.2.1 Indentation elastic modulus and hardness

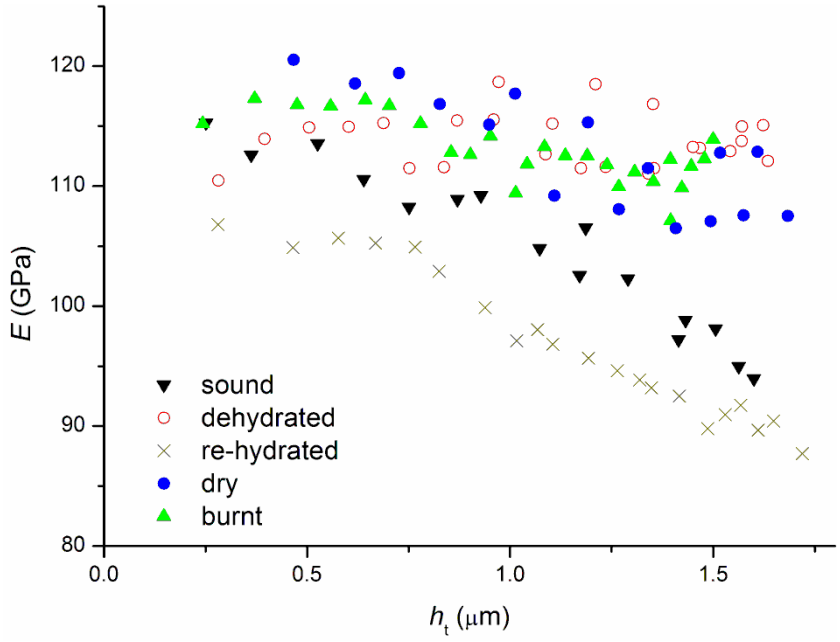

(a)

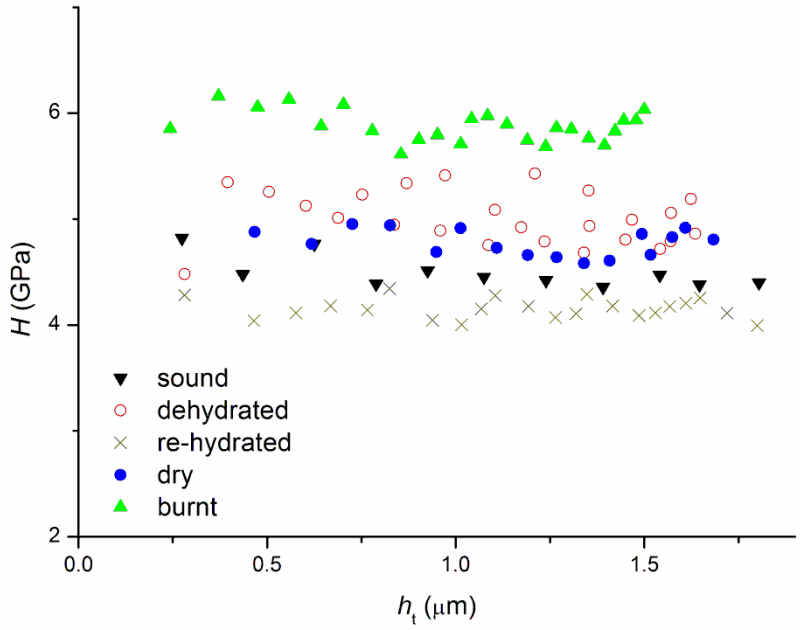

(b)

Fig. 7-1 Elastic modulus (a) and hardness (b) of enamel under different treatments with a Berkovich indenter.

As illustrated in Fig. 7-1a, healthy enamel showed decreasing elastic modulus values from ~120 to 100 GPa with increasing contact depth, h_t. After dehydration, the decreasing

trend of elastic modulus disappeared and *E* values stabilized at ~115 GPa, which was the same as the burnt sample. After the ethanol desiccated sample was re-soaked in water, the elastic modulus showed a decreasing trend but with the value decreasing from ~85 to 65 GPa. After subsequent drying at room temperature, the *E* value went back to the normal range of sound enamel, 110-120 GPa. All the treatments showed significantly different values compared to sound enamel (Table. 1).

Table 7-1 Elastic modulus and hardness of enamel with different treatments

Treatments	Elastic modulus (GPa)	Protein Shear Modulus (GPa)	Hardness (GPa)
Sound	104.85 ± 6.81	0.114 ± 0.032	4.49 ± 0.25
Dehydrated	113.84 ± 2.24*	0.165 ± 0.021*	5.01 ± 0.25*
Re-hydrated	96.78 ± 6.16	0.077 ± 0.012*	4.15 ± 0.10*
Dry	112.9 ± 4.86*	0.164 ± 0.042*	4.78 ± 0.13*
Burnt	113.48 ± 2.91*	Nil	5.94 ± 0.34*

(* means the group is statistically different to sound enamel, $P<0.05$)

Indentation hardness is the value of contact pressure at maximum load, which is a measure of the resistance of a material to permanent indentation. Results in Figure 7-1b and Table 7-1 illustrate that sound and burnt enamel had statistically the highest hardness values of ~6 GPa, followed by the dehydrated sample (~5 GPa). The softest sample was re-hydrated enamel with a hardness of just over 4 GPa. Drying in ambient laboratory of the re-hydrated sample raised the hardness of the sample by nearly 1 GPa.

The protein shear modulus values estimated from Eq. 7-1 and listed in Table 7-1, indicate that alcohol dehydrated and dry enamel has significantly higher values than in sound enamel. In contrast, the re-hydrated sample has a much lower value than sound enamel. Because matrix proteins and other organic components have been denatured during the heating procedure, shear modulus for the burnt samples was not calculated here.

7.2.2 Indentation creep behaviour

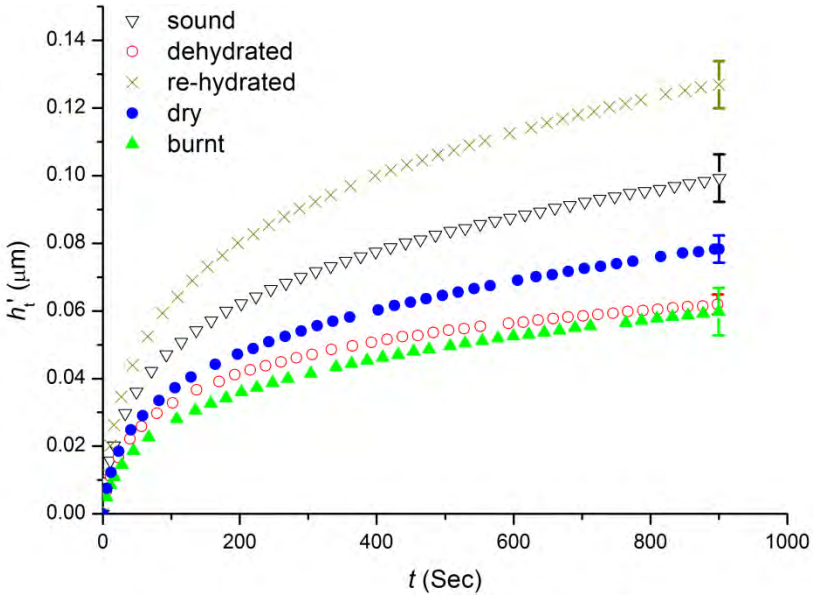

(a)

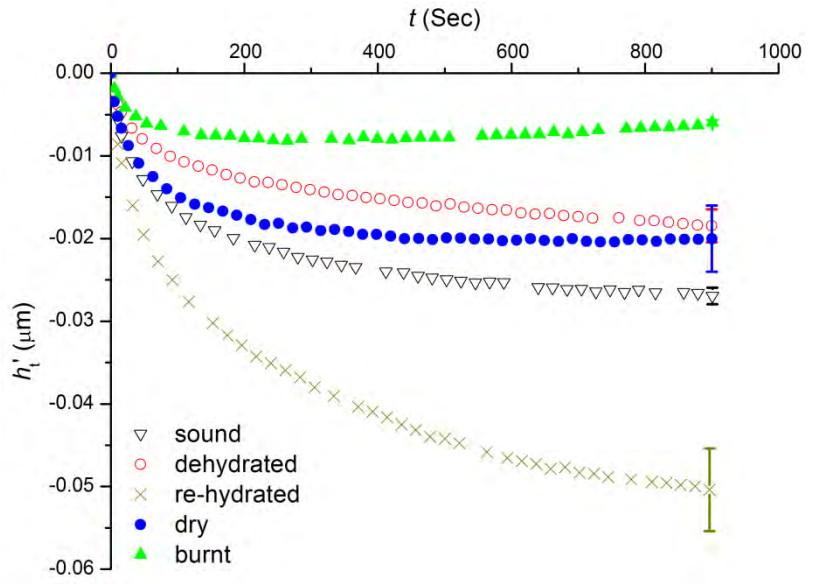

(b)

Fig. 7-2 Indentation depth against time, h_t'-t, curves of creep (a) and backcreep (b) of enamel under different treatments.

All the curves in Fig. 7-2 were the average value of at least 5 tests and the error bars at the end of the curves indicate the deviation of the data. The relative penetration depth, h_t', was calculated by subtracting the initial depth at the beginning of the holding time from the increasing depths during the holding period at maximum and minimum loads.

Creep data at maximum-load holding varied for different treatments (Fig. 7-2a). Sound enamel had a creep displacement of nearly 100 nm under watery environment, while the re-hydrated sample generated an additional ~20 nm. Alcohol dehydrated and burnt samples had similar creep curves, which were much lower than the other two samples. Dried enamel had a value between burnt and sound samples.

At the minimum-load holding period (called "*backcreep*" period), the recovery was most prominent again for the re-hydrated sample, which recovered ~20 nm more than sound enamel (Fig. 7-2b). The dehydrated sample had very limited backcreep while for burnt enamel it was negligible after the first 100 seconds because the displacement rate and limited backcreep were all within the limits of the nanoindentation systems thermal drift stability (~0.05 nm/sec).

The above results imply that at both the maximum and minimum loads different environment mediums may influence the creep behaviour of enamel. As hydroxyapatite crystals may be considered as chemically and thermally stable under these test conditions, this indicates that the small amount of protein inside enamel may influence mechanical properties of enamel.

7.2.3 SEM and EDX analysis

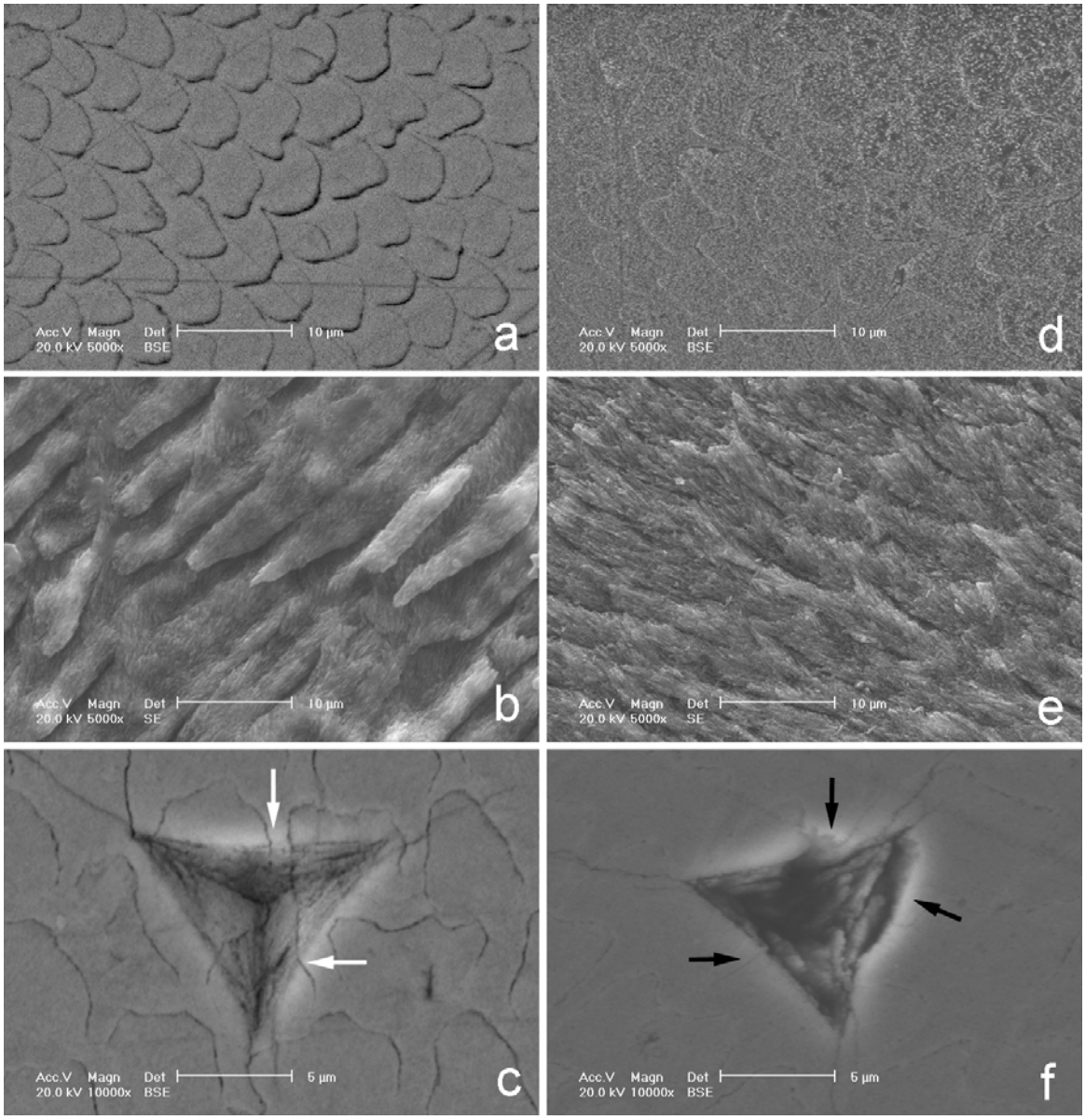

Fig. 7-3 SEM images comparing sound [a, b, c] and burnt enamel [d, e, f]. Images (a) and (d) are of the top surface while images (b) and (e) are of a cross section surface. Images (c) and (f) are of indentation impressions under a load of 250 mN on the top surface. (Cross sections of both samples, figure b and e, were etched by 37% H_3PO_4 for 5 seconds.)

Fig. 7-3 compares the sound and burnt enamel from directions parallel and perpendicular to the rods. After heating, the burnt sample became chalk white and fragile, but the rod structure of enamel still remained intact (Fig. 7-3d). However comparing the cross-section views of the two samples (Fig. 7-3b and e), it appears that heating made the

crystallites looser than for sound enamel. As a result, the entire rod structure looks rougher. These findings are similar to that described by other researchers on enamel and bone[21,22]. Sound enamel showed completely inelastic deformation without any prominent cracks (Fig. 7-3c). The white arrow in Fig. 7-3c illustrates that even at a rod gap along the boundary of the indent impression, no crack formation occurred. In contrast, burnt enamel exhibited typical brittle behaviour with a sharp indenter. The black arrows in Fig. 7-3f highlight brittle cracks at the edges and corners of the indent. Moreover, by comparing the centre of residual impressions, the deformed area of burnt enamel was much easier to etch with mild acid than sound enamel. Because of the similarity of dehydrated and re-hydrated samples to those of sound enamel, SEM images are not shown.

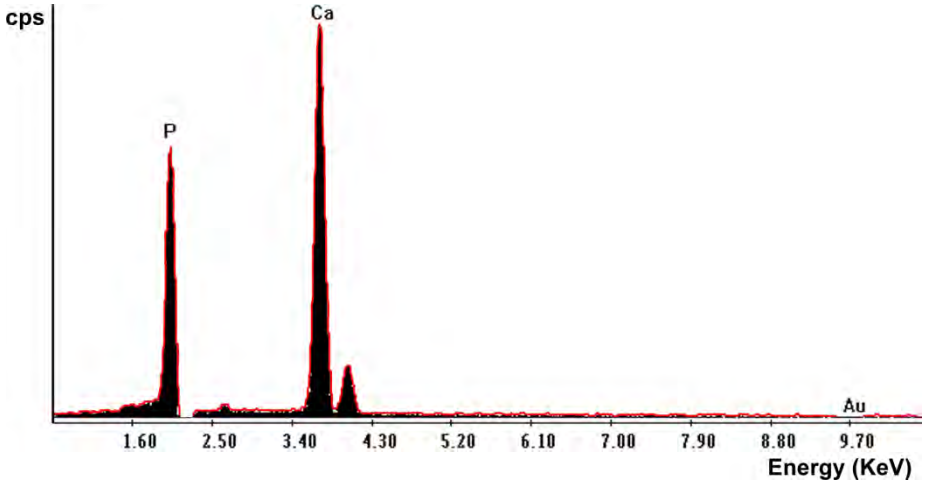

Fig. 7-4 Comparison of EDX spectrum on sound (black area) and burnt enamel (red line). (Two spectra completely overlapped.)

As illustrated in Fig. 7-4, EDX showed that sound and burnt enamel had exactly the same elemental composition, including the Ca to P ratio, which indicates no chemical changes of the inorganic component of enamel occurred during the heating procedure. This is in accordance with the XRD analysis on other heated calcified tissues [23].

7.3 Discussion

7.3.1 Possible roles of proteins in regulating mechanical behaviour of enamel

The functions of proteins for regulation of mechanical responses of enamel may be interpreted from the biopolymer[14] and sacrificial bond[24,25] characteristics of matrix proteins. We shall now consider the possible role each of these characteristics may play.

(1). Biopolymer

The proteins and other organic components within enamel may be regarded as a cross-linked biopolymer network. Viscoplastic properties of these biopolymers stem from the configurational rearrangements, disposition and interaction among the macromolecules in both their short- and long-range network interactions[14]. Under indentation load, the local re-distribution response of the structure is rapid, while the long-range interaction response is slow due to reduced stresses and the time-dependent molecular rearrangement Upon unloading, due to the memory effects associated with the cross-linked network, the molecules have a tendency to return to their initial form and positions[14].

(2). Sacrificial bond

Recently, the special mechanical responses of a recoverable domain bond within protein named the "sacrificial bond" was reported with the help of AFM[24,25]. Molecules that contain these bonds reveal saw-tooth pattern force-displacement curves under tensile loading and Rief et al.[24] demonstrated that every peak of the saw-tooth curve corresponded to a single domain unfolding. Such a domain structure also showed recovery upon unloading by refolding of the structure. The longer the delay before the next application of force, the more reformation of the bond occurred during relaxation. The value of the peak force of these saw-tooth curves for molecules within abalone shell varied from 100-400 pN[25]. Although the individual components of this type of bond may be weak (hydrogen bridges, hydrophobic interactions, etc.), because of the number in any one molecule, this multiple rupturing bond contributes significantly to the creep resistance and backcreep behaviour of structures containing them. By combining Jäger's staggered model[15] with the sacrificial bond theory[24], Ji and Gao[14] proposed a simple model to explain the roles of proteins between crystallites. Below is a schematically

modified version of their model for better understanding the contact deformation conditions that are relevant to the indentation of enamel (Fig. 7-5). This model may assist our understanding of the creep mechanisms at the crystallite level.

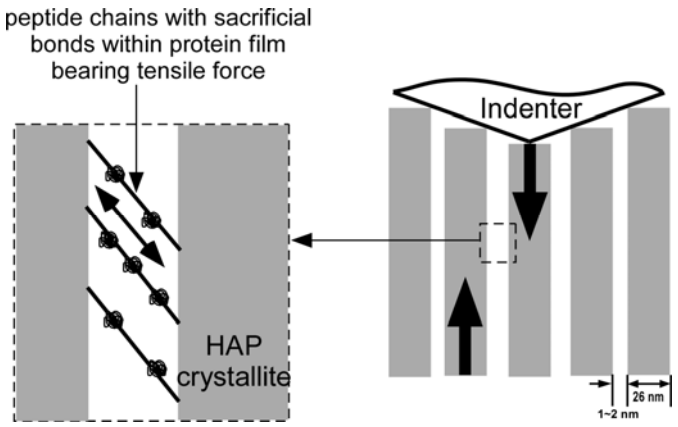

Fig. 7-5 Staggered model illustrates the functional response to shear strain of matrix proteins between HAP crystallites.

On the basis of the above model, creep behaviour may be considered as follows: during indentation loading procedure, the tip displacement causes shear movement of adjacent HAP crystallites (as black arrows shown in Fig. 7-5) causing a tensile force on the peptide chain of proteins linking the crystallites (as the double headed arrow shown in Fig. 7-5). This results in the unfolding of the sacrificial bonds during the hold period at maximum load and leads to further time dependent unfolding or creep behaviour. Upon unloading, refolding of peptide chains and the presence of residual elastic strains surrounding the residual impression enables the deformed material to recover inelastically. Moreover, at the rod level, the thick sheath with its higher protein organic content has much lower elastic modulus and hardness than the rod area [5]. This may also cushion the stress and limit the transfer of shear stress from one rod to the next. As a result, the existence of this protein thin film between HAP crystallites and protein rich sheath regulates the stress distribution on a large scale by its inelastic behaviour.

7.3.2 Experimental support

Firstly, by comparing the elastic modulus results between sound and dehydrated enamel (Fig. 7-1a), the decreasing trend of elastic modulus with contact depth was absent in the latter groups, and creep and backcreep of enamel were also partially blocked. In previous

studies[2,26], it was argued that the elastic modulus of enamel was controlled by the organic matrix and resulted in a decreasing trend with increment of contact depth or contact area at the micrometer level. Also, creep and backcreep are a consequence of the protein matrix deformation as HAP has minimal viscous behaviour. Therefore, the different responses of the dehydrated group are considered to be a consequence of the change of structure and function of mature enamel matrix proteins. This change may be interpreted by the well known specific biochemical function of ethanol.

The ethanol molecule has a radius of ~0.17 nm, which is small enough to enter most pores of a molecular-sieve like enamel[27]. Moreover, ethanol has a strong dehydration function and can change the conformation of a peptide chain within proteins[28,29]. Ethanol's amphiphilic properties enable it to be attracted simultaneously to both hydrophobic and hydrophilic targets, bind certain targets preferentially and displace water, leading to conformational changes of peptide chains of proteins[29]. One example is that ethanol may substitute hydrogen-bonded water between carboxyl group and NH group of peptide chain and affect biomechanical properties of the protein by changing its conformation (Fig. 7-6). Moreover, glycoproteins attract large volumes of water (up to 95%) and research on the glycoproteins of respiratory mucus indicated that the degree of hydration is very important in maintaining biological functions of glycoproteins[30]. Similarly, we may assume that dehydration of glycoproteins within an enamel matrix may have a vital influence on their mechanical properties and that ethanol dehydrates these types of proteins as well.

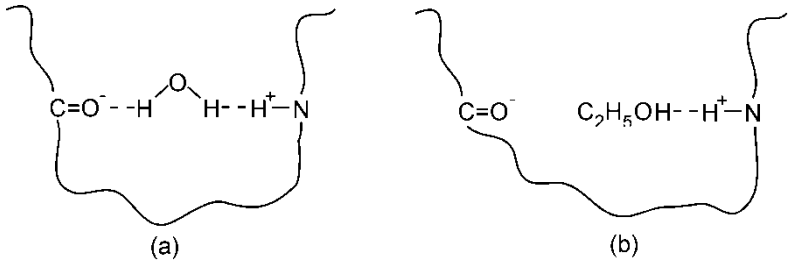

Fig. 7-6 Schematic illustration of peptide chain maintained by water (a), and changes in the presence of ethanol (b). The water hydroxyl group would be attracted to the carboxyl group of the peptide chain, and simultaneously the oxygen of water would be attracted to NH groups in the same chain. Alcohol, on the other hand, cannot bind both sites at the same time, because it has only a hydroxyl group to be attracted to NH groups. As a result, the conformation of the protein is changed. (Revised from Klemm[29])

Recently, another investigation on the role of alcohol in the fracture resistance of teeth[31] illustrated that chemical dehydration had a significant effect on the elastic modulus, strength, and fracture toughness of dentin and this effect is considered to be associated with increased cross-linking of the collagen molecules from intermolecular hydrogen-bonding, where water is replaced with weaker hydrogen-bond-forming solvents such as alcohol.

Secondly, by observing results from burnt enamel, a similar phenomenon was found for the elastic modulus – that is no decreasing trend with load exists (Fig. 7-1a). Other research on bone and enamel[23,32,33] has shown that heat treatment over a similar temperature range denatured matrix protein and collagen fibers, and the mechanical properties of a heated sample was influenced dramatically. Therefore, it is reasonable to assume that the protein matrix and water within our burnt enamel have been destroyed and removed. This may provide an explanation for the absence of backcreep. This supports our assertion that backcreep arises mainly from the presence of the protein matrix. By comparing burnt with dehydrated samples, the limited backcreep of the later may be explained as follows: although their biological functions have been blocked by ethanol, the matrix proteins may still act as biopolymers with some viscoelastic properties. In addition, the lubricating function of ethanol liquid inside dehydrated enamel should also be considered. In contrast, free water and loosely bound water were released from burnt enamel by heating to 300 ℃.

Furthermore, the shear modulus value of organic components of enamel also appears to be related to the different creep behaviour following different treatments (Table 7-1). Due to loss of water and/or changing of conformation, proteins in alcohol dehydrated and dry sample became stiffer than sound enamel. With higher *G* values, indicating that the biopolymer proteins are less plasticized, it is reasonable to anticipate less creep and backcreep for these two groups. On the other hand, additional plasticizing agents such as water in re-hydrated group may not only allow the proteins to recover but also lubricate the biocomposite system. Therefore, more creep and backcreep is not surprising.

Thirdly, SEM investigation provides visual evidence of the changes that take place in enamel without matrix proteins. Although the rod structures are still recognizable, the

HAP crystallites appeared looser in their arrangement with the absence of the protein "glue". This provided a better chance for acid to penetrate and etch the surface. This is why Figures 7-3d and 3e appear rougher than Fig. 7-3a and 3b, and indent impressions of the burnt sample were more seriously etched than their sound counterpart (Fig. 7-3c and 3f). The comparison of Fig. 7-3c and 3f also confirmed our assumption that the protein thin film redistributes the stresses. In the absence of a protective protein cushion between crystallites, the sample became brittle and fragile as indicated by the presence of cracks marked by black arrows. In contrast, with the protection of protein films, the entire structure can sustain high stresses without any cracks, even at the weak inter-rod junction, as highlighted by the white arrow in Fig. 7-3c.

7.3.3 Consideration of hierarchical structure of enamel

Why do burnt samples still have some creep ability? And why do re-hydrated samples have lower elastic modulus, hardness and greater creep and backcreep capacity? Responses to these questions may be interpreted from the hierarchical micro-structure of enamel.

After heating to 300 ℃, the organic matrix has lost all of its biological functions and the resultant enamel has modified mechanical properties. Crystallite-boundary sliding and densification may be the main creep and deformation mechanisms of this material with its fine micro-structure and porosity between the crystallites. Carbon particles between HAP crystallites originating from burning of the organic matrix may also act as a solid lubricant to promote sliding of adjacent crystallites. By comparing the force displacement responses with data from pure hydroxyapatite block (data not shown here), the hierarchial micro-structure contributes considerably to the creep behaviour of burnt enamel.

A comparison of creep and backcreep of sound and re-hydrated enamel, indicates that the later had an additional 20 nm in creep penetration depth and a similar amount of backcreep recovery. A possible explanation may be the over saturation of water within the enamel micro-structure following rehydration. Additional water may have contributed to more extensive creep and backcreep responses of the sample by softening or plasticizing the whole biocomposite system. Dehydration research on dentine indicated that polar solvents such as ethanol were found to result in shrinkage of hydrated dentine

matrix[34]. Therefore, it is reasonable to assume the re-hydration procedure may hyper-hydrate the peptide chains, swelling the enamel matrix. However, following 24 hours drying of the re-hydrated sample in an ambient environment, creep and backcreep behaviour decreased and were slightly lower than sound enamel. This indicates that water plays an important role in regulating the mechanical responses of enamel.

7.3.4 Clinical implications

Although this is a basic study of a natural biocomposite—enamel, there are still several practical implications for dental practitioners and material scientists. A range of different therapeutic materials and medicines are used in daily dental restorative and aesthetic treatments, such as cavity liner materials and adhesion bonding materials, disinfection solutions and tooth whitening products, all of which contain readily diffusible components. The consequence of these chemical reagents diffusing into enamel may have hazardous effects on the protein fragments and compromise the mechanical behaviour of enamel. Such effects have been reported in the case of bleaching of enamel[35]. This may reduce load bearing, wear behaviour and the lifetime of enamel. Therefore, a thorough investigation of the influence of these chemical reagents on the protein components of enamel will be an interesting and meaningful direction of future research.

7.4 Conclusions

This study identified that the mechanical properties of enamel are environmentally dependent. It is argued that such observations provide evidence of the role of mature enamel matrix proteins in regulating mechanical properties of sound enamel. The calculated shear modulus of the protein phase of enamel was also found to be significantly changed in the various environments. Pure ethanol partially blocked functions of matrix proteins by dehydrating the system, while heat treatment destroyed matrix proteins inside enamel. As a result, without deformable matrix proteins, the mechanical behaviour (especially creep response, modulus size dependence and fracture resistance) of different enamel samples noticeably changed. Comparing sound and treated enamel samples, matrix proteins endow enamel better performance as a load bearing calcified tissue. These observations suggest that, although proteins are only a minor part of the enamel composition, however with their biopolymer and perhaps sacrificial bond characteristics, they may regulate the mechanical properties of enamel by redistributing stresses inelastically. The results presented support Spears' finite element model[6] of the role of protein on the elastic modulus of enamel and Jäger's model[15] for creep of calcified tissues.

7.5 References

1. Habelitz S, Marshall SJ, Jr GWM, Balooch M. Mechanical properties of human dental enamel on the nanometre scale. Archives of Oral Biology. 2001;46:173-83.
2. He LH, Fujisawa N, Swain MV. Elastic modulus and stress–strain response of human enamel by nanoindentation. Biomaterials. 2006;27:4388-98.
3. Xu HHK, Smith DT, Jahanmir S, et al. Indentation damage and mechanical properties of human enamel and dentin. J Dent Res. 1998;77:472-80.
4. White SN, Luo W, Paine ML, Fong H, Sarikaya M, Snead ML. Biological organization of hydroxyapatite crystallites into a fibrous continuum toughens and controls anistropy in human enamel. J Dent Res. 2001;80(1):321-7.
5. Ge J, Cui FZ, Wang XM, Feng HL. Property variations in the prism and the organic sheath within enamel by nanoindentation. Biomaterials. 2005;26:3333-9.
6. Spears IR. A three-dimensional finite element model of prismatic enamel: a re-appraisal of the data on the Young's modulus of enamel. J Dent Res. 1997;76:1690-7.
7. Shimizu D, Macho GA, Spears IR. Effect of prism orientation and loading direction on contact stresses in prismatic enamel of primates: Implications for interpreting wear patterns American Journal of Physical Anthropology. 2005;126(4):427-34
8. Jiang Y, Spears IR, Macho GA. An investigation into fractured surfaces of enamel of modern human teeth: a combined SEM and computer visualisation study Arch Oral Biol. 2003;48(6):449-57
9. Spears IR, van Noort R, Crompton RH, Cardew GE, Howard IC. The effects of enamel anisotropy on the distribution of stress in a tooth. Journal of Dental Research. 1993;72:1526-31.
10. Maas MC, Dumont ER. Built to last: The structure, function, and evolution of primate dental enamel. Evolutionary Anthropology. 1999;8(4):133-52.
11. Moss-Salentijn L, Moss ML, Yuan MS-t. The ontogeny of mammalian enamel. Rotterdam: Balkema; 1997. 5-30 p.
12. Boyde A, Martin LB. The microstructure of primate dental enamel. New York: Plenum Press; 1984. 341-67 p.
13. Waters NE. Some mechanical and physical properties of teeth. In: Vincent J, Curry J (eds). The mechanical properties of biological materials. Cambridge: Cambridge University Press, 1980:99-134.
14. Ji B, Gao H. Mechanical properties of nanostructure of biological materials. Journal of the Mechanics and Physics of Solids. 2004;52:1963-90.
15. Jäger IL, Fratzl P. Mineralized collagen fibrils: a mechanical model with a staggered arrangement of mineral paticles. Biophysics Journal. 2000;79:1737-46.
16. Gao H, Ji B, Jäger IL, Arzt E, Fratzl P. Materials become insensitive to flaws at nanoscale: Lessons from nature. PNAS. 2003;100(10):5597-600.
17. Koenigswald Wv, Sander PM. Tooth enamel microstructure. In: Cate RT (ed). Oral histology : development, structure, and function (5^{th} Edition). Rotterdam: Balkema, 1997:267-80.
18. Zhou J, Hsiung LL. Biomolecular origin of the rate-dependent deformation of prismatic enamel. Appl Phys Lett. 2006;89:051904.
19. Bembey AK, Bushby AJ, Boyde A, Ferguson VL, Oyen ML. Hydration effects on the micro-mechanical properties of bone. Journal of Materials Research. 2006 Aug;21(8):1962-8.
20. Bembey AK, Oyen ML, Bushby AJ, Boyde A. Viscoelastic properties of bone as a function of hydration state determined by nanoindentation. Philosophical Magazine. 2006 Nov-Dec;86(33-35):5691-703.
21. Palamara J, Phakey PP, Rachinger WA, Orams HJ. The Ultrastructure of Human Dental Enamel Heat-treated in the Temperature Range 200'C to 600'C. J Dent Res. 1987;66(12):1742-7.
22. Raspanti M, Guizzardi S, Pasquale VD, Martini D, Ruggeri A. Ultrastructure of heat-deproteinated compact bone. Biomaterials. 1994;15(6):433-7.
23. Catanese J, Featherstone JDB, Keaveny TM. Characterization of the mechanical and ultrastructural properties of heat-treated cortical bone for use as a bone substitute. J Biomed Mater Res. 1998;45:327–36.
24. Rief M, Gautel M, Oesterhelt F, Fernandez J, Gaub H. Reversible unfolding of individual titin immunoglobulin domains by AFM. Science. 1997;276:1109-12.
25. Smith B, Schaffer T, Viani M, et al. Molecular mechanistic origin of the toughness of natural adhesives, fibres and composites. Nature. 1999;399:761-3.
26. Zhou J, Hsiung LL. Depth-dependent mechanical properties of enamel by nanoindentation. J Biomed Mater Res. 2006;In Press.

27. Darling AI, Mortimer KV, Poole DFG, Ollis WD. Molecular sieve behavious of normal and carious human enamel. Arch Oral Biol. 1961;5:251-73.
28. Klemm WR. Dehydration: A New Alcohol Theory. Alcohol. 1989;7:49-59.
29. Klemm WR. Biological Water and Its Role in the Effects of Alcohol. Alcohol. 1998;15(3):249-67.
30. Puchelle E, de Bentzmann S, Zahm JM. Physical and functional properties of airway secretions in cystic fibrosis-therapeutic approaches. Respiration. 1995;62(Suppl. 1):2-12.
31. Nalla RK, Kinney JH, Tomsia AP, Ritchie RO. Role of alcohol in the fracture resistance of teeth. J Dent Res. 2006;85(11):1022-6.
32. Wang X, Bank RA, TeKoppele JM, Agrawal CM. The role of collagen in determining bone mechanical properties. Journal of Orthopaedic Research. 2001;19:1021-6.
33. Holcomb DW, Young RA. Thermal Decomposition of Human Tooth Enamel. Calcif Tissue Int. 1980;31:189-201.
34. Pashley DH, Agee KA, Carvalho RM, Lee KW, Tay FR, Callison TE. Effects of water and water-free polar solvents on the tensile properties of demineralized dentin. Dent Mater. 2003;19(5):347-52.
35. Nizam BRH, Lim CT, Chng HK, Yap AUJ. Nanoindentation study of human premolars subjected to bleaching agent. J Biomech. 2005;38(11):2204-11.

Chapter 8

Characterization of nanoindentation induced residual stresses in human enamel by Raman micro-spectroscopy

Enamel is the hardest and the calcified tissue material with the highest elastic modulus and has the specific function of cutting and grinding food. The microstructural architecture of enamel varies from species to species and appears to have evolved to cope with the specific requirements associated with the source of food[1]. Of particular importance is the ability of enamel to survive sustained localized contact over millions of chewing and non specific loading cycles experienced. It is also known from comparative observations of primates that the structure of enamel was influenced by different food type and evolved to meet these functional needs[2,3]. Therefore, the deformation mechanisms and the stress distribution mode in relation to the structural characteristics of enamel are an essential factor to genuinely understanding this natural biocomposite material. Unfortunately, most techniques for material analysis such as SEM, TEM are unable to directly quantify stress distribution within the sample.

Although Raman spectroscopy has long been used in biomaterial research for compositional identification[4-7], measurement of stress with this technique is relatively novel in the biomaterials field. The relationship between mechanical stress and the position of Raman vibrational modes attributed to functional groups present in inorganic materials has been discussed theoretically[8,9] and been widely used in material and mechanical fields[10,11], and to a limited extent for biomaterials[12]. The relationship between the peak position of Raman vibrational modes of interest and applied stress can be investigated and calibrated by using standard samples with a loading apparatus. By assuming the axes of principal stress correspond to the main crystallographic directions of the crystal, the relationship can be expressed as:

$$\Delta\nu = \Pi_{ij}\sigma_{ij}, \quad (8\text{-}1)$$

where $\Delta\nu$ is the spectral shift of the selected Raman band, σ_{ij} and Π_{ij} are the stress and the piezo-spectroscopic coefficient, respectively[13]. Pezzotti reported the Π value of ν_1 phosphate band of a standard hydroxyapatite (HAP) sample under uniaxial stress, as 2.45

- 2.95 cm^{-1}/GPa[13,14]. This provides a convenient basis for measurement of stress by Raman microspectroscopy of dental hard tissues.

This is the first report of the application of Raman microspectroscopy for stress measurement of dental hard tissues. The aim of this study is to verify if this technique can be used for such biomaterials and to investigate the nanoindentation induced residual stress distribution on enamel in respect of its hierarchical structure.

This chapter is based on the following published manuscript:

- HE, L.H., CARTER, E.A. & SWAIN, M.V. (2007) Characterization of nanoindentation induced residual stresses in human enamel by micro-Raman spectroscopy. *Analytical and Bioanalytical Chemistry,* 389, 1185- 1192.

8.1 Material and methods

8.1.1 Enamel Samples

Three healthy premolar teeth, extracted for orthodontic reasons were prepared and indented as the method described in chapter 3. The force used for indentation was 100 mN for all samples and indenters. At least five indents from each indenter were made on each enamel sample and fifteen indents from each indenter on the HAP sample. The distance between two separate indents was more than 40 μm to avoid the influence of residual stresses from adjacent impressions. After indentation the enamel samples were stored in Hanks solution (typically for 1 week) until they were investigated with micro-Raman spectroscopy. Four Berkovich impressions, four spherical impressions and one intact sample area were selected randomly from three enamel samples and another eight different impressions (four for each indenter) and one sample area were selected from HAP sample for Raman mapping.

8.1.2 Raman Micro-spectroscopy

Spectra were collected using a Renishaw Raman InVia Reflex Microscope (Renishaw plc., Wotton-under-Edge, UK), equipped with an air-cooled charge-coupled device (CCD) camera. The spectrometer is fitted with holographic notch filters and two gratings (1200 mm/line (visible) 2400 mm/line (NIR)). The attached microscope is a Leica DMLM and is equipped with three objectives (×50/0.75 NA, ×20/0.40 NA, ×5/0.12 NA) and a trinocular viewer which accommodates a video camera allowing direct viewing of the sample.

Sample excitation was achieved using either an Argon ion laser (Modu-Laser, Utah, USA) emitting at 514.5-nm or a NIR diode laser (Renishaw plc., Wotton-under-Edge, UK) emitting at 830-nm. Daily calibration of the wavenumber axis is required and is achieved by recording the Raman spectrum of silicon (1 accumulation, 10 seconds) for both static and extended modes. If necessary, an offset correction is performed to ensure that the position of the silicon band is 520.50 ± 0.10 cm^{-1}. Spectra were not corrected for instrument response. The spectral resolution of the instrument using 514.5-nm excitation, a slit width of 65 μm and a 2400 l/mm grating was ~1.4 cm^{-1} and was determined by measuring the full width half height of the neon peak centred at 2350 cm^{-1}. The

spectrometer was controlled by PC with instrument control software (Renishaw WiRE™ 2.0 Service Pack 9).

Raman maps were collected by mounting the sample on the computerised X-Y translational mapping stage and using the WiRE™ software to define an area for analysis and the required step size. Raman maps with dimensions of ~10 μm × 10 μm^2 were defined for each enamel and HAP sample, the x and y step sizes were 1 μm. The spectral acquisition parameters were as follows: static mode, grating position centered at 960.00 cm^{-1}, 1 scan, 1 s exposure, ×50 objective. The laser power at the sample was ~7 mW for 514.5-nm and ~94 mW for 830-nm excitation.

To establish if the natural fluorescence of enamel influenced the position of the phosphate band, observed at ~960 cm^{-1}, addtional experiments were undertaken as follows: two sound, non-indented areas, were selected for the investigation. The instrument parameters were as follows: static mode, grating position centered at 960.00 cm^{-1}, 1 scan, 5 s exposure, ×50 objective. At the first point (Area 1), 20 spectra were collected sequentially from the same spot. The sample was then moved a distance of ~20 μm in the y direction and the experiment was repeated twice at the same spot (Area 2 and Area 2A). The spectra were curve fitted as per the method used in the paper: the initial parameters of a 50% Gaussian and 50% Lorentzian mixture in the range of 1000-900cm^{-1}, which means only a limited baseline was included in the fitting processes.

Data Manipulation: A representative spectrum from the map dataset was curve fitted using the initial parameters of a 50% Gaussian and 50% Lorentzian mixture and the resultant curve fitting parameters were saved. A map of the position of the $\nu_1(PO_4)$ band was then produced by curve fitting the individual spectra within the map dataset using the previously saved parameters. Although the nominal instrumental resolution is between 1 to 2 cm^{-1} it is possible to measure relative Raman shifts as small as 0.01 cm^{-1} provided that the S/N ratio is better than ~20[15].

8.2 Results

8.2.1 Force-displacement curves of nanoindentation

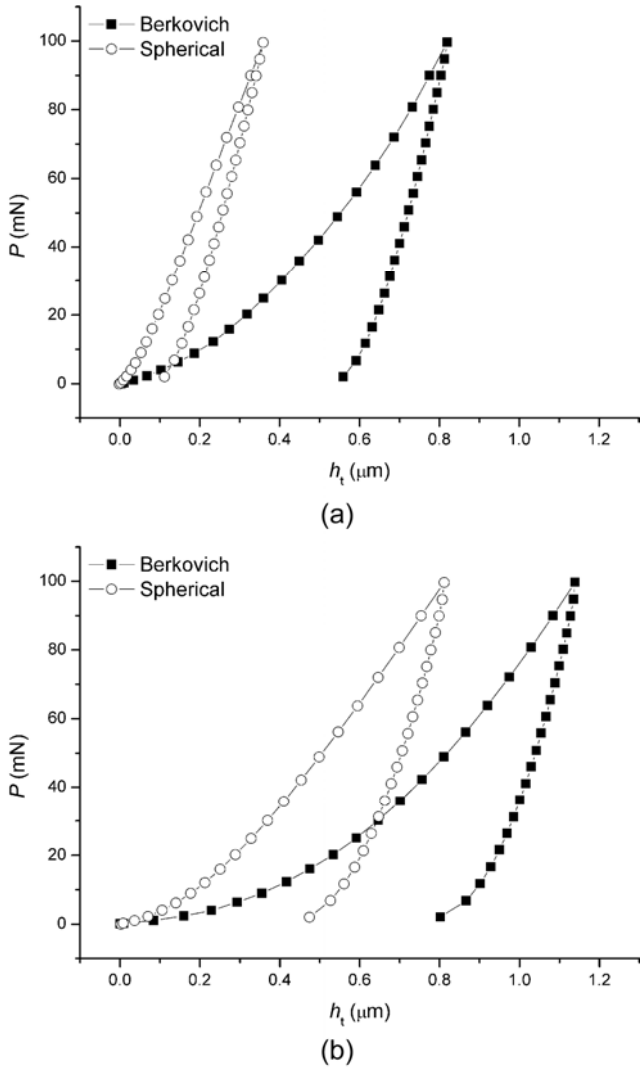

Fig. 8-1 Sample force-displacement curves of (a) HAP and (b) enamel samples by Berkovich and spherical indenters

Fig. 8-1 presents the force-displacement curves for HAP (Fig. 8-1a) and enamel (Fig. 8-1b) The area enclosed by load and unload curve is termed the plastic deformation energy (U_p), which is the energy absorbed by the sample. Under the same indentation force, enamel has a bigger indentation displacement, which means it is more deformable than HAP. The samples absorbed significantly higher U_p, especially the HAP sample, when the impressions were made with the Berkovich indenter compared to the spherical indenter.

8.2.2 Representative Raman spectra

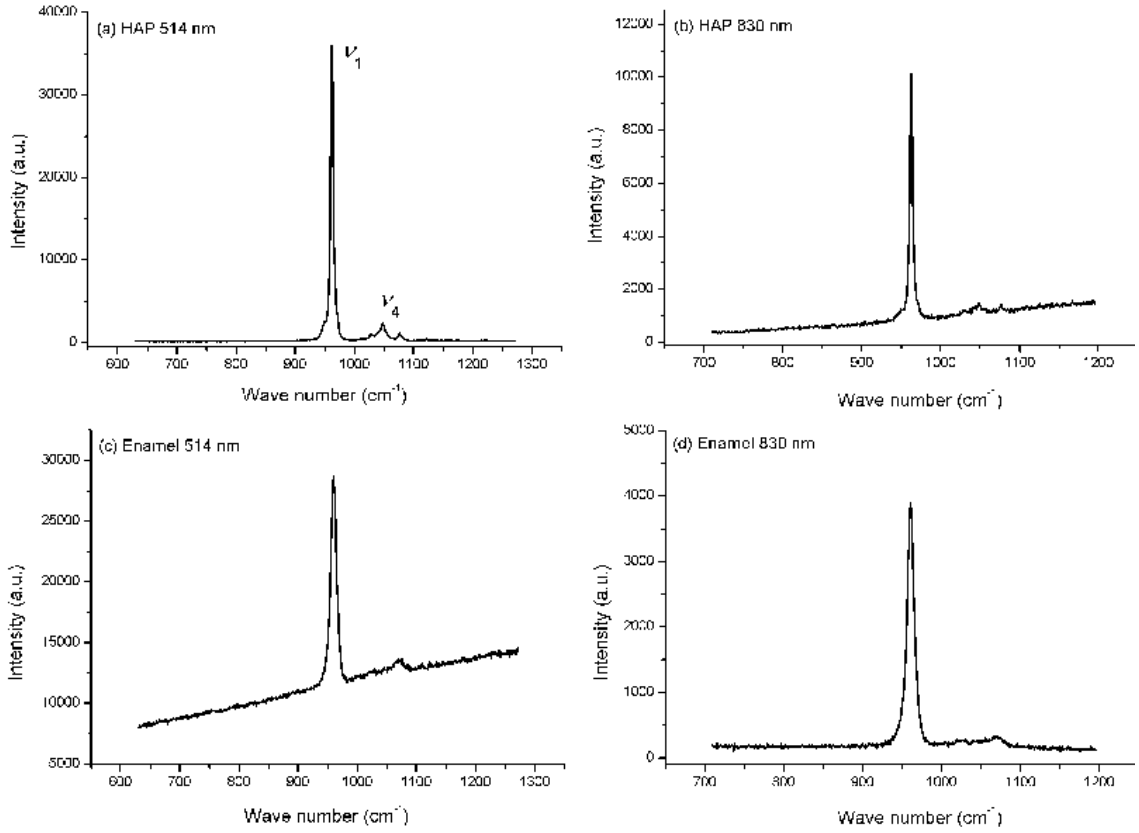

Fig. 8-2 Sample spectra of enamel and HAP using different excitation sources.

The HAP samples produced high quality, well resolved spectra with both 514.5- and 830-nm excitation (Figs 8-2a and b). Within the spectral range of 1200 – 700 cm^{-1}, two phosphate bands at 960 cm^{-1} (ν_1) and 1071 cm^{-1} (ν_4) were observed. The enamel sample spectrum collected with 514.5-nm excitation (Fig. 8-2c) exhibits a considerable fluorescent background, while the spectrum collected with 830-nm excitation (Fig. 8-2d) produced significantly less fluorescence. Comparison of these spectra reveals that regardless of excitation wavelength the ν_1 mode is broader in the enamel spectra than the HAP.

8.2.3 The influence of fluorescence on $\nu_1(PO_4)$ band position

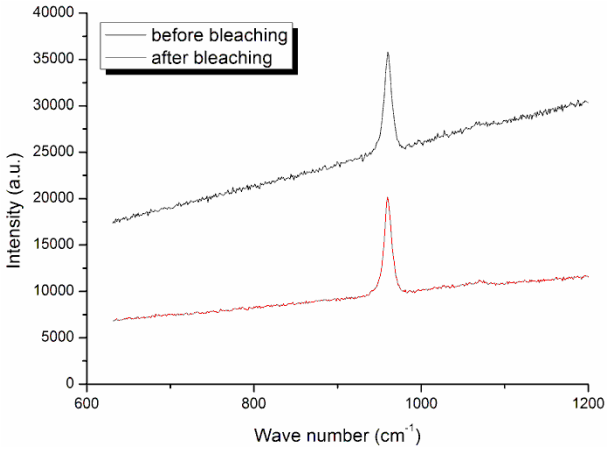

Fig. 8-3 The first (before bleaching, t=0 s) and the last spectrum (after bleaching, t=130 s) of the 20 spectra sequentially collected from Area 1. (Spectra are to scale)

Fig. 8-3 illustrates that repeated scans on the same point bleached the sample significantly, as is evidenced by the intensity (y-axis). However, the position of $\nu_1(PO_4)$ band before and after bleaching was 960.28 and 960.31, respectively, which indicates that fluorescent background did not influence the band position value.

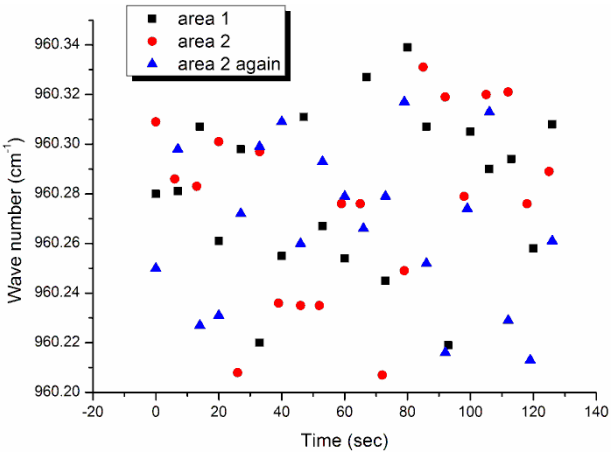

Fig. 8-4 $\nu_1(PO_4)$ band position of all three experiments from two different sound areas of enamel.

Fig. 8-4 is a plot of the position of the $\nu_1(PO_4)$ band of the spectra collected from the three experiments. The position of the band is 960.28 ±0.05 cm^{-1}, no time dependent trends are observed. Laser bleaching of the sample and fluorescent background (the tilted baseline) did not influence the accurate calculation of $\nu_1(PO_4)$ band position.

8.2.4 Representative Raman stress maps

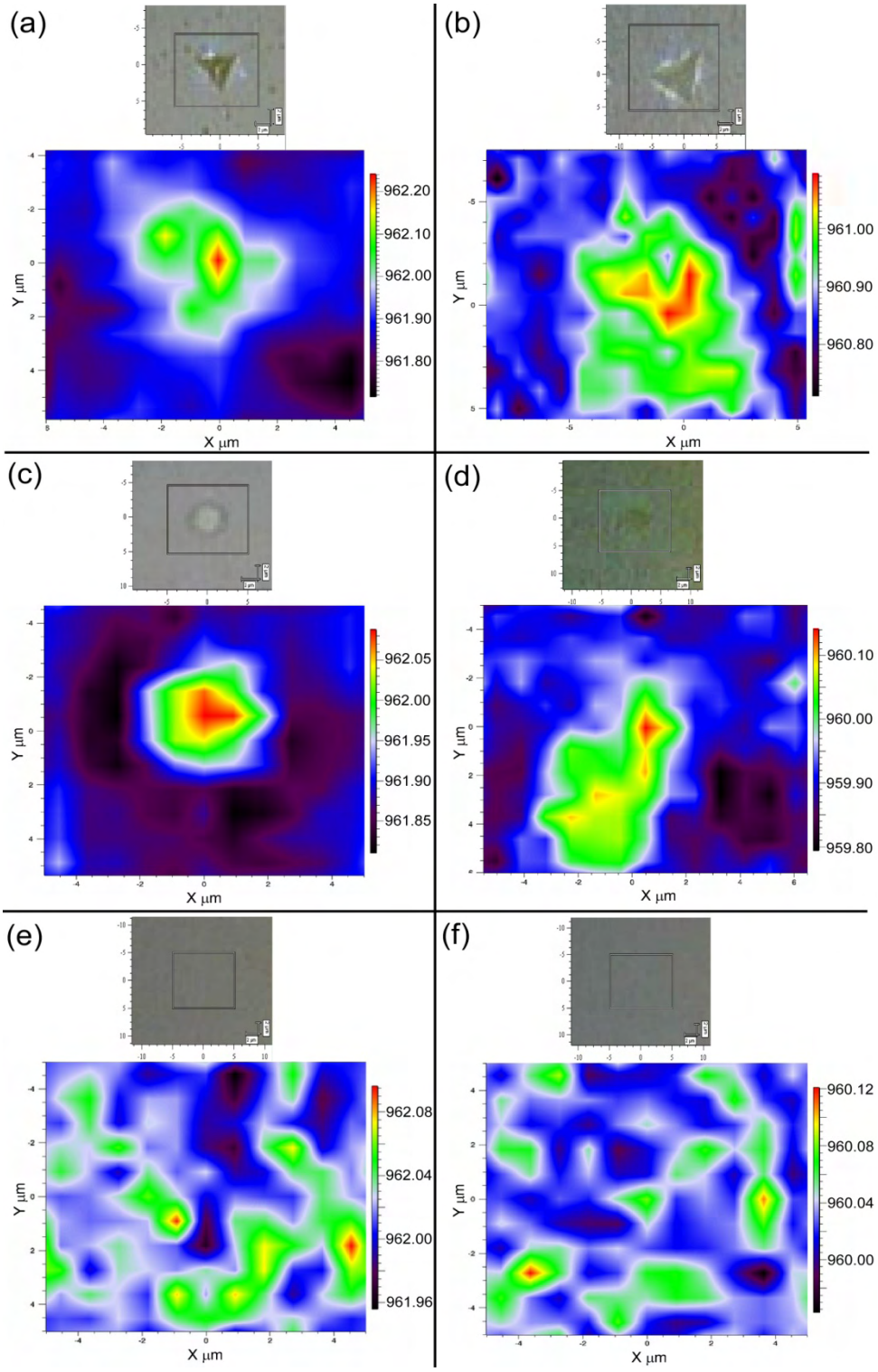

Fig. 8-5 Sample stress maps of Berkovich (a) (b) and 10 µm spherical (c) (d) indenters from both HAP (a) (c) and enamel (b) (d) samples (514.5 nm excitation). (e) and (f) are non-indent control areas of HAP and enamel, respectively. (The color bars at the right side of the maps have the dimension of cm-1).

Stress variation within and around the indentation impressions are reflected as a shift in the position of the ν1 band as shown in Figs. 8-5a to d, with the images of the control samples presented in Figs. 8-5e and f. For the HAP sample, the band shift was usually restricted to within the indent impression area. The highest band shift position was located at the centre of the residual impression, which was the highest compressively stressed region for both Berkovich and spherical indents. The maps of the Berkovich impression show the lowest band position correlates to the stress-free intact surface (Fig. 8-5a), while in the maps of spherical impression the lowest band position was located around the impression (dark blue area in Fig. 8-5c), because of local stress relaxation associated with the formation of a ring crack surrounding the impression. In contrast, the band position maps of enamel were more complex and less regular and, for most maps, the shift in the band position extended into the intact area (Figs. 8-5b and d). Additional maps illustrating the same characteristics are available in supplementary documents.

Maps in Fig. 8-5 have been interpolated by the Renishaw WiRE™ 2.0 software for better illustration. By definition, interpolation is a method of constructing new data points from a discrete set of known data points. Interpolation here means that the software generates more data points between two adjacent real measured data points to smooth the map. This procedure does not change the nature of the map but only improves the quality of the map for easy reading.

8.2.5 Comparison of 830-nm and 514.5-nm excitation wavelengths

Table 8-1 Band shift range of ν_1 vibrational mode from different excitation sources

Sample	Indenter	Band shift range	
		830 nm	514.5 nm
HAP	Berkovich	0.10±0.02	0.56±0.03
	Spherical	0.09±0.03	0.17±0.02
Enamel	Berkovich	0.17±0.03	0.54±0.04
	Spherical	0.22±0.02	0.37±0.04

Statistical analysis (*t*-test) shows that the extent to which the position of ν_1 mode shifts is distinctly different for the two excitation wavelengths ($P<0.05$) for both samples (Table 8-1). The most significant shift in the position of this band is observed when using 514.5-nm excitation. Notably, there is no statistical difference in the shift of the position of the ν_1 mode for the spectra of the HAP samples acquired with 830-nm excitation. These results indicate that the 514.5-nm excitation wavelength is the most appropriate of the two wavelengths used in this investigation for stress detection.

8.3 Discussion

8.3.1 Raman spectrum of hydroxyapatite in enamel

Previous investigation of hydrothermally prepared hydroxyapatite by Raman spectroscopy illustrated the presence of four main fundamental vibrational modes ν_1, ν_2, ν_3 and ν_4[16]. The most intense and sharp band, ν_1, is assigned to the symmetrical stretching of the tetrahedron of oxygen atoms surrounding the phosphorous atom (the free PO_4^{3-} atom has T_d symmetry)[14]. For dental calcified tissues, as recorded by this investigation and reported by other researchers, this Raman band is located at 960 cm^{-1} [4]. Because it is an intense, unique and quite distinct band the ν_1 band has been selected for stress characterization[13] and damage detection[17,18] for biomineralized tissues. The results of this study also confirmed that this is a suitable band for stress mapping of mineralized tissue.

The width of the Raman ν_1 band is related to the existence of long-range order in the crystalline structure[14]. The more crystalline the structure the narrower is the band. In this study, the ν_1 band was found to be broader in the enamel spectrum than that of the sintered HAP spectrum. This indicates that the hydroxyapatite crystals in enamel are less regular or more defective than those of HAP as anticipated due to the natural mineralization procedure of enamel and the organic components within enamel.

8.3.2 Factors influence stress detection

Crystal symmetry, long-range order in the crystalline structure, the polarization and propagation directions of the incident and scattered light with respect to the crystal axes as well as the crystal phonon modes will influence the intensity and shape of a Raman band[14,19]. Therefore, several factors can influence stress detection by Raman spectroscopy.

The first factor is stress direction. Theoretical and experimental reports all concluded that, there is no unique general relationship between the Raman spectral parameters (particularly Raman shift) and stress and such relationships can only be deduced for special simple cases[8,9]. He *et al.*'s piezo-spectroscopic investigation[20] indicated the stress direction at the crystal level influences the crystal spectrum and, if the principal stress is not parallel to main crystallographic direction, a transformation matrix is required for adjustment. The direction of the hydroxyapatite crystallites vary within enamel rod unit

because of the natural biomineralization procedure[21,22]. This means, even under uniaxial load, the stress on different crystallites could vary with respect to the main crystographic direction and makes accurate prediction of stress from shifts in the positions of Raman bands more difficult. Furthermore, it has been reported that the relationship between stress and band position may not be linear for a non-uniformly strained sample[23]. Therefore, in this study, the peak shift was not converted into stress values.

The second factor is the excitation wavelength. Raman spectra are obtained from a volume which is dependent upon the sample response (absorption and refractive index), excitation wavelength and the objective aperture of the microscope. Analysis has shown that the penetration depth of the focused laser beam can vary from tens of nanometers to several millimeters and thus sample a large volume of the strained structure[9]. Studies have also illustrated that the penetration depth can be markedly reduced by choosing a wavelength suitable for resonance Raman [11]. Furthermore, each point within this volume scatters light with a Raman band characteristic of the local stress at that point. Therefore, the final spectrum is an average value of each point within the sampled volume. In this study, the stress field around an indentation impression is highly localized and dependent upon indenter shape. If the laser penetrates too deep and generates a relatively large collecting volume, the spectra are less likely to reflect local stress because the band position is an average of the whole excitation volume. Under this condition, the average value of the peak position will not be sensitive enough to describe the localized stress field. Table 1 is evidence to support this argument. A shorter laser wavelength provides information about stress near to the sample surface[24], which explains why the shift in the peak position was more significant when using 514.5-nm compared to 830-nm excitation, as the residual indentation stress only exists in a limited subsurface volume near the indent impression. Moreover, the theoretical calculation of the diameter of these two laser beams is 0.837 and 1.35 μm for 514.5-nm and 830-nm, respectively. In another words, when using the 830-nm excitation wavelength there was a greater depth penetration and a larger detection area which also in all likelihood decreased its sensitivity for stress detection.

To the question of sample fluorescence on influence of the Raman bands, there are no satisfactory theoretical explanations till now. But, to enamel samples, we do find low level fluorescence especially with 514.4 nm laser (Fig. 8-2). Therefore, we did the

additional experiment to confirm that this fluorescence will not influence the accuracy of band position acquisition. Results showed that laser exposure significantly reduced the fluorescent background of the spectrum (Fig. 8-3). The fluorescent background originating from the enamel sample did not influence the $\nu_1(PO_4)$ band position (Fig. 8-4). Although the accuracy of the spectrometer system can be as high as 0.01 cm^{-1}, from this investigation, a ±0.05 cm^{-1} error should be noted from 514.5 nm laser excitation. However, we observed a band shift of ±0.5 cm^{-1} in our stress measurements which is a factor of 10 greater than the error measurement (Fig. 8-5). Furthermore, diffuse laser light spreads out around the area of analysis. This subsequently bleaches the adjacent areas of the sample. Therefore, the initial spectra collected within the map will have a fluorescent background, however, the remainder of the spectra do not have a very strong fluorescent background, if any fluorescence at all.

8.3.3 Residual Stress within different materials

The position of the $\nu_1(PO_4)$ Raman band shifts because of the stress stored in the hydroxyapatite crystals, which was introduced by the indentation load and was observed as plastic deformation energy, U_p, in the indentation force-displacement curve (Fig. 8-1). The spherical indents on the HAP sample absorbed much less plastic deformation energy, Up, than all the other indentations and were associated with much lower residual stresses, which can be reflected as the $\nu_1(PO_4)$ Raman band shift. In Table 8-1, the Raman band shifts of the spectra from samples with spherical indent impressions are statistically lower than those from Berkovich indent impressions.

As with most natural biomaterials, enamel shows distinctive structural hierarchy[21]. The smallest structural units are needle-like hydroxyapatite crystals which are ~20 nm in thickness. In healthy human enamel, these hydroxyapatite crystallites are organized and bundled together by organic molecules to form larger-scale structures called cylindrical enamel prisms. Crystallites in the central region of the prism are parallel, while those near the edge of the prism usually have an angle of nearly 60° to the longitudinal axis of prism[22]. The arrangement of prisms determines the next hierarchical level unit associated with enamel types. Human enamel has ~5 μm diameter prisms encapsulated by a thin layer of sheaths which are arranged parallel in a direction perpendicular to the dentino-enamel junction (DEJ) from dentin to the outer enamel surface. In some areas, prisms

may twist together or change the direction slightly to reinforce the whole enamel structure[25,26]. This hierarchical structure endows enamel high facture toughness[22] and anisotropic elastic modulus[27] and fracture patterns[28], all of which are related to the anisotropic microstructural architecture, as interpreted by Spears et al. in their finite element models[29,30].

Results of this study support these models as the residual stresses are distributed in a more complex way by the hierarchical structure, the stress distribution pattern of enamel was less regular than that of homogeneous sintered HAP (Fig. 8-1). Fig. 8-5 illustrated that the highest stresses were located at the centre of the indent impressions. For HAP samples, the residual stress was mainly limited within the indent impression, which is consistent with the contact mechanical theories. In contrast, residual stress fields for the enamel samples were far bigger than the indent impressions. Rod units were believed to redistribute the stress in a more complex manner. To confirm this statement, additional SEM images of the indentation was attached in Fig. 8-6 in comparison with the Raman stress map, which illustrated that the indentation stress distribution was affected by the rod unit structure of the biocomposite.

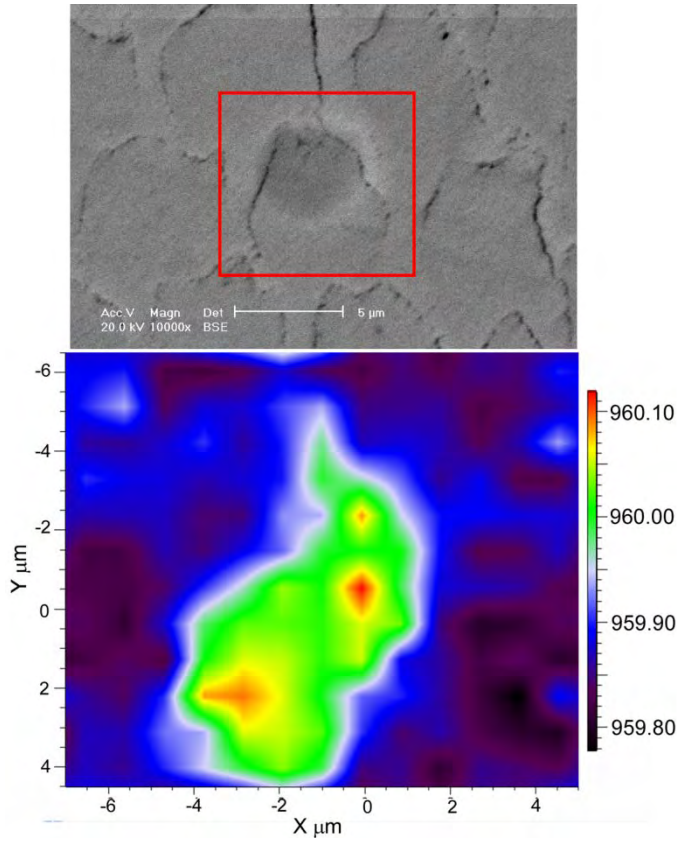

Fig. 8-6 Sample stress map of 10 µm spherical indent impression on enamel and its correlated SEM image. SEM clearly showed rod unit structure and the indent impression was located at the head part of one rod. Consequently, the indentation stress distribution was regulated by this rod structure as: stress only extended within the rod unit and was shielded by the rod-interrod interface.

8.4 Conclusions

Raman microspectroscopy has been successfully used to monitor nanoindentation induced residual stresses on human enamel and sintered HAP. Several conclusions have been drawn, namely:

- Raman microspectroscopy can be used as a unique stress meter with excellent spatial resolution for stress distribution mapping of nanomechanical biomaterials.
- Despite florescence originating from the organic matrix, 514.5-nm is a more appropriate excitation source than the NIR excitation wavelength of 830-nm for enamel stress detection.
  - Extended laser exposure prior to data collection significantly reduced the fluorescent background of the spectrum.
  - The fluorescent background originating from the enamel sample did not influence the $\nu_1(PO_4)$ band position.
  - Although the accuracy of the spectrometer system has been reported within the literature to be as high as 0.01 cm^{-1}, from this investigation and for these samples, a ± 0.05 cm^{-1} error was found to exist when using an excitation wavelength of 514.5-nm. A shift of ± 0.5 cm^{-1} was observed in the Raman spectra of samples which had been indented which is a factor of 10 greater than the error measurement.
- Comparison of enamel with homogeneous HAP, showed the hierarchical structure influenced the residual stress distribution on enamel sample.

The deformation and toughening mechanisms of natural biocomposites are not well understood. Raman microspectroscopy is a novel, non-destructive and high resolution technique which can be used to explore the stress distribution and crack propagation mechanisms of natural biocomposites.

8.5 References

1. Maas MC, Dumont ER. Built to last: The structure, function, and evolution of primate dental enamel. Evol Anthro. 1999;8(4):133-52.
2. Spears IR, Crompton RH. The mechanical significance of the occlusal geometry of great ape molars in food breakdown J Hum Evol. 1996;31(6):517-35
3. Maas MC, OLeary M. Evolution of molar enamel microstructure in North American Notharctidae (primates). J Hum Evol. 1996;31(4):293-309
4. Schulze KA, Balooch M, Balooch G, Marshall GW, Marshall SJ. Micro-Raman spectroscopic investigation of dental calcified tissues. J Biomed Mater Res. 2004;69A:286-93.
5. Wentrup-Byrne E, Armstrong CA, Armstrong RS, Collins BM. Fourier transform Raman microscopy mapping of the molecular components in a human tooth. J Raman Spectr. 1997;28:151-8.
6. Carden A, Morris MD. Application of vibrational spectroscopy to the study of mineralized tissues (review). J Biomed Opt. 2000;5(3):259-68.
7. Penel G, Leroy G, Rey C, Bres E. MicroRaman Spectral Study of the PO_4 and CO_3 Vibrational Modes n Synthetic and Biological Apatites. Calcif Tissue Int. 1998;63:475-81.
8. Ganesan S, Maradudin AA, Oitmaa J. A lattice theory of morphic effects in crystals of diamond structure. Ann Phys. 1970;56(2):556-94.
9. Atkinson A, Jain SC. Spatially Resolved Stress Analysis Using Raman Spectroscopy. J Raman Spectrosc. 1999;30:885-91.
10. Schmidt U, Ibach W, Muller J, Weishaupt K, Hollricher O. Raman spectral imaging - A nondestructive, high resolution analysis technique for local stress measurements in silicon. Vibr Spectr. 2006;42:93-7.
11. Dietrich B, Dombrowski KF. Experimental challenges of stress measurements with resonant micro-Raman spectroscopy. J Raman Spectr. 1999;30:893-7.
12. Pezzotti G, Sakakura S. Study of the toughening mechanisms in bone and biomimetic hydroxyapatite materials using Raman microprobe spectroscopy J Biomed Mater Res. 2003;65A(2):229-36.
13. Pezzotti G. Raman piezo-spectroscopic analysis of natural and synthetic biomaterials. Anal Bioanal Chem. 2005;381:577-90.
14. Pezzotti G. Introducting a unique measurement for biomaterial nanomechanics. Key Eng Mater. 2003;240-242:893-900.
15. Bonera E, Fanciulli M, Batchelder DN. Stress Mapping in Silicon: Advantages of Using a Raman Spectrometer with a Single Dispersive Stage. Appl Spec. 2002;56(5):560-3.
16. Blakeslee KC, Condrate RA. Vibrational spectra of hydrothermally prepared hydroxyapatites. J Am Ceram Soc. 1971;54:559-63.
17. Timlin JA, Carden A, Morris MD, Rajachar RM, Kohn DH. Raman spectroscopic imaging markers for fatigue-related microdamage in bovine bone. Anal Chem. 2000;72:2229-36.
18. Carden A, Rajachar RM, Morris MD, Kohn DH. Ultrastructural Changes Accompanying the Mechanical Deformation of Bone Tissue: A Raman Imaging Study. Calcif Tissue Int. 2003;72:166-75.
19. Loudon R. The Raman effect in crystals. Adv Phys. 1964;13:423-82.
20. He J, Clarke DR. Polarization dependence of the Cr3+ R-line fluorescence from sapphire and its application to crystal orientation and piezospectroscopic measurement J Am Ceram Soc. 1997;80:69-78.
21. Eisenmann DR. Enamel Structure. In: Cate RT (ed). Oral Histology. St. Louis, Missouri: Mosby, 1998:218-35.
22. White SN, Luo W, Paine ML, Fong H, Sarikaya M, Snead ML. Biological organization of hydroxyapatite crystallites into a fibrous continuum toughens and controls anistropy in human enamel. J Dent Res. 2001;80(1):321-7.
23. Pinardi K, Jain SC, Willander M, Atkinson A, Maes HE, Overstraeten RV. A method to interpret micro-Raman experiments made to measure nonuniform stresses: Application to local oxidation of silicon structures. J Appl Phys. 1998;84:2507-12.
24. Wolf ID. Micro-Raman spectrocopy to study local mechancial stress in silicon integrated circuits. Semicond Sci Technol. 1996;11:139-54.
25. Macho GA, Jiang Y, Spears IR. Enamel microstructure—a truly three-dimensional structure. J Hum Evol. 2003;45:81-90.

26. Radlanski RJ, Renz H, Willersinn U, Cordis CA, Duschner H. Outline and arrangement of enamel rods in human deciduous and permanent enamel. 3D-reconstructions obtained from CLSM and SEM images based on serial ground sections. Eur J Oral Sci. 2001;109:409-14.
27. Cuy JL, Manna AB, Livi KJ, Teaford MF, Weihs TP. Nanoindentation Mapping of the Mechanical Properties of Human Molar Tooth Enamel. Arch Oral Biol. 2002;47:281-91.
28. Xu HHK, Smith DT, Jahanmir S, et al. Indentation damage and mechanical properties of human enamel and dentin J Dent Res. 1998;77(3):472-80
29. Spears IR. A three-dimensional finite element model of prismatic enamel: a re-appraisal of the data on the Young's modulus of enamel. J Dent Res. 1997;76:1690-7.
30. Shimizu D, Macho GA, Spears IR. Effect of prism orientation and loading direction on contact stresses in prismatic enamel of primates: Implications for interpreting wear patterns Am J Phys Anthro. 2005;126(4):427-34

Chapter 9

Conclusions and Implications

Based on the above nanoindentation investigations on the mechanical behaviour of enamel, generally speaking, the hierarchical microstructure of enamel and the small amount of protein remnants in mature enamel played important roles in regulating the mechanical behaviour of this biocomposite. This may be appreciated from the following different perspectives:

- Indentation stress-strain relationship of enamel is more comparable with that of a metallic material rather than brittle ceramics such as pure hydroxyapatite (chapter 4).
- At the micro scale, the elastic modulus of enamel is regulated by its rod structure, in which the precisely arranged hydroxyapatite crystallites are adhered together by protein fragments (chapter 5).
- Moreover, the residual stress distribution of enamel is also regulated by its rod structure, due to this anisotropic arrangement of hydroxyapatite crystallites and protein fragments (chapter 8).
- The existence of protein remnants within enamel result in certain in-elastic behaviours such as high energy absorption and creep deformation, which are unique when compared with brittle ceramics (chapter 6).
- The change of the environment of enamel samples such as dehydration and burning blocks and eliminates the functions of proteins. Therefore, the resulting mechanical behaviour of enamel was observed to change significantly (chapter 7).

Enamel has long been regarded as a bioceramic[1] which is hard but brittle. This research illustrated a totally different aspect of the biocomposite, namely in-elastic or metallic like mechanical behaviour. This novel outcome provides both material developers and clinical practitioners many valuable implications:

- The mechanical properties of composite material can be manipulated by adjusting the hierarchical microstructure and addition of a viscous second-phase component. Several attempts such as self-assembly[2] of hydroxyapatite crystallites and multi-phase composite design[3] have been attempted to optimise the mechanical properties of the man-made materials.

- Due to the size and structural limitations of natural enamel, it is difficult to employ standard material test methods and criteria into the dental materials testing field. Therefore, nanoindentation techniques and the relevant measuring methods such as indentation stress-strain relationship and indentation creep should be considered as new and more appropriate methods for dental material evaluation and selection.
- From a clinical point of view, metallic materials such as cast alloys and amalgam may be a better choice for restorations than hard ceramics, which may cause excessive wear of opposing teeth. By considering the aesthetic needs of dental materials, composites are good choice but this category of dental materials needs further development to enhance the mechanical properties and reduce the shrinkage stresses during curing.

Based on the above findings, possible further research directions include:

- Detail investigations on the protein remnants in mature enamel. This includes biochemical e.g. proteomics and vibrational spectroscopy analyses.
- From the conclusion of current investigation, dental bleaching and laser treatments may have potential hazardous effects on tooth hard tissues. Therefore, further observations at this point are essential.
- Further theoretical and numerical analyses on natural hard biocomposites in respect to their microstructure and composition will benefit the material development and composite design.

Reference:

1. Robinson C, Connell S, Kirkham J, Shorea R, Smith A. Dental enamel—a biological ceramic: regular substructures in enamel hydroxyapatite crystals revealed by atomic force microscopy. J Mater Chem. 2004;14(14):2242-8
2. Chen H, Clarkson BH, Sun K, Mansfield JF. Self-assembly of synthetic hydroxyapatite nanorods into an enamel prism-like structure. J Coll Inter Sci. 2005;288:97-103.
3. Soh MS, Sellinger A, A.U.J Y. Dental nanocomposite. Curr Nanosci. 2006;2:373-81.